(9) PROFESSIONAL PAPER 245 (11) Jun 79

(6)

THE ACCELEROMETER METHODS OF OBTAINING AIRCRAFT PERFORMANCE FROM FLIGHT TEST DATA (DYNAMIC PERFORMANCE TESTING).

(10) William R. Simpson

(12) 403

The ideas expressed in this paper are those of the author. The paper does not necessarily represent the views of either the Center for Naval Analyses or the Department of Defense.

(14) CNA-PP-245

CNA Operations Evaluation Group

CENTER FOR NAVAL ANALYSES
2000 North Beauregard Street, Alexandria, Virginia 22311

PREFACE

There are, in general, two basic methods of obtaining aircraft performance from flight test data. Aircraft performance is defined here as engineering data which can be used to realistically represent the aircraft capabilities (i.e., specific range, turning performance, acceleration time, time-to-climb, etc.). The first of these methods, the Direct method, is to fly a particular maneuver of interest and mathematically correct this maneuver to a given set of standard conditions. Several similar maneuvers at different flight conditions are then combined in a composite map representing one aspect of the aircraft performance. For example, families of stabilized points at different constant values of W/δ are used to represent aircraft specific range; or specific excess power is calculated from several accelerations at different altitudes and combined to represent the ability of the aircraft to change its energy state.

The Indirect method is more subtle and has its basis deeper in theory. By this method, a group of aerodynamic and propulsion parameters are developed which in themselves are only numbers and do not represent performance. These parameters are not tied to a specific maneuver or maneuver type, but in general relate the physical forces required to achieve a certain flight condition. Such parameters for an aircraft would be the drag coefficient, lift coefficient, thrust available, fuel flow requirements, etc. However,

these parameters can be combined with known facts about the airframe and propulsion system in such a fashion as to compute airplane performance. For example, the airplane drag polar and thrust-fuel flow requirements can be coupled to develop aircraft specific range data.

Any valid flight test program can pursue either the Direct method or the Indirect method of obtaining aircraft performance within certain limitations. In general, basic flight test maneuvers may be placed into three categories:

- Steady state maneuvers: excess thrust is essentially zero (example - steady point).
- Quasi steady state maneuvers: excess thrust is not necessarily zero, but the normal load factor remains near unity (example - climb or acceleration).
- Dynamic maneuvers: normal load factor deviates from unity because of test technique (example - wind-up turn or rollercoaster).

The data acquisition technique for extraction of aerodynamic and performance data will generally consist of either:

- Airspeed - altitude measurements (energy method).
- Position measurements (radar or camera method).
- Longitudinal and normal accelerometer measurements (hereafter referred to as the accelerometer method).

With the advent of highly accurate accelerometers, the dynamic maneuvers have become attractive for development of aerodynamic data -

when obtaining aircraft performance using the Indirect Method. Accelerometers sense the inertial or total acceleration acting on an aircraft, and their value can be converted directly into force by multiplying by airplane gross weight. Aircraft longitudinal acceleration data are used to mathematically compute excess thrust for use in constructing a drag polar. Dynamic maneuvers offer significant savings in time and cost over the conventional time consuming steady state and quasi steady maneuvers for generating aerodynamic data. Several USAF, USN, and Grumman aircraft engineering programs have established that the drag polar shape (not absolute level) can be obtained to within ±3 percent data accuracy from dynamic maneuvers with time savings of 70 to 90 percent over conventional methods.

Because these techniques offer such tremendous advantages, and because these techniques require increased care in application, this document is compiled as a guide to those who wish to apply the techniques.

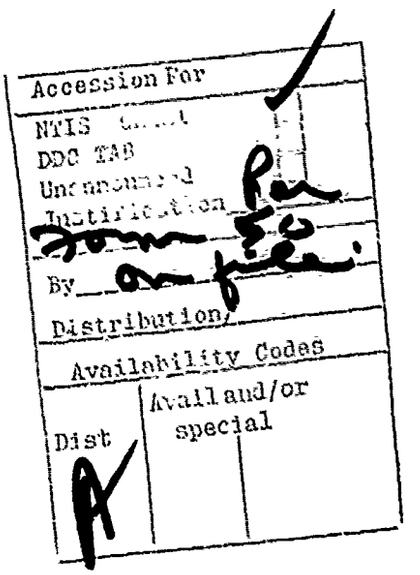

FORWARD

This document is the result of several years of research into accelerometer methods. Programs were conducted by the United States Air Force at Edwards' Air Force Base in California, and the Grumman Aerospace Corporation in Calverton, New York, as well as the U.S. Naval Air Test Center at Patuxent River, Maryland. Each of these programs was undertaken with U.S. Navy participation.

These intensive research programs represent the combined work of many specialists without whom the development of effective methods of determining aircraft performance by using onboard accelerometers could not have been possible. The author wishes to acknowledge the contributions of:

Mr. Wayne Olson, Air Force Flight Test Center

Mr. Willie Allen, Air Force Flight Test Center

Mr. Everret Dunlap, Air Force Flight Test Center

Mr. C. Porter Laplant, Grumman Aerospace Corporation

Mr. Chuck Sewell, Grumman Aerospace Corporation.

Mr. William Branch, U.S. Naval Air Test Center.

While making such acknowledgement, the author assumes full responsibility for the textual material presented in this report. Comments relative to the material contained herein are solicited, and should be addressed to the author at the Center for Naval Analyses, 1401 Wilson Boulevard, Arlington, Virginia 22209.

TABLE OF CONTENTS
CHAPTER 1

CHAPTER 2

CHAPTER 3

CHAPTER 4

CHAPTER 5

CHAPTER 6

CHAPTER 7

CHAPTER 8

CHAPTER 9

LIST OF ILLUSTRATIONS

LIST OF ILLUSTRATIONS

LIST OF TABLES

THE ACCELEROMETER METHODS OF DETERMINING AIRCRAFT PERFORMANCE (DYNAMIC PERFORMANCE TESTING)

CHAPTER 1

INTRODUCTION AND BACKGROUND

SUMMARY OF CHAPTER 1

1.1 The development of accelerometer methods for determining aircraft performance (popularly referred to as dynamic performance methods) was undertaken to reduce the total flight time required to determine the overall performance of an aircraft. The overall performance is taken to include climb, acceleration, turning, takeoff, and level flight performance, as well as other data used to define the capabilities of an aircraft. The accelerometer methods differ from conventional methods in that onboard accelerometers are used to measure longitudinal and normal load factors for the determination of aircraft excess thrust and lift. This first chapter introduces the subject of the accelerometer methods, the concepts of thrust and fuel flow modeling, and briefly addresses applications of accelerometer methods and presents results of three programs directed toward the development of these methods. Further expansion of each topic will be made in subsequent chapters.

1.2 In recent years, several aerospace industry agencies, both civilian and government, have investigated accelerometer methods for determining aircraft performance with some promising results. The accelerometer methods give an "instantaneous" measure of excess thrust which can then be used to calculate aircraft performance. The results of one such program are presented in reference 1-1. The accelerometer method was used in this case to generate drag polars from dynamic(i.e., push-pull or wind-up turn) maneuvers. Based on the promising results of this and other programs, and motivated by the potential savings in flight time achieved the accelerometer methods are presently being used as standard procedures in aircraft performance evaluation programs. The Air Force Flight Test Center (AFFTC) in conjunction with the Aerospace Research Pilot School (ARPS) organized a flight test program to define and document dynamic performance test techniques for both subsonic and supersonic flight. The United States Air Force (USAF) invited participation by the United States Navy(USN) in this program.

1.3 Test project flying began in March, 1971, with Navy participation beginning in February. The test aircraft utilized on this program were an A-7D assigned to ARPS and an FB-111A undergiong normal Category II testing (performance and stability and control tests) at the AFFTC. The A-7D was also the same aircraft that was used for Category II performance tests the

year before, so that conventionally acquired data was available for both aircraft. Both test aircraft were equipped with special instrumentation applicable to dynamic performance, including Systron-Donner accelerometers mounted in the noseboom of both aircraft. A similar accelerometer was mounted in the cockpit of the A-7D. Instrumentation requirements are reviewed in Chapter 5.

1.4 The Grumman Aerospace Corporation (GAC) had proposed to the Navy the use of the accelerometer methods for development, envelope expansion, and demonstration of the F-14A performance. Consequently, Navy participation in the AFFTC/ARPS program was terminated in October 1971, to provide an input to the GAC performance testing program. Participation in the GAC performance testing program continued through June 1972. The purpose of Navy participation in the GAC program was to monitor the development of accelerometer test methods and further expand the expertise gained in the Air Force program. Of the several F-14A aircraft tested, all were provided with Systron-Donner accelerometers mounted near the aircraft center of gravity. Dynamic techniques were used throughout Board of Inspection and Survey (BIS) and technical evaluation for the F-14A at Patuxent River, Maryland.

SYMBOLS

1.5 The following symbols are used in Chapter 1.

Symbol	Definition	Common Units	Metric Units
C_D	Drag coefficient	-	(-)
C_L	Lift coefficient	-	(-)
C_{L_V}	Lift slope of the AOA vane	1/radians	(1/radians)
cg	Aircraft center of gravity	percent MAC	(percent MAC)
F_{ex}	Excess thrust	lbs	(N)
g	Acceleration of gravity = 32.2 feet/seconds^2 @ sea level	ft/sec^2	(M/sec^2)
h	Altitude	ft	(M)
I_{Y_V}	Rotational mass inertia of the AOA vane system	lbs-sec^2/ft	(N-sec^2/M)
ℓ	AOA vane pivot length	ft	(M)
MAC	Mean Aerodynamic Chord	ft	(M)
M	Mach number	-	(-)
$N_{x_{FP}}$	Flight path load factor	-	(-)
P_s	Specific excess power	ft/sec	(M/sec)
q	Flight dynamic pressure	lb/ft^2	(N/M^2)
r	Radius of action	ft	(M)
R.F.	Range factor	air n.mi.	(Km)
S.R.	Specific range	air n.mi./lb	(Km/Kg)
Sv	AOA Vane area	ft^2	(M^2)
TSFC	Thrust Specific Fuel Consumption	lb-hr/lb	(N-sec/Kg)
V_t	True airspeed	ft/sec	(M/sec)
W	Aircraft gross weight	lbs	(Kg)
W_f	Fuel flow	lbs/hr	(Kg/sec)

Greek Symbols	Definition	Common Units	Metric Units
α	Angle of attack	deg	(deg)
ω_{n_v}	AOA vane natural frequency	cycles/sec	(cycles/sec)
ζ_v	AOA vane damping ratio	-	(-)
$\Delta\alpha_p$	Induced flow correction	deg	(radians)
$\dot{\theta}$	Pitch rate	deg/sec	(rad/sec)
ξ	Pressure ratio	-	(-)

Other	
$(\dot{})$	First time derivative
$(\ddot{})$	Second time derivative
$(\ )_i$	Indicated value
$(\ )_t$	True value
$(\ )_{PO}$	Power off

PERFORMANCE MEASUREMENTS METHODS

1.6 There are basically three generally accepted methods of obtaining aircraft performance data. These methods are denoted as:

- Airspeed/altitude (energy method)
- Position measurement (radar or camera method)
- Accelerometer (accelerometer or dynamic method).

The most convenient parameter with which to work in standardizing aircraft performance data is excess thrust. The excess thrust at a given flight condition, the flight path load factor, can be obtained by:

$$\frac{F_{ex}}{W} = \frac{\dot{h}}{V_t} + \frac{\ddot{V}_t}{g} = N_{x_{FP}} \qquad (1\text{-}1)$$

A complete derivation of this equation for the wind axis system is given in Chapter 2.

1.7 As related in reference 1-1, the bulk of performance test programs to date have made use of the airspeed/altitude (energy method). Usually, an airspeed indicator, altimeter, and clock are mounted on a photopanel, or these parameters are recorded on magnetic tape to gather performance data. Several schemes for processing the data have been developed. All schemes, however, require curve fit and differentiation to calculate the excess thrust.

1.8 Radar and camera data have been used to compute aircraft performance information in only isolated instances, although both

methods have yielded satisfactory results (reference 1-3). The accuracy in both cases depends primarily on the quality of the tracking data, which in turn depends on such factors as number of recording stations, range, elevation angle, etc.

1.9 Both the airspeed/altitude and position measurement methods are "time dependent" in that both methods require differentiation to resolve excess thrust. Any error of measurement in either of the methods is amplified by the differentiation process, and the magnitude of the time interval used for differentiation may have a decided bearing on the results.

1.10 The accelerometer method, or dynamic performance, on the other hand is "time independent" or instantaneous, in that a measurement of acceleration (or load factor) along the flight path is a direct measure of excess thrust. This "time independence" is attractive in that uncertainties incurred by data smoothing and differentiation required by other methods are avoided.

1.11 These methods can best be summarized by table 1-1, which is taken from reference 1-4. The table shows a rating for each method from the standpoint of accuracy, reliability, aircraft equipment required (least being considered best), and data processing effort (least required by engineering personnel considered best).

1.12 In order to obtain a direct measure of excess thrust, the accelerometer must be aligned, either mechanically or mathematically, to the flight path. Additionally, it must be protected from or corrected for environmental conditions. Mechanical alignment of

TABLE 1-1

A COMPARISON OF PERFORMANCE DATA GATHERING METHODS

Rating	Accuracy	Reliability	Aircraft Equipment Required	Data Processing Effort
1 (best)	Accelerometer	Airspeed/Altitude	Askania Camera	Radar
2	Askania Camera	Accelerometer	Radar	Accelerometer
3	Radar	Radar	Accelerometer	Askania Camera
4 (worst)	Airspeed/Altitude	Askania Camera	Airspeed/Altitude	Airspeed/Altitude

the accelerometer to the flight path can be achieved by mounting the accelerometer in the noseboom in such a way that the accelerometer remains aligned with the angle of attack vanes. Such a system is shown in figure 1-1.

1.13 The alternative method is to mount the accelerometer in a fixed position and mathematically align it with the flight path. This is usually done by mounting the accelerometer somewhere in the body of the aircraft where it can be environmentally controlled to eliminate temperature corrections. Additionally, it is preferred but not necessary that the accelerometer be mounted near the cg of the aircraft to minimize corrections associated with displacement from the cg. Such a system will be referred to as a body accelerometer, and if mounted near the aircraft cg will be referred to as a cg accelerometer. The principles involved in each system are identical, however, the transformation equations are different for the systems. When resolving flight path accelerations, each system will be considered separately. A complete derivation of the required coordinate transformations is given in Chapter 2.

1.14 The accelerometer methods (as will be shown in subsequent chapters) require increased care in analysis over conventional methods. Also, the instrumentation accuracies required are greater in the accelerometer methods. Therefore, the overall goals in any program utilizing the accelerometer methods should be a decreased flight time as compared with conventional methods, and/or a definition

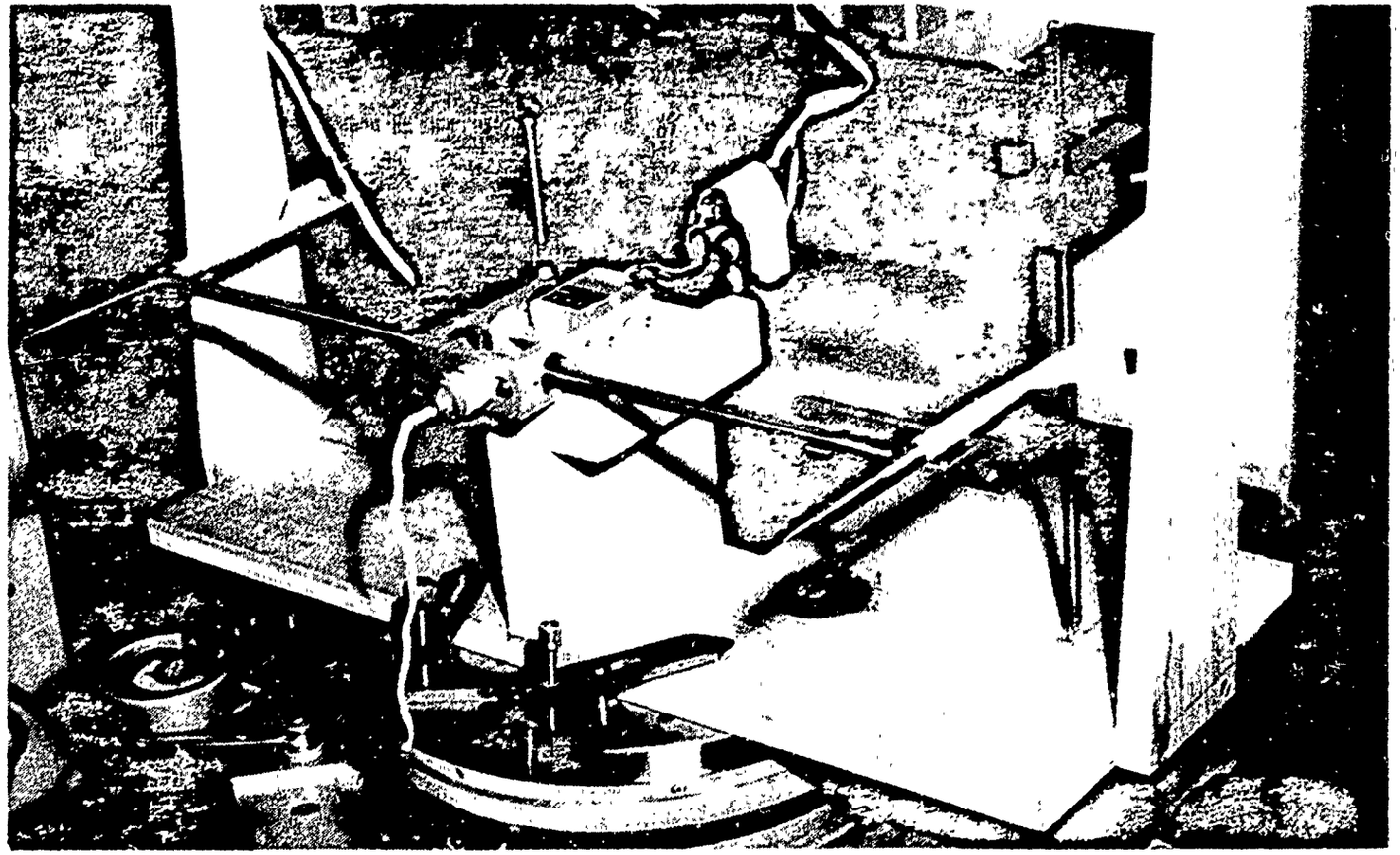

FIG. 1-1: VANE MOUNTED ACCELEROMETER SYSTEM
(This system will be referred to as a flight path accelerometer FPA)

of a mathematical model with increased confidence (as discussed in Chapter 3). If an accurate measurement of excess thrust is assumed, it will be shown that both can be accomplished.

1.15 The basic mathematical model concerning the performance engineer is based on drag, thrust available, and a thrust/fuel flow relation or thrust specific fuel consumption (TSFC) relation. Each mathematical component may be very complicated, but with all three components defined, aircraft performance capabilities can be computed. It is assumed (though not necessarily) that the interdependence of the above three relations is such that several different combinations of components will yield aircraft performance. That is, if drag was calculated incorrectly high, and if the TSFC was correspondingly low, the specific range would be correct. For example, the level flight thrust required is equal to drag and:

$$S.R. = \frac{V_t}{W_f} \quad . \tag{1-2}$$

For a TSFC of one, drag is numerically equal to fuel flow, when drag is incorrectly high, say 10 percent, then there is a corresponding decrease in TSFC to .9090. So that the flight generated TSFC map is entered with 1.1 times the drag thus yielding the correct value of fuel flow. Similarly, with high drag and high thrust available, a correct value of excess thrust can be obtained to yield aircraft acceleration performance or climb performance. Thus, if the thrust were incorrectly measured by normal parametric methods, the actual aircraft performance can be derived as long as the thrust measurement was consistent in the range of measurement.

Using the normal parametric measure of thrust for the calculation of aircraft performance will be referred to as thrust modeling. A more detailed analysis of aircraft mathematical modeling is presented in Chapter 3. The thrust model, in order to obtain accurate drag and fuel flow data, must be accurate. The drag data is needed for comparison with design data, etc. However, operational data can be derived without an "accurate" thrust if the thrust is "repeatable."

1.16 Basic laboratory calibrations of the Systron-Donner accelerometers was undertaken to give insight into the measurement obtained. The Systron-Donner accelerometers consist of a pendulus mass system whose electrical output is directly proportional to acceleration. This is described in greater detail in reference 1-4. The output of the accelerometer was range extended for higher resolution. Calibration was undertaken by the following methods:

- Ultradex Head
- Rate Table Calibration
- Environmental Chamber Testing.

A detailed explanation of each of these procedures is given in Chapter 6.

INFLIGHT CORRECTIONS

1.17 In addition to laboratory calibrations of the accelerometer, flight tests, ground checks, and analytical methods were employed to obtain:

- Noseboom bending
- Angle of attack vane system lag response
- Angular rate effects
- Angle of attack noseboom upwash.

1.18 Boom bending calibrations were accomplished by statically loading the nose boom to represent flight loads. For the A-7D installation, the bending due to inertia loads was .022 degrees/ g . Boom bending due to aerodynamic loads was considered to be part of the aircraft upwash. More details on boom bending are supplied in Chapters 6 and 7, respectively.

1.19 Angle of attack vane system lag response was obtained by determining the rotational inertia of the system in the laboratory (see Chapter 7 for methods and derivations), and applying the dynamic analysis and random input equations. The vane system lag response is a primary function of the vane system natural frequency (ω_n) and damping (ζ_v). These parameters are in turn a function of system geometry (ℓ, S_v, and C_{L_V}) flight conditions (q, V_t), and system rotational inertia (I_{Y_V}). In practice, the correlation was found to be small when dealing with low rate maneuvers.

1.20 Angular rate effects were analytically calculated for corrections to both angle of attack and indicated accelerations. The measurement of angle of attack was directly affected by the radius of action to the vanes (r) and the magnitude of the pitch rate ($\dot{\theta}$), and could consequently be deleted for low pitch rate maneuvers. Corrections to indicated acceleration were a primary function of angular rates and the moment arm between the accelerometer and cg. A complete derivation together with corrective procedures for these effects is given in Chapter 2.

1.21 Noseboom upwash was determined by several flight test methods:

- Attitude gyro method
- Horizon reference method
- Photographic method
- Energy method.

A complete description of the various methods of obtaining aircraft upwash is given in Chapter 7. The energy method was chosen in the final analysis as being the most advantageous. In the energy method, a stabilized point is performed with the accelerometer being resolved through the indicated angle of attack. The average longitudinal acceleration, as computed by airspeed/altitude time histories, is compared to the average longitudinal acceleration measured by the accelerometer. The difference between the two is related to up wash by the appropriate accelerometer transformation equations. Figure 1-2 shows the results of one series of points.

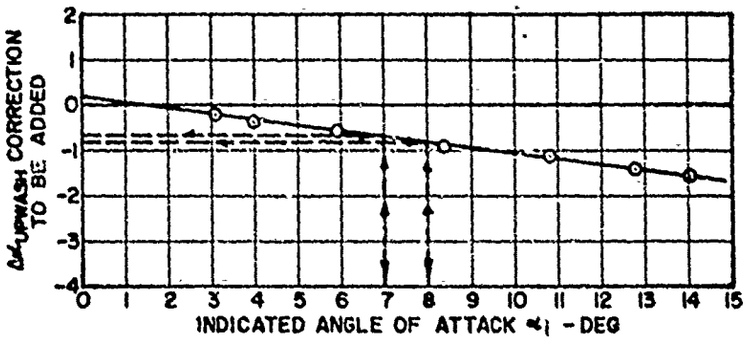

FIG. 1-2: ANGLE OF ATTACK UP WASH

The high quality of the data allows for greater confidence with fewer data points. Additionally, since the stabilized point flight test method is employed, the data can be taken concurrently with airspeed calibration or other stabilized point data.

1.22 Figure 1-2 also serves to point out the relation of body and flight path accelerometers to angle of attack. The body accelerometer readings are transformed through the angle of attack, while the flight path accelerometer readings are transformed through the corrections to angle of attack. As shown in figure 1-2, for the systems thus far tested, the corrections to angle of attack are an order of magnitude smaller than the angle of attack (approximately 10:1), so that the flight path accelerometer is much less sensitive to errors in measured angle of attack. This point is expanded with mathematical examples given in Chapter 7. The body accelerometers, on the other hand, are less sensitive to pitch rates due to their proximity to the cg. This combination of factors is the primary tradeoff to be considered when choosing an accelerometer package where environmental control problems are not a major consideration.

MANEUVERS FOR THE ACCELEROMETER METHODS

QUASI STEADY-STATE MANEUVERS

1.23 The quasi steady-state maneuvers are those maneuvers which are performed at near 1g conditions, but excess thrust is not necessarily zero; such maneuvers would be: climbs, descents, stabilized points, accelerations, decelerations, etc. The major advantages of the quasi steady-state maneuvers are: the low pitch rates involved (small associated corrections); and the simple, known test techniques (less pilot learning time). Additionally, the number of productive maneuvers increases (reduced test time), and a direct comparison to the energy method is available (increased confidence). A direct comparison with energy methods is desirable because on an average, the two methods should agree. Additionally, at each point the two should be on the order of magnitude equivalence thereby giving an independent check on the functioning of instrumentation and validity of data reduction procedures which in turn increases the confidence level of the data. The disadvantages of the quasi steady-state maneuvers are: the lack of maneuvering data (greater or less than nominal 1g); and the increased flight time to obtain the same data when compared with dynamic maneuvers. A complete description of each of the quasi steady-state and dynamic maneuvers is included in Chapters 3 and 8.

1.24 Figure 1-3 shows the advantage of being able to compare energy methods with accelerometer methods. The maneuvers were

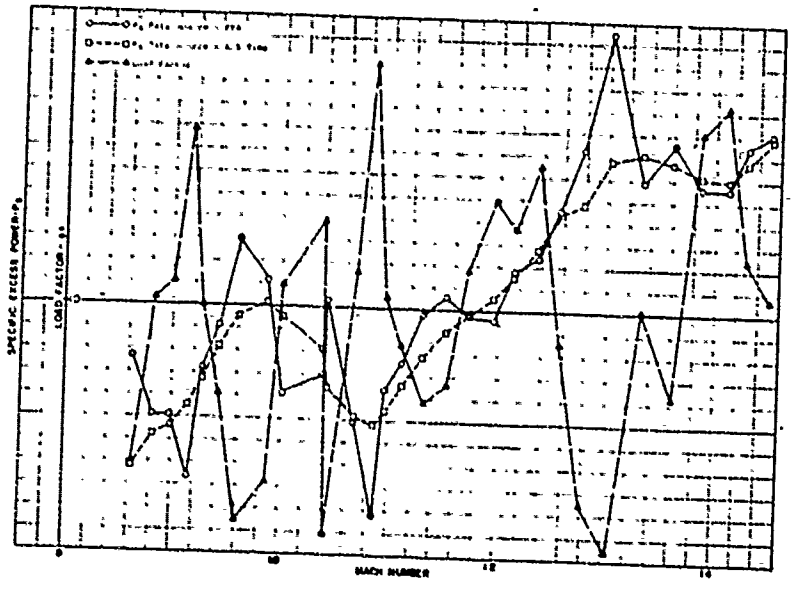

FIG. 1-3: SPECIFIC ENERGY METHOD COMPARISON

flown with the pilot "chasing" altitude, i.e., trying to hold a constant pressure altitude for simplication of the airspeed/ altitude (energy method) data reduction. Consequently, the change in load factor is greater exaggerated over typical acceleration data. The figure serves to show the direct correspondence of specific excess power (P_s), or rate of climb potential at zero change in airspeed, and excess thrust (F_{ex}) with load factor as measured by the accelerometer, while the energy method exhibits a much reduced sensitivity due to the differentiation process.

1.25 Figure 1-4 shows the thrust modeling drag polar obtained from a typical subsonic acceleration and climb. The data scatter is ±3 percent about the subsonic (Mach number .7 and below) drag polar line. It can be expected by conventional technique to obtain a data scatter of ±5 percent, as taken from the equivalent USAF Category II data.

1.26 Figure 1-5 shows the thrust modeling drag polar obtained during typical supersonic accelerations at 30-, 40-, and 50,000 feet with contractor predicted drag polar shapes. A data scatter of ±5 percent is present with most data falling in the 3 percent category. Part of the data scatter here is due to the Mach number range over which the data was sorted. That is, a point on the low side of the 1.3 to 1.4 Mach range could be -5 percent while on the high side of the range at +5 percent. For supersonic data, the dynamic maneuvers yield the better data as discussed in Chapters 3 and 8,

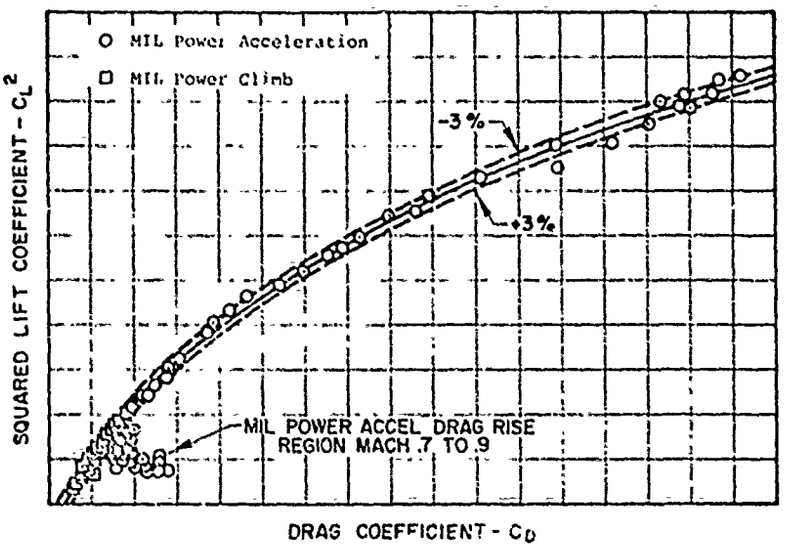

FIG. 1-4: SUBSONIC DRAG POLAR OBTAINED DURING ACCELERATIONS AND CLIMBS

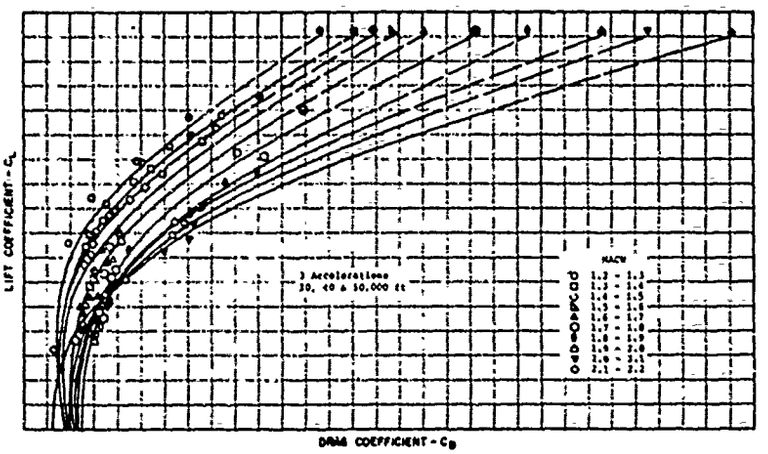

FIG. 1-5: SUPERSONIC DRAG POLAR OBTAINED DURING LEVEL ACCELERATIONS

and in the next section. It can be expected, by conventional techniques that this data will not be readily available.

1.27 Similar data is obtained during decelerations. Decelerations data low power settings may be performed over the same range as acceleration data, and the two may be compared to ascertain power effects. Climb and descent data have the particular advantage of being able to be performed at near constant Mach number, and drag polar data exhibit less scatter as all points can be corrected to a constant Mach number. (These corrections are discussed in Chapter 4.)

DYNAMIC MANEUVERS

1.28 The dynamic maneuvers are those maneuvers which are done at g levels greater than 1.2g or less than 0.8g. Such maneuvers would be roller coasters, wind-up turns, and wind-down turns. A complete description of each of these maneuvers is included in Chapters 3 and 8. The advantage of the dynamic maneuvers are its rapidity (less than 1 minute), its ability to be done at near constant Mach number, and the ability to reach higher and lower lift coefficients or angles of attack than can be reached in the quasi steady-state maneuvers. The disadvantages are: the pilot learning time involved to obtain "good" maneuvers, the inability to avoid sizeable pitch rates, and the inability to compare with energy methods.

1.29 The primary concern in the dynamic maneuver is the smooth transition from one g level to the next. Under high pitch

rate and high pitch acceleration conditions, the corrections to the accelerometer readings (as derived in Chapter 2) can become larger than the measured accelerations. The data scatter is directly proportional to both of these parameters (pitch rate and pitch acceleration). This may be due to the fact that the corrective procedures are inadequate or from other sources, such as flow disturbances due to angular rates, but these effects can be minimized by performing the maneuvers at relatively low pitch rate, and near zero pitch acceleration.

1.30 Figure 1-6 shows the result of a high rate maneuver. The maneuver was performed at 0.1 cycles per second for two cycles, or a total of 20.0 seconds. The data is also compared with the normal Category II (Air Force Stability and Performance Evaluation) data taken on the same aircraft. The dynamic maneuver shows excessive data scatter (±7 percent), but shows a much larger number of useful data points taken in 20 seconds than in three flights of Category II data. While the data in its present form is useless, it tends to show the potential of the dynamic maneuvers. It should be noted that a slightly different fairing would have resulted at the low C_L range if the dynamic data was taken alone. It should also be noted that the high C_L for which data can be obtained has been doubled by the use of the dynamic maneuver.

1.31 Figure 1-7 shows the results of a lower rate maneuver (approximately one cycle in 25 seconds). The data consists also

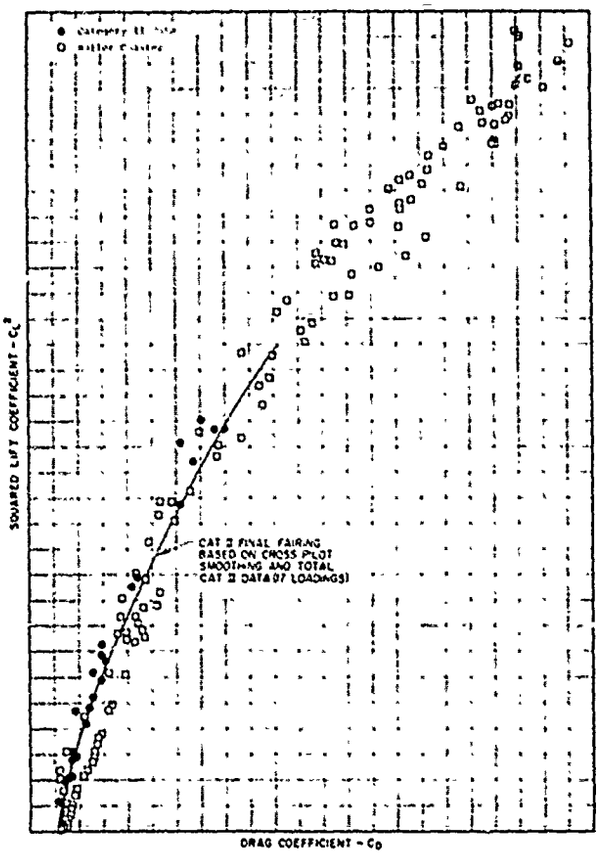

FIG. 1-6: HIGH RATE DYNAMIC MANEUVER

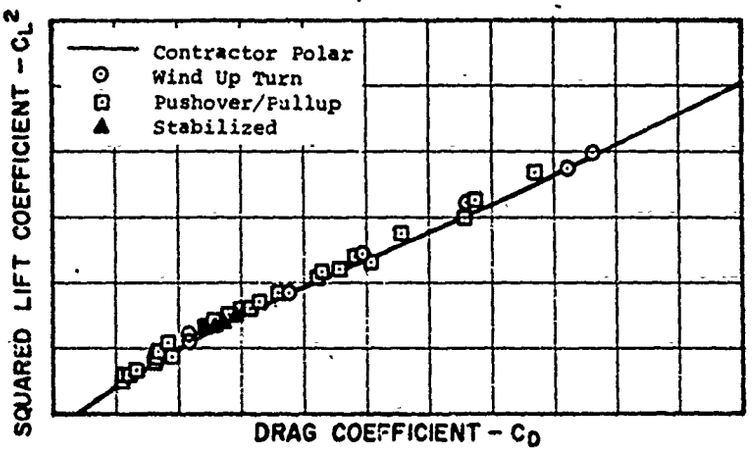

FIG. 1-7: SLOW RATE DYNAMIC MANEUVER

of wind up turn and stabilized point-total test time of less than 3 minutes. Here the data scatter is considerably less (±2 percent) and the data agrees nicely with the contractor predicted line. The dynamic maneuvers combined with accelerometer methods can reduce total flight time while giving data with a high level of confidence.

FUEL FLOW MODELING

1.32 It became apparent rather early in the development of these methods that the obtaining of performance data was no longer limited by the determination of drag or thrust available as with conventional techniques. With a good method of measuring excess thrust, a series of accelerations and climbs will yield both drag and thrust available. The limiting factor appeared to be the generation of a thrust/fuel flow relation which must be done at stabilized engine conditions. The generation of thrust/fuel flow for many military aircraft can be done conventionally. Since many external store loadings are usually flown, the thrust/fuel flow is only a gas generator characteristic and does not, therefore, depend on loading. For a test program with extensive external store loadings, one loading can be flown conventionally for four or more flights, and subsequent data can be flown by accelerometer methods in one or more flights per loading using the generated thrust/fuel flow relationships in the mathematical model.

1.33 Fuel flow modeling offers an alternative for programs that are extremely time constrained or on aircraft that have engines which cannot be used to adequately measure thrust by parametrics (as in the early turbofan families which were operable before the adequate parametrics were developed).

1.34 The first clue to the validity of the fuel flow modeling concept is the interdependency of the performance parameters as

THIS
PAGE
IS
MISSING
IN
ORIGINAL
DOCUMENT

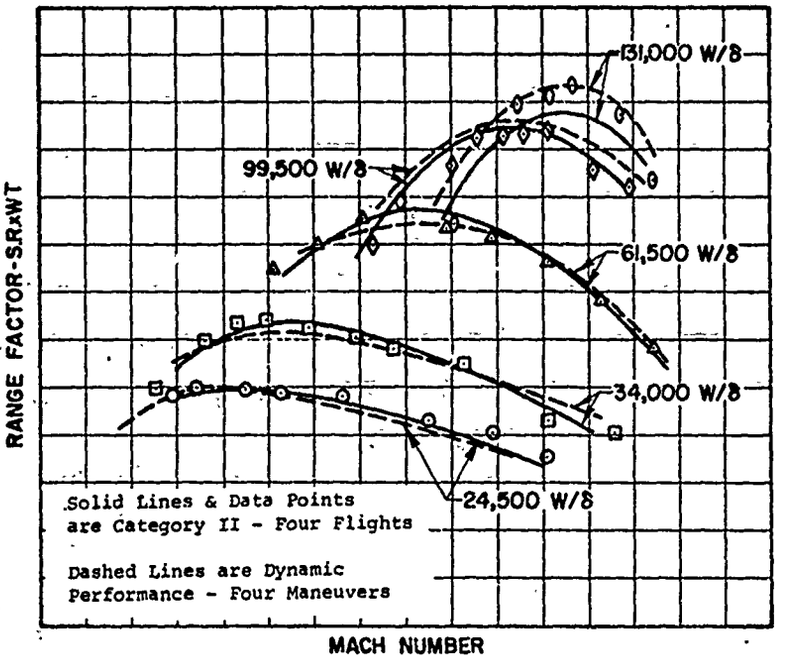

FIG. 1-8: FUEL FLOW MODELING DATA

dashed lines represent accelerometer method/fuel flow model data. The Category II data represents four flights, while the accelerometer method represents four maneuvers: a constant Mach climb; a constant Mach descent; and level accelerations at 20,000 and 5,000 feet. The obvious advantage of the fuel flow modeling technique is the tremendous savings in flight time. The fuel flow model used was the LTV-Allison specification, which was chosen so that no flight data was introduced and no information other than that available to the flight test engineer at the time of an evaluation would be required. Similar results have been obtained using other fuel flow relations (such as Category II test results) and other aircraft (FB-111A). Application of fuel flow modeling techniques are discussed further in Chapter 3.

ADDITIONAL AREAS OF INVESTIGATION

1.37 In addition to the areas already discussed, preliminary investigations have been made into the use of the accelerometer methods, for determining takeoff and landing performance. Here, the accelerometer data are integrated to reproduce data previously obtained by runway or Askania cameras. Figure 1-9 shows one such analysis. Main wheel rpm was used to determine lift-off time, or the time to begin integrating altitude. All accelerometer calculations were made by using onboard instrumentation entirely, which in essence, gives an onboard self-contained takeoff and landing data gathering capability. A further discussion of this and other applications of accelerometer methods is contained in Chapter 9.

1.38 Additional work has begun, but as yet uncompleted, in the area of transonics. Such schemes as integrating the accelerometer data to obtain transonics Mach number and determination of transonic performance data are being investigated. Also, the use of inertial navigation systems is being considered, since accelerations and angular relations are normal outputs. The advantages and disadvantages of this system are as yet undetermined. Finally, optimization of flight programs for the most efficient acquisition both stability and control and performance data are being considered. This final point is discussed further in Chapter 3.

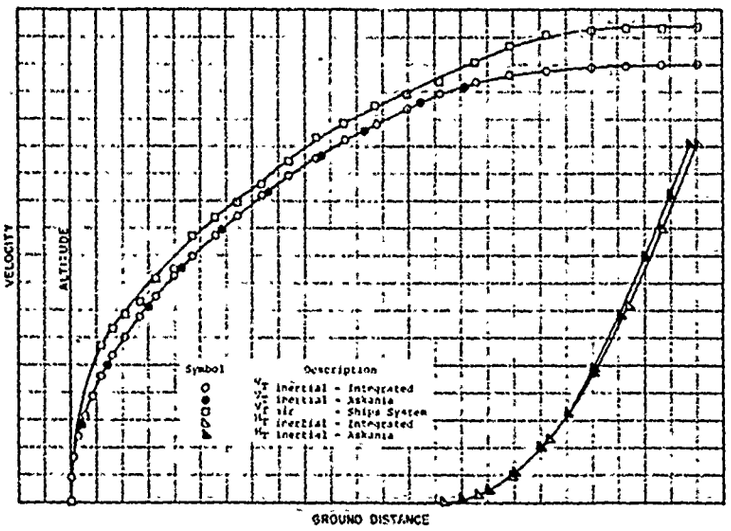

FIG. 1-9: SELF CONTAINED TAKEOFF DATA

CONCLUDING REMARKS TO CHAPTER 1

1.39 This chapter has presented an overview of the concepts and philosophy of the accelerometer methods of obtaining aircraft performance with application and examples from the flight test development programs at EAFB and GAC. A brief discussion has been applied to the aircraft model, calibration procedures, maneuvers, and data techniques. The remainder of the report will amplify these topics.

1.40 It has been shown that use of the accelerometer method of obtaining aircraft performance can result in a tremendous savings of flight time. Conversely, for the same amount or even lesser amounts of flight time than required by conventional techniques, much higher amounts of useful flight data can be had. Finally, accelerometer methods allow for a fuller definition of flight operating characteristics in areas where conventional techniques yield little or no data. Attention will now be turned to the mechanisms by which the accelerometer methods work, the primary equation development for an aircraft in the wind axis system.

REFERENCES TO CHAPTER 1

1-1. Grumman Aerospace Corporation, Report No.ADR-07-01-70.1, "Development of Dynamic Methods of Performance Flight Testing," by P. Pueschel,Unclassified, August 1970.

1-2. USAF, Edwards AFB, FTC-TD-71-1, "Theory of the Measurement and Standardization of Inflight Performance of Aircraft," by E.Dunlap and M. Porter, Unclassified, April 1977.

1-3. Flight Research Division,Air Force Flight Test Center AC-65-7, "A Comparison of Several Techniques for Determining Aircraft Test Day Climb Performance," by R. Walker, Unclassified, June 1965.

1-4. USAF, Edwards AFB, FTC-TR-68-28, "Final Report, Flight Path Accelerometer System," by J. Nevins, Unclassified, Dec 1968.

THE ACCELEROMETER METHODS OF DETERMINING AIRCRAFT PERFORMANCE (DYNAMIC PERFORMANCE TESTING)

CHAPTER 2

THE DEVELOPMENT OF PRIMARY EQUATIONS

SUMMARY OF CHAPTER 2

2.1 Primary equations for the use of onboard accelerometer data (both flight path and body mounted) for determining aircraft performance are developed. Primary equations are those mathematical relationships which relate measured quantities to useful parameters. They are distinguished from secondary and analysis equations in that the latter are used to either standardize or separate effects in the data. Reference materials are cited, or methods are presented for obtaining all parameters necessary in the use of the primary equations, with the exception of angle of attack and accelerometer data which because of their complex nature are treated separately in Chapters 6 and 7, respectively. In cases where sufficient reference materials are not available, the equations are derived. An equation summary is presented for the user who does not wish to go through the development procedures.

INTRODUCTION TO CHAPTER 2

2.2 The relation of measured quantities to some desired information about a system has been a problem facing the experimentalist since the first experiments were performed. The problem arises from the inability to measure directly a desired quantity in all instances. Many measurements by parametrics are taken as a matter of course. For example, engine pressures and temperatures are measured to infer engine thrust output. Other parametric measurements are more subtle, such as the measurements of airspeed and altitude, which are, in reality, parametrically measured by pressures and mechanically converted to the desired parameters in the output instrument.

2.3 With onboard accelerometers, then the question arises: Given the measurement of aircraft acceleration, how does one arrive at aircraft performance parameters? In order to answer this question, the aircraft force balance system must be examined. Additionally, the measurement of acceleration must be examined to determine its relation to the aircraft system. Finally, examination must be made of factors which affect either the aircraft force balance system or the measurement of accelerations. This then, will be the approach followed.

SYMBOLS

2.3 The following symbols are used in Chapter 2.

Symbol	Definition	Common Units	Metric Units
a_1, a_2	Acceleration in the subscripted direction	ft/sec^2	(m/sec^2)
a	Accelerometer	-	-
C_{L_α}	Lift coefficient partial derivative with angle of attack	1/radians	(1/radians)
cg	Center of gravity	% MAC	(% MAC)
D	Drag force	lb	(N)
d	Derivative indicator (differential)	-	-
E_s	Specific energy	ft	(m)
F	Force, thrust, drag, etc., with subscript	lb	(N)
g	Acceleration of gravity	ft/sec^2	(m/sec^2)
h	Altitude	ft	(m)
L	Lift	lb	(N)
ℓ	Length	ft	(m)
M	Mach number	none	none
m	Mass	slug	(kg)
MAC	Length of mean aerodynamic chord	ft	(m)
n	Load factor in subscripted direction	none	none
P_a	Ambient pressure	lb/ft^2	(N/m^2)
q	Dynamic pressure	lb/ft^2	(N/m^2)

Symbol	Definition	Common Units	Metric Units
r	Radius or distance in subscripted direction	ft	(m)
S	Area of wing	ft^2	(m^2)
t	Time	sec	(sec)
V	Velocity (airspeed)	ft/sec	(m/sec)
W	Weight	lb	(N)
W_a	Airflow	slugs/sec	(kg/sec)
Greek Symbol			
α	Angle of attack (aircraft reference above flight path positive)	deg	(deg)
β	Sideslip angle	deg	(deg)
γ	Flight path angle (climb attitude positive)	deg	(deg)
Δ	Change or correction to a parameter	-	-
Δ_{a_m}	Misalignment (with subscripts)	deg	(deg)
ζ	Damping ratio	none	none
θ	Pitch attitude (nose up positive)	deg	(deg)
$\Delta\alpha_{BB}$	Boom bending	deg	(deg)
π	3.14159	none	none
σ	Aircraft heading	deg	(deg)
Σ	Summation	-	-
τ	Thrust inclination angle (longitudinal offset)	deg	(deg)
ρ	Air denisty	$slugs/ft^3$	(kg/m^3)

Greek Symbol	Definition	Common Units	Metric Units
ϕ	Bank angle (right wing down positive)	deg	(deg)
ψ	Yaw angle (airplane nose right positive)	deg	(deg)
ω	Angular rate	deg/sec	(deg/sec)
ω_n	Natural frequency	cycles/sec	(cycles/sec)
ω_d	Damped frequency	cycles/sec	(cycles/sec)
γa	Ratio specific heats for air - 1.40 at standard temperature	-	-

SUBSCRIPTS AND SUPERSCRIPTS:

Symbol	Definition
( ) A/C	Aircraft
( ) B	Body reference
( ) BB	Boom bending
( ) ex	Excess
( ) FPA	Flight Path Accelerometer
( ) g	Gross
( ) i	Indicated
( ) m	Misalignment
( ) n	Net
( ) o	Initial condition
( ) p	Pitch rate
( ) r	Ram
( ) T, t	True quality
( ) u, upwash	Upwash

Symbol	Definition
( ) x	X-axis (flight path)
( ) y	Y-axis (lateral)
( ) z	Z-axis (flight path perpendicular)
( )1, 2, 3, 4	Condition point
$(\dot{})$	First time derivative
$(\ddot{})$	Second time derivative
$\triangleq$	Equal by definition

AIRCRAFT FORCE BALANCE

2.4 The various forces contributing to a change in specific energy (E_s) of an aircraft can be found by analyzing figure 2-1. The E_s is a measure of the total kinetic and potential energy of an aircraft. For ease of calculation, forces will be resolved parallel and perpendicular to the direction of flight (wind axis system). In the general case, the aircraft may be taken to be both climbing and accelerating. The simplified model developed herein assumes wings level flight at zero sideslip for the purpose of clarity. The effects of bank angle and sideslip will be discussed later. Additionally, the gross thrust vector is assumed to lie in the x-z plane. Toe-out effects can be accounted for by simply viewing the gross thrust vector as the in-plane component.

2.5 Resolving forces along the flight path and assuming the mass change to be instantaneously zero:

$$\Sigma F_x = ma_x \tag{2-1}$$

$$F_g\cos(\alpha+\tau) - F_r - D - W\sin\gamma = \frac{W}{g}a_{x_{A/C}} = \frac{W}{g}\frac{dV_t}{dt} \tag{2-2}$$

defining the net thrust (F_n) as:

$$F_n = F_g\cos(\alpha+\tau) - F_r \quad . \tag{2-3}$$

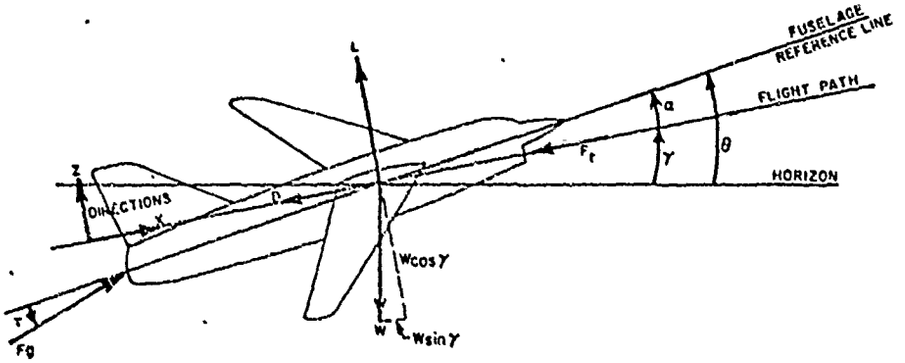

FIG. 2-1: AIRCRAFT FORCE BALANCE DIAGRAM

Equation 2-2 can be rewritten as:

$$F_n - D - W\sin\gamma = \frac{W}{g}\frac{dV_t}{dt} \tag{2-4}$$

or

$$F_{ex} \triangleq F_n - D = W\left(\frac{1}{g}\frac{dV_t}{dt} + \sin\gamma\right) \tag{2-5}$$

2.6 The ram drag (F_r) is assumed to act along the flight path and can be obtained from onboard inlet instrumentation or engine manufacturer's curves of airflow (W_a) and by the equation:

$$F_r = W_a V_t \,. \tag{2-6}$$

2.7 For forces perpendicular to the flight path, the equation becomes:

$$\Sigma F_z = ma_z \tag{2-7}$$

$$L - W\cos\gamma + F_g\sin(\alpha+\tau) = \frac{W}{g}a_{z_{A/C}} \tag{2-8}$$

or

$$L = W\left(\cos\gamma + \frac{a_{z_{A/C}}}{g}\right) - F_g\sin(\alpha+\tau) \,. \tag{2-9}$$

Equations 2-5 and 2-9 become the force balance equations of the aircraft in the two dimensional wind axis system (assuming zero sideslip and wings level).

2.8 Having resolved the force balance equations of the aircraft and defined excess thrust and lift as functions of accelerations, the next step is to select an accelerometer package for measuring

these accelerations. The accelerometer package can be either mounted in the boom and mechanically connected to the angle of attack vanes where it is free to align itself with the flight path of the aircraft, or it can be hard mounted in the body of the aircraft. Each case will be examined separately.

FLIGHT PATH ACCELEROMETER PACKAGE

2.9 The angular relations of the flight path accelerometer can be resolved through the use of figure 2-2. For clarification, angle of attack system misalignment, boom bending, and dynamic errors in angle of attack have been eliminated from the figure. The α_t referred to here is the true angle of attack of the boom reference line, and under 1g conditions, this will be the true angle of attack since the upwash calibration will include the aerodynamic boom bending. In the general case of accelerated flight, the boom bending term ($\Delta\alpha_{BB}$) should be added at this point so that:

$$\alpha_t = \alpha_i + \Delta\alpha_{upwash} + \Delta\alpha_{BB} \qquad (2\text{-}10)$$

where $\Delta\alpha_{BB}$ is a function of normal acceleration at the boom and pitch acceleration ($\dot{\theta}$) and is determined from laboratory calibrations as discussed in reference 2-1 and chapter 6. Further effects of angular rates and their derivatives are given in paragraphs 2.25 to 2.28. The accelerometer is aligned with the angle of attack vane with the exception of a misalignment angle due to mechanical fitting (Δa_m) . The determination of these misalignments which may, in general, be different for the normal and flight path axes is discussed in detail in chapter 6. The accelerometer flight path axis is then misaligned from the flight path by:

$$\Delta\alpha_{total} = \Delta\alpha_{upwash} + \Delta a_m + \Delta\alpha_{BB} \quad . \qquad (2\text{-}11)$$

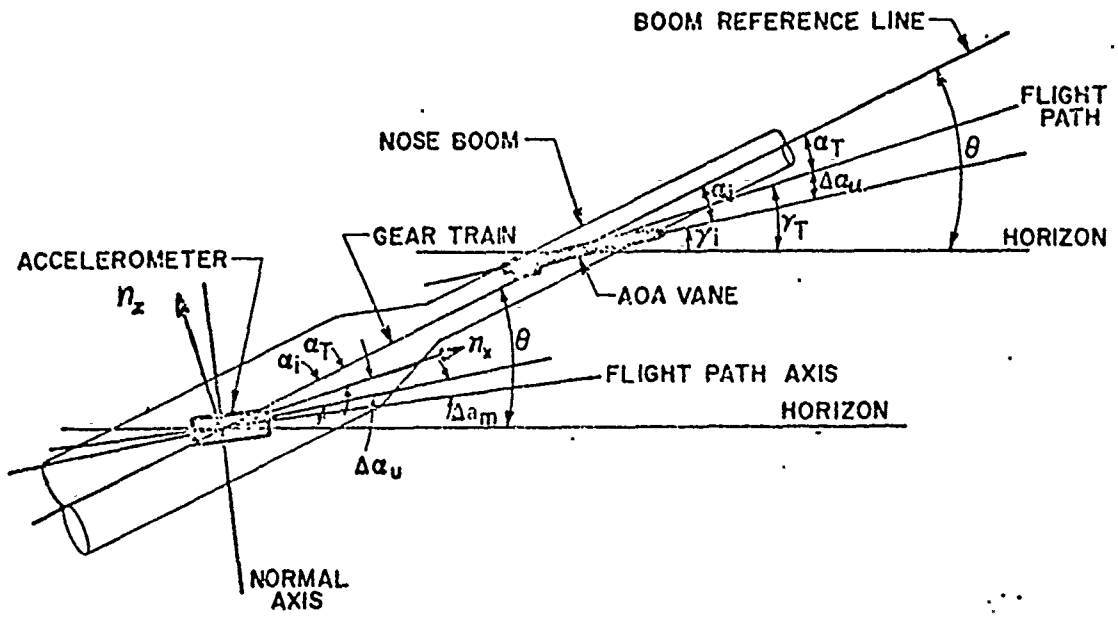

FIG. 2-2: FLIGHT PATH ACCELEROMETER BALANCE DIAGRAM

2.10 Resolving the readings of the accelerometer to the proper axes (along and perpendicular to the flight path):

$$a_{x_{FPA}} = a_{x_{i_{FPA}}} \cos\left(\Delta\alpha_u + \Delta a_{m_{x_{FPA}}} + \Delta\alpha_{BB}\right) - a_{z_{i_{FPA}}} \sin\left(\Delta\alpha_u + \Delta a_{m_{z_{FPA}}} + \Delta\alpha_{BB}\right) \quad (2\text{-}12)$$

$$a_{z_{FPA}} = a_{x_{i_{FPA}}} \sin\left(\Delta\alpha_u + \Delta a_{m_{x_{FPA}}} + \Delta\alpha_{BB}\right) + a_{z_{i_{FPA}}} \cos\left(\Delta\alpha_u + \Delta a_{m_{z_{FPA}}} + \Delta\alpha_{BB}\right) \quad (2\text{-}13)$$

It is often more convenient to work with the accelerations in g units or measurements of load factors, and the accelerometers will be calibrated in terms of load factor such that the above equations become:

$$n_{x_{FPA}} = n_{x_{i_{FPA}}} \cos\left(\Delta\alpha_u + \Delta a_{m_{x_{FPA}}} + \Delta\alpha_{BB}\right) - n_{z_{i_{FPA}}} \sin\left(\Delta\alpha_u + \Delta a_{m_{z_{FPA}}} + \Delta\alpha_{BB}\right) \quad (2\text{-}14)$$

$$n_{z_{FPA}} = n_{x_{i_{FPA}}} \sin\left(\Delta\alpha_u + \Delta a_{m_{x_{FPA}}} + \Delta\alpha_{BB}\right) + n_{z_{i_{FPA}}} \cos\left(\Delta\alpha_u + \Delta a_{m_{z_{FPA}}} + \Delta\alpha_{BB}\right) . \quad (2\text{-}15)$$

Equations 2-14 and 2-15 represent the accelerometer readings corrected to the wind axis system. The meaning of these values as they relate to the accelerometer force balance can be constructed by analyzing figure 2-3.

2.11 Resolving the accelerations along the perpendicular to the flight path, the following equations are obtained:

$$a_{x_{FPA}} = a_{x_{A/C}} + g \sin\gamma \quad (2\text{-}16)$$

$$a_{z_{FPA}} = a_{z_{A/C}} + g \cos\gamma . \quad (2\text{-}17)$$

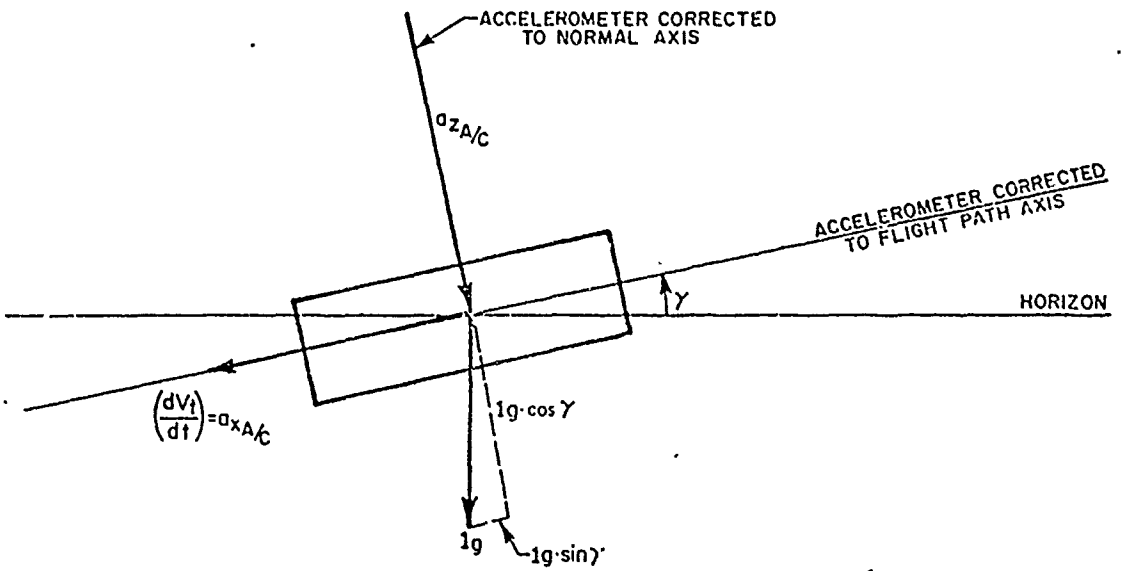

FIG. 2-3: TRANSFORMED AXIS ACCELEROMETER BALANCE DIAGRAM

Or again transforming the equations to load factor for convenience, the equations become:

$$n_{x_{FPA}} = \frac{a_{x_{A/C}}}{g} + \sin \gamma \qquad (2\text{-}18)$$

$$n_{z_{FPA}} = \frac{a_{z_{A/C}}}{g} + \cos \gamma. \qquad (2\text{-}19)$$

By definition, the acceleration along the flight path of an aircraft ($a_{x_{A/C}}$) is the time rate of change of the true velocity along the flight path $\frac{dV_t}{dt}$ which yields:

$$n_{x_{FPA}} = \frac{1}{g} \frac{dV_t}{dt} + \sin \gamma. \qquad (2\text{-}20)$$

Combining equations 2-5 and 2-20:

$$F_{ex} \triangleq F_n - D = W(n_{x_{FPA}}) \quad . \qquad (2\text{-}21)$$

Equation 2-21 is the singularly most important relation to the accelerometer method. It relates the wind axis longitudinal load factor with aircraft gross weight directly to excess thrust.

Combining equations 2-9 and 2-19:

$$L = W(n_{z_{FPA}}) - F_g \sin(\alpha+\tau) \quad . \qquad (2\text{-}22)$$

Equation 2-22 relates the wind axis normal load factor to aerodynamic lift.

2.12 In order to more fully develop the resolved accelerations as they fit into the picture of overall aircraft performance, the determination of longitudinal load factor can be further expanded with the aid of the velocity diagram of figure 2-4. From the breakdown of the aircraft velocity components:

$$\sin \gamma = \frac{dh}{dt} \frac{1}{V_t} \tag{2-23}$$

combining equation 2-23 with equation 2-20:

$$n_{x_{FPA}} = \frac{1}{g} \frac{dV_t}{dt} + \frac{dh}{dt} \frac{1}{V_t} \quad . \tag{2-24}$$

The specific energy (E_s) of an aircraft is given by:

$$E_s = h + \frac{V_t^2}{2g} \tag{2-25}$$

and the time rate of change of specific energy is given by:

$$P_s = \dot{E}_s = \frac{dh}{dt} + \frac{V_t}{g} \frac{dV_t}{dt} = (n_{x_{FPA}})V_t \quad , \tag{2-26}$$

where equation 2-26 relates the time rate of change of specific energy and the longitudinal load factor at each velocity point.

2.13 It has been shown then, that the resolved components of longitudinal and normal load factor will yield information about the aircraft excess thrust and aerodynamic lift. Additionally, it has been shown that the longitudinal load factor together with velocity gives information with regard to the time rate of change of aircraft specific energy.

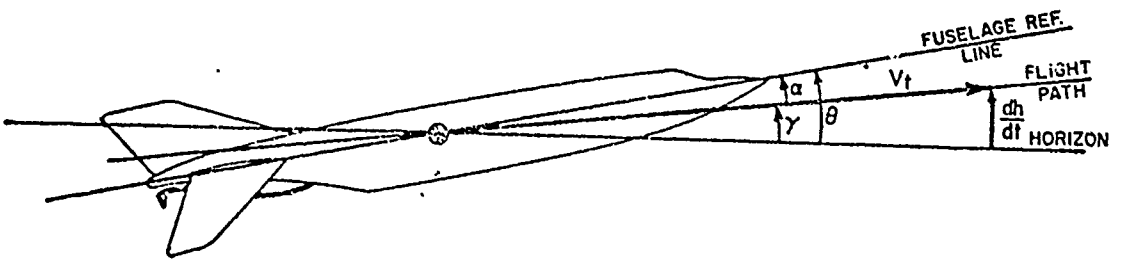

FIG. 2-4: AIRCRAFT VELOCITY DIAGRAM

BODY MOUNTED ACCELEROMETER PACKAGE

2.14 The data analysis procedures for the body mounted package becomes more complex when it is considered that the body mounted accelerometer is not aligned with the flight path but stays near the fuselage reference line. Thus, angle of attack, as well as corrections to angle of attack, enter into the overall calculations. Therefore, errors in measured angle of attack will be introduced which were not present with the flight path accelerometer. The forces acting on the body accelerometer can be resolved by analyzing figure 2-5.

2.15 The angle of attack vane is misplaced by the upwash at the boom and any boom bending due to rate effects (further effects of angular rate are discussed in paragraphs 2.25 to 2.30), so that the true angle of attack is given by:

$$\alpha_t = \alpha_i + \Delta\alpha_{upwash} + \Delta\alpha_{BB} \quad . \tag{2-27}$$

The body accelerometer is further misplaced by a mechanical misalignment (Δa_m). Resolving accelerations parallel and perpendicular to the flight path (as with the flight path accelerometer), the following equations are obtained:

$$n_{x_B} = n_{x_{i_B}} \cos\left(\alpha_t + \Delta a_{m_{x_B}}\right) - n_{z_{i_B}} \sin\left(\alpha_t + \Delta a_{m_{z_B}}\right) \tag{2-28}$$

and

$$n_{z_b} = n_{x_{i_B}} \sin\left(\alpha_t + \Delta a_{m_{x_B}}\right) + n_{z_{i_B}} \cos\left(\alpha_t + \Delta a_{m_{z_B}}\right) \quad , \tag{2-29}$$

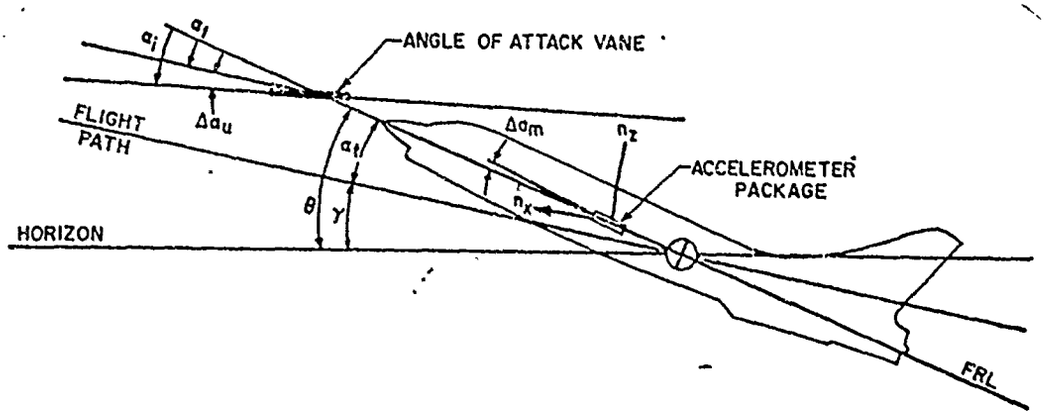

FIG. 2-5: BODY MOUNTED ACCELEROMETER BALANCE DIAGRAM

and, with the use of figure 2-5, it can be seen that:

$$n_{x_B} = \frac{a_{x_{A/C}}}{g} + \sin \gamma \qquad (2\text{-}30)$$

$$n_{z_B} = \frac{a_{z_{A/C}}}{g} + \cos \gamma \ . \qquad (2\text{-}31)$$

2.16 With the accelerometer readings referred to the wind axis system, figures 2-3 and 2-4 apply as well as the analysis of paragraphs 2.11, 2.12, and 2.13, so that equations 2-21, 2-22, and 2-26 apply as summarized below:

$$F_{ex} \triangleq F_n - D = W \cdot n_{x_B} \qquad (2\text{-}32)$$

$$L = W(n_{z_B}) - F_g \sin(\alpha+\tau) \qquad (2\text{-}33)$$

$$\dot{E}_s = (n_{x_B})V_t \ . \qquad (2\text{-}34)$$

BANK ANGLE EFFECTS

AIRCRAFT FORCE BALANCE

2.17 In the general case, the aircraft will not maintain a wings level altitude so that it becomes necessary to evaluate the effect of bank angle on the equation set. Since the wind axis system is used, introducing bank angle into figure 2-1 induces a side force component in the weight vector equal in magnitude to $W \sin \phi$ and the z direction component of weight becomes $W \cos \gamma \cos \phi$. All other vectors remain the same since the axis system (for wind axis analysis) has rolled with the aircraft. Thus, equation 2-9 becomes:

$$L = W\left(\cos \gamma \cos \phi + \frac{a_{z_{A/C}}}{g}\right) - F_g \sin(\alpha+\tau) \qquad (2\text{-}35)$$

FLIGHT PATH ACCELEROMETER

2.18 In the flight path accelerometer, the transformation equations under non-zero bank angle are unaffected since the accelerometer remains aligned with the wind axis system. The transformed accelerations of figure 2-3, however, show the effect of the 1 g vector being rotated out of plane so that equation 2-19 becomes:

$$n_{z_{FPA}} = \frac{a_{z_{A/C}}}{g} + \cos \gamma \cos \phi \qquad (2\text{-}36)$$

when equation 2-36 is combined with equation 2-35, equation 2-22 is the result, or:

$$L = W(n_{z_{FPA}}) - F_g \sin(\alpha+\tau) \quad . \qquad (2\text{-}22)$$

In the wind axis system then, non-zero bank angle does not affect the equation set when the flight path accelerometer is used.

BODY ACCELEROMETER PACKAGE

2.2.2 In the body accelerometer, the problem is further complicated in that the accelerometer is not aligned with the flight path and must be transformed through the angle of attack. Resolving the accelerations along and perpendicular to the flight path, we obtain equation 2-29:

$$n_{z_B} = n_{x_{i_B}} \sin\left(\alpha_t + \Delta a_{m_{x_B}}\right) + n_{z_{i_B}} \cos\left(\alpha_t + \Delta a_{m_{z_B}}\right) \qquad (2\text{-}29)$$

$$n_{z_B} = \frac{a_{z_{A/C}}}{g} + \cos\gamma \cos\phi \,, \qquad (2\text{-}37)$$

which again can be combined with equation 2-35 to yield:

$$L = W\left(n_{z_B}\right) - F_g \sin(\alpha_t + \tau) \quad . \qquad (2\text{-}38)$$

It can be seen that the equation sets are unaltered by the addition of bank angle.

SIDESLIP EFFECTS

2.20 In the general case, small values of sideslip will cause a misalignment of the acceleration vectors in the lateral plane. As explained in reference 2-1 and Chapter 6, lateral misalignments (which are the equivalent of sideslip) create negligible errors if they are less than 3 degrees. If this assumption is too restrictive, the case of non-zerosideslip must be considered. Additionally, a three-axis accelerometer must be considered in that correcting the equations without lateral accelerations may be more in error than completely ignoring the correction. In the case of sideslip, the normal axis accelerations are not affected since they are perpendicular to the plane of action of sideslip. The corrective procedures for the flight path axis can be shown with figure 2-6.

2.21 The n_x term is rotated out of plane by β, and a component of $n_y \sin \beta$ is introduced such that:

$$n_{x_{FP}} = n_x \cos \beta + n_y \sin \beta \, . \qquad (2\text{-}39)$$

The two terms tend to have a cancelling effect as shown in the diagram, but this is not always the case.

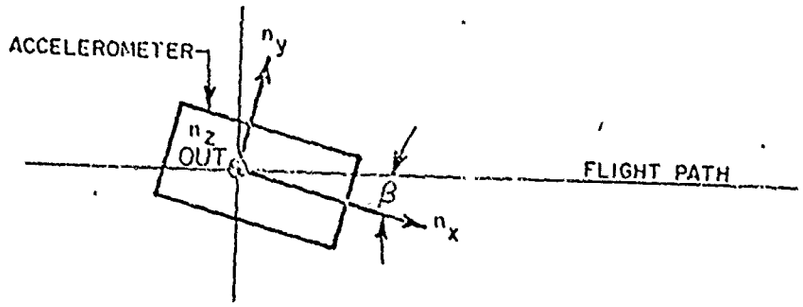

FIG. 2-6: ACCELEROMETER SIDESLIP DIAGRAM

FULLY DEVELOPED COORDINATE TRANSFORMATIONS

2.22 The fully developed equations for a three-axis system with bank angle and sideslip and no simplifying assumptions about misalignments are given below. Additionally, no angular rate or angular acceleration corrections are made. These will be dealt with in the next section. Finally, no cross-axis sensitivity has been introduced since it is basically a calibration problem and is dealt with in Chapter 6.

FLIGHT PATH ACCELEROMETER

2.23 The coordinate transformations for the flight path accelerometers are:

$$n_{x_{FPA}} = n_{x_i}\cos\left(\Delta\alpha_u+\Delta a_{m_{x_{FPA}}}\right)\cos\beta-n_{z_i}\sin\left(\Delta\alpha_u+\Delta a_{m_{z_{FPA}}}\right)\cos\beta+n_{y_i}\sin\beta \qquad (2\text{-}40)$$

$$n_{z_{FPA}} = n_{x_i}\sin\left(\Delta\alpha_u+\Delta a_{m_{x_{FPA}}}\right)+n_{z_i}\cos\left(\Delta\alpha_u+\Delta a_{m_{z_{FPA}}}\right) . \qquad (2\text{-}41)$$

For additional detail discussion, consult reference 2-2.

BODY ACCELEROMETER

2.24 The coordinate transformations for the body mounted accelerometer package are:

$$n_{x_B} = n_{x_i}\cos\left(\alpha_t+\Delta a_{m_{x_B}}\right)\cos\beta+n_{y_{i_B}}\sin\beta-n_{z_{i_B}}\sin\left(\alpha_t+\Delta a_{m_{z_B}}\right)\cos\beta , \qquad (2\text{-}42)$$

and

$$n_{z_B} = n_{x_{i_B}} \sin\left(\alpha_t + \Delta a_{m_{x_B}}\right) + n_{z_{i_B}} \cos\left(\alpha_t + \Delta a_{m_{z_B}}\right) \quad . \tag{2-43}$$

For additional detail discussion, consult reference 2-3.

ANGULAR RATE EFFECTS

2.25 The angular rate effect on an accelerometer located some distance from the cg induces accelerations which are reflected in the accelerometer readings. As illustrated in figure 2-7, the rotational rate (ω) creates an acceleration in the two axes of the plane of rotation. The centripetal acceleration (a_1) is created by the rotation as:

$$a_1 = r\omega^2 \quad . \tag{2-44}$$

The rotational acceleration (a_2) is created by the rate of change of rotation rate as:

$$a_2 = r\dot{\omega} \quad . \tag{2-45}$$

2.26 In the general case of rotation about all three axes, the cross product produces an acceleration perpendicular to the plane of rotation of a given pair of rotational vectors. In general, the accelerations as measured by the accelerometer can be corrected for angular rates and then corrected back to the cg. Alternately, the acceleration readings can be corrected to the cg and then the cg accelerations corrected for angular rates. For the body accelerometers, the latter method is easier and yields:

$$n_{x_{net}} = n_{x_i} + \frac{1}{g}\left[r_x(\dot{\theta}^2+\dot{\psi}^2)+r_y(\ddot{\psi}-\dot{\phi}\dot{\theta})+r_z(\ddot{\theta}+\dot{\phi}\dot{\psi})\right] \quad , \tag{2-46}$$

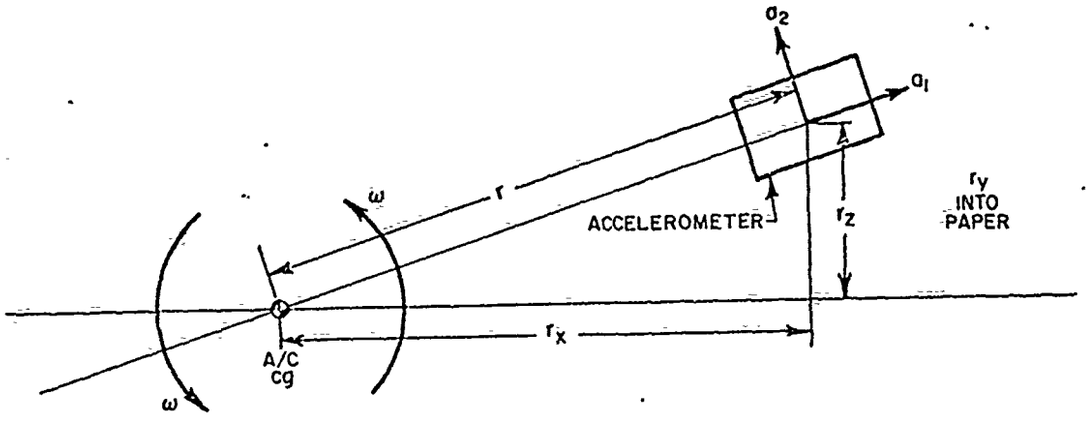

FIG. 2-7. ROTATIONAL DYNAMICS

and

$$n_{z_{net}} = n_{z_i} + \frac{1}{g}\left[-r_x(\ddot{\theta}-\dot{\phi}\dot{\psi})+r_y(\ddot{\phi}+\dot{\psi}\dot{\theta}) +r_z(\dot{\theta}^2+\dot{\phi}^2)\right] . \quad (2\text{-}47)$$

This method is employed in reference 2-2, which also includes corrective procedures for the lateral axis, i.e.;

$$n_{y_{net}} = n_{y_i} + \frac{1}{g}\left[-r_x(\ddot{\psi}-\dot{\phi}\dot{\theta})+r_y(\dot{\phi}^2+\dot{\psi}^2) - r_z(\ddot{\phi}-\dot{\psi}\dot{\theta})\right] . \quad (2\text{-}48)$$

The corrected accelerations are computed by replacing $n_{x_{net}}$, $n_{z_{net}}$, and $n_{y_{net}}$ for n_{x_i}, n_{z_i}, and n_{y_i}, respectively, in the coordinate transformations. The corrected normal acceleration can then be used to compute boom normal acceleration to determine boom bending by:

$$n_{z_{BB}} = n_{z_B} + \frac{1}{g}\left[X\alpha(\ddot{\theta}+\dot{\phi}\dot{\psi}) - Y\alpha(\ddot{\phi}+\dot{\psi}\dot{\theta}) - Z\alpha(\dot{\theta}^2+\dot{\phi}^2)\right] . \quad (2\text{-}49)$$

Further effects of boom bending are discussed in reference 2-1 or Chapter 6.

2.27 For the flight path accelerometer, it becomes more convenient to correct the accelerations for angular rates at the accelerometer and then correct back to the cg. So that:

$$n_{z_{BB}} = n_{z_{FPA}} , \quad (2\text{-}50)$$

and

$$n_{x_{FPA_{CG}}} = n_{z_{FPA}} + \frac{r}{g}\left[(\dot{\theta}^2+\dot{\psi}^2)\cos\alpha-(\ddot{\phi}\ddot{\psi}-\ddot{\theta})\sin\alpha\right] \qquad (2\text{-}51)$$

$$n_{z_{FPA_{CG}}} = n_{z_{FPA}} + \frac{r}{g}\left[(\dot{\theta}^2+\dot{\psi}^2)\sin\alpha+(\ddot{\psi}\ddot{\phi}-\ddot{\theta})\cos\alpha\right], \qquad (2\text{-}52)$$

where r is the distance from accelerometer to cg along a radial. This analysis technique together with a complete derivation of the above relation is presented in reference 2-2.

2.28 In summary, when dealing with body accelerometers, it is more convenient to correct the accelerometer readings to the cg prior to coordinate transformation. Thus, equations 2-46, 2-47, and 2-48 are employed prior to coordinate transformation, and equation 2-49 is used for boom bending calculations. When dealing with flight path accelerometers, it is more convenient to calculate the local acceleration at the accelerometers so that equation 2-50 can be used for boom bending calculations, and equations 2-51 and 2-52 are applied after coordinate transformation. Of course, either accelerometer package can mathematically be treated by either technique.

PRIMARY EQUATION SUMMARY

FLIGHT PATH ACCELEROMETER

2.29 The final accelerations along and perpendicular to the flight path are computed as:

$$n_{x_{FPA_{CG}}} = n_{x_i}\cos\left(\Delta\alpha+\Delta a_{m_{x_{FPA}}}\right)\cos\beta - n_{z_i}\sin\left(\Delta\alpha+\Delta a_{m_{z_{FPA}}}\right)\cos\beta + n_{y_i}\sin\beta + \frac{r}{g}\left[(\dot\theta^2+\dot\psi^2)\cos\alpha_t - (\ddot\phi\psi-\ddot\theta)\sin\alpha_t\right] \quad (2\text{-}53)$$

and

$$n_{z_{FPA_{CG}}} = n_{x_i}\sin\left(\Delta\alpha+\Delta a_{m_{x_{FPA}}}\right)+n_{z_i}\cos\left(\Delta\alpha+\Delta a_{m_{z_{FPA}}}\right) + \frac{r}{g}\left[(\dot\theta^2+\dot\psi^2)\sin\alpha_t+(\ddot\psi\phi-\ddot\theta)\cos\alpha_t\right], \quad (2\text{-}54)$$

where $\Delta\alpha = \sum_{i=1}^{n}\Delta\alpha_i$ or $\Delta\alpha$ is the total of all corrections to angle of attack as detailed in reference 2-4 and Chapter 7.

BODY MOUNTED ACCELEROMETER

2.30 The final accelerations along and perpendicular to the flight path are computed as:

$$n_{x_{B_{CG}}} = n_{x_{net}}\cos\left(\alpha_t+\epsilon_{x_B}\right)\cos\beta - n_{z_{net}}\sin\left(\alpha_t+\epsilon_{z_B}\right)\cos\beta+n_{y_{net}}\sin\beta \quad (2\text{-}55$$

and

$$n_{z_{B_{CG}}} = n_{x_{net}}\sin\left(\alpha_t+\epsilon_{x_B}\right)+n_{z_{net}}\cos\left(\alpha_t+\epsilon_{z_B}\right), \quad (2\text{-}56.$$

where

$$n_{x_{net}} = n_{x_{i_B}} + \frac{1}{g}\left[r_x(\dot{\theta}^2+\dot{\psi}^2)+r_y(\ddot{\psi}-\dot{\phi}\dot{\theta})+r_z(\ddot{\theta}+\dot{\phi}\dot{\psi})\right] \quad (2\text{-}57)$$

$$n_{z_{net}} = n_{z_{i_B}} + \frac{1}{g}\left[-r_x(\ddot{\theta}-\dot{\phi}\dot{\psi})+r_y(\ddot{\phi}+\dot{\psi}\dot{\theta})+r_z(\dot{\theta}^2+\dot{\phi}^2)\right] \quad (2\text{-}58)$$

and

$$n_{y_{net}} = n_{y_{i_B}} + \frac{1}{g}\left[-r_x(\ddot{\psi}+\dot{\phi}\dot{\theta})+r_y(\phi^2+\psi^2)-r_z(\ddot{\phi}-\dot{\psi}\dot{\theta})\right] . \quad (2\text{-}59)$$

AIRCRAFT FORCE BALANCE

2.31 With the measured quantities corrected and resolved to the proper axes, the primary equations for the determination of aircraft excess thrust, lift, and time rate of change of specific energy are as follows:

$$F_{ex} \triangleq F_n - D = W \cdot n_x \quad (2\text{-}60)$$

$$L = W \cdot n_z - F_g \sin(\alpha_t + \tau) \quad (2\text{-}61)$$

$$\dot{E}_s = n_x V_t \ , \quad (2\text{-}62)$$

where

$$n_x = n_{z_{B_{CG}}} \quad \text{or} \quad = n_{x_{FPA_{CG}}} \quad (2\text{-}63)$$

and

$$n_z = n_{z_{B_{CG}}} \quad \text{or} \quad = n_{z_{FPA_{CG}}} . \quad (2\text{-}64)$$

The latter equations depend only on the accelerometer package in use.

2.32 The aircraft force balance equations can now be expanded to yield the normal aircraft performance parameters as follows:

Equation 2-60 becomes:

$$C_D = \frac{F_n - W \cdot n_x}{q\,s} = \frac{F_n - W \cdot n_x}{\frac{1}{2}\rho\, V_t^2\, S} = \frac{F_n - W \cdot n_x}{\frac{\gamma a}{2}\, P_a M^2 S} \quad (2\text{-}65)$$

Equation 2-61 becomes:

$$C_L = \frac{W \cdot n_z - F_g \sin(\alpha_t + \tau)}{\frac{1}{2}\rho V_t^2 S} = \frac{W \cdot n_z - F_g \sin(\alpha_t + \tau)}{\frac{\gamma a}{2} P_a M^2 S} \quad (2\text{-}66)$$

2.33 Equations 2-60 through 2-62 are convenient when applying flight test data to the direct methods of determining aircraft performance, while equations 2-65 and 2-66 are more convenient when applying flight test data to the indirect methods of determining aircraft performance.

CONCLUDING REMARKS TO CHAPTER 2

2.34 The aircraft accelerations yield very useful data for defining aircraft performance. Extreme care, however, must be exercised when using measured accelerations to insure proper values of resolved accelerations. These resolved acceleration values are directly adaptable to either the direct or indirect methods of determining aircraft performance.

REFERENCES TO CHAPTER 2

2-1. Naval Air Test Center, Flight Test Technical Memorandum 5-73, "Developing the Airplane Drag Polar and Lift Slope Curve From Flight Test Data Using Onboard Accelerometers," by W.R. Simpson, Unclassified, 15 May 1973.

2-2. Edwards Air Force Base, USAF Document No. F7C-TD-71-1, "Theory of the Measurement and Standardization of In-Flight Performance of Aircraft," by E.W. Dunlap and M.B. Porter, Unclassified, April 1971.

2-3. Grumman Aerospace Corporation, Report No. ADR-07-01-70.1, "Development of Dynamic Methods of Performance Flight Testing," by P. Pueschel, Unclassified, August 1970.

2-4. Naval Air Test Center, Flight Test Technical Memorandum 2-75, "The Determination of Aircraft Angle of Attack," by W.R. Simpson, Unclassified, 27 March 1975.

2-5. USAF Aerospace Research Pilot School, USAF Document No. FTC-TIH-70-1001, "Performance," Unclassified, May 1970.

2-6. Naval Air Test Center, Technical Memorandum 76-3, "The Development of Primary Equations for Use of Onboard Accelerometers in Determining Aircraft Performance," by W.R. Simpson, Unclassified, 19 April 1977.

THE ACCELEROMETER METHODS OF DETERMINING AIRCRAFT PERFORMANCE (DYNAMIC PERFORMANCE TESTING)

CHAPTER 3

MATHEMATICAL MODELING CONCEPTS

SUMMARY OF CHAPTER 3

3.1 Basic math modeling concepts are presented for use with the accelerometer methods of obtaining aircraft performance. Components of the math model are discussed with reference to thrust modeling and fuel flow modeling. Each maneuver is discussed as it fits into the overall picture of accelerometer methods and mathematical modeling. The concept of the optimum flight profile, its application, and an example are presented. Basic considerations in program planning are also discussed.

INTRODUCTION TO CHAPTER 3

3.2 It has been shown in Chapter 2 that the measurement of onboard aircraft acceleration can be used to deduce aerodynamic lift and excess thrust. These relations are given by:

$$F_{ex} \triangleq F_n - D = Wn_x \tag{2-21}$$

$$L = Wn_z - F_g \sin(\alpha_t + \tau) \tag{2-22}$$

or, rearranging equation (2-21):

$$D = F_n - Wn_x \quad . \tag{3-1}$$

It becomes convenient when dealing with aerodynamic forces to deal with the force coefficients such that:

$$C_L = \frac{L}{qS} = \frac{Wn_z - F_g \sin(\alpha_t + \tau)}{qS} \tag{3-2}$$

and

$$C_D = \frac{D}{qS} = \frac{F_n - Wn_x}{qS} \quad . \tag{3-3}$$

These coefficients are non-dimensional and are related to one another as discussed in the chapter. The primary goal of mathematical modeling will be to define the aircraft performance mathematically. In order to do this, the engine output requirements must be known (both thrust and fuel flow), and the engine thrust available must

be known. The difference between the engine thrust output available and the engine thrust output required will give a measure of the rate of change of airspeed or altitude, and the fuel flow will give the rate of change of aircraft weight and fuel consumption. The engine output required to maintain level, non-accelerating flight can be obtained by setting excess thrust equal to zero in equation (2-21):

$$F_N = D \quad . \tag{3-4}$$

It becomes important, then, to know the aircraft thrust available, drag, and fuel flow at each point.

SYMBOLS

3.3 The following symbols are used in Chapter 3:

Symbol	Definition	Common Units	Metric Units
A_{CA}	Accelerometer cross-axes sensitivity	g/g	(g/g)
C_D	Drag coefficient	-	(-)
C_L	Lift coefficient	-	(-)
$C_{L_{eff}}$	Effective lift coefficient	-	(-)
$C_{L_{PON}}$	Power-on lift coefficient	-	(-)
$C_{L_{POFF}}$	Power-off lift coefficient	-	(-)
$C_{L_{T_{POFF}}}$	Power-off trimmed lift coefficient	-	(-)
C_{F_G}	Gross thrust coefficient	-	(-)
$\Delta C_{L_{TRIM}}$	Incremental tail lift coefficient required to trim	-	(-)
C_M	Coefficient of moment	-	(-)
$\bar{c}$	Mean geometric chord of wing	inch	(CM)
D_{INT}	Interference drag	lb	(N)
D_{RAM}	Ram drag (sometimes F_R)	lb	(N)
D_{SPIL}	Spillage drag	lb	(N)
FRL	Fuselage reference line	-	(-)
F_G	Gross thrust	lb	(N)
F_R	Ram drag (also D_{RAM})	lb	(N)

Symbol	Definition	Common Units	Metric Units
F_{ex}	Excess thrust	lb	(N)
F_n	Net thrust ($F_g - D_{RAM}$)	lb	(N)
F_{N_E}	Equivalent net thrust $\{F_{G_E} \cos(\alpha+\tau) - D_{RAM} - D_{SPIL}\}$	lb	(N)
F_{G_E}	Equivalent gross thrust ($F_G \cos \varepsilon - D_{INT}$)	lb	(N)
g	Acceleration of gravity	ft/sec^2	(M/sec^2)
Hp	Pressure altitude	ft	(M)
h_R	Ram drag moment arm	ft	(M)
L_T	Tail lift moment arm	ft	(M)
L	Lift	lb	(N)
M	Mach number	-	(-)
m	Mass	$lb\ sec^2/ft$	(Kg)
n_x, n_z	Sensitive accelerometer reading along the indicated axis	g	(g)
$n_{x_{net\ corr}}$ $n_{z_{net\ corr}}$	Accelerometer reading corrected for cg and rotation effects	g	(g)
n_{x_D}	Longitudinal load factor along drag axis	g	(g)
$n_{x_{D_E}}$	Longitudinal load factor calculated via energy method	g	(g)
$n_{z_{LIFT}}$	Load factor along lift axis	g	(g)
N	Engine speed	RPM or %	(%)
p	Longitudinal body accelerometer misalignment	deg	(deg)
P_a	Ambient pressure	lb/ft^2	(N/M^2)
q	Normal body accelerometer misalignment	deg	(deg)

Symbol	Definition	Common Units	Metric Units
q	Free stream dynamic pressure	lb/ft^2	(N/M^2)
$r_{x,y,z}$	Location of accelerometer package in x,y,z axis	ft	(M)
R_N	Reynolds number	-	(-)
RNI	Reynolds number index	-	(-)
S	Wing area	ft^2	(M^2)
SR	Specific range	n.mi./lb fuel	(KM/Kg
TSFC	Thrust Specific Fuel Consumption	lb-hr/lb thrust	(N-sec/Kg
V_T	True airspeed	kt	(KM/hr)
V_{MAX}	Maximum airspeed	kt	(KM/hr)
W	Gross weight	lb	(Kg)
W_a	Airflow	lb/sec	(Kg/sec)
W_f	Fuel flow	lb/hour	(Kg/sec)
Y_T	Gross thrust moment arm	ft	(M)

Greek Symbols	Definition	Units	
α	Angle of attack	deg	(deg)
τ	Thrust inclination	deg	(deg)
ε	Thrust toe out from FRL	deg	(deg)
γ	Flight path angle	deg	(deg)
ψ	Yaw angle	deg	(deg)
θ	Pitch angle	deg	(deg)
ϕ	Roll angle	deg	(deg)
δ	Ratio of ambient pressure to sea level standard	-	(-)
θ	Ratio of ambient temperature to sea level standard	-	(-)
1,2,etc.	Iteration number	-	

THE BASIC MATHEMATICAL MODEL

3.4 The basic mathematical model concerning a performance engineer will be based on drag, thrust available, and thrust fuel flow relations. Each mathematical component may be very complicated but with all three components defined, it is assumed that the complete aircraft performance can be calculated. It is further assumed that the interdependency of these relationships is such that several different component combinations will yield similar aircraft performance as discussed in paragraph 1.15 of chapter 1. In defining the basic mathematical model, each component will be examined in detail.

AIRPLANE DRAG POLAR

3.5 The airplane drag polar depicts the relation of the airplane power-off trimmed lift coefficient as a function of the trimmed drag coefficient and Mach number. A typical drag polar is presented in figure 3-1.

3.6 The meaning of the power-off trimmed lift coefficient can be better visualized by referring to figure 3-2. $C_{L_{POFF}}$ is defined as the aerodynamic lift of the airplane exclusive of the lift produced by the thrust vectors:

$$C_{L_{PON}} = C_{L_{POFF}} + C_{F_G}$$

or

$$C_{L_{POFF}} = C_{L_{PON}} - C_{F_G} \quad . \tag{3-5}$$

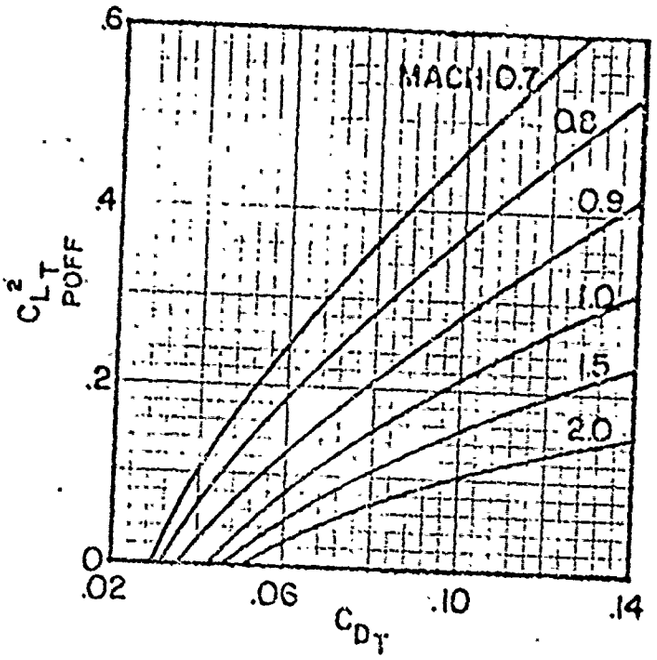

FIG. 3-1: TYPICAL DRAG POLAR

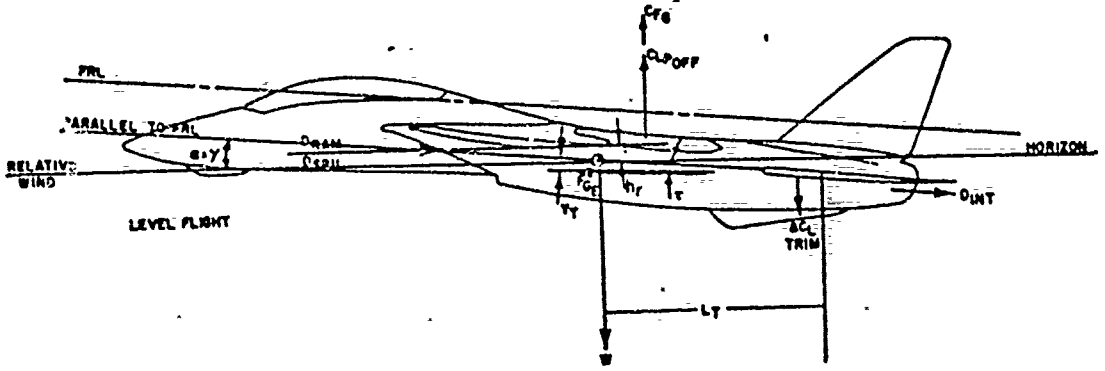

FIG. 3-2: FREE BODY DIAGRAM OF AIRPLANE LIFT AND DRAG VECTORS

Including the tail lift term required to trim the airplane in the desired flight condition, the equation becomes:

$$C_{L_{TRIM}} = C_{L_{PON}} - C_{F_G} + \Delta C_{L_{TRIM}} \quad . \tag{3-6}$$

The term $\Delta C_{L_{TRIM}}$ can be determined by summing moments around the center of gravity (cg), and setting them equal to zero:

$$C_{M_{TRIM}} = +\Delta C_{L_{TRIM}}\left(\frac{L_T}{\bar{c}}\right) + \left[\frac{F_{G_E}}{qS}\frac{Y_T}{\bar{c}}\right] + \left[\frac{(D_{RAM}+D_{SPIL})}{qS}\left(\frac{h_R}{\bar{c}}\right)\right] = 0 \tag{3-7}$$

rearranging:

$$-\Delta C_{L_{TRIM}}\left(\frac{L_T}{\bar{c}}\right) = \left[\frac{F_{G_E}}{qS}\left(\frac{Y_T}{\bar{c}}\right)\right] + \left[\frac{(D_{RAM} + D_{SPIL})}{qS}\left(\frac{h_R}{\bar{c}}\right)\right] \tag{3-8}$$

or

$$\Delta C_{L_{TRIM}} = -\left[\frac{F_{G_E}}{qS}\left(\frac{Y_T}{L_T}\right) + \frac{(D_{RAM} + D_{SPIL})}{qS}\left(\frac{h_R}{L_T}\right)\right] \quad , \tag{3-9}$$

and substituting back into equation 3-6:

$$C_{L_{TRIM}} = C_{L_{PON}} - C_{F_G} - \left[\frac{F_{G_E}}{qS}\left(\frac{Y_T}{L_T}\right) + \frac{(D_{RAM} + D_{SPIL})}{qS}\left(\frac{h_R}{L_T}\right)\right]. \tag{3-10}$$

The term C_{F_G} is the thrust component in the lift axis and is defined, by using figure 3-2 as:

$$C_{F_G} = \frac{F_{G_E}\sin(\alpha+\tau)}{q\,S} \quad . \tag{3-11}$$

Note that h_R is a function of vertical and horizontal cg position and angle of attack; Y_T is a function of vertical and horizontal cg; and L_T is a function of angle of attack and horizontal cg.

3.7 The drag coefficient calculated from measured conditions is adjusted for drag effects associated with non-standard conditions. Among them is a trim correction for power. This correction stems from the fact that the tail lift required to trim results in an incremental tail incidence which is itself related to a ΔC_L, hence, a ΔC_D. Correction to a standard cg is required since an incremental tail incidence is required for cg variation from standard, resulting again in a ΔC_D. Maneuvers with associated pitch rates, i.e., dynamic maneuvers, result in incremental tail incidence, also resulting in a ΔC_D. A correction to a standard Reynolds Number (R_N) is also required since skin friction R_N relates to a drag increment. Incremental drag corrections are also made to adjust data to a standard Mach number and a standard constant load factor. Other adjustments, such as those for airplane elasticity can be applied if deemed necessary.

3.8 All the above adjustments should be given due consideration when constructing a drag polar; however, a large amount of information is required before many of the corrections can be made. In these considerations, the total data acquisition cost must be weighed against the requirements for quality and quantity of the final data product.

3.9 Detailed correction procedures for each of the items mentioned in this section are given in Chapter 4.

LIFT SLOPE CURVE

3.10 The lift slope curve consists of the power-off trimmed lift coefficient as a function of true angle of attack and Mach. A typical plot is presented in figure 3-3. The angle of attack is usually referenced to the fuselage reference line. The measured angle of attack must be corrected for upwash effects, nose boom bending, vane lag response, and pitch rates in order to obtain a true angle of attack. These corrections are detailed in Chapter 5.

THRUST-FUEL FLOW RELATION

3.11 The thrust-fuel flow relation is depicted in figure 3-4. Note that this curve is applicable for only one altitude, hence, one curve for each altitude of interest or for enough altitudes to enable interpolation is required. This curve can be established for zero bleeds on the engine for baseline data or for standard bleed requirements. Adjustments for bleed effects should be considered when applying these curves.

THRUST AVAILABLE

3.12 Thrust available characteristics are depicted in figure 3-5. For many applications, it is desirable to have the contributing components to net thrust separated as is summarized in figure 3-6. The spillage drag and interference drag components are derived from wind tunnel tests and adjusted for flight test results obtained throughout the development phase of an aircraft/propulsion system.

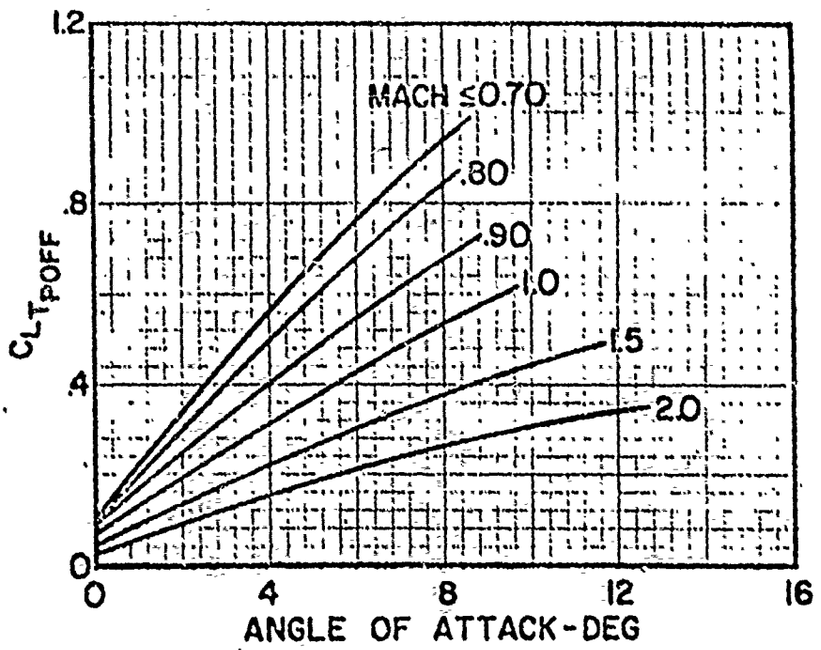

FIG. 3-3: TYPICAL LIFT SLOPE CURVE

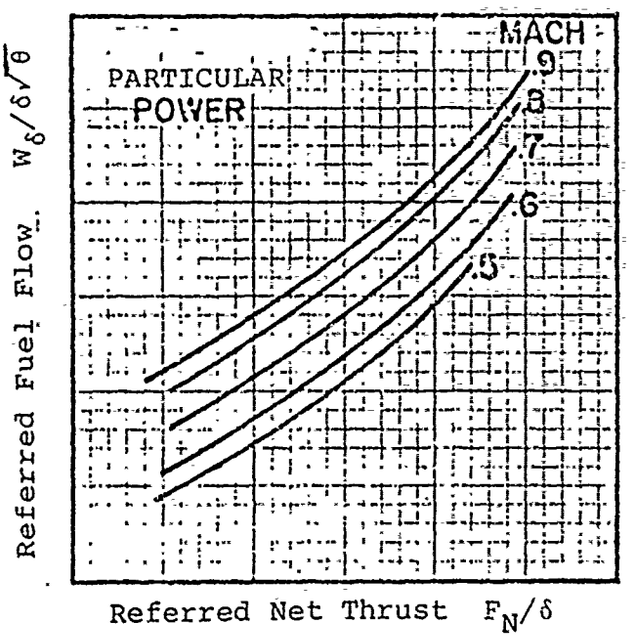

FIG. 3-4: TYPICAL THRUST-FUEL RELATION

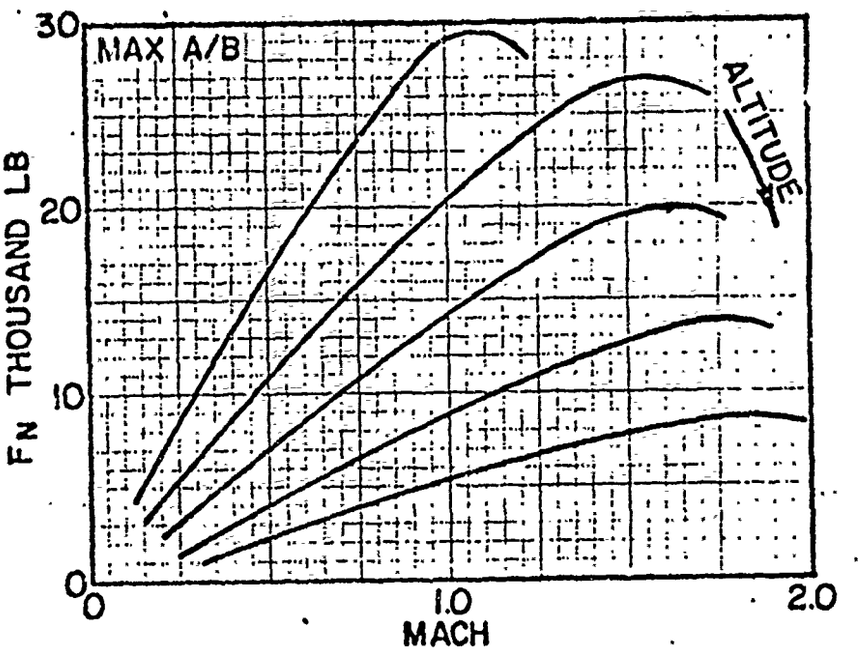

FIG. 3-5: TYPICAL THRUST AVAILABLE CHARACTERISTICS

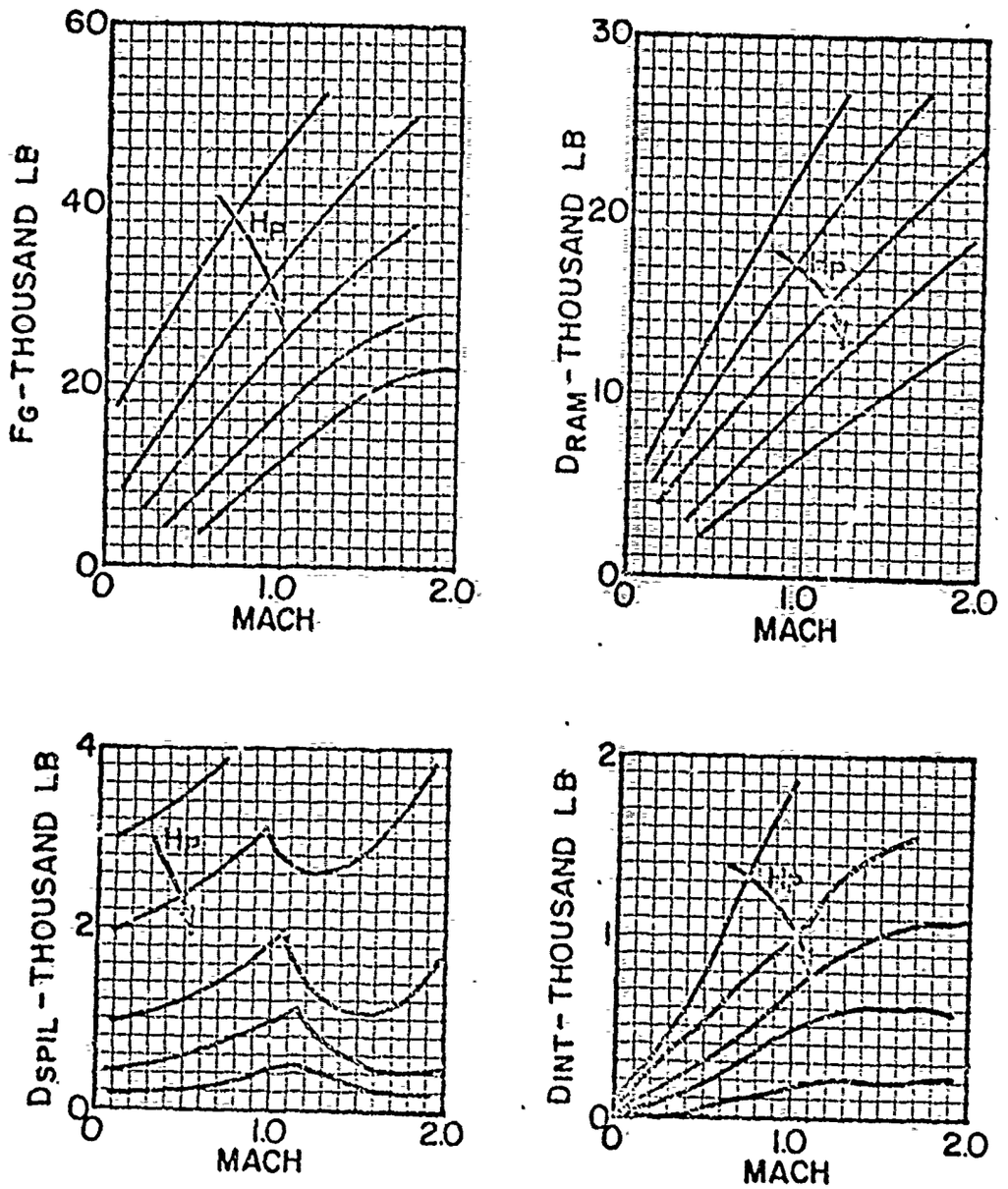

FIG. 3-6: TYPICAL COMPONENTS COMPRISING NET THRUST

THRUST RPM CURVE

3.13 Assuming for the moment, that the aircraft configuration is defined and aircraft performance is to be predicted, there arises a need for the determination of the aircraft gross thrust. As was shown in Chapter 2:

$$F_n = F_G \cos(\alpha+\tau) - F_R \quad , \tag{3-12}$$

or:

$$F_G = \frac{F_n + F_R}{\cos(\alpha+\tau)} \quad . \tag{3-13}$$

The ram drag component can be determined from contractor airflow curves as:

$$F_R = \frac{W_a V_T}{g} \quad , \tag{3-14}$$

where airflow (W_a) is usually a function of rpm (N). We then need to be able to predict engine rpm for a given flight condition, and this may be done as shown in figure 3-7.

OTHER RELATIONS

3.14 When trying to predict non-standard performance, several other relations will be necessary to correct to non-standard conditions. These corrective procedures are discussed in detail in Chapter 4.

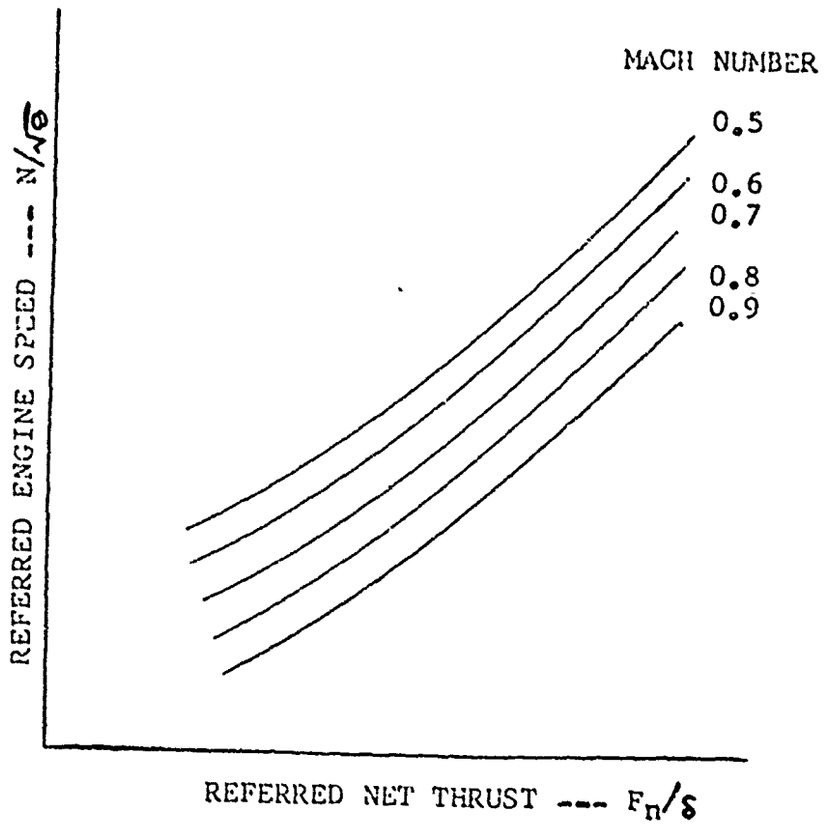

FIG. 3-7: THRUST-RPM CURVE

APPLYING THE MATHEMATICAL MODEL

3.15 The five curves (figures 3-3 through 3-7) related above are to be used to predict the performance of an aircraft at a flight condition. This can be extended to maneuvers by considering flight conditions during the maneuver and numerically integrating to obtain the predicted performance during the maneuver. The flight condition will consist of a Mach number, load factor, gross weight, altitude, and throttle condition. Initially, the effective aircraft C_L, is calculated as:

$$C_{L_{eff}} = \frac{Wn_z}{qS} \quad . \tag{3-15}$$

This is used on the first iteration to determine angle of attack and gross thrust. The $C_{L_{eff}}$ is used together with Mach number, and the trimmed lift curve (figure 3-3) to determine angle of attack(α_1). The $C_{L_{eff}}$ is then used with Mach number and the drag polar (figure 3-1 to determine drag coefficient (C_{D_1}). For iteration:

$$F_{N_1} = C_{D_1} qS \quad . \tag{3-16}$$

Using F_{N_1}/δ and the thrust rpm curve, $(N/\sqrt{\theta})_1$ is obtained. Using contractor curves for airflow (W_{a_1}), ram drag is calculated by:

$$F_{R_1} = \frac{W_{a_1} V_T}{g} \tag{3-17}$$

and gross thrust becomes:

$$F_{G_1} = \left(F_{N_1} + F_{R_1}\right)/\cos(\alpha_1 + \tau) \quad . \tag{3-18}$$

From this point, $C_{L_{POFF}}$ is computed by:

$$C_{L_{POFF}} = \frac{Wn_z - F_{G_1} \sin(\alpha_1 + \tau)}{qS} \quad , \tag{3-19}$$

and the process is repeated (i.e., determine α_2 from $C_{L_{POFF}}$ and Mach, C_{D_2} from $C_{L_{POFF}}$ and Mach, F_{N_2}, F_{R_1}, F_g, and finally, $C_{L_{POFF}}$). The iteration ceases when $C_{L_{POFF}}$ becomes the same value each time within some tolerance. The final values of α, F_n, C_D, $C_{L_{POFF}}$ are used in further calculations. For climbs and accelerations, figure 3-5 yields, for a given Mach number and altitude, the $\frac{F_N}{\delta}$ available and:

$$\left(\frac{F_N}{\delta} \text{ available}\right)\delta - C_D qS = F_{ex} \quad . \tag{3-20}$$

For level flight data, figure 3-4 thrust fuel flow is used with:

$$\frac{F_N}{\delta} = \frac{C_D qS}{\delta} \tag{3-21}$$

to give

$$W_f = \left(\frac{W_f}{\delta\sqrt{\theta}}\right)\delta\sqrt{\theta} \tag{3-22}$$

and

$$SR = \frac{661.48\ M\sqrt{\theta}}{W_f} = \frac{V_t}{W_f} \quad . \tag{3-23}$$

These parameters can be further expanded to yield time to climb, rate of climb, fuel used, etc., depending upon the maneuver performance sought.

FUEL FLOW MODELING

3.16 In the basic discussion of the mathematical model, it was assumed that the interdependency of the parameters was such that several combinations of mathematical components will yield the aircraft performance. This point is discussed in Chapter 1 (paragraph 1.15). It has also become apparent that with the accelerometer methods, obtaining performance is no longer limited by the determination of thrust available or drag. With the accelerometer methods, thrust available and drag can be obtained quickly by a series of accelerations and climbs at the power setting for which thrust available is desired. The limiting factor to determine aircraft performance is the determination of a thrust fuel flow relation. Conventionally, this is done by a laborious series of stabilized points. The generation of thrust fuel flow for many programs done on military aircraft can be done conventionally at only a small penalty. Most military aircraft are tested for a large number of external store loadings, and the thrust fuel flow relation is independent of external loading in that it is only a gas generator characteristic. One loading can be flown by conventional techniques for four or more flights, and subsequent loadings can be flown by the accelerometer methods in one or more flights using the generated thrust fuel flow relation.

3.17 The alternative for programs that are extremely time-constrained, or on aircraft that have engines which cannot be used

to adequately measure thrust by parametrics, is fuel flow modeling. This point is further discussed in Chapter 1 (paragraph 1.33).

3.18 The validity of the fuel flow model approach is tied to the interdependency of the performance parameters and is dealt with in Chapter 1 (paragraph 1.34). This can be further extended by analogy. In the mathematical approach, there is a three component determinant of performance. For example:

$$x + y + z = \text{performance} \quad ,$$

where x, y, and z may have many values to define performance and where x is analogous to thrust required, y is analogous to thrust available, and z is analogous to fuel flow. The interdependency of the relations can be expressed by:

$$y = C_o z \quad , \tag{3-24}$$

which is analogous to thrust being a function of fuel flow, and C_o is dependent on flight parameters. If in the analogous equation set, a value is assigned to z, then the interdependency dictates a value of y. Next, a flight test is performed yielding performance, such that:

$$x + y + z = \text{performance} \quad , \tag{3-25}$$

so that the value of x is defined. Any value can be assigned to z, and the values of x and y will change, but performance does not.

3.19 By analogy, if a thrust fuel flow relation is assumed, and for each of the flight tests performed, thrust is inferred by fuel flow and the thrust fuel flow relation, then the solutions have been constrained to one set of values. This, then, is a definition of fuel flow modeling. A thrust fuel flow relation is assumed. Thrust output is inferred by fuel flow and the assumed thrust fuel flow relation. Excess thrust is measured by the accelerometers, and drag (thrust required) is calculated by equation 3-3.

3.20 In theory, any relationship which can be assumed can be used (example, TSFC = constant); however, this can make the thrust available and drag polars very complicated functions, and may introduce parameters not normally considered (such as altitude lines on a drag polar). If this happens, more flight data may be required to define these deviations than can be saved by the fuel flow modeling approach. In practice, a fuel flow map which is as close to actual as possible is needed. This makes the analysis easier by eliminating undesired parametrics and gives more confidence in the data.

3.21 The thrust fuel flow map to be used can be obtained from a number of sources. Contractor flight tests prior to turning the aircraft over to the Navy for evaluation, engine manufacturer curves, or specification curves can be used. In addition, Naval Air Propulsion Test Center (NAPTC) test cell data can be used. Finally, stabilized points taken for airspeed calibration and upwash determination can be used as anchor points to modify the relations available. If necessary, the fuel flow relation can be determined by conventional techniques

and applied to the data taken. An example of data taken by fuel flow modeling technique, with a comparison to conventional data is given in Chapter 1 (paragraph 1.36 and figure 1-7).

3.22 In aircraft where the normal parametric measurement of thrust is adequate and consistent, both the thrust modeling and fuel flow modeling techniques can be used as independent checks. For example, if the thrust modeling technique and the fuel flow modeling technique are both assumed correct, then the thrust modeling method can be solved for nozzle coefficients in flight where this data would not be otherwise available.

3.23 With the math modeling concepts defined, and with both thrust modeling and fuel flow modeling techniques available, it is well to describe the flight techniques and maneuvers available for defining these models. The contribution of each maneuver to the mathematical model will be examined.

TEST MANEUVERS

3.24 The test maneuvers requried to generate data for the indirect approach are basically the same as those performed when evaluating performance via the direct approach. The one additional set of maneuvers are the dynamic maneuvers, consisting primarily of wind-up and wind-down turns, accel-decel and pushover pull-up tests. These test maneuvers can be classified into three areas:

- Steady state maneuvers where excess thrust is zero or near zero. These points minimize data adjustments and provide the baseline for all aerodynamic and propulsion maps. In-flight assessment of onboard accelerometer misalignments can also be evaluated.
- Quasi steady maneuvers where the normal load factor is near one but excess thrust is not zero. These maneuvers, such as climbs, descents, accelerations, are relatively easy to perform and require no special test techniques. Pitch rates are low, thus minimizing associated corrections to lift and drag data. These maneuvers also enable a direct comparison of results obtained from onboard accelerometers with results obtained using energy analysis techniques. This enables a ready assessment of the validity of accelerometer outputs and provides confidence to extend the use of accelerometers to dynamic maneuvers.

- Dynamic maneuvers where the normal load factor may vary significantly from one and excess thrust is not zero. These include wind-up and wind-down turns and push-pull maneuvers. These maneuvers can be performed over a small time period, at or near a constant Mach and yield data at somewhat higher and lower C_L values than either the steady or quasi steady maneuvers. Special test techniques are required and inherent pitch rates have to be accounted for in more sophisticated data analysis techniques. Additionally greater accuracy in the instrumentation system is required. Chapter 5 gives an analysis of instrumentation requirements. Comparison with energy techniques cannot be accomplished with these maneuvers; hence, all in-flight errors associated with instrumentation must be determined from preceding steady points and quasi steady maneuvers.

TEADY STATE TEST MANEUVERS

teady Points

.25 These maneuvers are 1 g steady points, such as performed in W/δ series; however, a unique combination of gross weight and ltitude is not required. These points can be at any Mach number t any flight condition; the only constraint is that the airplane is n the proper configuration for the desired test results. The test echnique requires stabilization for approximately two minutes;

Usually, a minimum of one minute is required to allow the engine(s) to stabilize; data is then recorded for approximately one additional minute. This enables a complete, concise definition of the energy state of the airplane, and even more important, an assessment of the validity of longitudinal accelerometer readings; hence, an extremely accurate determination of airplane drag. A time history of a typical steady point showing the determination of the incremental drag associated with non-steady conditions is presented in figure 3-8. With the figure is also the listing of average measured values and the corrections to the measured values. It can be seen that the two methods differ by some 9 percent, as demonstrated by a .0084 g difference between the computed $(\dot{E}/V_T)$ and the measured values. Steady point maneuvers provide, however, only one data point at the test Mach number for the applicable aerodynamic and propulsion maps. Typical data output is summarized in figure 3-9. From steady points tail trim requirements can be defined along with extensive propulsion data. Additionally, in-flight checks on angle of attack upwash can be made.

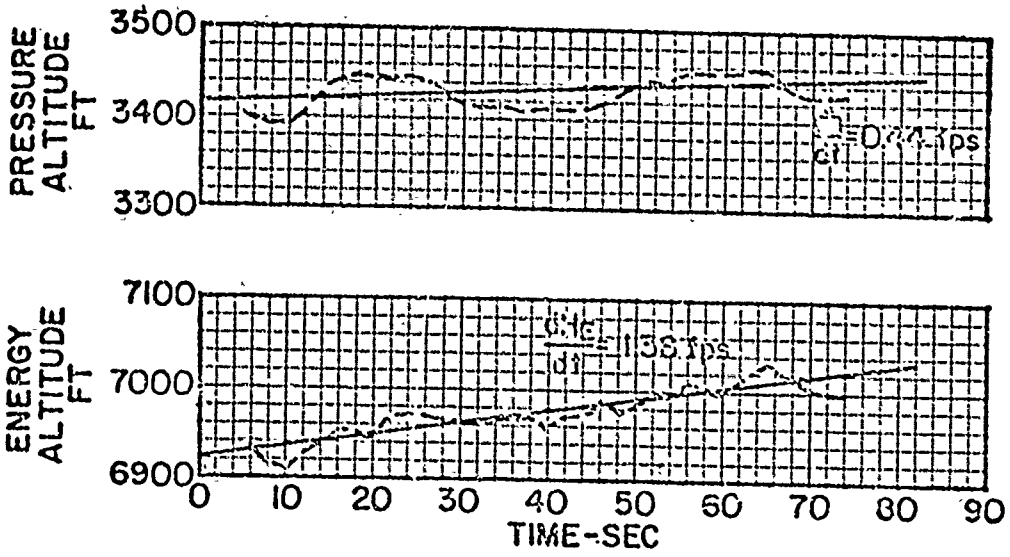

FIG. 3-8: TIME HISTORY OF A STEADY POINT

Average Measured Values

W_t : 61,000 lbs.

V_T : 476 fps

θ : 3.73 deg.

N_{X_D} : 0.0113 g

C_D : 0.0426

Adjustments

$$N_{X_{D_E}} = \frac{E}{V_T} = \frac{1.38}{476} = 0.0029$$

$$\Delta N_{X_D} = N_{X_{D_{MEAS}}} - N_{X_{DE}} = 0.0084 \text{ g}$$

$$F_{ex} = 512 \text{ lbs.} (\Delta N_{X_D} \cdot W_t)$$

ΔC_D = 0.0039 or 9 percent of measured value of C_D

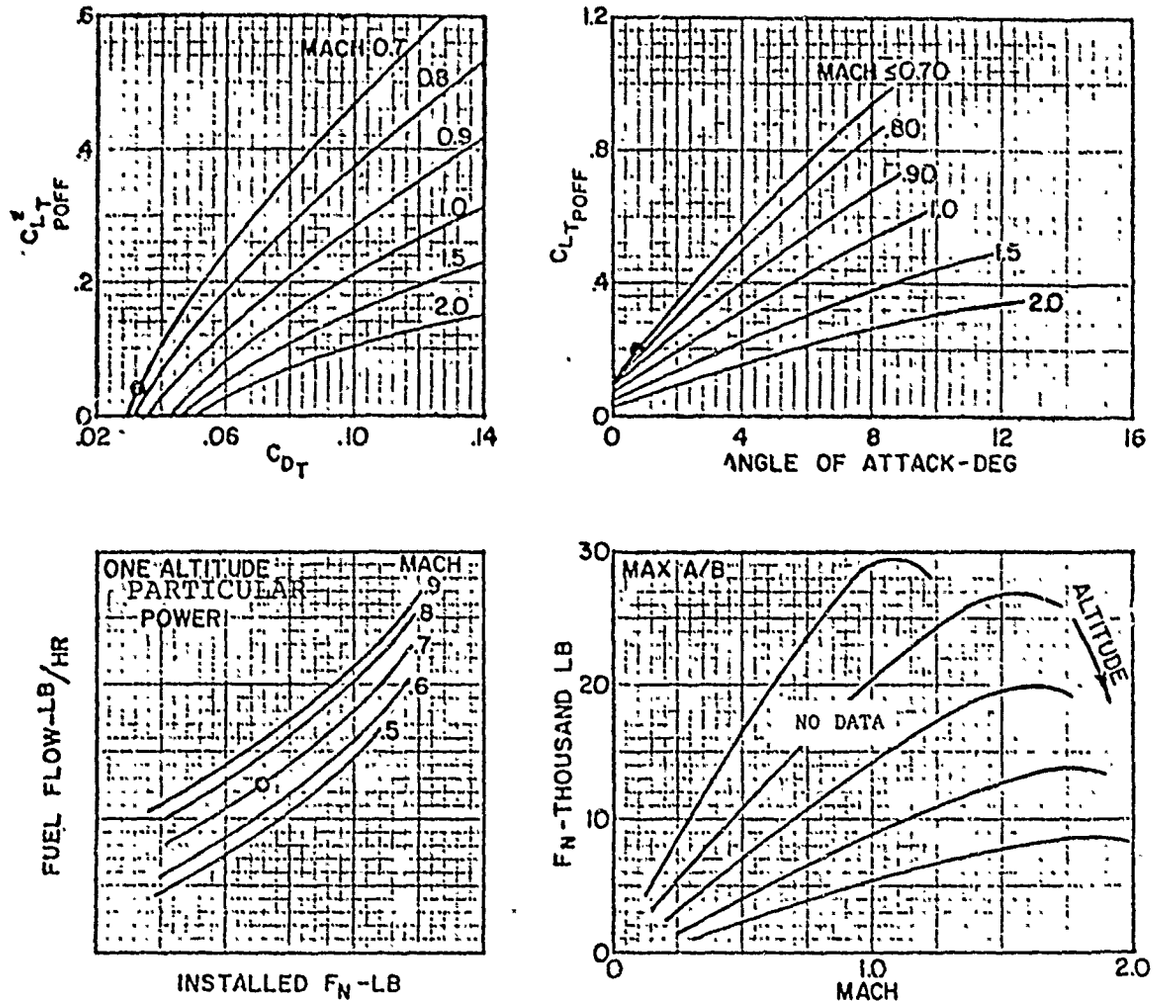

FIG. 3-9: DATA OUTPUT FROM A STEADY POINT MANEUVER

Steady State Turns

3.26 These maneuvers are thrust limited steady state turns where excess thrust is at or near zero. They provide aerodynamic data at higher values of C_L than the 1 g steady points, closely approximated by a multiple of the load factor, i.e., $\frac{Wn_z}{qS}$. The recommended technique is to stabilize in 1 g flight at V_{MAX} for either MIL or Max A/B thrust. Once the engines have stabilized, proceed with a series of steady turns at various Mach numbers or airspeeds, holding thrust constant. Usually, a 10-second burst of data is all that is practical under these conditions. This maneuver is of secondary importance in gathering data for the indirect approach, but nonetheless, useful aerodynamic data can be extracted if a series of thrust limited turns are to be performed to evaluate performance directly. Typical data output is summarized in figure 3-10.

QUASI STEADY TEST MANEUVERS

Level Flight Accelerations

3.27 These maneuvers are flown with either MIL or Max A/B thrust over a range of airspeed from V_{MIN} to V_{MAX} (or limit "q") at various altitudes. They provide 1 g excess thrust characteristics, steady state V_{MAX} (if obtainable), acceleration characteristics, such as time, fuel, distance, plus lift and drag characteristics, tail, trim data, and thrust available data. Special emphasis must be placed on the importance of maintaining as close to unity load

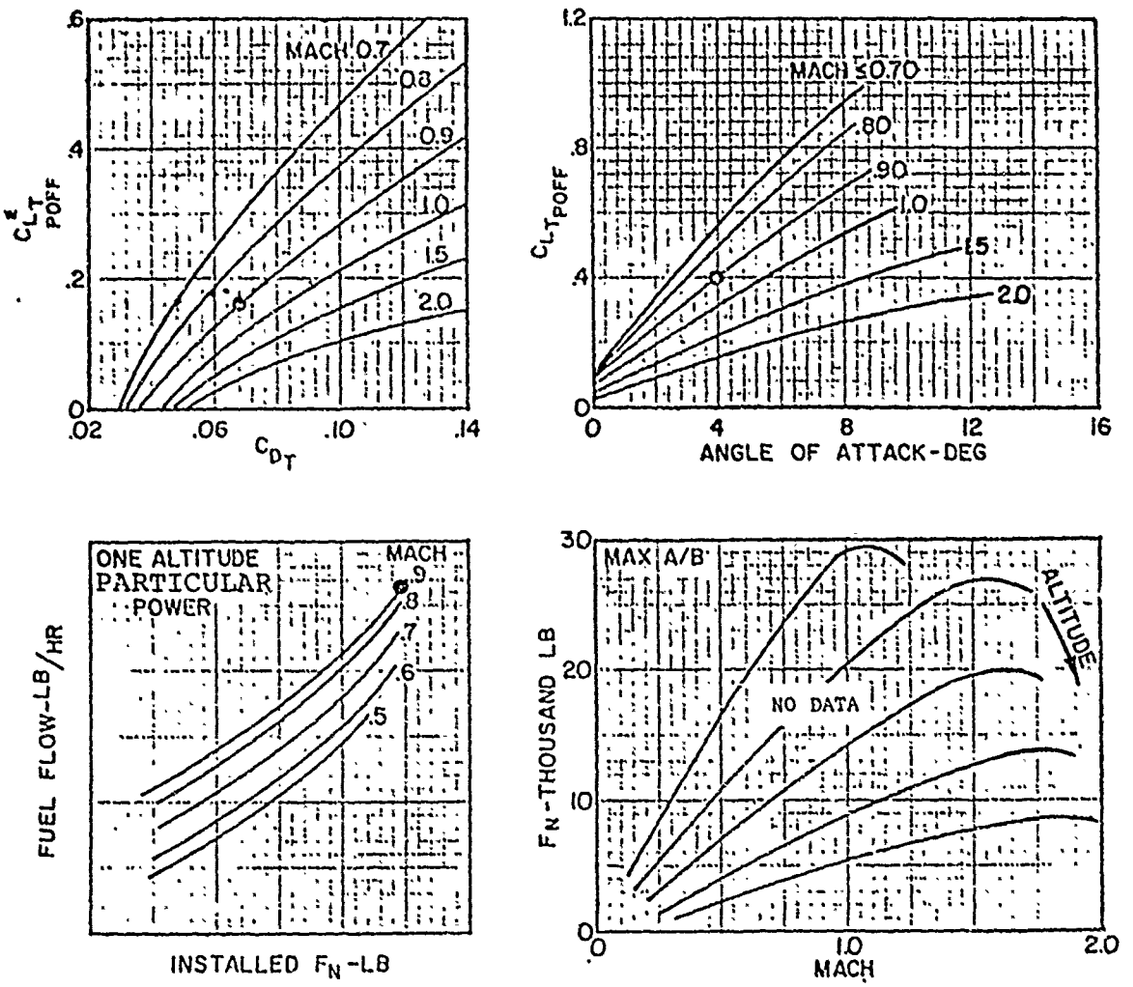

FIG. 3-10: DATA OUTPUT FROM STEADY STATE TURNS

factor as possible during the maneuver. Large variations in load factor cause excessive corrections in trimmed lift and drag calculation, hence, scatter in the data. Typical time histories of level acceleration are presented in figure 3-11 and 3-12.

3.28 Note the effect in figures 3-11A and 3-11B of normal load factor on the calculation of n_{x_D}. The variation of ±0.1g results in a peak-to-peak variation in n_{x_D} of 0.015g or 750-pound excess thrust, 6 percent of the total value at this flight condition. The large variation in load factor results from the pilot chasing altitude as vividly illustrated in figure 3-11A. Figures 3-12A and 3-12B illustrate a much better accleration run with the normal load factor varying only about ±0.05g, resulting in a significantly improved n_{x_D} calculation. Note also, the small variation in altitude throughout the maneuver. The recommended technique for level acceleration is to maintain constant altitude until the transonic region is approached, then fly constant attitude through the transonic region. Once the pitot-static system has settled down, again pick up the reference altitude. Above all, do not chase altitude.

3.29 Aerodynamic data can be presented in the form illustrated by figure 3-13. Additionally, the acceleration runs provide aerodynamic and propulsion data as summarized in figure 3-14.

Wings Level Deceleration

3.30 This maneuver is usually performed after an acceleration run. The thrust is reduced to a setting between IDLE and MIL, such as to

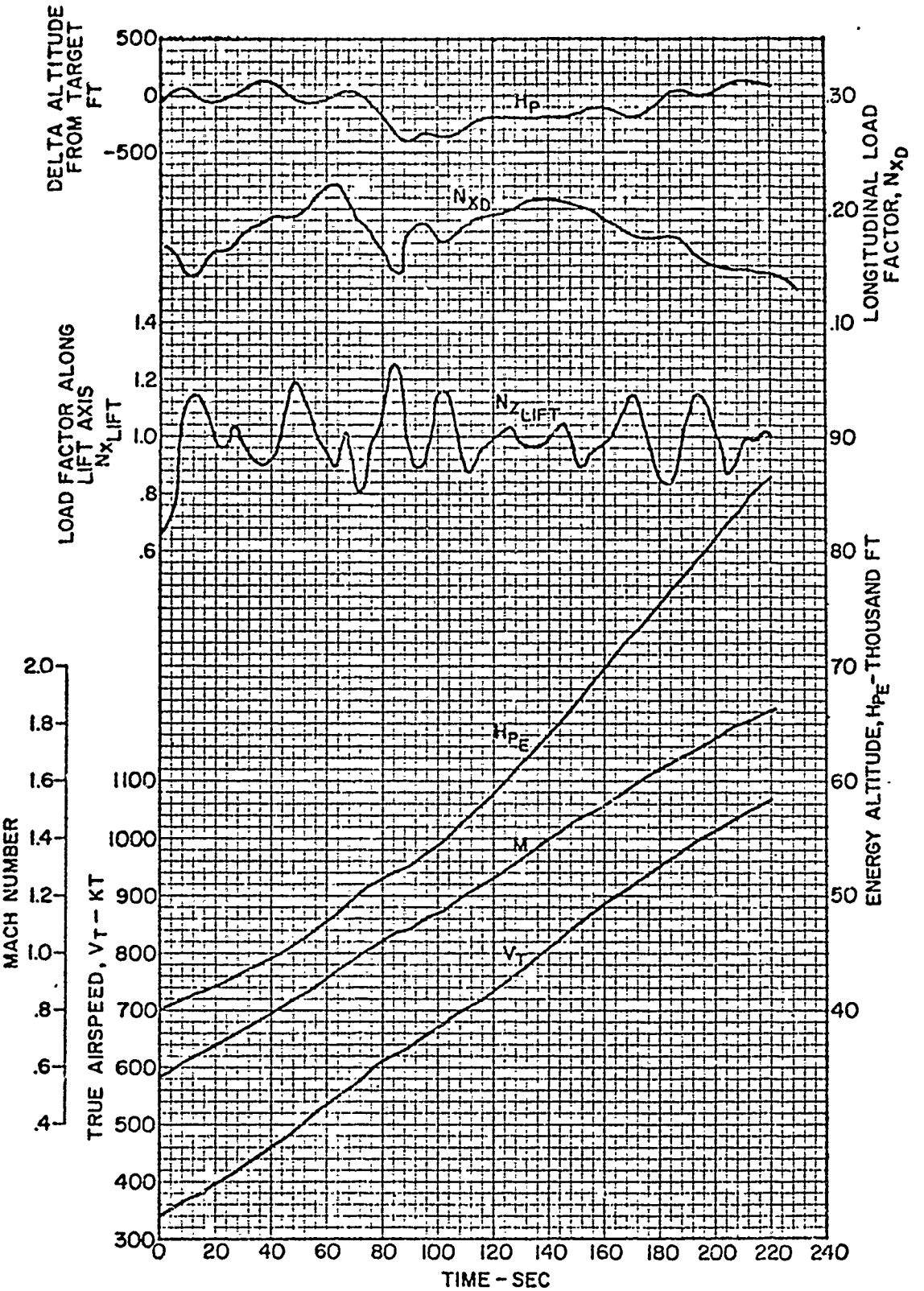

FIG. 3-11A: TIME HISTORY OF A LEVEL FLIGHT ACCELERATION

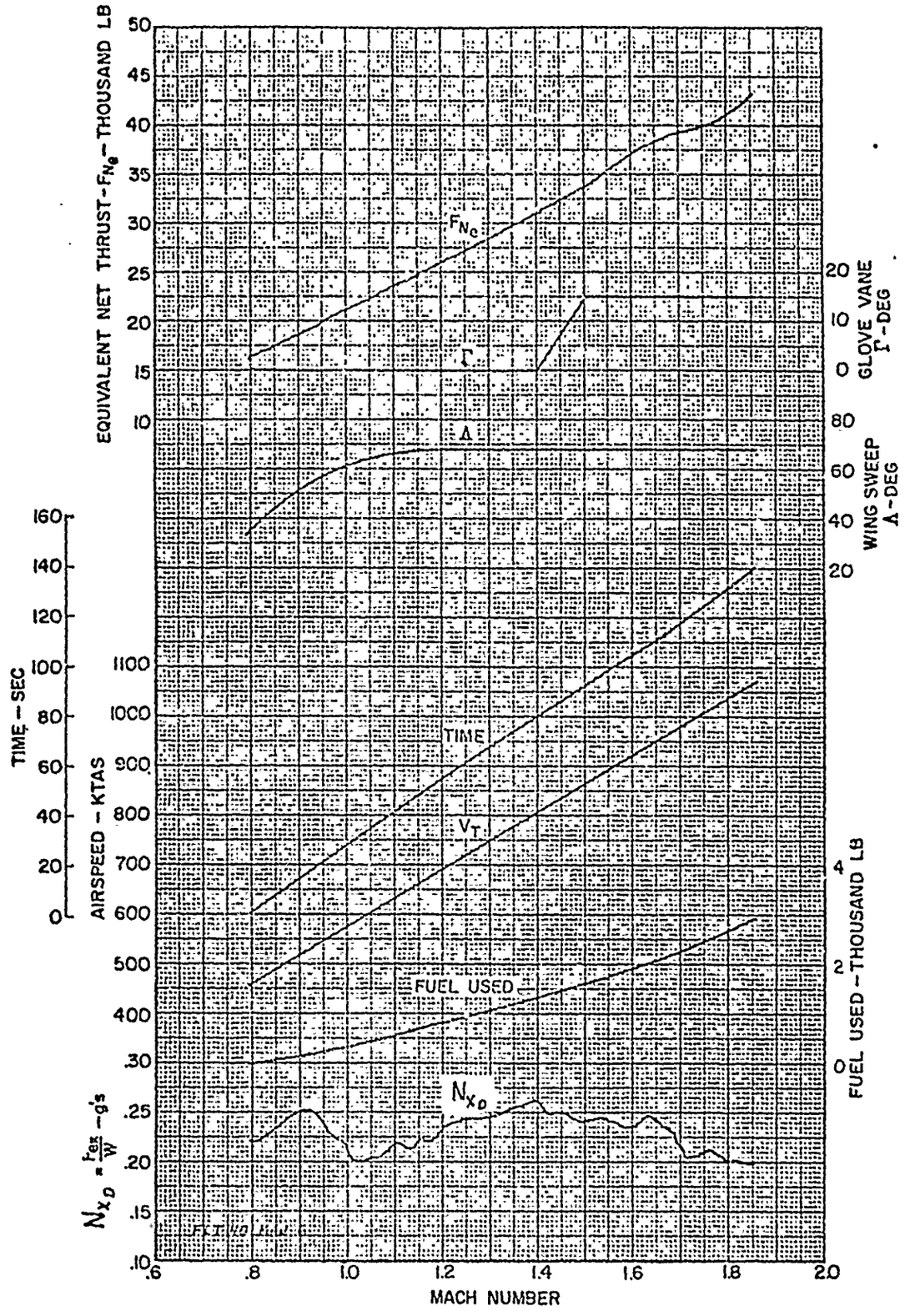

FIG. 3-11B: LEVEL FLIGHT ACCELERATION CORRECTED TO STANDARD CONDITIONS

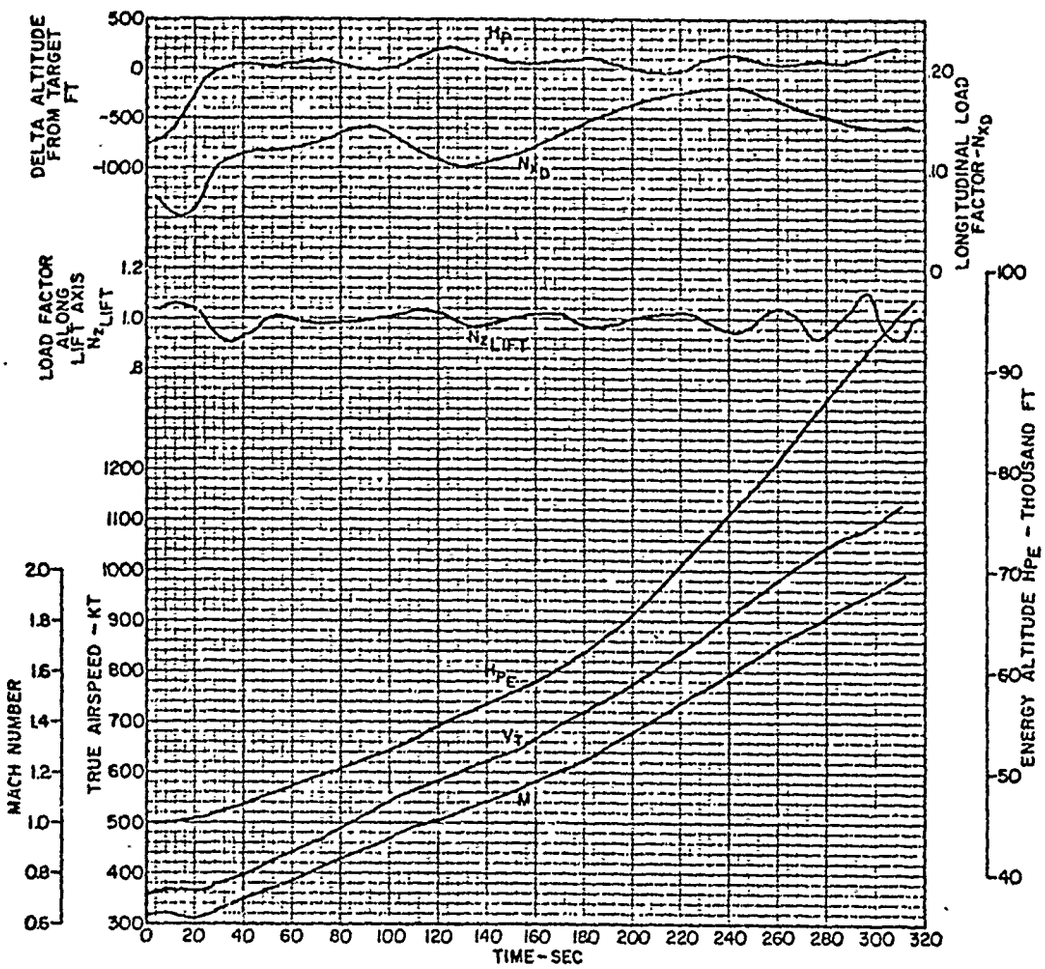

FIG. 3-12A: TIME HISTORY OF A LEVEL FLIGHT ACCELERATION

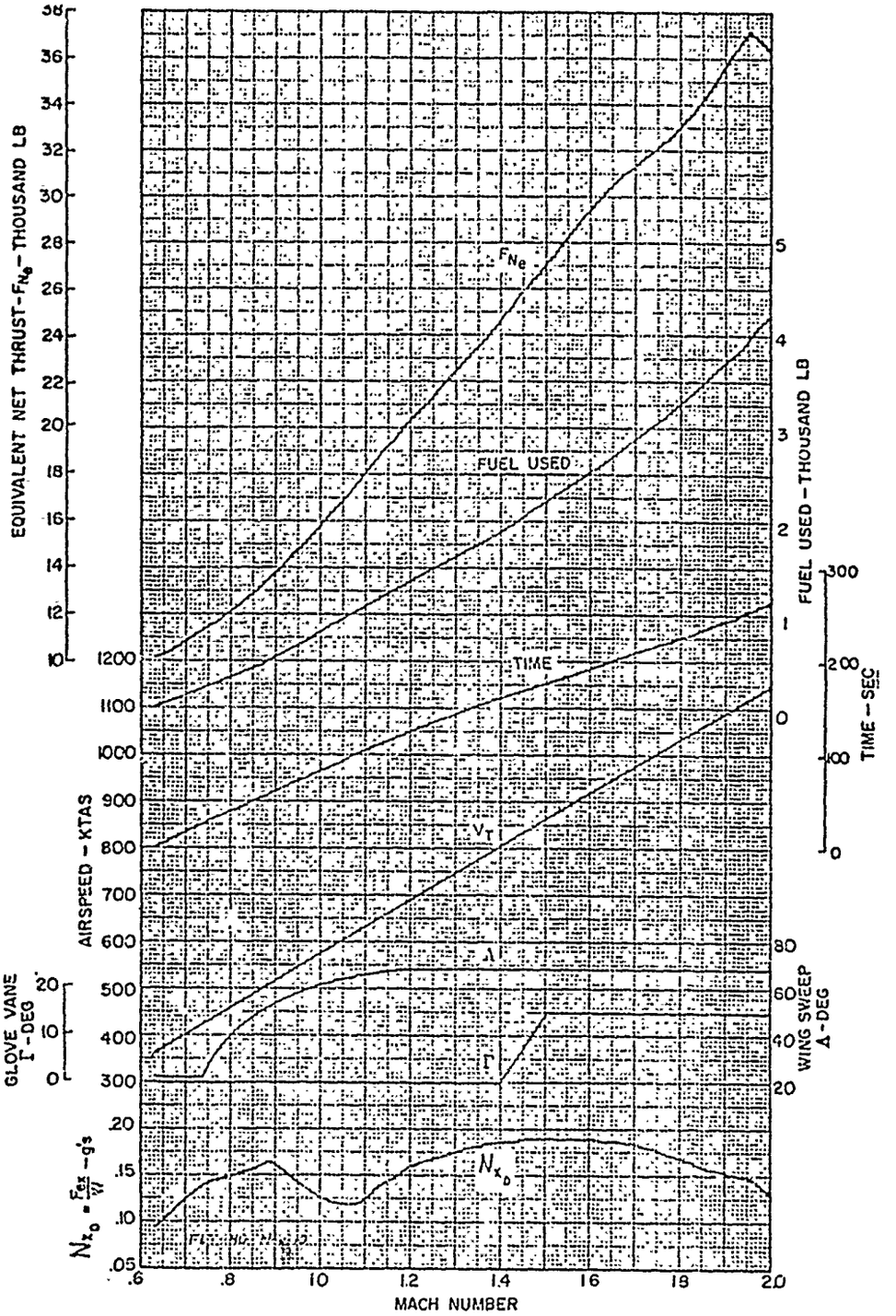

FIG. 3-12B: LEVEL FLIGHT ACCELERATION CORRECTED TO STANDARD CONDITIONS

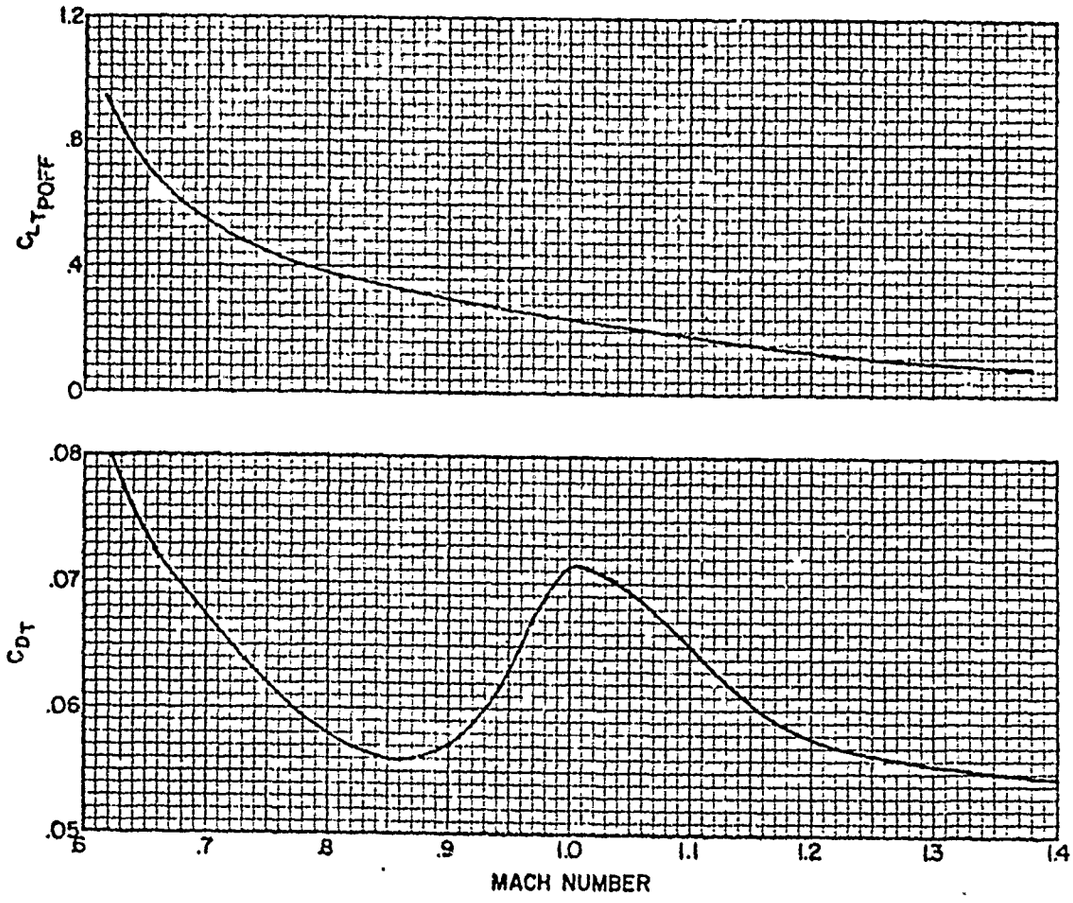

FIG. 3-13: LIFT AND DRAG CHARACTERISTICS FROM LEVEL FLIGHT ACCELERATION RUN

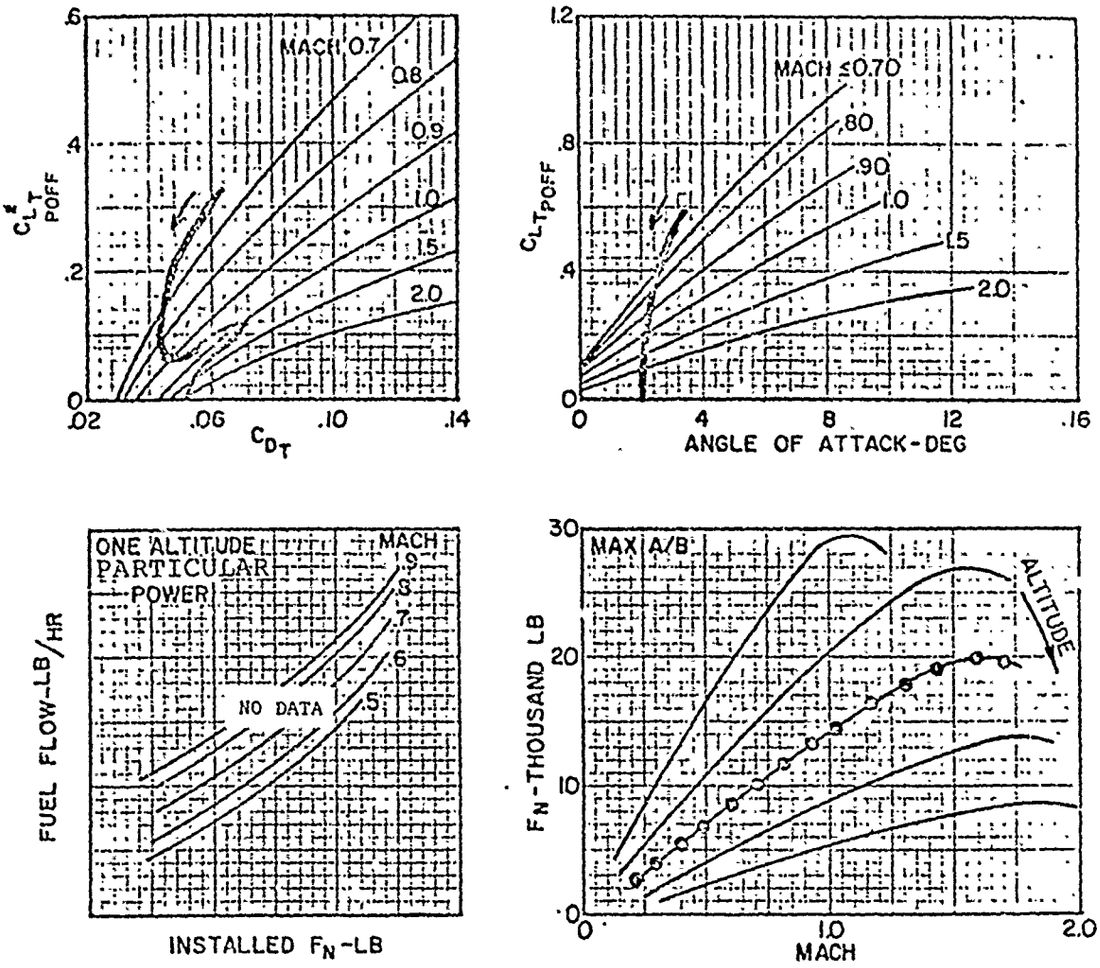

FIG. 3-14: TYPICAL DATA OUTPUT FROM ACCELERATION RUNS

yield the desired minimum speed point. Once the thrust is set, it is not changed throughout the maneuver. Care should be taken to keep load factor as near unity as possible and corrections should be made smoothly. Typical data output is presented in figure 3-15.

Constant Mach Climbs

3.31 These maneuvers are no different than any other climb, with the one criteria that they are flown on a constant Mach schedule. Pilot technique requires smooth adjustments to the schedule. Abrupt, jerky motions must be avoided. Typical data output is summarized in figure 3-16. Techniques for making small corrections in Mach are detailed in Chapter 4.

DYNAMIC MANEUVERS

Constant Mach Wind-Up Turns

3.32 These maneuvers are performed at or near a constant Mach and are preceded by a trim point in order to obtain a drag reference and to assess the longitudinal accelerometer reading. The thrust required for level flight at the trim point is maintained throughout the maneuver. The maneuver is entered and load factor is smoothly applied, keeping pitch rate and pitch acceleration to a minimum. Pitch rate should, in general, be kept below 2 degrees/second, in order to keep data correction to a minimum; however, the final data output will dictate the magnitude of acceptable pitch rate. The rate of application of load factor should not be used as a basic

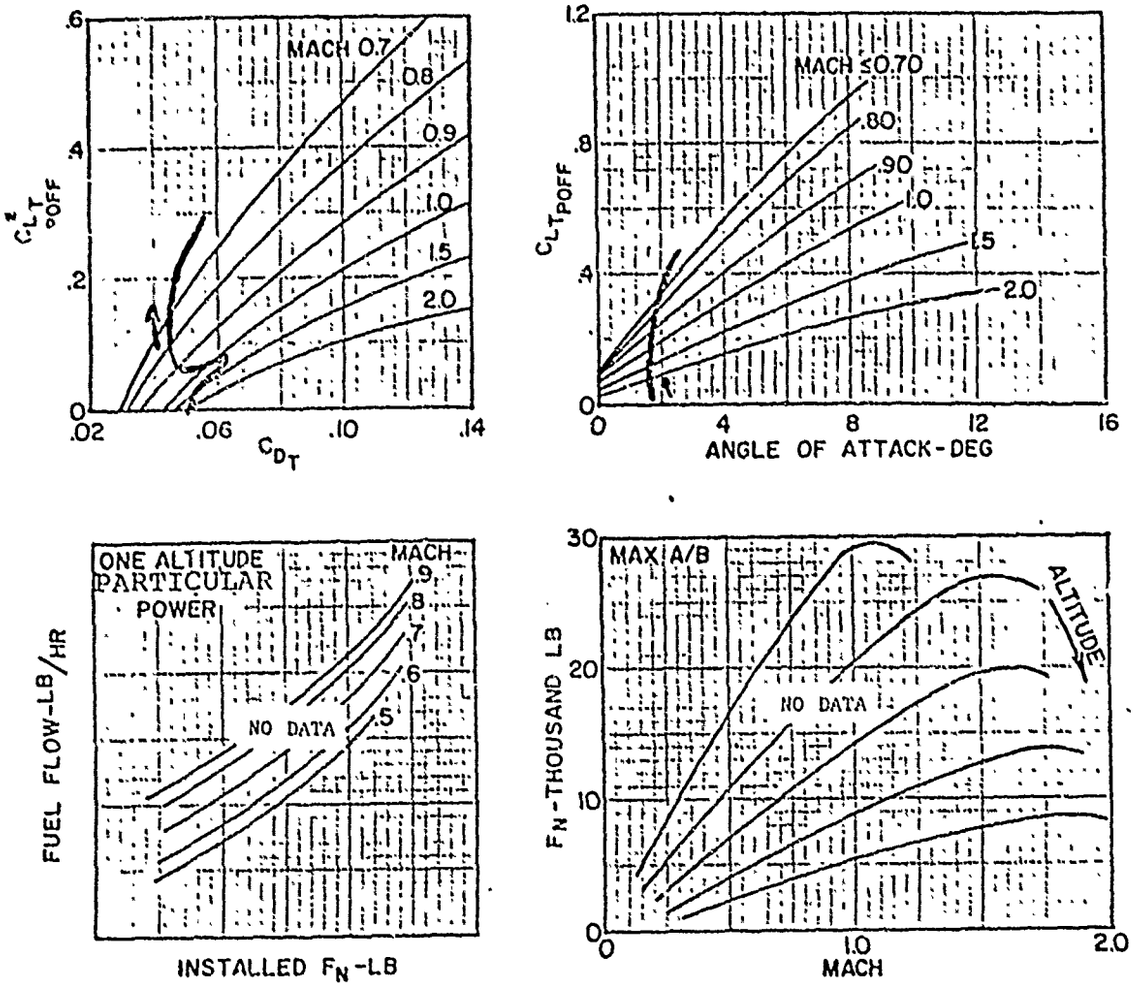

FIG. 3-15: TYPICAL DATA OUTPUT FROM WINGS LEVEL DECELERATION

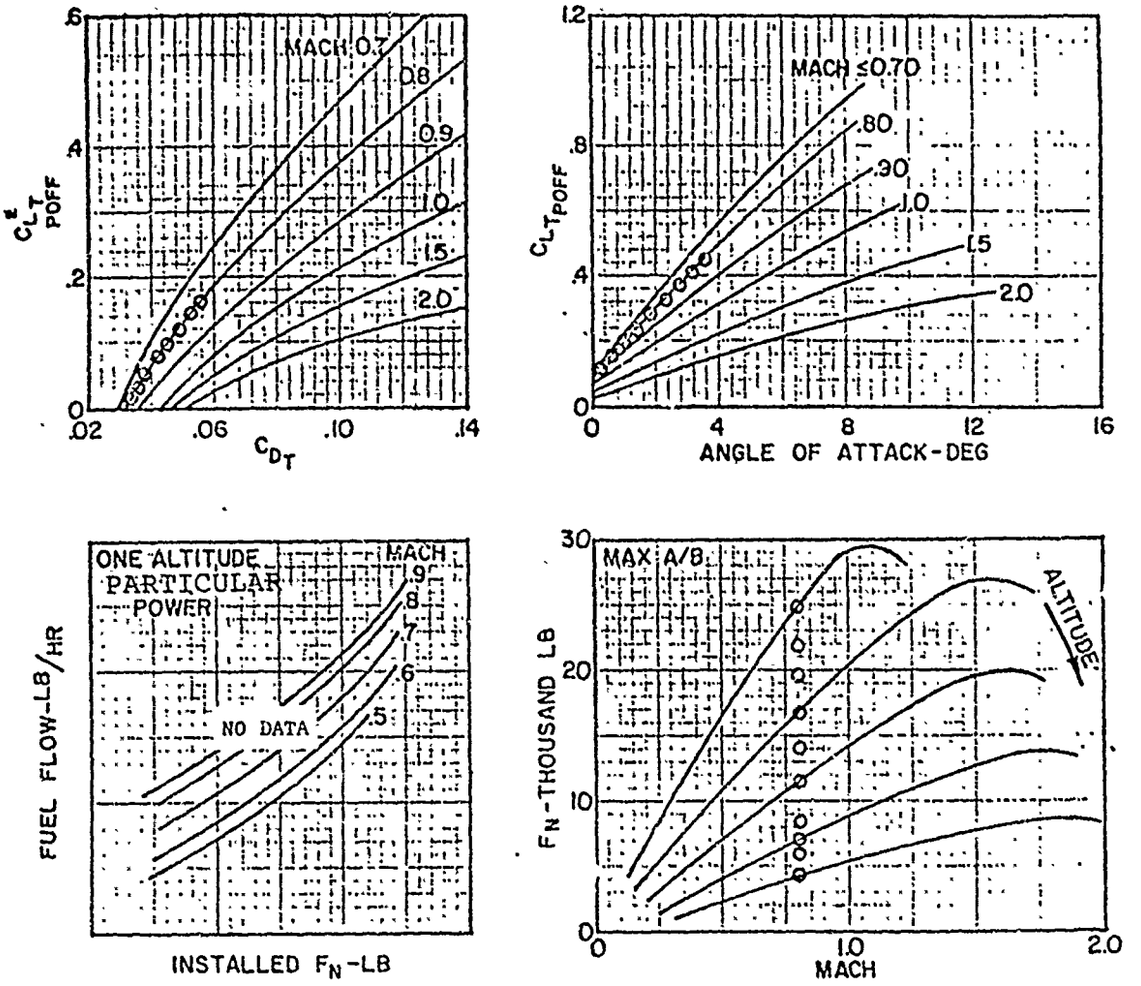

FIG. 3-16: TYPICAL DATA OUTPUT FROM CONSTANT MACH CLIMBS

guideline, since the rate will obviously change for various flight conditions. Additionally, the maneuver need not be carried to buffet onset or limit g,since buffet obviously affects accelerometer readings, hence, data quality. A smooth maneuver performed to 3 g provides much better data than a rapid, jerky maneuver to 5, 6, or 7 g s. The Mach should be maintained closely, trading-off alticude for airpseed if required. As a general guideline, the Mach number should be maintained within ±0.03. Typical data output for the indirect approach of obtaining performance data is summarized in figure 3-17.

Push-Over/Pull-Up

3.33 The push-over/pull-up maneuver is performed at or near a constant Mach number and is preceded by a stabilized point for the same reason as in the wind-up turn maneuver. Smooth application of load factor and pitch rate is very important. If the maneuver is done too quickly, high pitch rates and high pitch accelerations cannot be avoided. If the pitch rate is too low, unacceptable excursions in Mach and altitude cannot be avoided. Adequate pilot training in this maneuver is a prerequisite to useful data. A time history of a typical maneuver is presented in figure 3-18. The maneuver can be started by performing a smooth push-over or by pulling to a slight nose-high attitude, followed by a smooth push-over. During the push-over, the load factor generally should not be less than 0.0 to 0.5 g. A smooth pull-up is performed to target

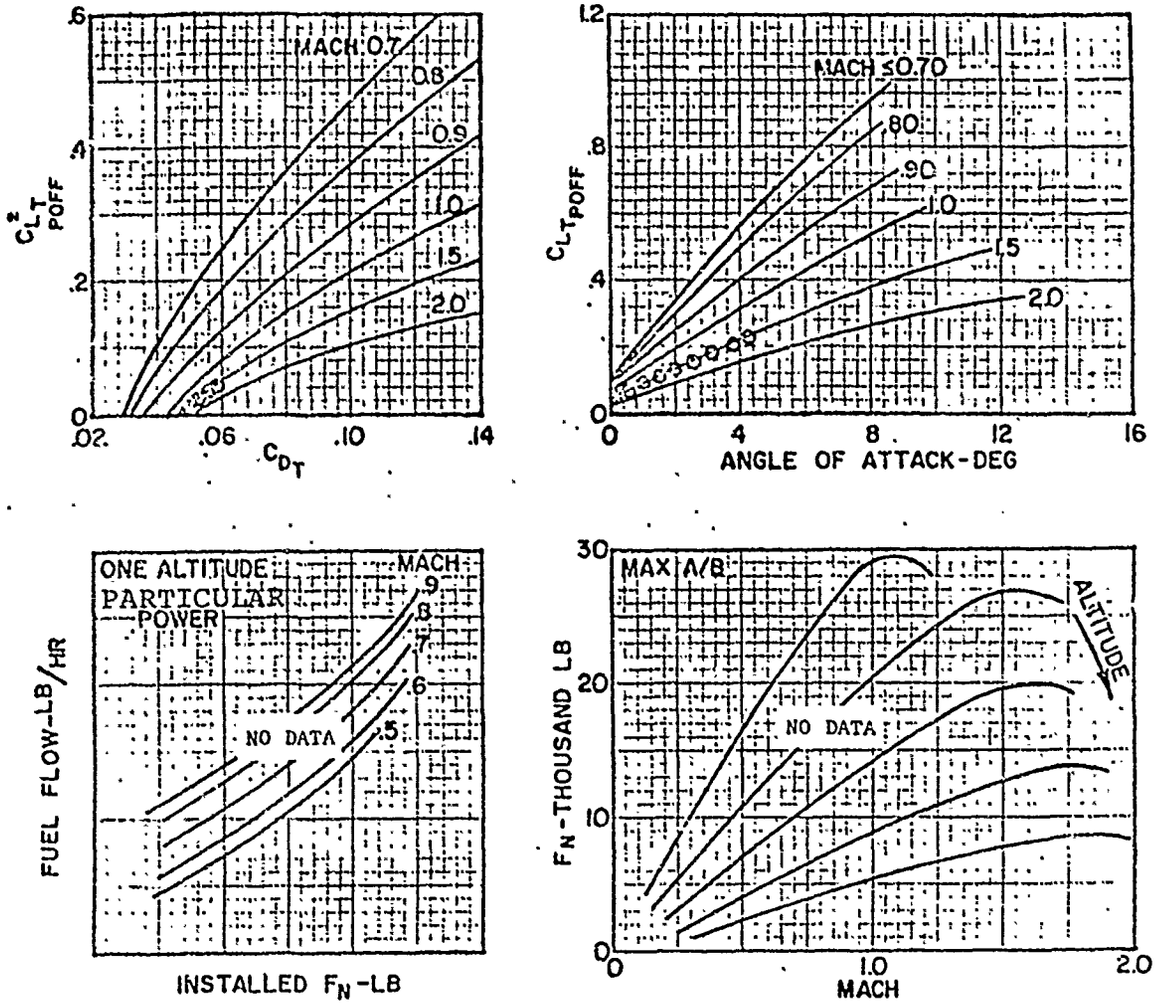

FIG. 3-17: TYPICAL DATA OUTPUT FROM A CONSTANT MACH WIND-UP TURN

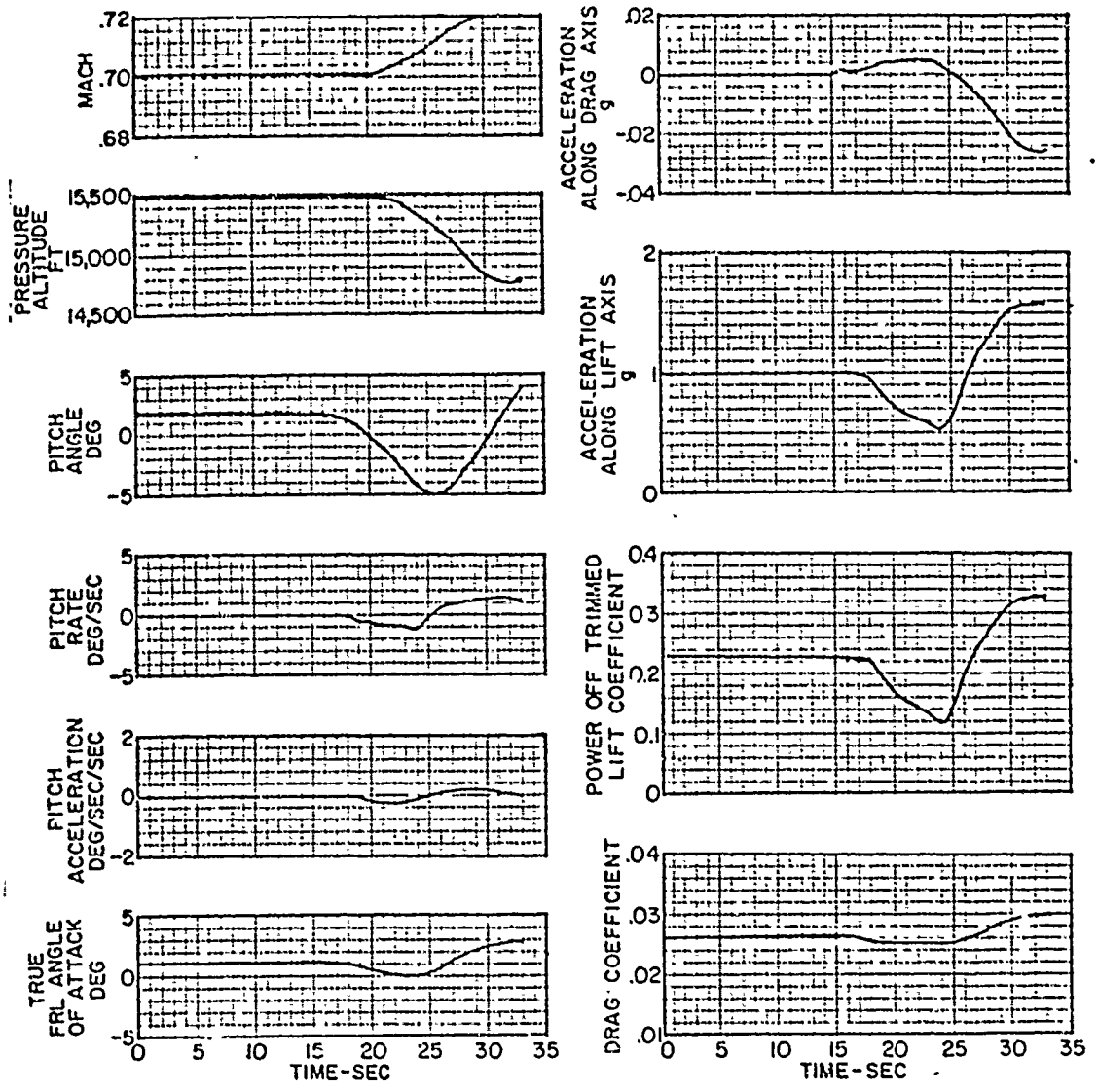

FIG. 3-18: TIME HISTORY OF A TYPICAL PUSH-OVER/PULL-UP MANEUVER

load factor, usually less than 2.0 g. The maneuver can be terminated or continued for another cycle; however, the aerodynamic data will be over the same range of values. In cases where the drag at zero lift is desired, smooth push-overs to zero g can be performed but require excellent pitch technique to maintain a constant Mach. Pitch rates less than 2 degrees/second are normally acceptable, while the acceptable Mach variation and altitude excursions are a function of the particular flight condition. Pitch rate effects are detailed in Chapter 2. Corrections for variations in Mach and altitude are detailed in Chapter 4. Note that the thrust setting for the initial trim point is maintained throughout the maneuver. The final data plot of the drag polar will verify the validity of each maneuver. Typical aerodynamic data output is summarized in figure 3-19.

Wind-Down Deceleration

3.34 These maneuvers include MIL or Max A/B wind-down decelerations either by the constant load factor constant altitude technique or by the constant deceleration rate constant attitude technique. In addition to supplying aerodynamic data, these maneuvers are used in conjunction with level acceleration to generalize thrust limited turning performance. The deceleration rate in the latter technique should be kept at 1 to 2 knots per second. Obviously, care must be taken in planning fuel management when conducting Max A/B decelerations, which are usually preceded by a Max A/B acceleration. The two maneuvers could easily require a total of 6 minutes at altitude

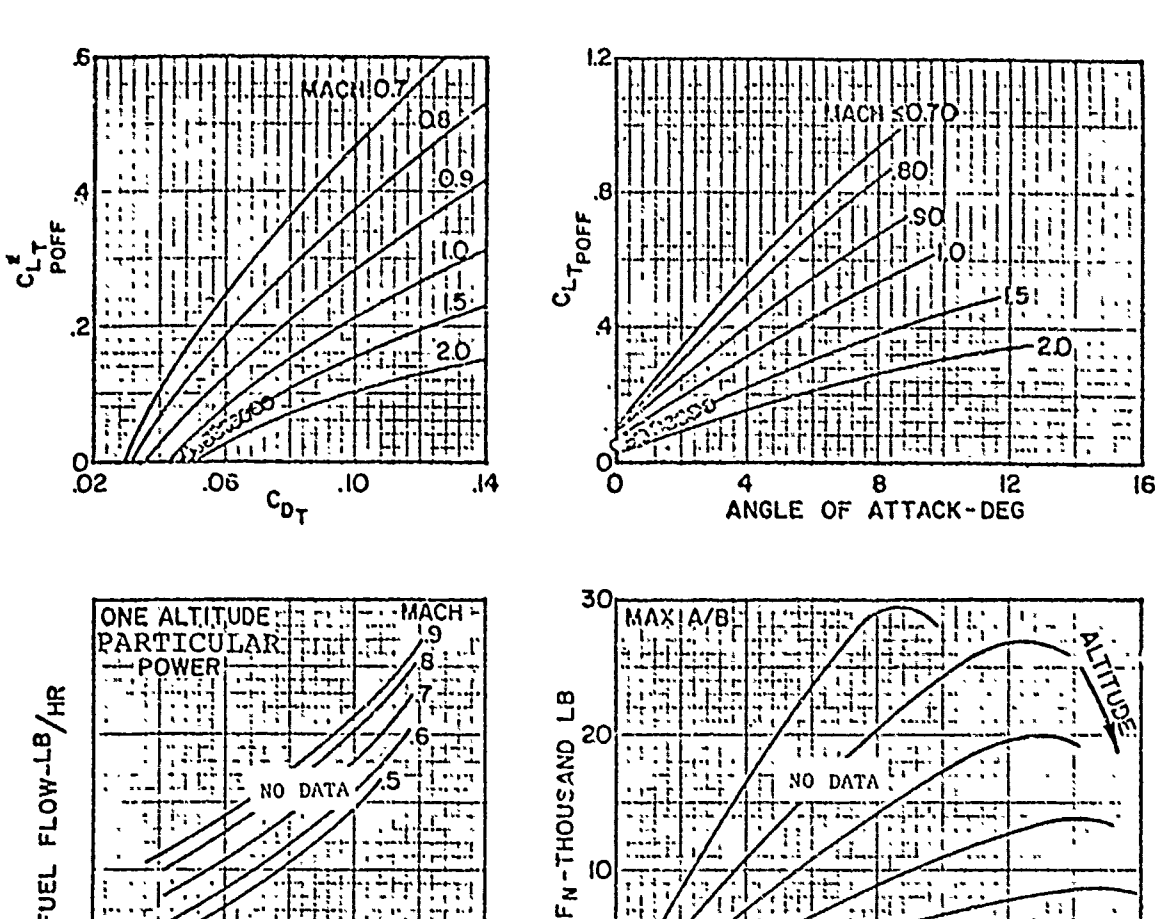

FIG. 3-19: TYPICAL DATA OUTPUT FROM A PUSH-OVER/PULL-UP MANEUVER

consuming nearly 1,200 pounds of fuel per minute per engine. At low altitude, the constraint may be the maximum load factor which is required to be held over an extended time period. It is not unlikely that a constant 5 g turn may have to be sustained for 2 to 3 minutes. Physiological factors being considered, the deceleration maneuver at low altitude may have to be done in parts, i.e., decelerate from V_{MAX} to some convenient Mach, terminate the maneuver, then accelerate back to the cut-off Mach and decelerate to V_{MIN} or another convenient cut-off Mach. Typical data yield for the indirect analysis procedure is presented in figure 3-20.

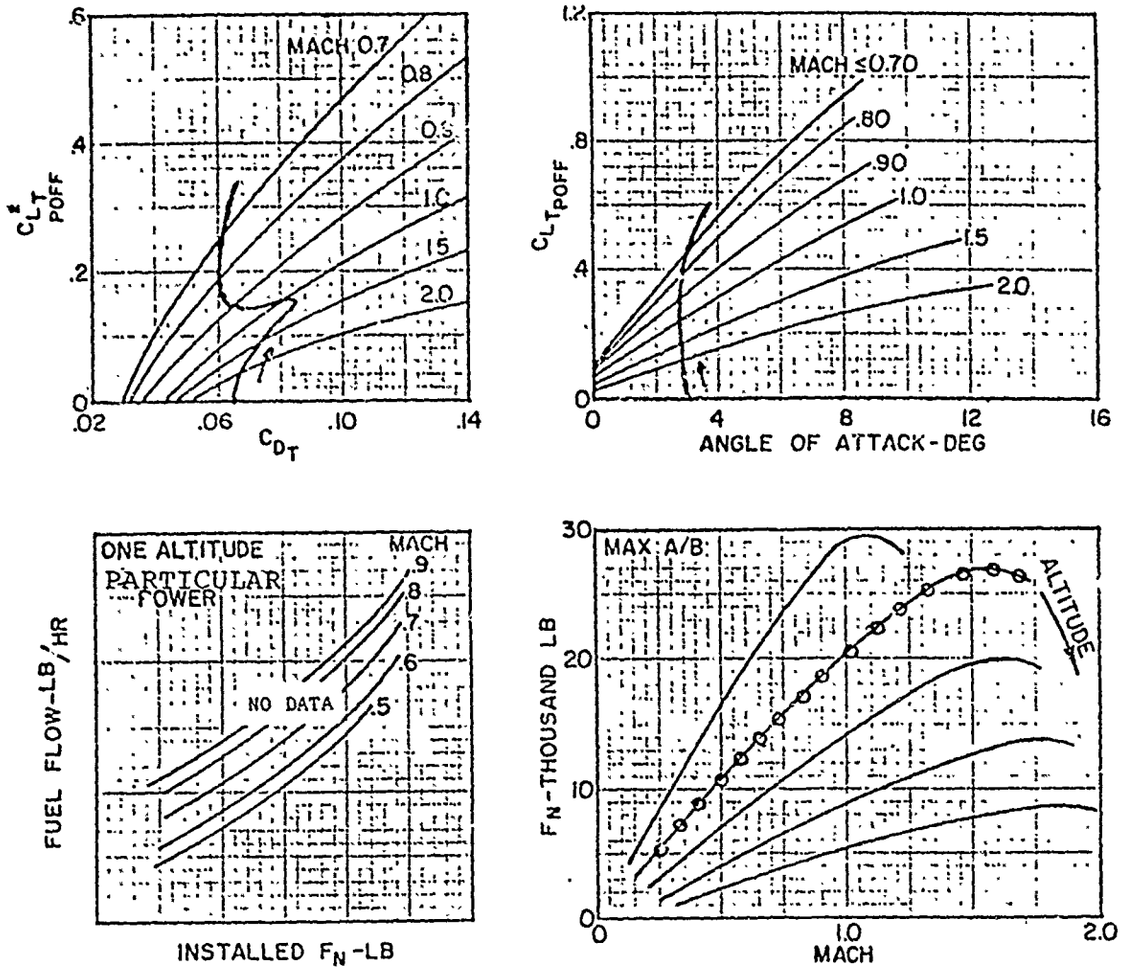

FIG. 3-20: TYPICAL DATA OUTPUT FROM A WIND-DOWN DECELERATION

3.35 Given the general trend of aerodynamic and propulsion data as obtained from the different maneuvers, the project team can consider a flight profile which will yield the maximum amount of data. Each project has different constraints and objectives which will provide the guidelines for maneuver selection. For instance, if only the drag increment of a group of stores was desired, it would not be necessary to do a full-blown performance evaluation. A subsonic trim point (below the drag rise) followed by a push-over/pull-up maneuver and wind-up turn will provide adequate results for comparison to a reference condition as depicted for the F-14A in figure 3-21. The drag analysis may be extended to include a constant Mach climb, level accelerations at one or two altitudes, and wind-up turn maneuvers at several Mach numbers.

THE OPTIMUM FLIGHT PROFILE

3.36 With each of the maneuvers defined in its relation to the mathematical model, it is now possible to combine these maneuvers in such a way as to define certain portions of the model. For example, climbs at .7M and .8M combined with descents at .75M and .85M will define a major portion of the drag polar from .7M to .85M, or accelerations at several altitudes will define the thrust available. The most efficient method of obtaining data from these maneuvers is to link them in consecutive order of flight sequence, so that the pilot can smoothly translate from one maneuver to the next with minimum set-up time between maneuvers. This then is a definition of the optimum flight profiles. It is the linking of maneuvers in flight sequence, in such a manner as to obtain the maximum data yield contribution to the mathematical model in the minimum flight time. The concept can be further extended to include the sequencing of maneuvers to answer a specific performance problem. For example, mission profile alternatives where only certain portions of the envelope are explored with the aircraft both loaded and unloaded (expendable stores dropped) on the same flight.

3.37 Figure 3-22 will give an example of the optimum flight profile. It is based on the A-7D, but can be applied to any aircraft. The profile was constructed so as to yield the maximum performance data in the minimum flight time. In the A-7D tested, onboard instrumentation recording time was limited to 130 minutes

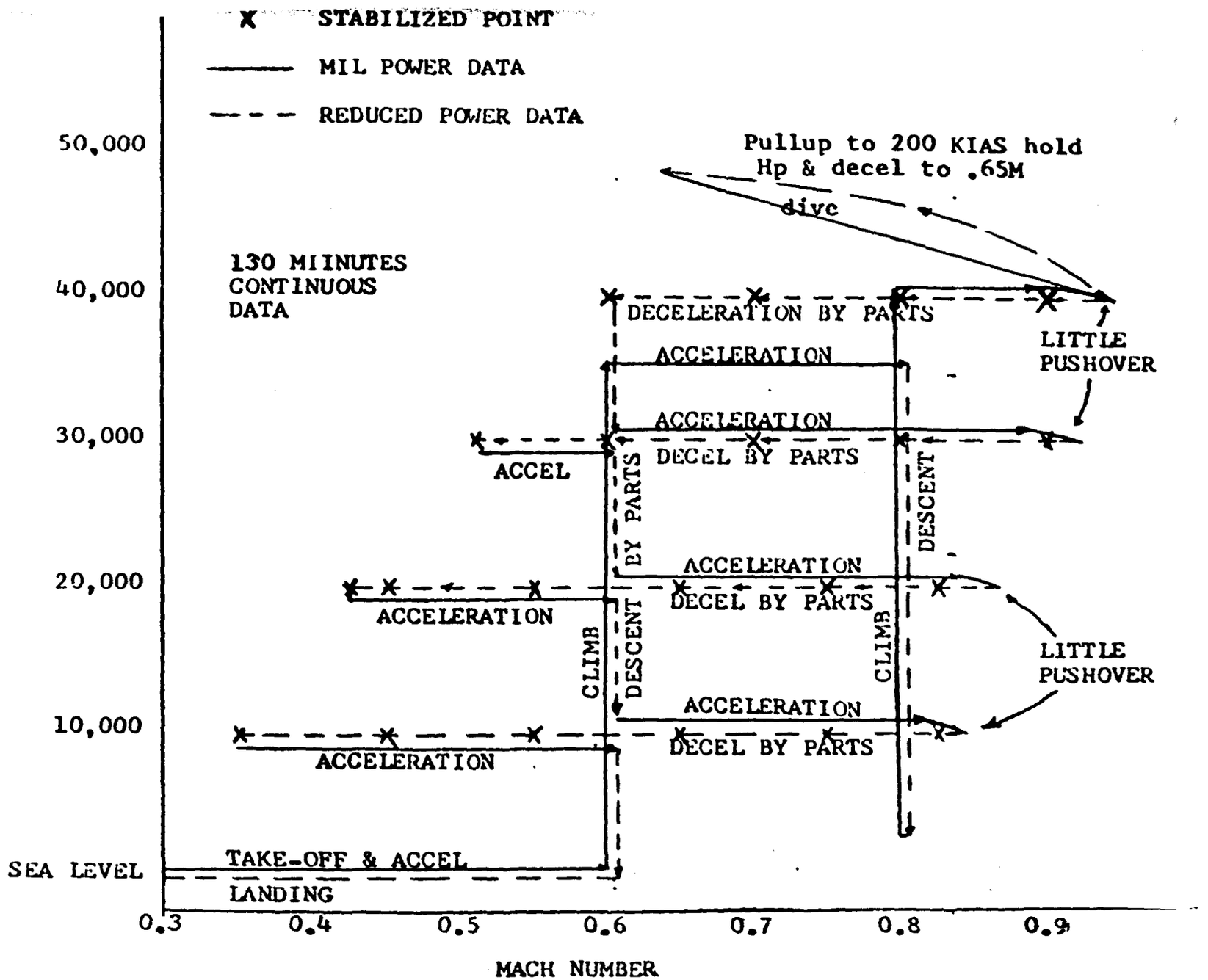

FIG. 3-22: TYPICAL OPTIMUM FLIGHT PROFILE

and prevented the investigation of the maneuvering flight regime. With longer recording times available and an adequate supply of fuel onboard, the stabilized point data could be followed by a roller-coaster and wind-up turn. It can be noted that all maneuvers in the profile will yield useful data, and therefore, the instrumentation need only be turned on at take-off and turned off at landing. This allows the pilot to concentrate more fully on the execution of the profile. A detailed discussion of optimum flight profiles is given in Chapter 8, together with additional examples of developed profiles.

OPTIMUM FLIGHT PROFILE - DATA YIELD

3.38 An attempt will be made to analyze the data yield of the optimum flight profile as given in figure 3-22. The data will be the same as that given in the appropriate section for each maneuver.

DRAG POLAR

3.39 The drag polar data yield will be similar to that shown in figure 3-23. The power effects shown on the data may or may not be present. The stabilized point data are used as the anchor points for curve fairings.

THRUST AVAILABLE

3.40 The thrust available data yield will be similar to that shown in figure 3-24. Several gaps appear in the thrust available data (high and low altitude), and these may be filled in by subsequent data or cross plotting and use of the family shapes for the curves.

OTHER CURVES

3.41 In addition to the data presented, stabilized points are used for the thrust fuel flow relation and thrust rpm data, and all data points are placed on the lift curve. The stabilized points are additionally used for the determination of angle of

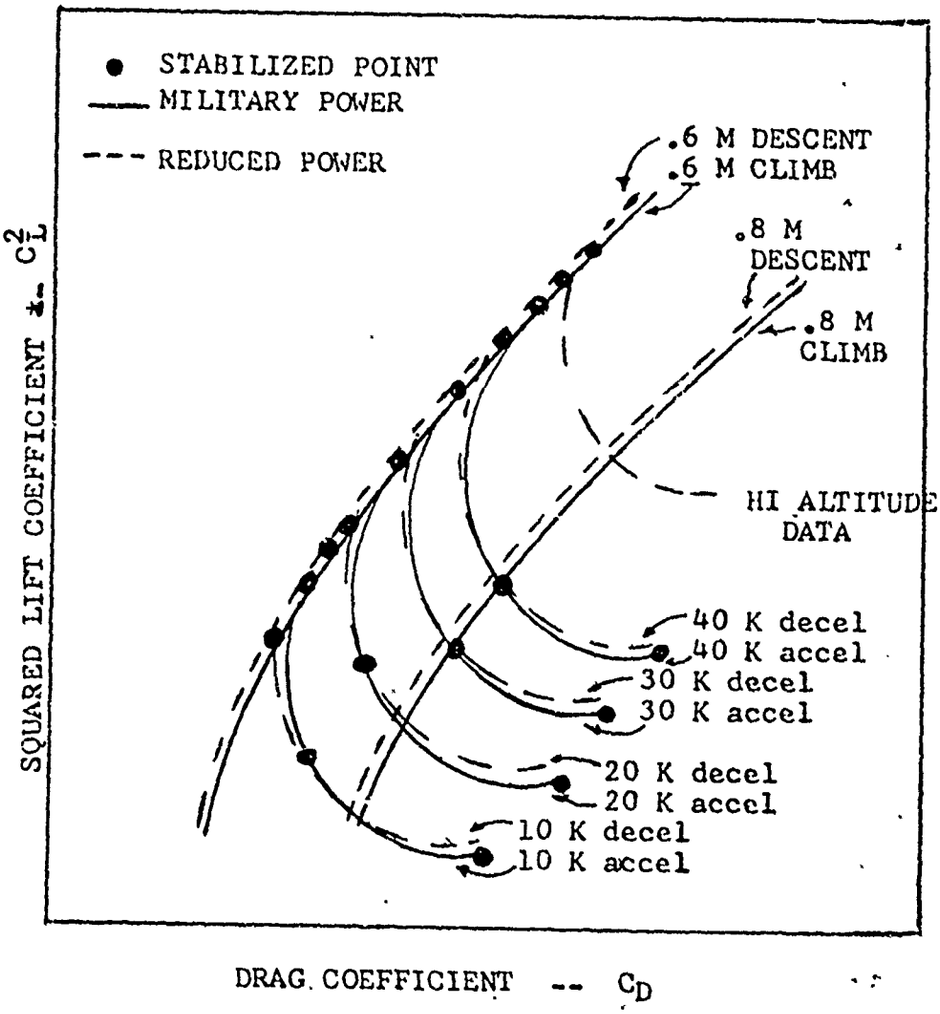

FIG. 3-23: OPTIMUM FLIGHT PROFILE
DRAG DATA YIELD

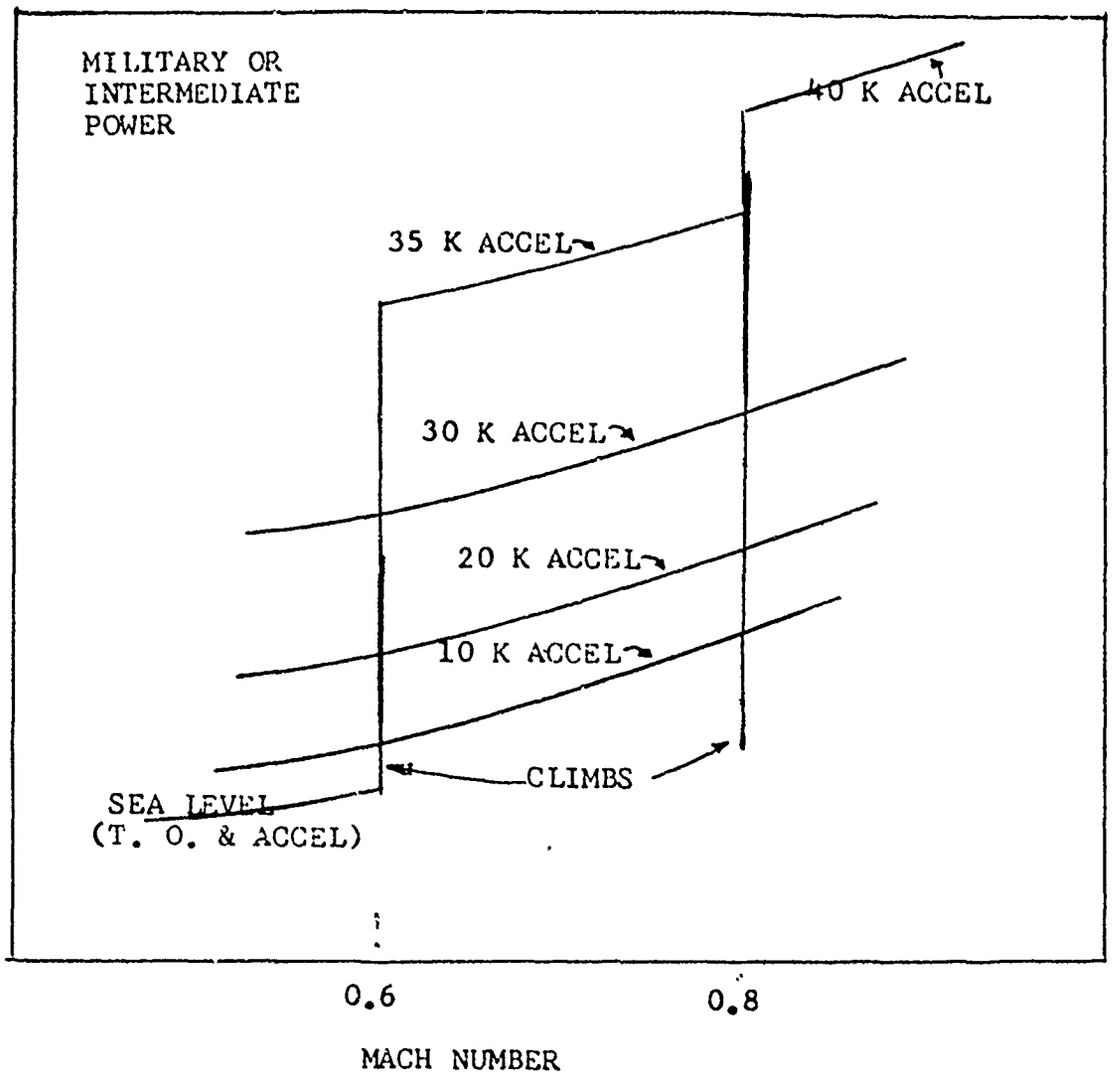

FIG. 3-24: THRUST AVAILABLE DATA YIELD FROM THE OPTIMUM FLIGHT PROFILE

attack upwash and tail trim. If a pace plane were available, the stabilized points could additionally be used for airspeed calibration although the time consumed at each point would probably increase to 2 or 3 minutes to allow both aircraft to stabilize.

PROGRAM PLANNING

3.42 When planning a program utilizing the mathematical model concept with the accelerometer methods, it is important to consider what data is already available. If adequate installed engine data is available, fuel flow modeling may be considered. Additionally, if large amounts of flight data are available in certain portions of the flight envelope, it may be advantageous to only verify the data in this region, and completely document data in the portions of the flight envelope sparsely explored. Additionally, data obtained previously can be used to verify or invalidate certain simplifying assumptions. Such questions as the following can be answered:

- Is the drag polar independent of Mach number below .7M?
- Is the drag rise with Mach number independent of C_L?
- Do trim drag and power effects become large enough to require correcting?

If the answers to the above questions are known, the flight time to obtain performance can possibly be further reduced.

3.43 Finally, each flight should be mapped out to ascertain whether enough data has been generated to answer the basic performance problems. In programs combined with stability and control evaluations, maneuvers being flown for stability data may have value as performance data. Certain trim points prior to the

execution of stability and control maneuvers, climbs, and descents, as well as accelerations and decelerations between data points can all yield useful performance data. Some maneuvers (such as wind-up turns) may be common to both types of evaluation programs.

CONCLUDING REMARKS TO CHAPTER 3

3.44 Mathematical modeling offers an effective means of predicting aircraft performance. Either thrust modeling or fuel flow modeling techniques can be employed. Basic maneuvers, such as climbs and acceleration, can be used to generate the necessary components of the mathematical model from flight test data.

REFERENCES TO CHAPTER 3

3-1. USAF Aerospace Research Pilot School, FTC-T1H-70-1001, Edwards AFB, "Performance," Unclassified, May 1970.

3-2. Boeing Company, D6-1420, "Jet Transport Performance Methods," Unclassified, May 1969.

3-3. USAF, Edwards AFB, 6273, "Flight Test Engineering Handbook," by R.M. Herrington, et el, Unclassified, Jan 1966.

3-4. U.S. Naval Test Pilot School, Patuxent River, Maryland, "Aircraft and Engine Performance," by F.S. Peterson, et al, Unclassified, 1 May 1962.

3-5. GAC Report ADR-07-01-70.1, "Development of Dynamic Methods of Performance Flight Testing," Unclassified, Aug 1970.

3-6. Air Force Flight Test Center, Report FTC-TD-71-1, "Theory of the Measurement and Standardization of In-Flight Performance of Aircraft," by E. Dunlap, Unclassified, April 1971.

3-7. Flight Test Division NATC Technical Memorandum 5-73, "Developing the Airplane Drag Polar and Lift Slope Curve From Flight Test Data Using Onboard Accelerometers," by W.R. Simpson, Unclassified, 15 May 1973.

3-8. Flight Test Division NATC Technical Memorandum 1-75, "Test Procedures for the Indirect Approach of Determining Aircraft Performance," W.M. Branch, Unclassified, 9 Jan 1975.

THE ACCELEROMETER METHODS OF DETERMINING AIRCRAFT PERFORMANCE (DYNAMIC PERFORMANCE TESTING)

CHAPTER 4

SECONDARY AND ANALYSIS EQUATIONS

THE ACCELEROMETER METHODS OF DETERMINING AIRCRAFT PERFORMANCE (DYNAMIC PERFORMANCE TESTING)

CHAPTER 4

SECONDARY AND ANALYSIS EQUATIONS

SUMMARY OF CHAPTER 4

4.1 Secondary and analysis equations are presented for the determination of aircraft lift and drag. Secondary and analysis equations are those equations used to standardize to a given set of conditions, or separate certain effects in the data. Where possible, derivations are presented and methods are given. A summary of corrective equations is given for those who do not wish to go through the development. This chapter is intended primarily to supplement the primary equation development of Chapter 2, and the mathematical modeling concepts of Chapter 3.

INTRODUCTION TO CHAPTER 4

4.2 In applying the mathematical modeling concept to the data taken by the accelerometer methods, or any other methods, it is often convenient to standardize to a given set of conditions. This set of standard conditions is normally dictated by the analysis to be used. For example, when determining the drag polar at a given Mach number and wing sweep combination, it would be convenient if all data were taken at the same cg location and every point were at the exact same Mach number and wing sweep. Under such conditions, each data point will be of equal importance to the curve shape, and the analysis will not be complicated by small deviations in Mach number, wing sweep, or cg position. Unfortunately, it is very difficult to maintain such a rigid set of requirements, in that the cg in most aircraft moves with fuel consumption and it is very difficult for the pilot to set a given wing sweep exactly, or to hold an exact Mach number under varying flight conditions. In a given set of flight data to be analyzed, the Mach number, wing sweep, and cg will invariably cover a range of values. For ease of analysis then, it will be convenient to standardize each data point to a given set of conditions.

4.3 In addition to standardizing to a given set of conditions, certain effects may introduce unwanted parameters in the problem, for example, the thrust effect on C_L or the tail mispositioning

which results in aircraft angular rates. When deriving a drag polar, the aerodynamic C_L is given as a function of the aerodynamic C_D, and non-aerodynamic terms (i.e., thrust) must be removed. Additionally, the trim drag or zero lift drag is a function of the aircraft geometry, and for a given configuration is a function of movable control surface positions. Such movable control surface positions will include rudders, ailerons, elevators, spoilers, maneuver flaps, etc. In the general case of spoilers, maneuver flaps, etc., each value will be associated with a different configuration. Rudders and ailerons are seen to have only a small effect and for level flight data are seldom misplaced from the zero force position by appreciable quantities. The zero force positions for these control surfaces are dictated by lateral and vertical cg movements which for most aircraft are small. When ailerons are used for roll control, small forces are usually all that is required, due to the large moment arm. For these reasons, corrections to drag polar data for these surfaces will be excluded from further discussion. The individual case must be the prime consideration. The elevators, or tail position is dictated by the longitudinal cg which may vary over a considerable distance, and the tail surface is a major contributor to the lift in many aircraft. It is, therefore, necessary to correct for tail position at each point to insure that trim drag effects are accounted for properly.

4.4 Summarizing, then, the data taken by accelerometers must be standardized for analysis purposes. Such standarization will include:

- Center of gravity (cg)
- Wing sweep
- Mach number
- Load factor
- Standard atmospheric conditions.

In addition, the drag and lift data must be corrected for:

- Thrust effects
- Pitch rate trim effects
- Roll rate trim effects (tail used for roll control).

SYMBOLS

4.5 The following symbols are used in Chapter 4.

Symbol	Definition	Common Units	Metric Units
C_D	Drag coefficient	none	(-)
C_f	Friction coefficient	none	(-)
C_L	Lift coefficient	none	(-)
cg	Center of gravity	length or % MAC	(%MAC)
D	Drag	lbs	(N)
F_g	Gross thrust	lbs	(N)
F_R	Ram drag (sometimes D_{RAM})	lbs	(N)
g	Acceleration of gravity	ft/sec^2	(M/sec^2)
h_r	Ram drag moment arm	ft	(M)
h_p	Pressure altitude	ft	(M)
i_s	Tail incidence	deg	(deg)
ℓ_t	Tail length to cg	ft	(M)
L	Lift	lbs	(N)
M_{THRUST}	Thrust moment	ft-lbs	(N-M)
M	Mach number	none	(-)
n_x	Longitudinal load factor	g	(g)
n_z	Normal load factor	g	(g)
P_a	Ambient pressure	lbs/ft^2	(N/M^2)
q	Dynamic pressure	lbs/ft^2	(N/M^2)
R_N	Reynolds number	none	(-)
S	Wing area	ft^2	(M^2)
T_a	Ambient temperature	^oF	(^oC)

Symbol	Definition	Common Units	Metric Units
S_{wet}	Wetted area	ft^2	(M^2)
W	Weight	lbs	(Kg)
Y_t	Gross thrust moment arm	ft	(M)

Greek Symbols	Definition	Common Units	Metric Units
α	Angle of attack	deg	(deg)
γ	Flight path angle	deg	(deg)
Δ	Increment	deg	(deg)
δ_e	Elevator position	deg	(deg)
θ	Pitch attitude	deg	(deg)
$\dot{\theta}$	Pitch rate	deg/sec	(deg/sec)
Λ	Wing sweep	deg	(deg)
τ	Thrust inclination	deg	(deg)
τ_t	Tail effectiveness parameter	-	(-)
∂	Partial derivative		
$\left.\frac{\partial(1)}{\partial(2)}\right\|_{(3)=(4)}$	Partial derivative of (1) with respect to (2) at (3)=(4).		

Subscripts	Definition
ALT	Altitude
cg	Center of gravity
e	Elastic
eff	Effective
L	Lift, Left
LF	Load factor

Subscripts	Definition
M	Mach number
P.E.	Power effect
P.O., P_{off}	Power off
P.T.	Pitch trim
R	Right
R.T.	Roll trim
S	Standard
T	Tail, trim
t	Test
TPO	Trim power off
TEMP	Temperature
W	Wing
Λ	Wing sweep
1, 2, etc.	Condition state

Others	
$\therefore$	Therefore
$\hat{\ }$ or $\dot{\ }$	Wind tunnel or predicted
$\triangleq$	Defined as
f(x)	Function of x

CORRECTIONS TO BE MADE TO ALL DATA

4.6 For the purposes of analysis, the aerodynamic data must be corrected as given in the introductory paragraph for:

- Thrust effects
- Pitch rate trim effects
- Roll rate trim effects (tail used for roll control).

Each of these effects will be examined separately, and methods will be developed to correct for these effects. In each of the corrective procedures that follow, the basic method of approach is to treat the aerodynamic quantity as a first order Taylor series expansion about its function space. For example:

$$C_L = f(\alpha, M, \dot{\theta}, n_z, \ldots)$$

then

$$C_L = C_{L_0} + \frac{\partial C_L}{\partial \alpha} \Delta\alpha + \frac{\partial C_L}{\partial M} \Delta M + \frac{\partial C_L}{\partial \dot{\theta}} \Delta\dot{\theta} + \frac{\partial C_L}{n_z} \Delta n_z \ \ldots$$

with higher order terms neglected. The problem is then reduced to a determination (either by flight test or by estimated data) of the partial derivatives. Certain parameters, where explicit forms exist, will be corrected by the derived relationships.

4.7 From the classical definition of lift coefficient:

$$C_L = \frac{n_z W}{qS} \quad . \tag{4-1}$$

This is the effective lift coefficient of the system and includes all forces (aerodynamic and others) acting on the airframe. This parameter is referred to as the effective lift coefficient $\left(C_{L_{eff}}\right)$.

$$C_{L_{eff}} = \frac{n_z W}{qS} \quad . \tag{4-1a}$$

It has been shown in equation 2-7 of Chapter 2 that the aerodynamic lift is given by:

$$L = n_z W - F_g \sin(\alpha + \tau) \quad . \tag{2-7}$$

This removes the thrust effect on the lift term by removing the thrust component in the lift direction. This aerodynamic lift is referred to as the power-off lift, since the power component has been removed. So that:

$$C_{L_{POFF}} = \frac{n_z W - F_g \sin(\alpha+\tau)}{qS} \quad . \tag{4-2}$$

Figure 4-1 shows that this component is not the only contributor to the power-off situation.

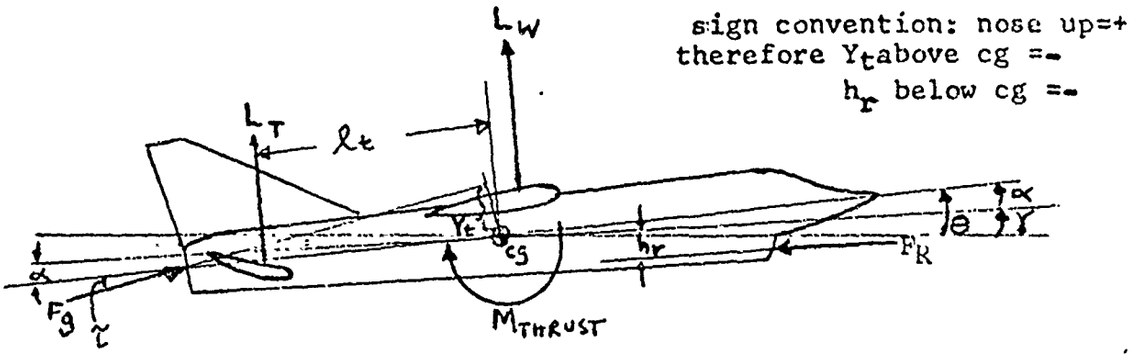

FIG. 4-1: AIRCRAFT MOMENT BALANCE DIAGRAM

4.8 It can be seen from figure 4-1, that in order to completely remove the thrust effect from the problem, the associated moments of thrust, as well as the force vectors, must be removed. As in flight, when the pilot removes an imbalance of moments by deflecting a control surface, the aircraft must be mathematically brought to the "trimmed" condition. The moment about the cg created by the thrust vectors, F_g and F_R (where F_R is taken to be ram drag, spillage drag, and any other forces assigned to the production of thrust), is given by:

$$\Delta M_{THRUST} = F_g Y_t + F_R h_r \text{ (nose down)}. \tag{4-3}$$

In order to counteract this moment, an incremental lift at the tail must be applied, such that:

$$\Delta L_{T_t} = F_g Y_t + F_R h_r \tag{4-4}$$

or

$$\Delta C_{L_{P.E.}} = \frac{F_g Y_t + F_R h_r}{\ell_t q S} . \tag{4-5}$$

The sign of the ΔC_L is such that a nose-up moment is created on the tail, and is negative for the situation shown. Consequently, the trimmed power-off lift coefficient $\left(C_{L_{TPO}}\right)$ is given by:

$$C_{L_{TPO}} = C_{L_{PO}} + \Delta C_{L_{P.E.}} . \tag{4-6}$$

4.9 It should be noted here that Y_t is a function of aircraft cg and airframe geometry, while h_r is also a function of angle of attack. This stems from the assumption that the ram drag acts along the flight path. A more complete detailed analysis of these vectors, and an expansion to the case of lateral offset including methods for determining the values of h_r and Y_t are included in reference 4-1.

4.10 It is perhaps best to review the physical meanings of the above equations. Equation 4-1 gives the effective lift coefficient of the airframe including all thrust vectors and moments. Equation 4-2 gives the aerodynamic-only lift coefficient of the airframe (thrust vector removed), while equation 4-6 gives the equivalent trimmed aerodynamic lift coefficient with no power. From equations 4-2 and 4-5, equation 4-6 can be rewritten as:

$$C_{L_{TPO}} = \frac{n_z W - F_g \sin(\alpha+\tau)}{qS} + \frac{F_g Y_t + F_R h_r}{\ell_t qS} , \qquad (4-7)$$

with the power effects completely removed from the system.

4.11 The test drag coefficient corresponds to the test tail incidence position, or the $C_{L_{P.O.}}$ from equation 4-2. It is now necessary to adjust the drag coefficient by trimming the tail to the power-off condition corresponding to equation 4-7. The procedure for correcting the drag coefficient is not straightforward and depends upon wind tunnel data available for the aircraft

being tested. Also, the effects of the trim drag to the overall aircraft drag may be small and the correction may be omitted (for instance, if the values of Y_t and h_r are significantly small). The procedures below are based on typical wind tunnel data available, and may have to be modified depending on the data at hand.

4.12 The aerodynamic or wind tunnel data assumed available is shown in figures 4-2, 4-3, and 4-4. For a given Mach number, angle of attack combination, the $\frac{\partial i_s}{\partial C_L}$ can be obtained from figure 4-2. The increment of tail required to trim out the thrust moment can be obtained by combining this partial derivative with equation 4-5 as follows:

$$\Delta i_{s_{P.E.}} = \frac{\partial i_s}{\partial C_L} \Delta C_{L_{P.E.}} \quad . \tag{4-8}$$

For symmetrical tails, in the range below tail stall, the data may be the same for all values of α, assuming $\Delta i_s = \Delta \alpha_{tail}$. For small delta tail increments, only small errors will be introduced using predicted data. Utilizing the predicted data or wind tunnel data will be signified by $\hat{(\ )}$. Since predicted data is being used, it will be necessary to generate predicted C_Ls for the given conditions, such that:

$$\left(\hat{C}_{L_{P.O.}}\right) = f\left(M, \alpha_t, i_{s_{test}}\right) \tag{4-9}$$

and

$$\left(\hat{C}_{L_{TPO}}\right) = f\left(M, \alpha_t, i_{s_{test}} + \Delta i_{s_{p.e.}}\right) \quad , \tag{4-10}$$

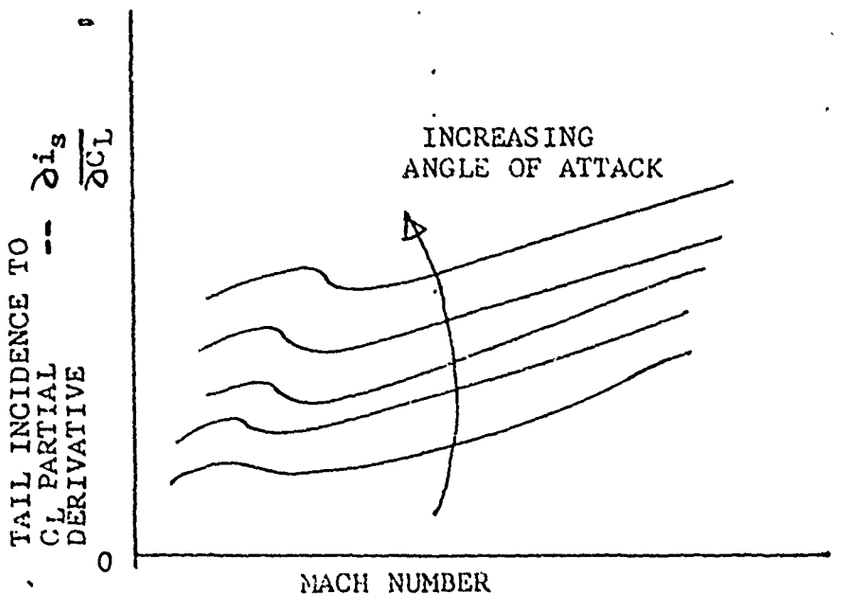

FIG. 4-2: TYPICAL AERODYNAMIC OR WIND TUNNEL TAIL EFFECTIVENESS DATA

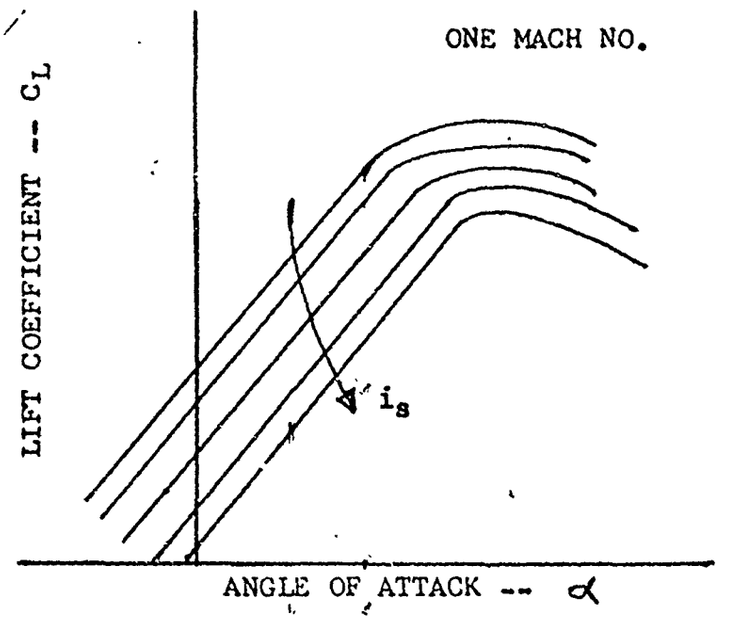

FIG. 4-3: TYPICAL AERODYNAMIC OR WIND TUNNEL TRIMMED LIFT DATA

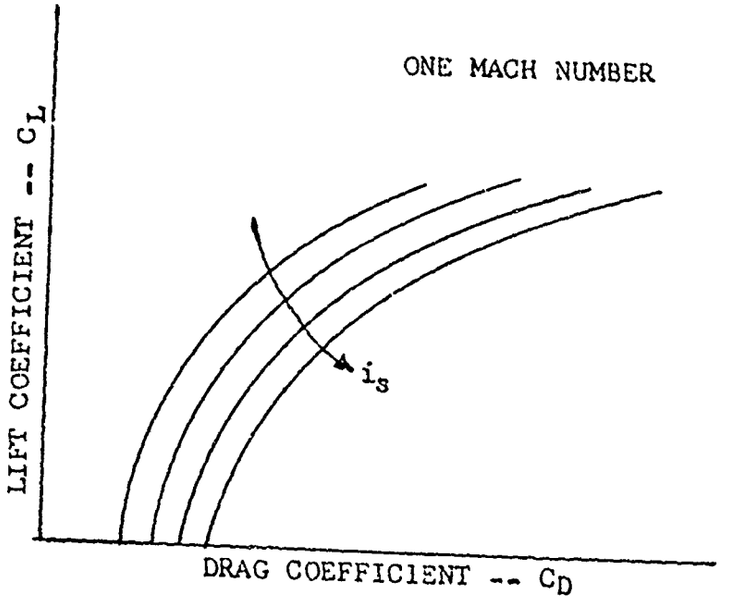

FIG. 4-4: TYPICAL AERODYNAMIC OR WIND TUNNEL DRAG POLAR

as taken from figure 4-3. These C_L values will be used together with figure 4-4 to generate C_D values. In this manner, figure 4-4 is entered with the predicted values, such that:

$$\left(\hat{C}_{D_{P.O.}}\right) = f\left(M, \left(\hat{C}_{L_{P.O.}}\right), i_{s_{test}}\right) \tag{4-11}$$

and

$$\left(\hat{C}_{D_{TPO}}\right) = f\left(M, \left(\hat{C}_{L_{POT}}\right), i_{s_{test}} + \Delta i_{s_{P.E.}}\right) , \tag{4-12}$$

and finally, the drag increment created by trimming out thrust moments is given by the difference between equations 4-11 and 4-12 as:

$$\Delta C_{D_{P.E.}} = \left(\hat{C}_{D_{P.O.}}\right) - \left(\hat{C}_{D_{TPO}}\right) , \tag{4-13}$$

and the power corrected, C_D , is given as:

$$C_{D_{TRIM}} = C_{D_{test}} + \Delta C_{D_{P.E.}} , \tag{4-14}$$

or from equation 3-3 of Chapter 3:

$$C_{D_{TRIM}} = \frac{F_n - W(n_x)}{qS} + \Delta C_{D_{P.E.}} \tag{4-15}$$

combining with equation 2-3 of Chapter 2:

$$C_{D_{TRIM}} = \frac{F_g \cos(\alpha+\tau) - F_R - W(n_x)}{qS} + \Delta C_{D_{P.E.}} . \tag{4-16}$$

Again, only negligible inaccuracies are introduced by using predicted data for small corrections.

PITCH RATE TRIM CORRECTION

4.13 Figure 4-5 shows the meaning of the pitch rate trim correction. For a given α, M combination, the aircraft pitch rate will be created by an imbalance of moments created by tail mispositioning from trimmed flight. The first step in the corrective process is to determine the tail mispositioning $\left(\Delta i_{s_{P.E.}}\right)$. Both theoretical and flight test methods are available, and both will be reviewed.

PITCH RATE TRIM CORRECTION (THEORETICAL)

4.14 The pitch rate trim correction to elevator position can be derived through the use of the stability and control equations for an aircraft in both the pull-up and level turn. For the pull-up (assumed constant α):

$$\frac{d\theta}{dt} = \frac{g(n_z-1)}{V_t} = \frac{d\gamma}{dt} \quad , \tag{4-17}$$

and for the level turn:

$$\frac{d\theta}{dt} = \frac{g}{V_t}\left(n_z - \frac{1}{n_z}\right) \quad . \tag{4-18}$$

A complete derivation of the above relationships is presented in reference 4-2, "Jet Transport Performance Methods," and reference 4-3, "TPS Stability and Control Manual," and these derivations will not be repeated here.

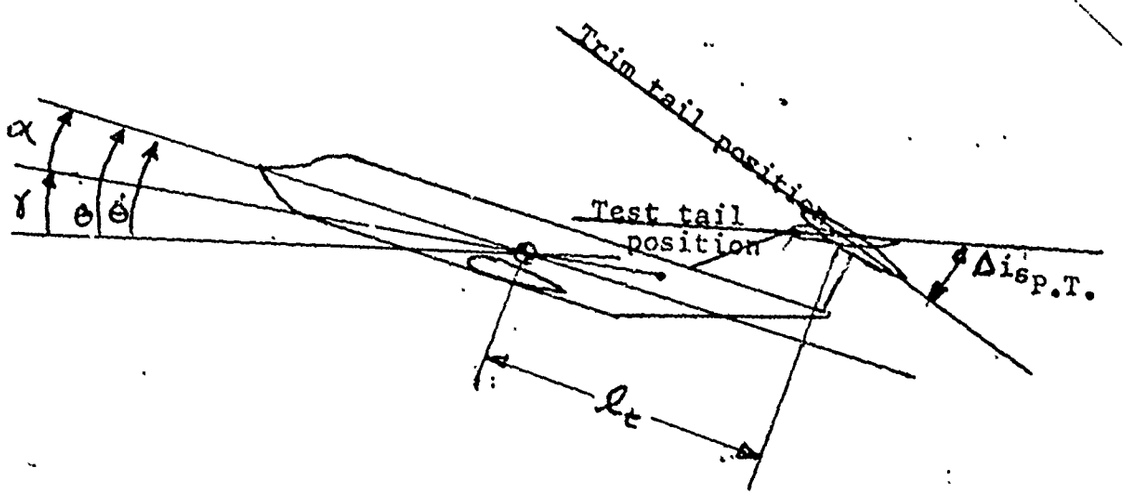

FIG. 4-5: PITCH RATE TRIM DIAGRAM

4.15 The angular rotation of the airplane in steady state maneuver imparts a change in flow around the stabilizer, and therefore, a change in angle of attack for the tail. This change creates a moment in such a direction as to damp the rotation. The change in angle of attack at the tail is:

$$\Delta\alpha_{tail} = \frac{(d\theta/dt)\ell_t}{V_t} \quad , \tag{4-19}$$

and the effective change in angle of attack at the tail due to the necessary change in elevator position is:

$$\Delta\alpha_{tail} = \left(\frac{d\alpha_{tail}}{d\delta_e}\right)\delta_e \quad . \tag{4-20}$$

The derivative $\frac{d\alpha_{tail}}{d\delta_e}$ is called the tail effectiveness parameter (τ_t) and for unit horizontal tails is equal to unity. For tails with elevators, appropriate methods of determining this parameter are given in reference 4-12. Thus,

$$\delta_e \text{ required} = \frac{(d\theta/dt)\ell_t}{(d\alpha_{tail}/d\delta_e)V_t}\,(57.3) \text{ in medians, where} \tag{4-21}$$

$$\frac{d\alpha_{tail}}{d\delta_e} = \tau_t \quad . \tag{4-22}$$

For lack of a bet er criterion for judging the damping of the rest of the aircraft, the damped tail position required is increased by 10 percent, so that:

$$\delta_{e_{\text{required damped}}} = \frac{63(d\theta/dt)\ell_t}{\tau_t V_t} \quad , \tag{4-23}$$

and the elevator position in general can be written as:

$$\delta_e = \delta_{e_o} - \frac{C_{L_{T.P.O.}}}{(\partial C_M/\partial \delta_e)} \left(\frac{dC_M}{dC_L}\right)_{FIXED} - \frac{63(d\theta/dt)\ell_t}{\tau_t V_t} \quad . \tag{4-24}$$

One further simplification is made for using wind tunnel tail effectiveness data:

$$\frac{\left(\frac{dC_M}{dC_L}\right)_{FIXED}}{\frac{\partial C_M}{\partial \delta_e}} = \frac{\partial \delta_e}{\partial C_L} \quad , \tag{4-25}$$

or

$$\frac{\partial \delta_e}{\partial C_L} = \frac{\partial is}{\partial C_L} \quad , \text{ for slab tails with } \tau_t = 1 \text{ the equation}$$

reduces to:

$$i_s = i_{s_o} - \frac{C_{L_{TPO}}}{1}\left(\frac{\partial is}{\partial C_L}\right) - \frac{63\ell_t}{V_t} \frac{d\theta}{dt} \tag{4-26}$$

Equations 4-17 and 4-18 may now be substituted into equation 4-26 and differentiated with respect to load factor:

$$\left(\frac{di_s}{dn_z}\right)_{\text{pull-up}} = \left[- \frac{63g\ell_t}{V_t^2} - \frac{C_{L_{TPO}}}{n_z}\left(\frac{\partial is}{\partial C_L}\right) \right] \quad , \tag{4-27}$$

and

$$\left(\frac{di_s}{dn_z}\right)_{\text{turn}} = \left[- \frac{63g\ell_t}{V_t^2}\left(1 - \frac{1}{n_z^2}\right) - \frac{C_{L_{TPO}}}{n_z}\left(\frac{\partial is}{\partial C_L}\right) \right] . \tag{4-28}$$

Equation 4-27 can be applied to push-over pull-up or rollercoaster data, as well as accelerations, climbs, and other wings level data. Equation 4-28 can be applied to wind-up and wind-down turns. These equations are used only to infer the tail angle mispositioning due to pitch rate and must be converted to trim drag as discussed later.

PITCH RATE TRIM CORRECTION (FLIGHT TEST)

4.16 The theoretical equations above make several restrictive assumptions, and it is better, if possible, to use flight data to ascertain the tail mispositioning due to pitch rate. The method employed is to generate a tail incidence required to trim curve as shown in figure 4-6. The curve is generated by slow accelerations, decelerations, climbs, and stabilized points and must be corrected for power effects and standardized to a given cg or cg as a function of Mach number as discussed in a later section. Maneuvers used to generate this curve should be near zero pitch rate.

4.17 The first step is to pull a value of $i_{s_{TRIM}}$ for the given α,M combination. This value is then adjusted to the test cg of the data point, using the test $C_{L_{TPO}}$ and:

$$i_{s_{TRIM\ required}} = i_{s_{TRIM}} + \Delta i_{s_{cg}} . \qquad (4\text{-}29)$$

This correction is derived in the section under cg standardization. The tail mispositioning, then, is simply given by:

$$\Delta i_{s_{P.T.}} = i_{s_{test}} + \Delta i_{s_{P.E.}} - i_{s_{TRIM\ required}} . \qquad (4\text{-}30)$$

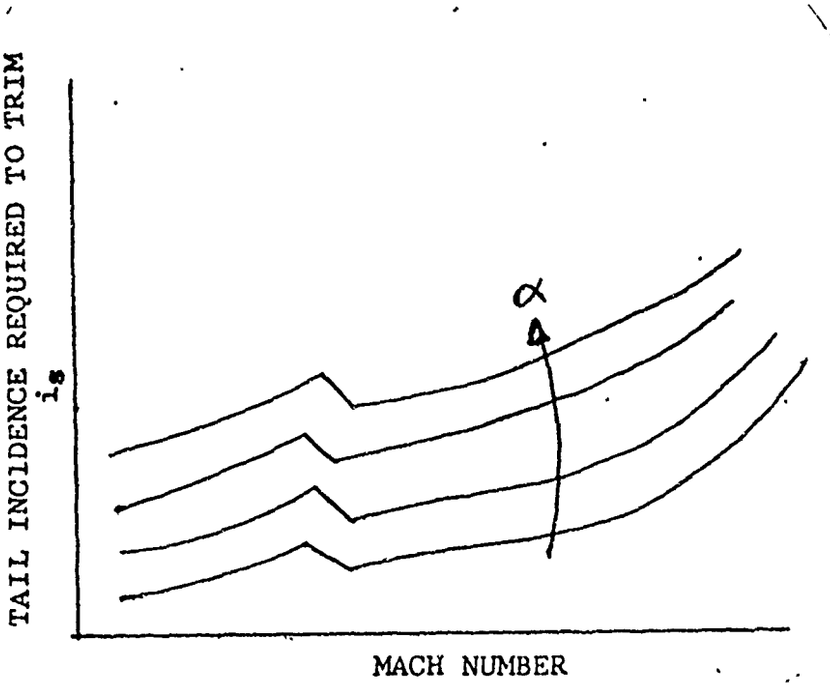

FIG. 4-6: TAIL INCIDENCE REQUIRED TO TRIM

With $\Delta i_{s_{P.T.}}$ defined by either theoretical or flight test methods, the trim drag and trim C_L can be defined as follows:

$$\left(\hat{C}_{L_{TPO}}\right) = f\left(M, \alpha_t, i_{s_{test}} + \Delta i_{s_{P.E.}}\right) \tag{4-31}$$

$$\left(\hat{C}_{L_{TPO}}\right)_{\theta=0} = f\left(M, \alpha_t, i_s + \Delta i_{s_{P.E.}} + \Delta i_{s_{P.T.}}\right) \tag{4-32}$$

as taken from figure 4-3. And:

$$\Delta C_{L_{P.T.}} = \left(\hat{C}_{L_{TPO}}\right) - \left(\hat{C}_{L_{TPO}}\right)_{\theta=0} \tag{4-33}$$

$$\left(C_{L_{TPO}}\right)_{\theta=0} = C_{L_{TPO}} + \Delta C_{L_{P.T.}} \quad . \tag{4-34}$$

The trim drag contribution is obtained from figure 4-4 as:

$$\left(\hat{C}_{D_{TPO}}\right) = f\left[M, \left(\hat{C}_{L_{TPO}}\right), i_{s_{test}} + \Delta i_{s_{P.E.}}\right] \tag{4-35}$$

and

$$\left(\hat{C}_{D_{TPO}}\right)_{\theta=0} = f\left[M, \left(\hat{C}_{L_{TPO}}\right)_{\theta=0}, i_{s_{test}} + \Delta i_{s_{P.E.}} + \Delta i_{s_{P.T.}}\right] \quad , \tag{4-36}$$

with the change in trim drag given by:

$$\Delta C_{D_{P.T.}} = \left(\hat{C}_{D_{TPO}}\right) - \left(\hat{C}_{D_{TPO}}\right)_{\theta=0} \tag{4-37}$$

and

$$C_{D_{TRIM,\theta=0}} = C_{D_{TRIM}} + \Delta C_{D_{P.T.}} \quad . \tag{4-38}$$

4.19 The corrected parameters for further standardization will then be:

$$C_D = C_{D_{TRIM,\dot{\theta}=0}} = C_{D_{test}} + \Delta C_{D_{P.E.}} + \Delta C_{D_{P.T.}} \quad (4\text{-}39)$$

$$C_L = C_{L_{TRIM,\dot{\theta}=0}} = C_{L_{PO}} + \Delta C_{L_{P.E.}} + \Delta C_{L_{P.T.}} , \quad (4\text{-}40)$$

and

$$i_s = i_{s_{test}} + \Delta i_{s_{P.E.}} + \Delta i_{s_{P.T.}} . \quad (4\text{-}41)$$

These parameters represent the trimmed aircraft at a given Mach number, angle of attack, and load factor with zero pitch rate and no power or thrust. In practice, the pitch rate correction need not be applied to low pitch rate maneuvers, such as slow accelerations and climbs, but need be applied to wind-up turns and rollercoasters.

ROLL TRIM CORRECTIONS
(TAIL USED FOR ROLL CONTROL)

4.20 When the tail is used for roll control, the preceding discussion applies to the average of the left and right tail positioning. The corrections for roll trim are quite simple. There is no correction to the C_L, since for rolling moments:

$$\Delta C_{L_{left}} = -\Delta C_{L_{right}} \qquad (4\text{-}42)$$

and

$$\Delta C_{L_{total}} = 0 \; . \qquad (4\text{-}43)$$

The total tail mispositioning will also be zero since each left and right tail are mispositioned by equal and opposite amounts.

4.21 There may, however, be a trim drag correction, and this may be figured as followed:

- Tail mispositioning is computed for both left and right tail positions, as under the pitch rate correction.
- Trim drag is computed for each tail surface as one-half the trim drag of a total tail displacement.
- $\Delta C_{D_{R.T.}} = \Delta C_{D_R} + \Delta C_{D_L}$ (4-44)

  Such that:

  $$C_D = C_D + \Delta C_{D_{R.T.}} \; . \qquad (4\text{-}45)$$

This correction will be generally small, since the signs of the left and right tail corrections will be generally opposite.

STANDARDIZATION

4.22 Standardization will need to be made to some extent in most of the data taken. The degree of standardization will depend upon the maneuver and the analysis applied. For instance, in an acceleration, standardization on load factor (i.e., 1.0g) eases the analysis, but it makes no sense to standardize on Mach number. In a wind-up turn, standardization on load factor makes no sense, while standardization on Mach number aids in the analysis. For a stabilized point, standardization on Mach number, load factor, cg, wing sweep, etc., may all be desirable. With the mathematical modeling approach (i.e., parametric extraction of performance from the mathematical components), standard day will apply only when extracting data from the mathematical model.

4.23 The basic areas of standardization to be considered, and as given in the introductory section, are:

- Center of gravity (cg)
- Wing sweep
- Mach number
- Load Factor
- Standard atmospheric conditions.

The center of gravity standardization will be dealt with first, since most of the data will require cg standardization.

4.24 A change in cg at a given test point (i.e., Mach number, angle of attack combination) will cause a change in the tail trim position which will, in turn, cause a change in the aircraft C_L and trim drag. As shown in figure 4-7, there are two moment contributors to the problem. The moment arm change produces an imbalance of moment, created by the wing lift as $L_W(\Delta cg)$ and the tail lift as $L_T(\Delta cg)$, which must be balanced by a corresponding change in tail lift through the moment arm $\ell_{t_{stand}}$ such that:

$$\underset{\text{nose down}}{\Delta L_T(\ell_t - \Delta cg)} = \underset{\text{nose up}}{L_W(\Delta cg) + L_T(\Delta cg)} \quad . \tag{4-46}$$

Noting from figure 4-6, that the total aircraft lift (L) is given by:

$$L = L_W + L_T \quad , \tag{4-47}$$

equation 4-46 can be rewritten as:

$$\Delta L_T(\ell_t - \Delta cg) = L(\Delta cg) \quad , \tag{4-48}$$

and in coefficient form:

$$\Delta C_{L_{cg}} = \frac{C_{L_{TPO}}(\Delta cg)}{(\ell_t - \Delta cg)} \quad , \tag{4-49}$$

where $C_{L_{TPO}}$ has been corrected for tail mispositioning due to angular rates, if necessary. Application of equation 4-49 is

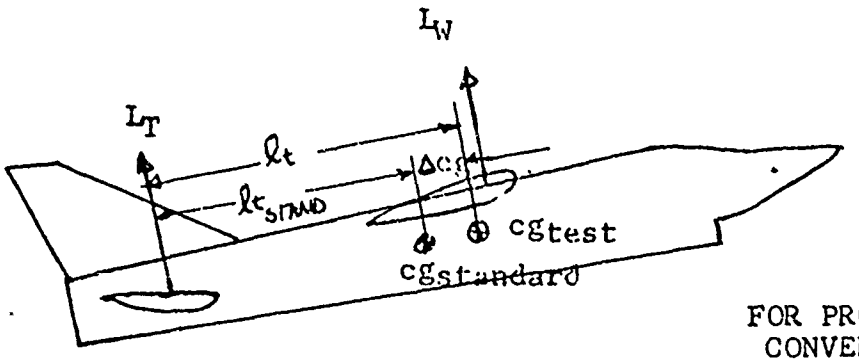

FOR PROPER SIGN CONVENTION

$\Delta cg = cg_{stand} - cg_{test}$

FIG. 4-7: AIRCRAFT MOMENT DIAGRAM CG EFFECT

straightforward, however, care must be taken in that the tail length and delta cg have the same units (i.e., either measured units of length, or ℓ_t is normalized with the length of the mean aerodynamic chord). The trimmed flight C_L would then be given by:

$$C_{L_{cg_S}} = C_{L_{TPO}} + \Delta C_{L_{cg}} \quad . \tag{4-50}$$

4.25 The tail increment required to trim can be obtained by the use of equation 4-49 and figure 4-2 as:

$$\Delta i_{s_{cg}} = \frac{\partial i_s}{\partial C_L} \Delta C_{L_{cg}} \quad , \tag{4-51}$$

and

$$i_{s_{cg_S}} = i_{s_{TRIM}} + \Delta i_{s_{cg}} \quad . \tag{4-52}$$

Again, predicted data can be used to obtain the trim drag increment as follows:

$$\left(\hat{C}_{L_{cg_T}}\right) = f\left(M, \alpha_t, i_{s_{TRIM}}\right) \tag{4-53}$$

and

$$\left(\hat{C}_{L_{cg_S}}\right) = f\left(M, \alpha_t, i_{s_{cg_S}}\right) \tag{4-54}$$

is taken from figure 4-3. And, from figure 4-4:

$$\left(\hat{C}_{D_{cg_T}}\right) = f\left[M, \left(\hat{C}_{L_{cg_T}}\right), i_{s_{TRIM}}\right] \tag{4-55}$$

$$\left(\hat{C}_{D_{cg_S}}\right) = f\left[M, \left(\hat{C}_{L_{cg_S}}\right), i_{s_{cg_S}}\right] \tag{4-56}$$

so that:

$$\Delta C_{D_{cg}} = \left(\hat{C}_{D_{cg_T}}\right) - \left(\hat{C}_{D_{cg_S}}\right) \qquad (4\text{-}57)$$

and

$$C_{D_{cg_S}} + C_{D_{TRIM}} + \Delta C_{D_{cg}} \quad . \qquad (4\text{-}58)$$

Although not explicitly stated, the correction assumes constant angle of attack.

CONSTANT MACH NUMBER
(MACH NUMBER STANDARDIZATION)

4.26 For certain maneuvers, such as rollercoasters, wind-up turns, and climbs, it is advantageous to standardize to a constant Mach number for analysis purposes. The Mach number correction, as in most corrective equations, assumes a constant angle of attack. From flight data at various altitudes, or by cross-plotting figures 4-3 and 4-5, figure 4-8 must be generated.

4.27 A change in Mach number at a constant angle of attack will be accompanied by a change in C_L, as taken from figure 4-7.

$$C_{L_{M_T}} = f(\alpha_t, M_t) \tag{4-59}$$

and

$$C_{L_{M_S}} = f(\alpha_t, M_S) \quad , \tag{4-60}$$

so that,

$$\Delta C_{L_M} = C_{L_{M_T}} - C_{L_{M_S}} \tag{4-61}$$

and

$$C_{L_{S_M}} = C_{L_{TPO}} + \Delta C_{L_M} \quad . \tag{4-62}$$

This change in C_L will cause a change in the associated tail trim which can be derived through equation 4-61 and figure 4-2 as:

$$\Delta i_{s_M} = \left(\frac{\partial i_s}{\partial C_L}\right) \Delta C_{L_M} \tag{4-63}$$

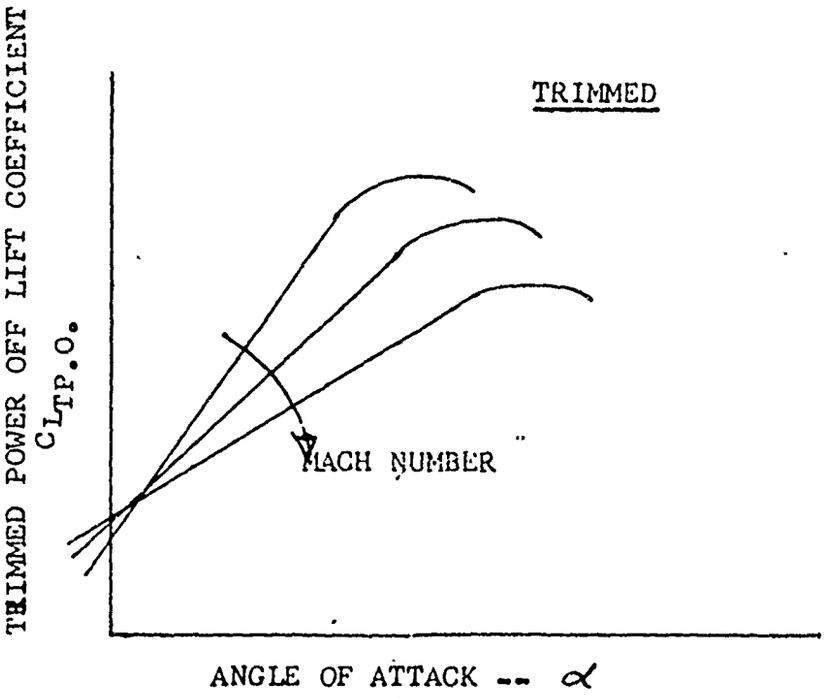

FIG. 4-8: TRIMMED LIFT CURVE

and

$$i_{s_{M_S}} = i_{s_{TRIM}} + \Delta i_{s_M} \quad . \tag{4-64}$$

The change in trim drag can be determined by the use of figure 4-9 which is either arrived at by flight test data or cross-plotted from figures 4-4 and 4-5, where:

$$C_{D_{M_T}} = f\left(M_T,\ C_{L_{TPO}}\right) \tag{4-65}$$

and

$$C_{D_{M_S}} = f\left(M_S,\ C_{L_{S_M}}\right) \quad . \tag{4-66}$$

Such that:

$$\Delta C_{D_M} = C_{D_{M_T}} - C_{D_{M_S}} \tag{4-67}$$

and

$$C_{D_{S_M}} = C_{L_{TPO}} + \Delta C_{D_M} \quad .$$

The Mach number correction, in effect, changes C_L, C_D, and i_s by equations 4-62, 4-64, and 4-67.

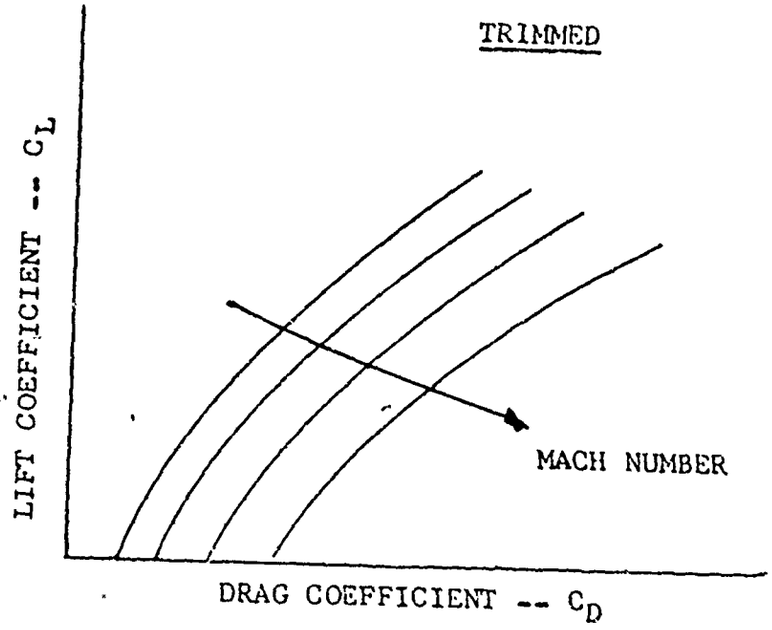

FIG. 4-9: TRIMMED DRAG POLAR

LOAD FACTOR CORRECTION
(LOAD FACTOR STANDARDIZATION)

4.28 For maneuvers, such as acceleration, deceleration, etc., it will be advantageous to apply the load factor standardization. The load factor correction runs along the C_L-C_D curve at a given Mach number such that:

$$C_{L_{S_{LF}}} = C_{L_{TPO}} \left(\frac{n_{z_s}}{n_{z_t}} \right) \tag{4-68}$$

or

$$\Delta C_{L_{S_{LF}}} = C_{L_{TPO}} \left(\frac{n_{z_s}}{n_{z_t}} - 1 \right) . \tag{4-69}$$

Generally, the aircraft angle of attack is changed to maintain the new C_L. Its value can be drawn from figure 4-7 as:

$$\alpha_{LF_t} = f\left(C_{L_{TPO}}, M_t \right) \tag{4-70}$$

$$\alpha_{LF_s} = f\left(C_{L_{S_{LF}}}, M_t \right) \tag{4-71}$$

and

$$\Delta\alpha_{LF} = \alpha_{LF_t} - \alpha_{LF_s} , \tag{4-72}$$

where the new angle of attack is given by:

$$\alpha_{S_{LF}} = \alpha_t + \Delta\alpha_{LF} . \tag{4-73}$$

The difference in drag at the new test point can be drawn from figure 4-8 as:

$$C_{D_{LF_t}} = f\left(C_{L_{TPO}}, M_t\right) \tag{4-74}$$

$$C_{D_{LF_S}} = f\left(C_{L_{S_{LF}}}, M_t\right) , \tag{4-75}$$

and

$$\Delta C_{D_{LF}} = C_{D_{LF_t}} - C_{D_{LF_S}} . \tag{4-76}$$

The new drag value is then given by:

$$C_{D_{S_{LF}}} = C_{D_{TRIM}} + \Delta C_{D_{LF}} . \tag{4-77}$$

Finally, the test tail incidence change can be obtained from figure 4-5 as:

$$i_{s_{LF_t}} = f\left(\alpha_t, M_t\right) \tag{4-78}$$

and

$$i_{s_{LF_s}} = f\left(\alpha_{S_{LG}}, M_t\right) , \tag{4-79}$$

where

$$\Delta i_{s_{LF}} = i_{s_{LF_T}} - i_{s_{LF_S}} \tag{4-80}$$

and the standard tail trim angle is given by:

$$i_{s_{s_{LF}}} = i_{s_{TRIM}} + \Delta i_{s_{LF}} . \tag{4-81}$$

WING SWEEP EFFECTS
(WING SWEEP STANDARDIZATION)

4.29 The preceding discussions apply to either a fixed wing sweep aircraft, a variable wing sweep aircraft at a constant wing sweep angle, or a variable wing sweep aircraft with the wing sweep angle as a function of Mach number. In the general case of a variable wing sweep aircraft where the wing can be placed in any position at any Mach number (within flight operating limits), there arises a need to standardize wing sweep. Wing sweep corrections are further complicated by the need for additional wind tunnel or predicted data, and these corrections should be avoided if possible. When planning a program, several detents in the wing sweep handle will aid in establishing the same wing sweep each time.

4.30 The corrections for wing sweep are straightforward and depend upon the wind tunnel or predicted data available. For example, if partial derivative information is available, the partial derivative data can be applied directly. If predicted drag polar and lift curves are available, then $\Delta C_L s$ at a constant angle of attack can be derived. These in turn can be converted to $\Delta C_D s$ and $\Delta i_s s$, as shown in the previous examples. An example follows in figure 4-10. The lift increment would be obtained from curve A of figure 4-10 as:

$$\left(\hat{C}_{L_{TPO_{\Lambda T}}}\right) = f\left(\alpha_t, M_t, \Lambda_t\right) \tag{4-82}$$

$$\left(\hat{C}_{L_{TPO_{\Lambda S}}}\right) = f\left(\alpha_t, M_t, \Lambda_s\right) , \tag{4-83}$$

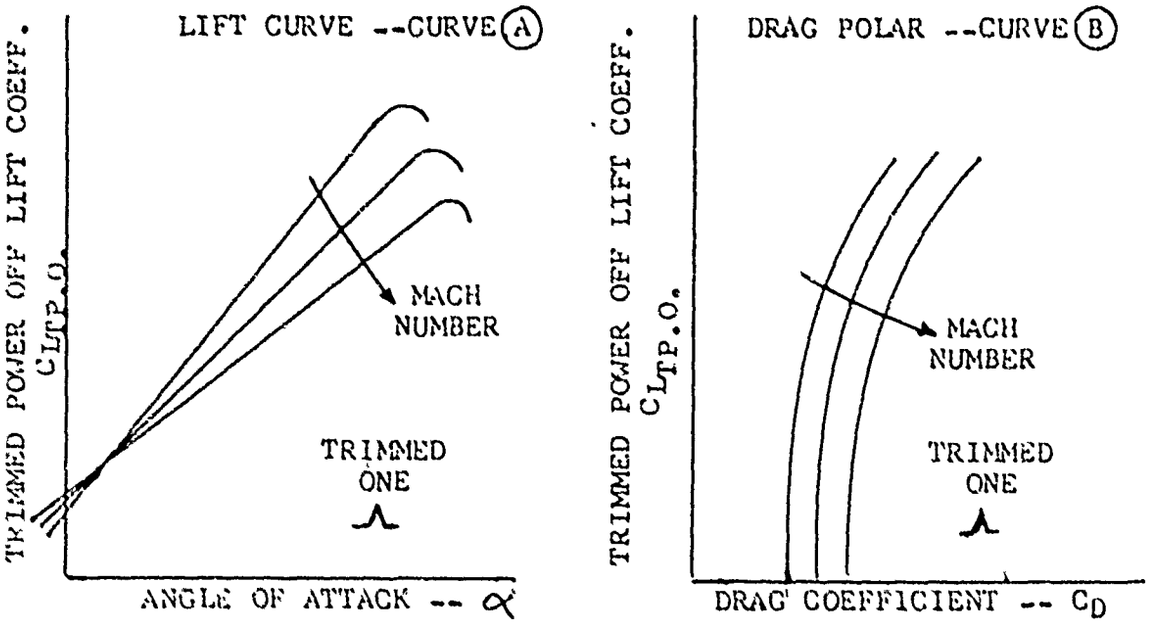

FIG. 4-10: LIFT CURVE AND DRAG POLAR AT CONSTANT WING SWEEP

and

$$\Delta C_{L_\Lambda} = \left(\hat{C}_{L_{TPO_{\Lambda T}}}\right) - \left(\hat{C}_{L_{TPO_{\Lambda S}}}\right) \quad . \tag{4-84}$$

The drag increment would be obtained from curve B of figure 4-10 as:

$$\left(\hat{C}_{D_{TRIM_{\Lambda T}}}\right) = f\left[\left(\hat{C}_{L_{TPO_{\Lambda T}}}\right), M_t, \Lambda_t\right] \tag{4-85}$$

$$\left(\hat{C}_{D_{TRIM_{\Lambda S}}}\right) = f\left[\left(\hat{C}_{L_{TPO_{\Lambda S}}}\right), M_t, \Lambda_s\right] \quad , \tag{4-86}$$

and

$$\Delta C_{D_\Lambda} = \left(\hat{C}_{D_{TRIM_{\Lambda T}}}\right) - \left(\hat{C}_{D_{TRIM_{\Lambda S}}}\right) . \tag{4-87}$$

The tail increment corresponding to the lift change can be obtained by the use of figure 4-2, which is again for a constant wing sweep, such that:

$$\Delta i_{s_\Lambda} = \left(\frac{\partial i_s}{\partial C_L}\right)_{\Lambda=\Lambda_t} \Delta C_{L\Lambda} \quad . \tag{4-88}$$

And, again, this correction is made at a constant angle of attack. Since data at every wing sweep is probably not available, interpolation between wing sweep curves will be required. As in the previous analyses, the increments are additive.

ALTITUDE EFFECTS

4.31 In general, the effects of altitude on airplane performance are reflected only to a small extent in the drag polar. It is suggested, that unless altitude effects show as more than a nominal (±2 percent) amount of scatter, that these effects be ignored. If larger effects are present, attempts to correct the polars to some standard altitude may be made as given in the following discussion.

4.32 The effects of altitude on drag are two-fold. There may, in general, be a Reynold's number effect and an aeroelasticity effect. Both will be discussed.

REYNOLD'S NUMBER

4.33 The Reynold's number effect may be two-fold. At high C_L values, the Reynold's number effect may be reflected in the wake drag due to separation, as shown in figure 4-11 as taken from reference 4-5. As shown in figure 4-11, the larger the wake the larger the pressure drag. The pressure drag effect shown only in the separation phenomenon and for conventional streamlined aircraft will show only at near stall or high C_L values where separation of flow occurs. Generally, at higher Reynold's numbers, a smaller wake will result at separation and lesser drag. The interest in the stall phenomenon will ususally be limited to a small altitude range (i.e., sea level to 20,000 feet), and consequently, a small

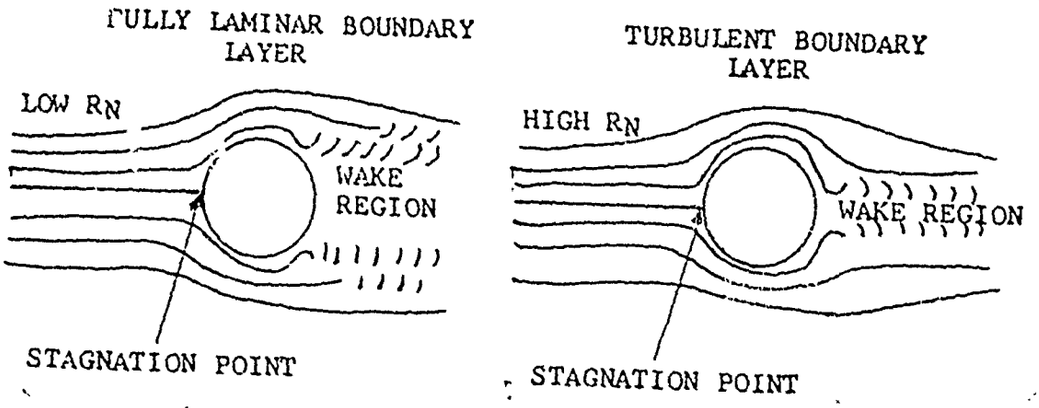

FIG. 4-11: REYNOLD'S NUMBER PRESSURE DRAG

R_N range at the stall speed, so that it will be eliminated from further discussion.

4.34 The second effect of Reynold's number is on the skin friction. At high C_L values or near-stall, the skin friction drag goes to zero where separation occurs so that the pressure drag R_N effect does not occur at the same point that the skin friction R_N effect occurs. At low subsonic speeds, the fore-body pressure drag is very small (assuming no separation), and the skin friction drag accounts for the major portion of the drag at zero lift. The importance of skin friction drag decreases as speed is increased, but is still a major portion of total drag at transonic speeds.

4.35 The flight Reynold's number is given by:

$$R_N = \frac{V_T \ell \rho}{\mu} \tag{4-89}$$

where

$$\rho = f(P_a, T_a) \tag{4-90}$$

$$\mu = f(T_a) \quad . \tag{4-91}$$

For test values, the test point ρ and μ are used, while for standard values the values of ρ and μ at standard conditions are used (i.e., when an attempt is made to correct all data to 35,000 feet, $\rho_{35} = \rho_{standard}$, and $\mu_{35} = \mu_{standard}$). A value of R_N should be computed both standard and test for each major component (i.e., wings, fuselage, nacelles,etc.), where ℓ is a characteristic length of each item in the direction of flow.

4.36 Correction for Reynold's number skin friction drag cannot be made without an assumption about the characteristics of the boundary layer. For normal flight Reynold's numbers, a 100 percent turbulent boundary layer can be assumed when calculating skin friction coefficients. The skin friction coefficients for both standard and test conditions can be computed by the incompressible Karman-Schoenherr formula which shows the closest agreement with experimental data and is given by:

$$0.242 = \sqrt{C_{f_i}} \log_{10}\left(C_{f_i} R_{e_x}\right) \quad , \tag{4-92}$$

where R_{e_x} is the Reynold's number based on length x, and C_{f_i} is the incompressible skin friction coefficient, for 100 percent turbulent boundary layer, and is solved graphically or by iteration. More details are provided in references 4-5, 4-6, and 4-10. The skin friction coefficients can be corrected by use of the Frankl-Voishel relation, as given in reference 4-10:

$$\frac{C_f}{C_{f_{M=0}}} = \frac{C_f}{C_{f_i}} = \left[1 + \frac{\gamma+1}{2} M^2\right]^{-.467} \quad . \tag{4-93}$$

4.37 Since equation 4-92 is not readily solvable by numerical techniques without iteration, wide acceptance in Europe has been accorded the Prandtl-Schlichting expression (reference 4-8) as given by:

$$C_{f_i} = \frac{.455}{(\log_{10} R_{e_x})^{2.58}} \tag{4-94}$$

which is more readily solvable for computer work. These skin friction coefficients should also be corrected for compressibility by the Frankl-Voishel relation (equation 4-93). It should be noted that the Prandtl-Schlicting relation (equation 4-94) is 2.7 percent higher than the Karman-Schoenherr relation (equation 4-92), at $R_{e_x} = 10^8$, but only negligable differences exist when working with the incremental drag.

4.38 The change in skin friction drag for each component can be computed by adjusting the skin friction coefficients to the aircraft reference area (usually the wing area). The skin friction coefficient is based on wetted area, or the area exposed to the free stream, such that:

$$\Delta C_f = C_{f_{R_N}}{}_{standard} - C_{f_{R_N}}{}_{TEST} \tag{4-95}$$

and

$$\Delta C_{D_i} = \Delta C_f \left(\frac{S}{S_{wet}} \right) , \tag{4-96}$$

where S_{wet} is computed for each aircraft component and ΔC_{D_i} is the component differential drag. The total aircraft drag differential is given as the sum of the component drag differention or:

$$\Delta C_{D_{TOTAL_{R_N}}} = \sum_{i=1}^{n} \Delta C_{D_i} , \tag{4-97}$$

for n components and the aircraft drag is given by:

$$C_D = \Delta C_{D_{TOTAL_{R_N}}} + C_{D_{TRIM}} . \tag{4-98}$$

4.39 As stated earlier, this correction should be small and need not be considered unless a large altitude effect is noted. Additionally, Reynold's number effects may still be present in the high C_L data because of the separation phenomenon noted earlier. Additional information on Reynold's number effects on drag is contained in references 4-5 through 4-11.

ELASTICITY

4.40 Aeroelasticity effects in the aerodynamic parameters is brought about by structural deformation of the airframe. There is some washout of the wing as it tries to relieve the lift load, and some absorption of moments due to fuselage bending and other structure deformation, and consequently, a reduced tail trim angle. Since the aeroelastic effects vary from airplane to airplane and corrective procedures are dependent on available wind tunnel data, they will not be dealt with here. The general corrective procedure would be to remove all of the elastic effects and correct to a rigid airplane, or to correct the data to an elastic airplane at a given altitude. Elasticity effects are further discussed in Chapters 6 and 7.

OTHER ATMOSPHERIC CONDITIONS

4.41 The basic development of the mathematical model will be taken at test atmospheric conditions where the calculations of q, V_T, etc., are based on test atmospheric conditions (pressures, temperatures, etc.). In application of the mathematical model, the aerodynamic parameters will be calculated by standard atmospheric conditions, thus in the calculation of:

$$q = \frac{\gamma_a}{2} P_a M^2 \qquad (4\text{-}99)$$

or

$$q = \frac{1}{2} \rho V_t^2 \quad . \qquad (4\text{-}100)$$

The values of P_a and ρ will be based on the standard atmospheric pressures and temperatures at the desired altitude. Certain maneuvers on the other hand, may be reduced to standard day, standard weight, etc., by the conventional methods given in references 4-10 and 4-11.

SECONDARY AND ANALYSIS EQUATION SUMMARY

4.42 The secondary and analysis equations can best be summarized in tabular form, as shown in tables 4-1 and 4-2. Table 4-1 deals with the corrections to be made to all data and table 4-2 deals with standardization equations. Aeroelasticity and R_N effects are not included since they will be applied only in isolated incidences.

TABLE 4-1

CORRECTIONAL EQUATIONS FOR LIFT AND DRAG

Effect	Lift Coefficient	Tail Incidence	Angle of Attack	Drag Coefficient
Power	$C_{L_{eff}} = \frac{n_z W}{qs}$ $C_{L_{P.O.}} = \frac{n_z W - F_g \sin(\alpha+\tau)}{qs}$ $\Delta C_{L_{P.E.}} = \frac{F_g Y_t + F_R h_r}{\ell_t qs}$ $C_{L_{TPO}} = C_{L_{P.O.}} + \Delta C_{L_{P.E.}}$	$\Delta i_{s_{P.E.}} = \left(\frac{\partial i_s}{\partial C_L}\right) \Delta C_{L_{P.E.}}$ $i_{s_{TRIM}} = i_{s_{TEST}} + \Delta i_{s_{P.E.}}$	$\Delta\alpha = 0$	$\Delta C_{D_{P.E.}} = f\left(\Delta C_{L_{P.E.}}, M_t, \Delta i_{s_{P.E.}}\right)$ $C_{D_{TRIM}} = C_{D_{TEST}} + C_{D_{P.E.}}$
Pitch Rate Trim	$\Delta C_{L_{P.T.}} = f\left(M, \alpha_t, \Delta i_{s_{P.T.}}\right)$ $\left(C_{L_{TPO}}\right)_{\dot{\theta}=0} = C_{L_{TPO}} + \Delta C_{L_{P.T.}}$	$\Delta i_{s_{P.T.}} = \left[-\frac{63 g \ell_t}{V_t^2} - \frac{C_{L_{TPO}}}{n_z}\left(\frac{\partial i_s}{\partial C_L}\right)\right] \cdot \left[n_z - 1\right]$ for pull-up $\Delta i_{s_{P.T.}} = \left[-\frac{63 g \ell_t}{V_t^2}\left(1 - \frac{1}{n_z^2}\right) - \frac{C_{L_{TPO}}}{n_z}\left(\frac{\partial i_s}{\partial C_L}\right)\right](n_z - 1)$ for turn OR: $\Delta i_{s_{P.T.}} = f\left(M, \alpha, i_s\right)$ from flight test $i_{s_{TRIM}} = i_{s_{TEST}} + \Delta i_{s_{P.T.}} + \Delta i_{s_{P.E.}}$	$\Delta\alpha = 0$	$\Delta C_{D_{P.T.}} = f\left(M, \Delta C_{L_{P.T.}}, \Delta i_{s_{P.T.}}\right)$ $C_{D_{TRIM}} = C_{D_{TEST}} + \Delta C_{D_{P.E.}} + \Delta C_{D_{P.T.}}$

TABLE 4-1
(Continued)

CORRECTIONAL EQUATIONS FOR LIFT AND DRAG

Effect	Lift Coefficient	Tail Incidence	Angle of Attack	Drag Coefficient
Roll Rate Trim (Tail used for roll control)	$\Delta C_{L_{R.T.}} = 0$	$\Delta i_{s_L} = f\left(M,\alpha,i_{s_L}\right)$ $\Delta i_{s_R} = f\left(M,\alpha,i_{s_R}\right)$ from flight test $\Delta i_s = \Delta i_{s_L} + \Delta i_{s_R} = 0$	$\Delta\alpha = 0$	$\Delta C_{D_{RT_L}} = f\left(M,\alpha,\Delta i_{s_L}\right)$ $\Delta C_{D_{RT_R}} = f\left(M,\alpha,\Delta i_{s_R}\right)$ $\Delta C_{D_{RT}} = \frac{\Delta C_{D_{RT_L}}}{2} + \frac{\Delta C_{D_{RT_L}}}{2}$ $C_D = C_{D_{TRIM}} + \Delta C_{D_{P.E.}} + \Delta C_{D_{P.T.}} + \Delta C_{D_{R.T.}}$

TABLE 4-2

STANDARDIZATION EQUATION FOR LIFT AND DRAG

Effect	Lift Coefficient	Tail Incidence	Angle of Attack	Drag Coefficient	Components
cg	$\Delta C_{L_{cg}} = \frac{C_{L_{TPO}}(\Delta cg)}{(\ell_t - \Delta cg)}$	$\Delta i_{s_{cg}} = \left(\frac{\partial i_s}{\partial C_L}\right)\Delta C_{L_{cg}}$	$\Delta\alpha = 0$	$\Delta C_{D_{cg}} = f\left(C_L, \alpha, M, \Delta i_{s_{cg}}\right)$	all data
Mach Number	$\Delta C_{L_{SM}} = f(\alpha_t, \Delta M)$	$\Delta i_{s_M} = f(\alpha_t, \Delta M)$	$\Delta\alpha = 0$	$\Delta C_{D_{SM}} = f\left(\Delta M, \Delta C_{L_{SM}}\right)$	For wind-up turns, climbs, descents, stabilized points, and rollercoasters
Load Factor	$\Delta C_{L_{S_{LF}}} = C_{L_{TPO}}\left(\frac{n_{z_s}}{n_{z_t}} - 1\right)$	$\Delta i_{s_{LF}} = f\left(\Delta\alpha_{LF}, M_t\right)$	$\Delta\alpha = f\left(\Delta C_{L_{S_{LF}}}, M_t\right)$	$\Delta C_{D_{LF}} = f\left(\Delta C_{L_{S_{LF}}}, M_t\right)$	Accelerations, decelerations, stabilized points
Wing Sweep	$\Delta C_{L_\Lambda} = f\left(\alpha_t, M_t, \Delta\Lambda\right)$	$\Delta i_{s_\Lambda} = \left(\frac{\partial i_s}{\partial C_L}\right)_{\Lambda=\Lambda_t} \Delta C_{L_\Lambda}$	$\Delta\alpha = 0$	$\Delta C_{D_\Lambda} = f\left(\Delta C_{L_\Lambda}, M_t, \Delta\Lambda\right)$	As needed

NOTES: All standardization values are additive (i.e., $C_L = C_L + \Delta C_L$, etc.).

CONCLUDING REMARKS TO CHAPTER 4

4.43 The corrective procedures outlined in this chapter are dependent upon the availability of wind tunnel data, and may have to be modified in the particular case. Certain corrections, such as the wing sweep correction, can be avoided (by placing detents in the wing sweep actuator, etc.), while others may be negligible. Some corrections will be necessary to all data (such as power effects), and the individual case must dictate the criterion.

4.44 With the conclusion of Chapter 4, the basic mechanics of the accelerometer method are concluded. Attention will now be turned to the instrumentation requirements dictated by the equation development.

REFERENCES TO CHAPTER 4

4-1. U.S. Naval Air Test Center, Flight Test Technical Memorandum 1-70, "Determination of Total Lift, Excess Thrust, and Longitudinal Acceleration in the High-Lift Configuration," by W. Branch, Unclassified, 16 April 1970.

4-2. The Boeing Company, Document Number D6-1420, "Jet Transport Performance Methods," Unclassified, May 1969.

4-3. U.S. Naval Training Pilot School, Technical Memorandum 103, "Fixed Wing Stability and Control Theory and Flight Test Techniques," by S.D. Langdon, Unclassified, August 1969.

4-4. U.S.A.F. Aerospace Research Pilot School, Document Number FTC-TlH-70-1001, "Performance," Unclassified, May 1970.

4-5. Pope, A. and K.L. Goin, "High-Speed Wind Tunnel Testing," John Wiley & Sons, Inc., New York, 1965.

4-6. Truitt, R.W., "Fundamentals of Aerodynamic Heating," The Ronald Press, New York, 1960.

4-7. Grumman Aerospace Engineering Corporation, Report No. 64-20, "Scale Corrections to Minimum Drag," by I.T. Waaland, Unclassified, April 1964.

4-8. Schlichting, H., "Boundary Layer Theory," McGraw-Hill, Inc., New York, 1960.

4-9. Grumman Aerospace Engineering Corporation, Report No. A51-335-R-69-1, "F-14A Basic Aerodynamic Data Required for Substantiation of Standard Aircraft Characteristics(U)," Confidential, August 1969.

4-10. Edwards Air Force Base, USAF Document No. 6273, "Flight Test Engineering Handbook," by Herrington, et al, Unclassified, January 1966.

4-11. U.S. Naval Test Pilot School, "Aircraft and Engine Performance," by F.S. Peterson, et al, Unclassified, 1 May 1962.

4-12. Perkins, Courtland D. and Robert E. Hage, "Airplane Performance Stability and Control," John Wiley & Sons, Inc., New York, 1949.

THE ACCELEROMETER METHODS OF DETERMINING AIRCRAFT PERFORMANCE (DYNAMIC PERFORMANCE TESTING)

CHAPTER 5

INSTRUMENTATION REQUIREMENTS

SUMMARY OF CHAPTER 5

5.1 Basic considerations of instrumentation and instrumentation accuracies are reviewed. The chapter presents an overview of instrumentation as used in the accelerometer methods and aircraft performance modeling. Details of accelerometer calibration and angle of attack determination are presented in subsequent chapters. A summary of instrumentation requirements is presented for quick reference.

INTRODUCTION TO CHAPTER 5

5.2 The equation development of the first four chapters has dealt mainly with converting measured quantities to meaningful flight test data. This data, in turn, will be used to generate a mathematical model of aircraft performance or a specific performance point. Some attention must now be turned to the measurements themselves. In this chapter, an attempt will be made to overview the instrumentation requirements. Additionally, instrumentation accuracy requirements will be analyzed, although more often than not, accuracy requirements will depend upon the individual aircraft being tested.

5.3 It should also be noted, that since aircraft today are instrumented for a variety of programs including performance, stability and control, weapons delivery, service suitability, etc., accuracy requirements may not always be constrained by performance data.

5.4 Finally, detailed discussions of accelerometer and angle of attack measurements have been deferred to later chapters in that these measurements are radically different from conventional data and require more detailed analysis.

SYMBOLS

5.5 The following symbols are used in Chapter 5.

Symbol	Definition	Common Units	Metric Units
A	Angular rate derivative or product	rad/sec^2	(rad/sec^2)
a	Speed of sound	kt or ft/sec	(m/sec)
A_e	Exhaust area	in^2	(cm^2)
D	Diameter	in	(cm)
F_g	Gross thrust	lbs	(N)
g	Acceleration of gravity ($32.2\ ft/sec^2$ or $9.80\ m/sec^2$ @ sea level standard)	ft/sec^2	(m/sec^2)
k	Probe recovery factor	-	-
mg	Milli-g = .001g	g	(g)
M	Mach number	-	-
OAT	Outside air temperature	^oF	(^oC)
P_a	Ambient pressure	lbs/ft^2	(N/m^2)
P_t	Total pressure	lbs/ft^2	(N/m^2)
P_{t_5}	Total pressure at station 5 (nozzle exit)	lbs/ft^2	(N/m^2)
P_{SSL}	Static pressure at sea level standard	lbs/ft^2	(N/m^2)
q	Dynamic pressure	lbs/ft^2	(N/m^2)
r_x, r_y, r_z	Center of gravity moment arm in the subscripted direction	ft	(m)

Symbol	Definition	Common Units	Metric Units
T_a	Ambient temperature	^{o}F	(^{o}C)
T_t	Total temperature	^{o}F	(^{o}C)
V_t	True airspeed	kt or ft/sec	(m/sec)
V_c	Calibrated airspeed	kt or ft/sec	(m/sec)
Greek Symbols			
γ_a	Ratio of specific heats for air (1.40 at normal temperatures)	none	none
γ_e	Ratio of specific heats of exhaust gases (1.33 at 1600^{o}R)	none	none
δ	Pressure ratio P_a/P_{SSL}	none	none
θ	Pitch attitude	deg	(deg)
$\dot{\theta}$	Pitch rate	deg/sec	(deg/sec)
$\ddot{\theta}$	Pitch acceleration	deg/sec^2	(deg/sec^2)
ϕ	Bank angle	deg	(deg)
$\dot{\phi}$	Roll rate	deg/sec	(deg/sec)
$\ddot{\phi}$	Roll acceleration	deg/sec^2	(deg/sec^2)
$\dot{\psi}$	Yaw rate	deg/sec	(deg/sec)
$\ddot{\psi}$	Yaw acceleration	deg/sec^2	(deg/sec^2)

5.6 The basic constituents of the instrumentation system should provide an overall end product with a given standard of accuracy. When using the mathematical modeling approach, certain parameters are needed more accurately than others. Also, certain parameter accuracies will depend upon the primary instrumentation to be used. Thus, as is shown in the section on inertial measurements and in Chapter 7 when dealing with angle of attack, the instrumentation accuracy requirements are dependent upon the accelerometer package chosen.

5.7 The instrumentation will be broken into the following categories of consideration:

- Basic pitot-static parameters
- Other basic aerodynamic parameters
- Accelerometer measurements
- Inertial measurements
- Engine parameters
- Airframe parameters
- Pilot display parameters.

Each category of instrumentation will have an effect on the end product and each will be analyzed separately.

5.8 To ensure rapid data turnaround, a magnetic tape system should be available for the test aircraft. It is assumed that the more sensitive parameters will be assigned

PCM channels due to the increased accuracy available, and that in general, the system will be a combination of PCM, PJM, and FM channels. The sampling rate should be a minimum of ten per second while the non-dynamic paramters (such as OAT) can be sampled at a much lower rate.

PITOT-STATIC INSTRUMENTATION

5.9 The accuracy requirement of pitot static information is constrained by several mathematical equations. The calculation of Mach number, true airspeed, altitude, and free air temperature affect several of the relations in the mathematical model; for instance, in the calculation of dynamic pressure (q) to convert drag to drag coefficient, or lift to lift coefficient. The calculation of airspeed and altitude are derived through the measurement of total and static pressures and these quantities should yield the desired accuracies of Mach number, etc. Additionally, these measurements are constrained by stability and control data measurements for stall speeds, and other tests.

The Altimeter

5.10 Most altitude measurements are made with a sensitive pressure gauge called an altimeter, scaled so that a pressure decrease indicates an altitude increase in accordance with the U.S. Standard Atmosphere (reference 5-1). If the altimeter is adjusted to 29.92 inches of mercury, the altimeter will read pressure altitude whether in a

standard or non-standard atmosphere. Further, discussion with equation development and altimeter schematics is given in reference 5-1. As taken from reference 5-1, the altimeters presently available and the expected characteristics are given in table 5-1.

The Airspeed Indicator

5.11 True airspeed (V_t) is the velocity of an aircraft with respect to the air through which it is flying. It is difficult to measure V_t directly. Instead, it is usually determined from calibrated airspeed (V_c), atmospheric pressure (P_a), and the atmospheric temperature (T_a). V_c is obtained from a conventional airspeed indicator; P_a is measured with an altimeter; and T_a is measured with a free air temperature probe. Additionaly details including equation development and airspeed indicator schematics are given in reference 5-1. As taken from reference 5-1, the airspeed indicators available at present and the expected characteristics are given in table 5-2.

The Mach Meter

5.12 Mach number is defined as the ratio of true airspeed to the local atmospheric speed of sound:

$$M = \frac{V_t}{a} \quad . \tag{5-1}$$

Mach number is of primary importance in the mathematical model of an aircraft's performance. For isentropic flow of a perfect gas,

TABLE 5-1

CURRENTLY AVAILABLE ALTIMETERS

Type	Range (Feet)	Readability (Feet)	Repeatability
C-12	0 to 50,000	5	±100 feet desired
C-19	0 to 80,000	5	±100 feet desired

TABLE 5-2

CURRENTLY AVAILABLE AIRSPEED INDICATORS

Type	Range (knots)	Readability (knots)	Repeatability
F-1	50 to 650	0.5	±1 knot desired low speed ±2 knots desired high speed
059	50 to 850	0.5	Same

Bernoulli's equation states:

$$\frac{P_t}{P_a} = \left(1 + \frac{\gamma_a - 1}{2} M^2\right)^{\frac{\gamma_a}{\gamma_a - 1}} \quad . \qquad (5\text{-}2)$$

For air, $\gamma_a = 1.40$, so that equation 5-2 becomes:

$$\frac{P_t}{P_a} = (1 + 0.2\, M^2)^{3.5} \quad . \qquad (5\text{-}3)$$

This equation relates free stream total and static pressures to Mach number and is good for supersonic as well as subsonic flight. The Machmeter then, is essentially a combination of the altimeter and the airspeed indicator. Further detailed equation development and Machmeter schematics are given in reference 5-1. As taken from reference 5-1, the accuracy of present systems is poor and cannot be used for flight test data. The instruments, however, can be used for safety of flight indications to the pilot. The Machmeters presently in use, as given by reference 5-1, are given in table 5-3.

OTHER BASIC AERODYNAMIC PARAMETERS

Free Air Temperature Probe

5.13 The atmospheric temperature is a measurement of the internal thermal energy of air. Therefore, it is a very important parameter in aircraft and engine performance. If the air surrounding the probe is brought to a complete stop adiabatically and the probe correctly senses the resulting temperature, then:

$$\frac{T_t}{T_a} = 1 + \frac{\gamma_a - 1}{2} M^2 \quad . \qquad (5\text{-}4)$$

TABLE 5-3

CURRENTLY AVAILABLE MACHMETERS

Type	Range	Readability	Repeatability
A1	0.3 to 1.0 0 to 50,000 feet	0.01	Determined by calibration
A2	0.5 to 1.5 0 to 50,000 feet	0.01	
G09501	0.7 to 2.5 0 to 60,000 feet	0.01	

For various reasons, such as radiation or heat leakage, most probes do not register the full adiabatic temperature rise. To account for these loses, equation 5-4 is written as:

$$\frac{T_t}{T_a} = 1 + \frac{\gamma_a - 1}{2} K M^2 , \qquad (5\text{-}5)$$

where K is an engineering adjustment factor called the probe recovery factor. Methods of determining this probe recovery factor, together with schematics of a typical bridge type probe are given in reference 5-1. The instruments available can be adapted to any range desired, and generally have a readability and accuracy of about $\pm 0.5^{\circ}C$ which is suitable for flight test work.

Angle of Attack

5.14 The angle of attack is of primary importance. Due to its complex nature and its vital importance to the accelerometer methods, it is discussed separately in Chapter 7. Closely associated with the angle of attack is boom bending term which is discussed in detail in Chapters 6 and 7. The basic accuracy sought is ±0.05 degrees as will be seen in Chapter 7; however, ±0.10 degrees is more realistic at the present time with available instruments.

Angle of Sideslip

5.15 Sideslip is of lesser importance to the accelerometer methods, although its accuracy requirement may be greater in stability and control programs. Generally, as discussed in Chapter 2, sideslip angles affect the accelerations through a coordinate transformation, and predominately through a cosine term so that for the normal range of ±10 degrees an acceptable accuracy of ±1.0 degrees can be obtained.

ACCELEROMETER MEASUREMENTS

5.16 The accelerometer parameters are, of course, the primary measurements with which to be dealt. The objective is to obtain a measurement as accurate as possible, consistent with the other measurements taken. The end product accuracy available is ±.001 g or 1 mg under laboratory conditions in the nominal range of ±1 g, and every effort should be made to maintain this accuracy level. The instrument range of the longitudinal axis (±.6 g in the normal test vehicles) is consistent with maintaining this accuracy by range extending the measurement. In the normal axis, however, the wider range of measurement restricts range extending capabilities, so that ±.001 g cannot be maintained by normal methods. Basic considerations in the calculation of aircraft lift coefficients and in the accuracy of aircraft weight are such that degraded accuracy is acceptable and for the normal axis, an error of ±.005 g (±5 mg) per g is acceptable. For the lateral axis, there is no problem with obtaining the desired

1 mg accuracy, however, the lateral axis effects on the calculated lift and drag are small and range extension may not be needed if ±.005 g can be maintained without it.

5.17 Several accelerometers are available at present, and the use of Systron-Donner accelerometers in the background research programs for all test aircraft must be deemed coincidental. The Conrac Corporation of Duarte, California under contract to the U.S.A.F. to develop a flight path accelerometer had chosen the Kistler Model 303B due to its small size and weight (reference 5-2).

5.18 As taken from reference 5-2, the FPA design goal of measuring the magnitude of acceleration along the flight path and vertical normal to it, within ±0.001 g, over the range of ±1.0 g along the flight path, and -1.0 to +7.0 g perpendicular to it, are within the design limitations of the force feedback-type accelerometer.

5.19 The force feedback accelerometer has the advantages of accuracy, size, stability, and cost over the other type of accelerometers considered. The conventional open loop type accelerometer does have the combined accuracy and resolution required. A recently developed open loop type accelerometer combines the proof mass and suspension in a single element utilizing either piezoelectric effects or variations in capacitance to measure acceleration. This approach has yet to demonstrate the reliability and stability required in the Flight Path Accelerometer (FPA) system. Weight, size, and cost of the unbalanced gyro accelerometer offset its accuracy and stability advantages over the other devices considered (references 5-3 and 5-4).

5.20 Catalog information on the operating characteristics of three force feedback acclerometers is presented in table 5-4 as taken from reference 5-2. The size and weight criteria which figure dramatically in the selection of the FPA may be of lesser importance in selecting a body-mounted package.

INERTIAL NAVIGATION SYSTEMS

5.21 Reference 5-2 also approaches the inertial flight path acceleration sensing system. Two methods of establishing an earth's reference were investigated. On approach involved mounting the accelerometers to the airframe with an earth-oriented reference, and the other features a four-gimbal platform utilizing Schuler tuning to establish the earth-oriented plane. Both approaches establish the instantaneous velocity vector of the aircraft with respect to the earth's coordinates. After due consideration, reference 5-2 concludes: "...the inertial approach for determining flight path accelerations was not pursued because of the inherent complexity of the system, large errors introduced during certain maneuvers, and difficulties in obtaining accurate three-dimensional local wind information."

5.22 General Dynamics utilized a modified Delco Carousel V inertial platform in its YF-16 test program (reference 5-5). Although a great deal of performance data was used from the platform, the aircraft was equipped with conventional instrumentation for data

TABLE 5-4

CURRENT ACCELEROMETER CAPABILITIES

Model	Kistler Model 305B	Systron-Donner Model 4310	Kearfott C702401
Threshold	5×10^{-6} g	1×10^{-5} g	1×10^{-6} g
Hysteresis	5×10^{-4} g	4×10^{-4} g	1×10^{-5} g
Scale Factor Error	2×10^{-4} g/g^2	1×10^{-3} g/g^2	2×10^{-6} g/g^2
Bias Error	1×10^{-3} g	1×10^{-3} g	1×10^{-3} g
Cross Coupling	0.010 g/g	0.002 g/g	10^{-5} rad/g
Natural Frequency	300 Hz	200 Hz	200 Hz
Temperature Sensitivity	3×10^{-4} g/^{o}F (5.4×10^{-4} g/^{o}C)	2×10^{-4} g/^{o}F (3.6×10^{-4} g/^{o}C)	5×10^{-6} g/^{o}F (9×10^{-6} g/^{o}C)
Temperature Range	-65 to 185 ^{o}F (-54 to 85^{o}C)	-40 to 200 ^{o}F (-40 to 93^{o}C)	-85 to 225 ^{o}F (-65 to 107^{o}C)
Size	1.0 in dia x 2.0 in (2.54cm dia x 5.08cm)	0.9in x 1.2in x 1.4in (2.3cm x 3cm x 3.5cm)	1.0in x 1.0in x 2.0in (2.5cm x 2.5cm x 5 cm)
Weight	3.4 ounces (96.5 grams)	4.5 ounces (127.7 grams)	3 ounces (85.1 grams)

backup, and the platform was not a production item. General Dynamics however, claims a highly successful program (the reader is referred to reference 5-5 for additional details).

5.23 More recent tests performed at the U.S. Naval Air Test Center, utilizing an A-7C at the Naval Test Pilot School (reference 5-6) gave a more optimistic evaluation of the use of an inertial navigation system. The A-7C combines an ASN-91 Tactical Computer (IBM) with an ASN-90 Inertial Measurement Unit (Singer Kearfott). The only modifications to the system were for the purpose of recording system parameters (one circuit board was modified). Reference 5-6 concludes: "An inertial system can be successfully used to derive the parameters which describe the motion of an aircraft."

INERTIAL MEASUREMENTS (ANGLES AND ANGULAR RATES)

5.24 The inertial measurement of bank angle (ϕ) , and pitch attitude (θ) effect the accelerometer equations in the coordinate transformation as given in Chapter 2. Additionally, as will be discussed in Chapter 7, the measurement of angle of attack upwash requires the measurement of pitch attitude by some methods. The basic accuracy sought in angle of attack (as shown in Chapter 7) is ± 0.10 degrees and this will be taken as the desired accuracy of the inertially measured angles.

5.25 In determining the accuracy necessary for the determination of angular rates and their derivatives, the limiting equation set

is the accelerometer rate corrections as given in equations 2-46 to 2-52 of Chapter 2. For example:

$$N_{x_{net}} = N_{x_i} + 1/g\left[r_x(\dot{\theta}^2+\dot{\psi}^2) + r_y(\ddot{\psi}-\dot{\phi}\dot{\theta}) + r_z(\ddot{\theta}+\dot{\phi}\dot{\psi})\right] \quad . \tag{2-46}$$

5.24 In order to preserve the .001 g (1 mg) accuracy in the corrected accelerometer reading, each additive term in the above equation should be more accurate than 1 mg. However, in the general case, the errors in terms will not be biased all in one direction so that maintaining 1 mg accuracy in each of the terms should induce only small errors. The x distance terms are the most critical in the above equations because in the general case, r_x will have the largest magnitude. The terms involving the r_x term in the angular rate correction equations are:

$$r_x\dot{\phi}^2,\ r_x\dot{\psi}^2,\ r_x\ddot{\theta},\ r_x\ddot{\phi}\ddot{\psi},\ r_x\ddot{\psi},\ r_x\ddot{\psi}\dot{\theta} \quad ,$$

so that each of these terms divided by g should maintain the desired 1 mg accuracy where the angular rates and derivatives are in radians per second and radians per second squared, respectively.

5.27 It can be seen in the above relations that $\frac{r_x A}{g}$ is the general form where A is the angular rate product or derivative. In general, for flight path accelerometers, the distance is from 30 to 50 feet or more so that for a 32-foot distance:

$$\frac{r_x \Delta A}{g} = .001 \tag{5-6}$$

$$\Delta A = .001 \text{ (rad/sec)}^2 \text{ or rad/sec}^2 \tag{5-7}$$

or

$$\Delta A = .238 \text{ deg/sec or } .057 \text{ deg/sec}^2 \quad . \tag{5-8}$$

In the general case, if the instrumentation system is available, .2 deg/sec and .05 deg/sec^2 is desired. However, in the practical case, accuracies of this magnitude for angular acceleration are either cost-prohibitive or not available so that an associated accuracy of ±.20 deg/sec or ±.10 deg/sec^2 for rate and rate derivative instruments is acceptable. For cg accelerometers, the accuracy requirement becomes less in that the r_x distance is much reduced. It can be seen, for instance, that an r_x value of 8 feet will yield an associated rate accuracy of four times the above accuracies. This then is one of the tradeoff values of body-mounted packages versus the flight path accelerometer. The flight path accelerometer shows reduced sensititivy to errors in angle of attack as detailed in Chapter 1, paragraph 1.22.

ENGINE PARAMETERS

5.29 The parameters required for the calculation of aircraft thrust are in general dependent upon the particular engine and airframe combination. For this reason, they will be dealt with only generally here. If the idealized thrust equations, as taken from reference 5-7, are examined:

subcritical flow,

$$\frac{F_g}{\delta} = \frac{29.4\ A_e \gamma_e}{\gamma_e - 1}\left[\left(\frac{P_{T_5}}{P_a}\right)^{\frac{\gamma_e - 1}{\gamma_e}} - 1\right] \tag{5-9}$$

and

supercritical flow,

$$\frac{F_g}{\delta} = 14.7\ A_e\left[(\gamma_e + 1)\left(\frac{P_{T_5}}{P_a}\right)\left(\frac{2}{\gamma_e + 1}\right)^{\frac{\gamma_e}{\gamma_e - 1}} - 1\right]. \tag{5-10}$$

Equation 5-9 is the most critical due to the fractional exponent. At the critical pressure ratio, a .03 change in the pressure ratio will create a 3 percent change in thrust with the other parameters being constant. This .03 change in pressure ratio corresponds to 1.62 percent at the critical pressure ratio, but due to the inaccuracies in the other parameters, a 1.0 percent accuracy is desired in the engine pressure ratios when dealing with the idealized thrust equations. This analysis applies mainly to turbojet engines, since this is the basic parametric form; however, for turbofan-type engines, the individual parametric thrust development must be considered.

5.30 In addition to the parameters required for thrust, the engine fuel flow must be monitored for use in the thrust fuel flow map. In general, in order to obtain a thrust fuel flow map which is good to 3 percent for the case where thrust is good to only 3 percent, the fuel flow must be accurate to ±0 percent. However, when plotting in rectangular coordinates, the curve accuracy will be given as the hypotenuse of the accuracy triangle, so that introducing ±1 percent scatter in fuel flow, yield ±3.16 percent scatter in the thrust fuel flow relation. For thrust modeling applications, then, the desired accuracy of fuel flow is ±1 percent.

5.31 For fuel flow modeling applications and an assumed TSFC (Thrust Specific (Fuel) Consumption) of one, the accuracy of fuel flow will be ±3 percent because the associated inaccuracies of thrust calculation are now in the measurement of fuel flow. So that the accuracy requirement fuel

flow decreases to ±3 percent for fuel flow modeling applications. This reduction in accuracy requirement is brought about by the fact that the thrust fuel flow map is taken as accurate by definition and is the basis for further performance calculations.

5.32 The final parameter to be considered with engine instrumentation is the aircraft gross weight. In some cases, the aircraft gross weight will be calculated from the integrated fuel flow and others from a survey of fuel remaining onboard. If the case of a ±3 percent measurement of aircraft gross weight is applied to a 50,000 pound aircraft at .5 g longitudinal acceleration, the resultant inaccuracy in excess thrust is ±1.5 percent. Under these conditions, the measurement of gross weight to ±3 percent are adequate.

AIRFRAME PARAMETERS

5.33 The airframe parameters to be considered will be mainly the movable control surface positions. These in turn will be used predominately to define the aircraft configuration. The accuracy requirements in defining the aircraft configuration are dependent, of course, upon the configurations to be tested. For instance, the requirement for a two-position speed-brake will simply be in or out. However, for a variable position speed-brake, the accuracy requirement is increased if several different configurations use the speed

[redacted]

[redacted]

[redacted]

[redacted] display for [redacted] certain parameters [redacted]. The [redacted] required are lesser than [redacted] "kneeboard" data will not [redacted] modeling approach.

5.37 The main accuracy requirement is that accuracy of precision asked of the pilot. For example, if the pilot is asked to hold .05 Mach number in a climb, his instrument should be capable of yielding this information. For this reason, the pilot display parameters will only be listed here:

a. Altitude - used for a baseline for data gathering and safety of flight.

b. Airspeed - again as a pilot setup parameter and safety of flight. At low Mach numbers, where Machmeters are inaccurate, the engineer should provide airspeed information to the pilot.

c. Mach number - required as a pilot setup parameter.

d. Longitudinal acceleration - desired but not required as an aid to the pilot in achieving stabilization. (See figure 5-1.)

e. Normal acceleration - required for dynamic-type maneuvers.

f. Angle of attack - required for safety of flight and dynamic-type maneuvers.

g. Pitch rate - required for dynamic-type maneuvers.

h. Fuel counts or fuel remaining - for quick calculation of aircraft gross weight.

i. Correlation

j. Engine monitor parameters - safety of flight

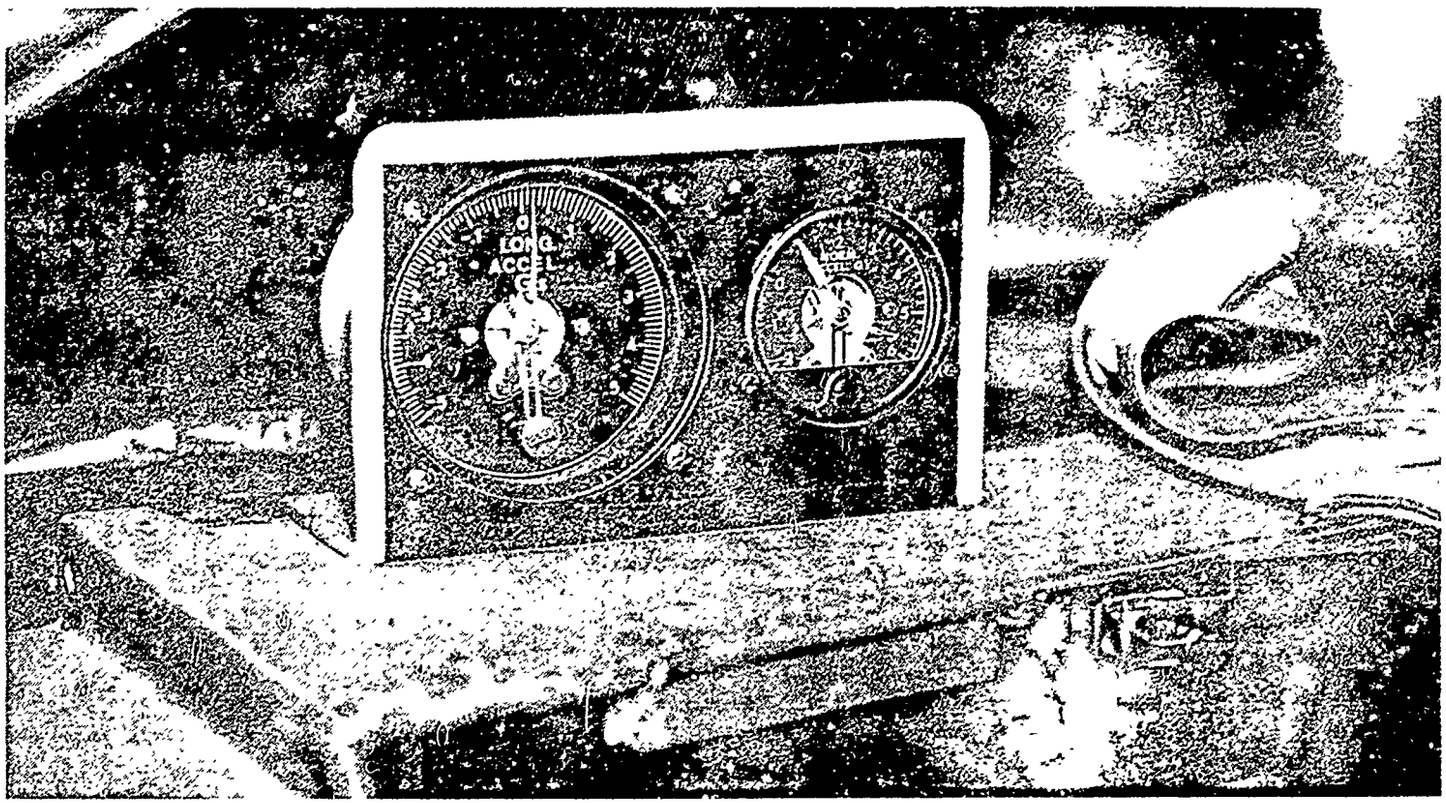

FIG. 5-1: PILOT DISPLAY OF LONGITUDINAL AND NORMAL ACCELERATIONS IN FB-111A

INSTRUMENTATION SUMMARY

5.38 The instrumentation accuracies desired will degrade somewhat from the laboratory conditions. It has been seen, that in research programs such as that conducted by Grumman on the A-6A (reference 5-8) or those conducted at Edwards Air Force Base, the Grumman Flight Test Facility, and Patuxent River as given in Chapter 1, a target accuracy of 3 percent can be maintained. It has been noted, however, that in production type programs, the accuracy degrades to about 5 percent. This is probably due to several reasons. During research programs, increased attention is paid to small items, such as calibration constants, etc. Additionally, research programs usually involve much fewer people than the production programs which are mainly concerned with gathering data. Finally, more careful attention is paid to handling, installing, and calibrating instruments in a research program.

5.39 The generalized instrumentation requirements and accuracy requirements are summarized in table 5-5.

TABLE 5-5

INSTRUMENTATION SUMMARY

Instrument	Desired Accuracy	Required Accuracy	Comments
Altimeter	±100 ft	±100 ft	
Airspeed Indicator	±1 kt slow ±2 kt fast	±1 kt slow ±2 kt fast	
Mach meter	±.02	±.05	
Free Air Temperature	±0.5°C	±1.0°C	
Angle of Attack	±0.05 deg	±0.10 deg	See Chap.7
Angle of Sideslip	±0.1 deg	±1.0 deg	
Longitudinal Accel.	±.001 g	±.001 g	
Normal Acceleration	±.001 g	±.005 g	
Lateral Acceleration	±.001 g	±.005 g	
Accelerometer Temp.	±1.0°C	As required by calibration	See Chap.6
Pitch Attitude	±0.05 deg	±0.10 deg	
Roll Attitude	±0.10 deg	±0.10 deg	
Pitch Rate	±0.20 deg/sec	±0.20 deg/sec	
Roll Rate	±0.20 deg/sec	±0.20 deg/sec	
Yaw Rate	±0.20 deg/sec	±0.20 deg/sec	
Pitch Accleration	±0.06 deg/sec^2	±0.10 deg/sec^2	
Roll Acceleration	±0.06 deg/sec^2	±0.10 deg/sec^2	
Yaw Acceleration	±0.06 deg/sec^2	±0.10 deg/sec^2	
Engine Pressure Ratio	±1%	±1%	
Thrust	±3% repeatable	±3% repeatable	
Fuel Flow	±1%	±1% thrust modeling ±3% fuel flow modeling	
Others	As required	As required	

CONCLUDING REMARKS TO CHAPTER 5

5.40 The instrumentation requirements for any program must be modified to fit the individual circumstances. The analyses contained in this chapter are general in nature and require detailed application. Two areas require further clarification and will be dealt with in the next two chapters. The instrumentation required and the accuracy requirements for the accelerometer methods are consistent with the requirements for conventional performance, with the exception of the accelerometer measurements and the measurement of angle of attack. Each of these will be the subject of separate chapters.

REFERENCES TO CHAPTER 5

5-1. U.S.A.F. Document No. 6273, "Flight Test Engineering Handbook," by Herrington et al., Unclassified, Jan 1966.

5-2. U.S.A.F. Document No. FTC-TR-68-28, "Final Report, Flight Path Accelerometer System," by J. A. Nevins, Unclassified, Dec 1968.

5-3. Royal Aircraft Establishment, TR-67183, "Performance Characteristics and Methods of Testing Force Feedback Accelerometers," by I.L. Thomas and R.H. Evans, Unclassified, Aug 1967.

5-4. Grumman Aircraft Engineering Corporation, RE-239J, "Advances in Inertial Guidance Components," by P.H. Savet, Unclassified, 1966.

5-5. A.I.A.A. Paper 75-32, "The Use of a Navigation Platform for Performance Instrumentation on the YF-16 Flight Test Program," Presented in Pasadena, California by J.N. Olhausen, Unclassified, Jan 1975.

5-6. U.S. Naval Air Test Center, Technical Memorandum TM-TPS-76-1, "Inertially Derived Flying Qualities and Performance Parameters," by W.C. Bowes and R.V. Miller, Unclassified, 16 Jun 1976.

5-7. U.S. Naval Air Test Center, Technical Memorandum 3-68, "Use of the Ratio of Specific Heats in the Determination of Turbojet Engine Thrust," by W. R. Simpson, Unclassified, 16 Apr 1970.

5-8. Grumman Aerospace Corporation, Report No. ADR-07-01-70.1, "Development of Dynamic Methods of Performance Flight Testing," By P. Pueschel, Unclassified, Aug 1970.

THE ACCELEROMETER METHODS OF DETERMINING AIRCRAFT PERFORMANCE (DYNAMIC PERFORMANCE TESTING)

CHAPTER 6

LABORATORY CALIBRATION PROCEDURES FOR SENSITIVE ACCELEROMETERS

SUMMARY OF CHAPTER 6

6.1 The laboratory calibration of sensitive accelerometers are essential to any program using the dynamic methods. Calibration techniques are presented for range extended sensitive accelerometers in high g and various environmental conditions.

INTRODUCTION TO CHAPTER 6

6.2 The purpose of the laboratory calibration of the accelerometer package is to correlate the accelerometer output with the measured load factor. Several methods will be used to place the accelerometer in a known or standard acceleration condition. The output of the accelerometer is simply a voltage which is proportional to the acceleration experienced.

6.3 In order to increase the output resolution, the accelerometer will be range extended. The purpose of the range extender is to take the accelerometer output (which is in the 0 to 5 volt range) and effectively increase the output. This is done by a series of numerical cutoffs and amplifiers giving two signals instead of one. The first signal takes the original 0 to 5 volt output and breaks it into digital segments. If there are 25 digital segments for 0 to 5 volt output, then each digital segment will be 0.20 volts. For example, if the voltage output were to read 2.500 volts, the digital signal would be 2.400 volts or 12 digital steps of 0.20 volts. The second signal takes the remainder of the signal and amplifies it to 0 to 5 volts, based on the digital cutoffs. In the example, 0.20 volts is amplified to 5-volt output or an amplification of 25 to 1. At the given point in the example, 0.10 volts remain after the digital cutoff at 2.4 volts. This signal is amplified 25 to 1, or to 2.50 volts. The result is two signals, a digital signal of 2.40 volts, and an amplified signal of 2.50 volts or 50 percent of the

5.0 volt range. Simply translated, then, there would be 12.5 digital steps. This allows the end accuracy of the output voltage to be amplified 25 to 1, so that any loss of recording accuracy will affect the signal at 1 to 25.

6.4 The procedures described in this Chapter were established with the Systron-Donner, two axis (Model 4310) systems in the Air Force Flight Test Center (AFFTC) laboratories. All calibrations were taken with the intent of maintaining ±.001 g (1 mg) accuracy of the longitudinal axis.

SYMBOLS

6.5 The following symbols are used in Chapter 6.

Symbol	Definition	Common Units	Metric Units
a	Acceleration	ft/sec^2	(m/sec^2)
C	Coefficient	-	-
d	Diameter	ft	(m)
e	Voltage	volts	(volts)
E	Modulus of elasticity	lbs/ft^2	(N/m^2)
g	Acceleration of gravity	ft/sec^2	(m/sec^2)
G	Gain	db	(db)
I	Area moment of inertia	ft^4	(m^4)
ℓ	Length	ft	(m)
M	Moment	ft-lbs	(N-m)
n	Step number	-	-
n	Load factor	g s	(g s)
r	Radius	ft	(m)
T	Temperature	deg F or R	(deg C or K)
V	Voltage	volts	(volts)
V_o	Zero voltage	volts	(volts)
W	Weight	lbs	(kg)
w	Weight per length	lbs/ft	(kg/m)
x	Length	ft	(m)
β	Rate table, radius-oriented misalignment angle	deg	(deg)
Δ	Increment	-	-

Symbol	Definition	Common Units	Metric Units
θ_1, θ_2	Pendulum-orientation angles	deg	(deg)
$\ddot{\theta}$	Pitch acceleration	deg/sec^2	(deg/sec^2)
θ	Ultradex head orientation	deg	(deg)
ϕ	Rate table, earth-oriented misalignment angle	deg	(deg)
γ	Voltage sensitivity	volts/step	(volts/step)
ω	Turn rate	deg/sec	(deg/sec)

Others

f( )	Function		
de/dstep	Step sensitivity	g s	(g·s)

Subscripts

r	Radial direction
i	Indicated
n	Normal
FP	Flight path
L	Local
amb	Ambient
o	Zero condition
x	Flight path direction
z	Normal to flight path
FPA	Flight path accelerometer

6.6 The first value of standard acceleration to be used will be the earth's gravitational field. For calibration of the total range of the flight path axis and the ±1.0 g range of the normal axis of the accelerometer, the static geocentric acceleration of gravity is sufficient. If the orientation of the accelerometer with respect to the earth's gravitation field is known accurately, the acceleration that the accelerometer is experiencing can be computed as a component of the earth's gravitational field. It should be noted that the value of g referred to here is the local acceleration of gravity, and this value should be used in subsequent calculations. In a test case, an Ultradex Head was mounted on a Collins Micro-Flat granite block in the AFFTC calibration laboratory.

6.7 The acclerometers were mounted as closely to zero-orientation as could be obtained by the sensitive levels available, as shown in figures 6-1 and 6-2. At this point, the alignment of the accelerometer is not assumed perfect, and the misalignment is computed by using the flight path accelerometer outputs at 0 degrees and 180 degree orientation (these should be the same for perfect alignment, since in both cases, the flight path axis experiences zero g s). The difference in electrical readings is equivalent to twice the misalignment, and the mid voltage, or average vlotage reading at these two settings is the true voltage for 0 or 180-degree orientation. This is further checked by recording normal acceleration at

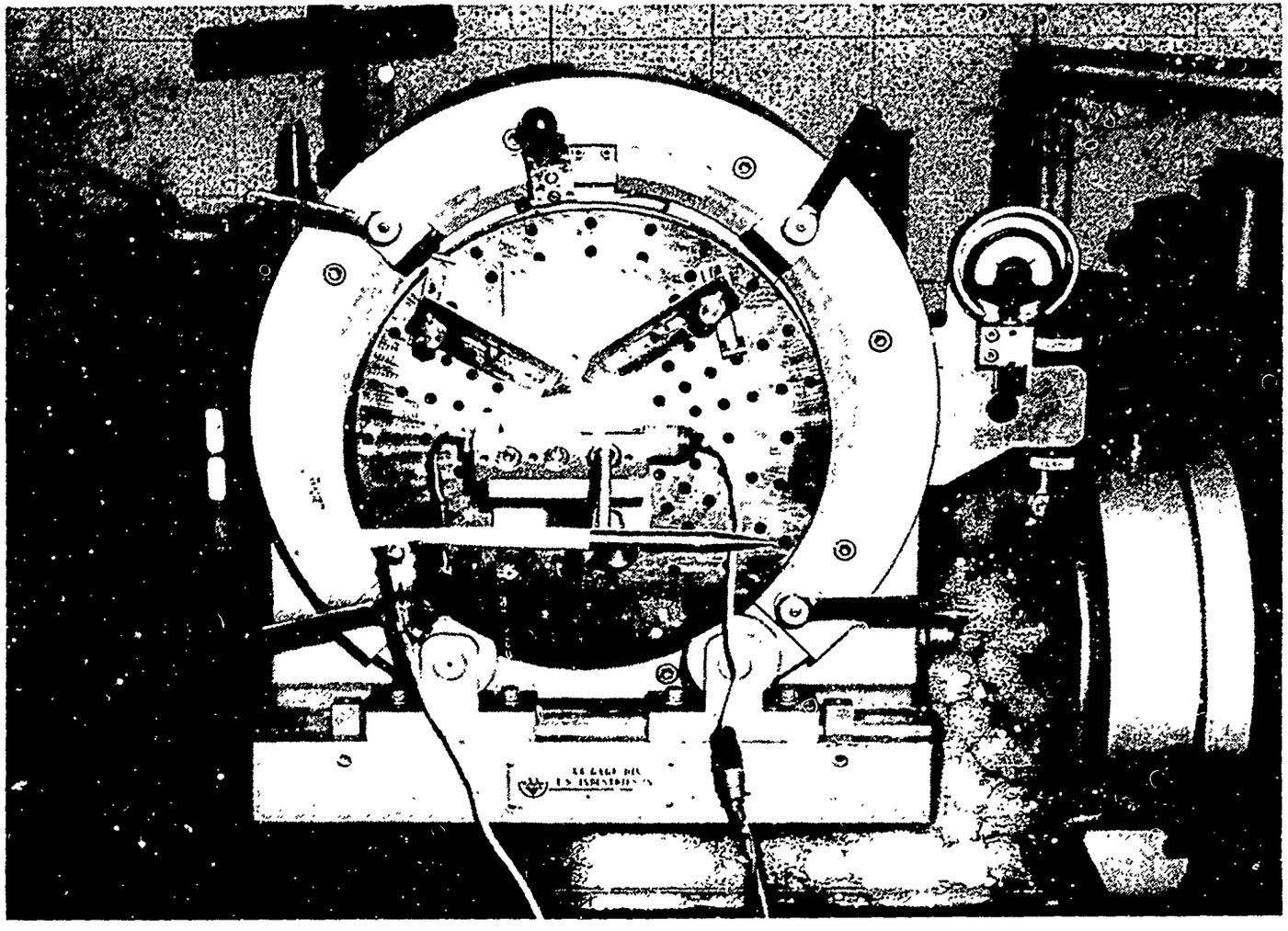

FIG. 6-1: ULTRADEX HEAD WITH ACCELEROMETER MOUNTED

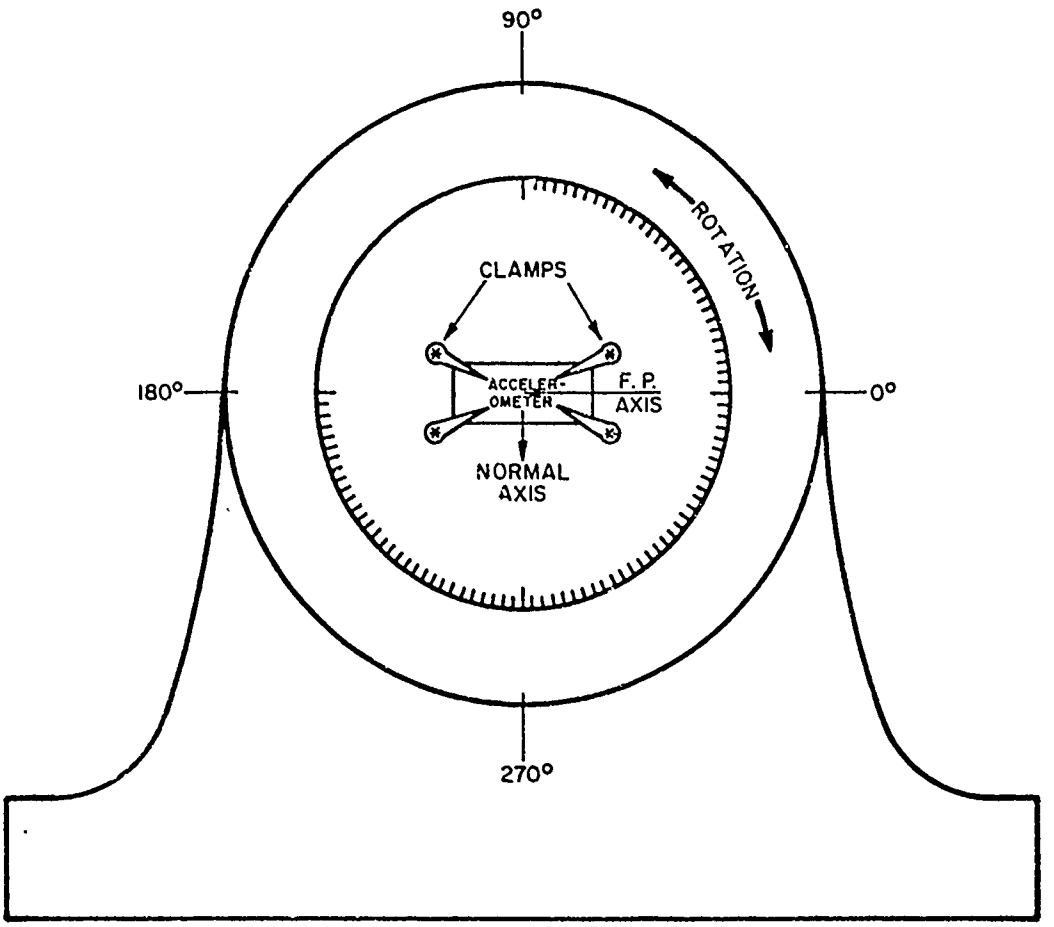

FIG. 6-2: ULTRADEX HEAD ANGULAR RELATIONS

the 90-degree and 270-degree orientation and a zero voltage is obtained for this axis. Misalignments in yaw for a three-axis system can be obtained similarly.

6.8 Readings of step and fine voltages are then taken at specified degree intervals on the Ultradex Head over the useful range (±0.6 g for the flight path axis and ±1.0 g for the normal axis). For higher values of acceleration, the rate table is required as discussed in a later section. The head/accelerometer misalignment is added to each point to give the true orientation of the accelerometer to the earth's gravitational field.

6.9 A mathematical model will be used to relate the voltage readings to acceleration. The mathematical model is based on the voltage readings and is obtained as follows:

$$n_x \text{ or } n_z = \left[\frac{V-V_o}{\gamma} + n\right] \frac{dg}{dstep} \qquad (6\text{-}1)$$

where dg/dstep = voltage sensitivity per step

V = range extended fine voltage

V_o = voltage reading at 0 g (from paragraph 6.6)

γ = voltage step sensitivity (volts per g)
(0.20 in the example of paragraph 6.2)

n = step number based on the digital cutoff voltage (coarse reading).

6.10 The step voltage is used to define a level for the overall reading and the step numbers should be defined by voltage readings. The voltage step may be defined as:

step 0 when g = 0 and $V = V_o$

step +1, +2, etc., when g > 0

step -1, -2, etc., when g < 0 .

In practice, the first term of equation 6-1 is simply the fraction of the step used such that n = [step + fractional step] x sensitivity. The standard value of load factor is determined as the component of the one g gravitational field (sine or cosine of $(\theta+\phi)$) where:

θ is the Ultradex Head orientation; and

ϕ is the accelerometer/head misalignment as determined in paragraph 6-6.

6.11 With the misalignment in both axes calculated, the orthagonality can be checked between these axes and the difference between the two axes from the 90 degrees or normal case can be used as a measure of cross-axis sensitivity.

6.12 The zero voltage (V_o) and the step numbers have been defined. The volts per step and dg/dstep can be obtained as in the example of paragraph 6-2 by dividing the full range output by the number of steps. These values will be coarse, and will probably not relate the load factor to voltage with enough accuracy. At each point, a value of load factor will be calculated from equation 6-1 and a standard value will be determined as in paragraph 6-10. The parameters of equation 6-1 will then be manipulated to arrive at the desired accuracy as given in the procedures below:

A. If data dispersion is excessive (see figure 6-3). An error in the volts per step constant(γ) can create a family of error lines with double values as shown in figure 6-3. The volts per step should be adjusted to minimize scatter. In a test case run, a difference of .047 volts/step reduced the dispersion from ±8 mg to ±3 mg and gave case B.

B. Data is linear, but not dispersed about zero (see figure 6-4). In the general case, if results similar to figure 6-4 are achieved, data reduction may cease, in that figure 6-4 may

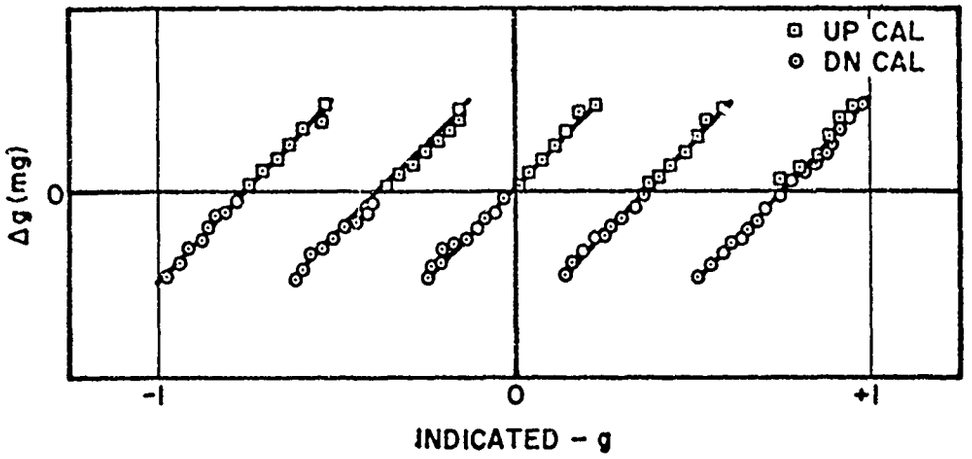

FIG. 6-3: EXCESSIVE DATA DISPERSION

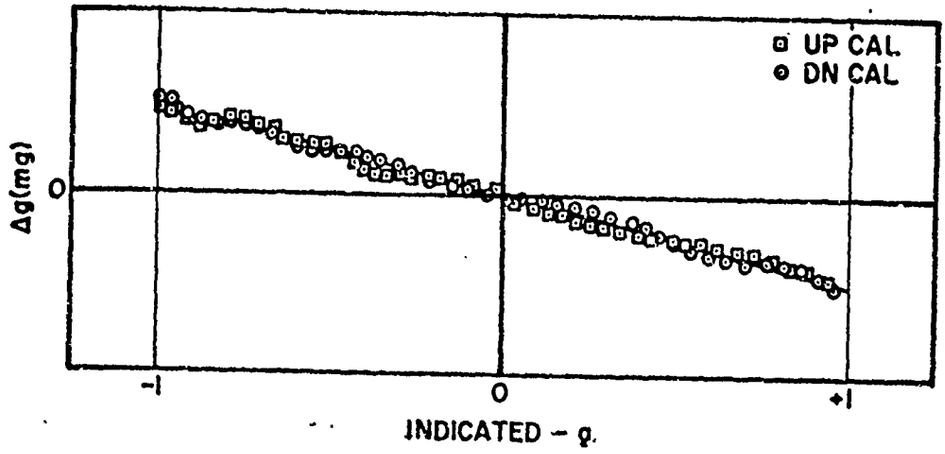

FIG. 6-4: LINEAR NON-ZERO SLOPE DATA

be applied as a calibration curve. However, adjusting the mathematical model to minimum error, so that no calibration curve is required, will greatly simplify the temperature calibration. If environmental problems are not severe (as with body accelerometers) or the accelerometer is under environmental control, figure 6-4 may be used as a calibration curve. In the general case of a flight path accelerometer without thermal control(so that temperature corrections are required),further refinement to equation 6-1 will be required. The slope of this line may be changed by adjusting the sensitivity parameter dg/dstep. In a test case, a change of .0009 g s/step reduced dispersion (rotated the line) from ±3 mg to ±1 mg. The procedure is to adjust the sensitivity parameter until a zero slope calibration curve is obtained.

C. Data is linear, zero slope, but not at a zero value (see figure 6-5). This indicates a small error in the zero voltage or a small adjustment in the zero voltage is necessary and correction can be made by adjusting the zero voltage by the amount indicated.

D. Data is not linear (see figure 6-6). The non-linearity, as shown in figure 6-6, may be caused by a non-linearity in the accelerometer output. In the systems thus far tested, non-linearity was considerably less than ±1 mg in the range of data acquisition. More than likely, the non-linearity is caused by an error in calculation of the measured Ultradex Head to accelerometer misalignment. The voltage difference is related to g which is

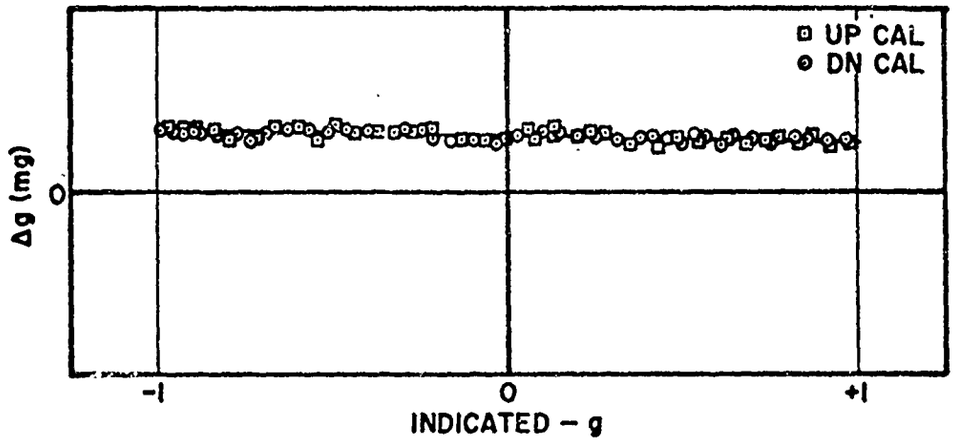

FIG. 6-5: LINEAR NON-ZERO VALUED DATA

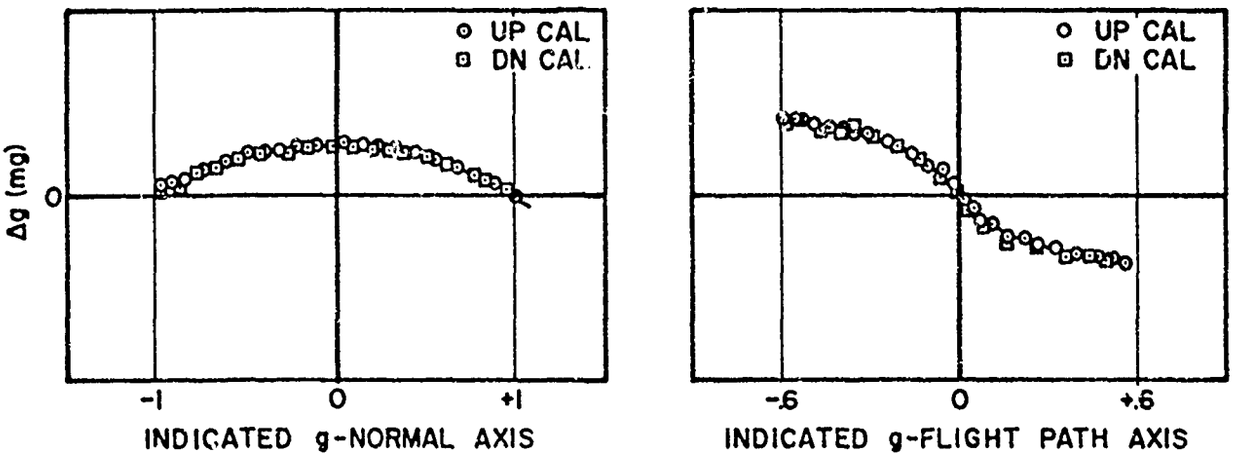

FIG. 6-6: NON-LINEAR DATA

then translated to angular measure by the arc sine or arc cosine (depending on the axis tested) to obtain a misalignment angle. In a test case, introducing an error of 9 minutes in misalignment angle leads to a peak in the normal axis of 4 mg (a change of 3 mg over the original ±1 mg). In practice, a combination of all of the above errors may be included in the original data. Refinements need not be taken beyond eliminating the double value of step A, since the resulting curve can be used as a calibration curve. But obtaining a mathematical model that does not require a calibration curve simplifies the analysis when temperature calibrations are considered. The final data should reduce to ±x mg where x is the accuracy desired (normally 1 mg).

ACCELEROMETER TEMPERATURE SENSITIVITY

6.21 Calibrating the accelerometer over a wide temperature range is desirable. For this reason, a temperature probe was mounted on the flight path accelerometer used in the AFFTC program. The probe consisted of a small spool of wire whose resistance was temperature sensitive. The probe used was made of Balco wire - 36 gauge (4.8 ohms/ft @ $0^{\circ}C$), and was wound to 50 ohms (just over 10 feet) for compatibility with output instruments. (Accelerometer models are available with temperature probes installed.) The probe may be calibrated at the same time as the accelerometer. The probe and accelerometer should be calibrated over the useful temperature range of the accelerometer (-40 to $+130^{\circ}F$ for the Systron-Donner Model 4310). The accelerometer is placed on a stand and a pendulum is mounted as shown in figure 6-13. With the vane earth-oriented by the pendulum and the accelerometer vane-oriented, there will be no change in the accelerometer position with the earth's gravitational field due to temperature warpage of the mounting stand or over floor. Standard g is given as the component of the earth's gravitational field. The value of standard g can then be changed by changing the accelerometer orientation with the pendulum as shown in figure 6-14.

6.22 Several results can be obtained. Looking again at the basic mathematical model:

$$g = \left[\frac{V-V_o}{\gamma} + n\right] dg/dstep \quad . \qquad (6\text{-}1)$$

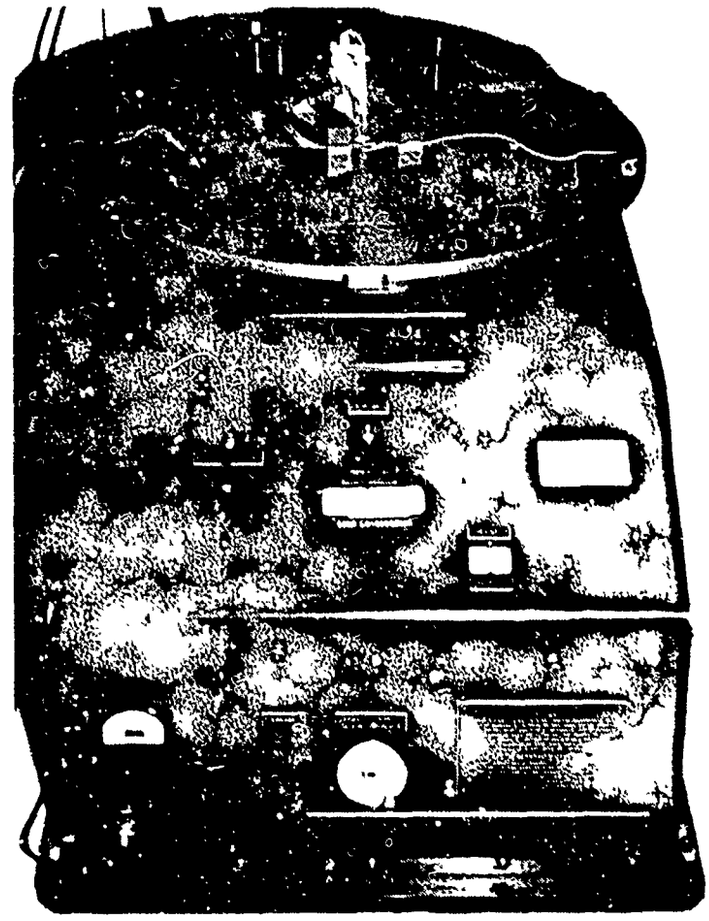

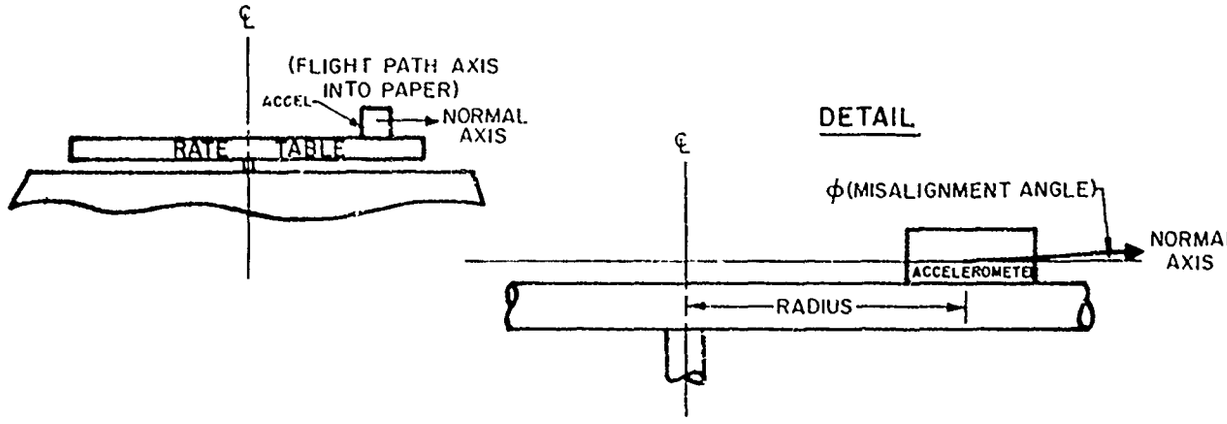

FIG. 6-7: RATE TABLE AND EARTH-ORIENTED MISALIGNMENT

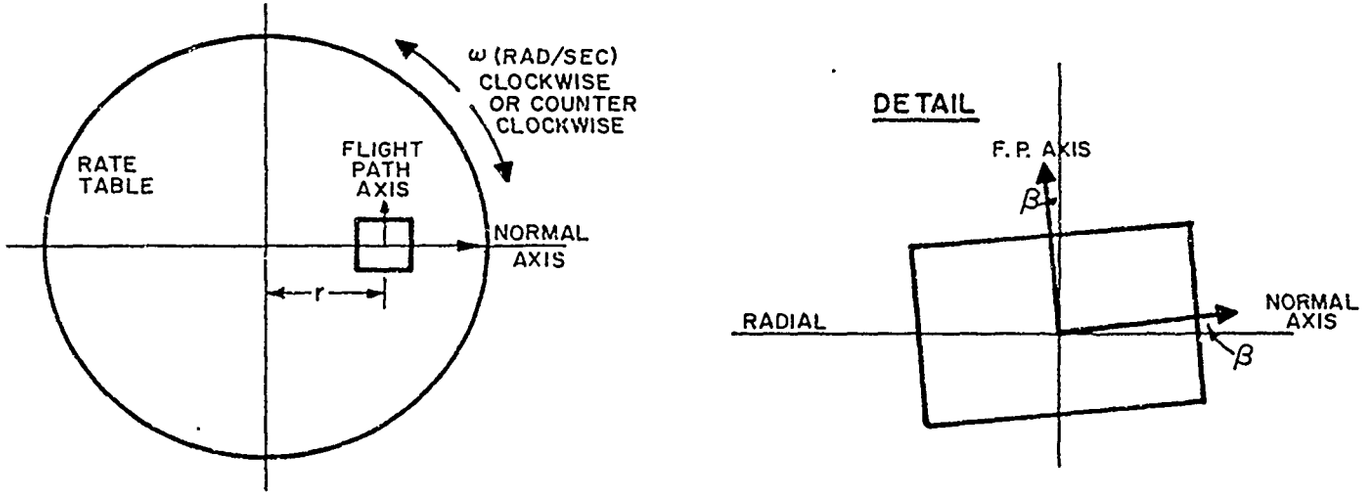

FIG. 6-8: RATE TABLE, RADIUS-ORIENTED MISALIGNMENT

Under running conditions, the acceleration outward along the radius (a_r), is given by:

$$a_r = r\,\omega^2 \quad , \tag{6-2}$$

where r is the radius of rotation and ω is the turn rate in rad/sec, the radial load factor will be given by:

$$n_r = \frac{r\omega^2}{g_L} \quad , \tag{6-3}$$

where g_L is the local acceleration of gravity and n_r is the radial load factor.

6.14 The indicated normal acceleration (n_{i_n}) is given as a component of the radial acceleration by:

$$n_{i_n} = n_r \cos\beta \cos\phi \tag{6-4}$$

or

$$n_{i_n} = \frac{r\omega^2}{g_L} \cos\beta \cos\phi \; . \tag{6-5}$$

The earth-oriented misalignment (ϕ) is determined from the procedure of paragraph 6.13, and the turn rate (ω) is measured by a counter. By keeping the turn rate small to keep the accelerations less than 1 g, the n_{i_n} can be computed from equation 6-1 and the measured voltages using the values obtained in the section on Ultradex Head Calibration. There are still two unknowns, r and β.

6.15 The indicated flight path acceleration $\left(n_{i_{FP}}\right)$ is given by its radial component or:

$$n_{i_{FP}} = n_r \sin \beta = \frac{r\omega^2}{g_L} \sin \beta \ . \qquad (6\text{-}6)$$

Once again, $n_{i_{FP}}$ is computed from equation 6-1. Dividing equation 6-6 by 6-5, and solving for β :

$$\beta = \tan^{-1}\left[\frac{n_{i_{FP}}}{n_{i_n}}\right]\cos \phi \ . \qquad (6\text{-}7)$$

With β known, the radius can be calculated by either equation 6-5 or 6-6. The process should be repeated for several values of n_r.

6.16 With the appropriate system geometry defined, the system can now be calibrated at turn rates high enough to exceed 1 g. The standard value of load factor will be given by:

$$n_s = \frac{r\omega^2}{g_L} \cos \beta \cos \phi \ . \qquad (6\text{-}8)$$

The standard value is used as a comparator to the value of load factor obtained from equation 6-1 at values greater than 1 g. The calibration can be continued until the maximum useful turn rate is reached as given by:

$$\omega_{max} = \left[\frac{n_{max\ useful}\ g_L}{r \cos \beta \cos \phi}\right] \text{rad/sec} \ . \qquad (6\text{-}9)$$

This process should be repeated with the accelerometer inverted to calibrate the negative range of the accelerometer. If an error or 1 mg is obtained at 1 g , the error at 6 g should be no more than 6 mg. If greater errors are obtained, the coefficients of the calibration equation (6-1) can be adjusted as discussed in the section on Ultradex Head.

APPLYING THE CALIBRATION

6.17 Step and fine traces will be used on either magnetic tape or oscillograph. It is important to know the location of the zero voltage. This can be obtained by placing a digital voltmeter in line with the system and orienting the accelerometer to zero voltage on each axis. Alternate methods include taking the midpoint of full scale deflections and using a pendulum to determine the flight path zero axis, or even setting a known orientation, and calculating the voltage or position from calibration data. For magnetic tape recording zero voltages, the step voltage is converted to an integer step number and g is calculated from the calibration equation:

$$g = \frac{V-V_o}{v} + n \quad dg/dstep \quad . \qquad (6\text{-}1)$$

For oscillograph data, the equation is:

$$g = n_{steps} \pm \text{fractional step} \quad dg/dstep \quad . \qquad (6\text{-}10)$$

It should be noted that the fractional step can be positive or negative as shown in figure 6-9.

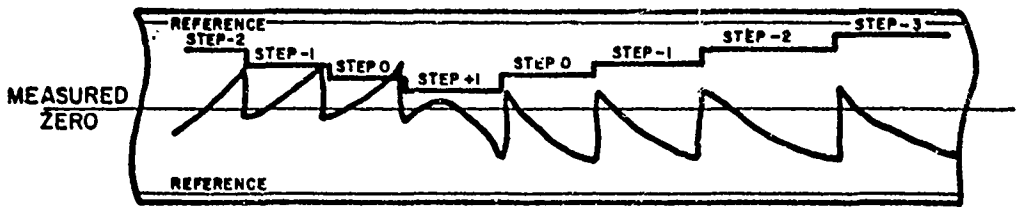

FIG. 6-9: OSCILLOGRAPH RECORD

ACCELEROMETER MISALIGNMENTS (INSTALLED)

6.18 For flight path accelerometers, the vane and accelerometer will, in general, not be mutually aligned. This causes a small error in the orientation of the accelerometer with respect to the aircraft flight path. This misalignment can be determined by earth orienting the vane with a pendulum. With the vane earth-oriented and no misalignment, the accelerometer flight path reading will be zero and the normal reading will be 1.0 g. In the general case, the flight path reading will be the sine of the misalignment angle. This can be checked by setting the vane at known angles as shown in figure 6-10. The vane system can be mounted at $\Delta\theta_1$, 0, or $\Delta\theta_2$ angles and the flight path axis of the accelerometer will experience the sine of the mounting angle plus misalignment.

6.19 For body accelerometers, the misalignment angle to be considered is the angle between the accelerometer orientation and the fuselage reference line. Figure 6-11 shows the body-mounted accelerometer misalignment. A sensitive inclinometer can be used to give the angle of the fuselage reference line with respect to the earth. If there is no misalignment, the flight path axis will experience the sine of this angle. In the general case, the flight path axis will experience the sine of the inclination plus misalignment.

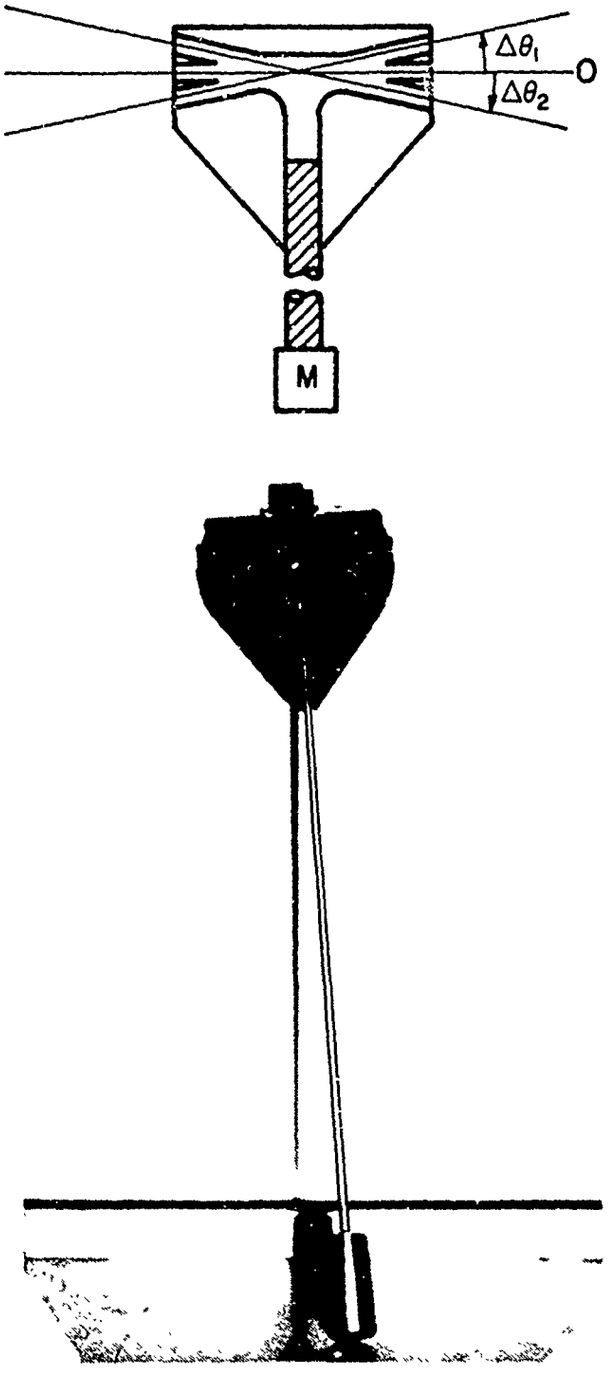

FIG. 6-10: PENDULUM MOUNT

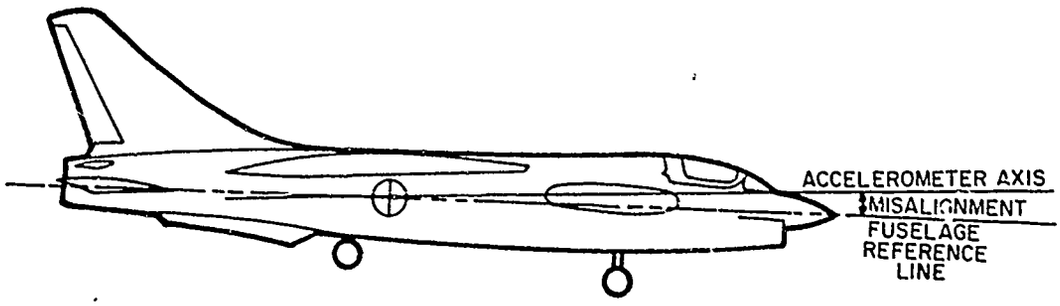

FIG. 6-11: BODY-MOUNTED ACCELEROMETER MISALIGNMENT

YAW MISALIGNMENT

6.20 Misalignments in yaw as shown in figure 6-12 are much more difficult to ascertain and must be obtained by surveying methods. However, in the practical case where accuracies of ±1 mg are sought, we can reasonably ignore this angle if it is determined to be less than 3 degrees. For example, under 0.5 g longitudinal acceleration, a 3-degree yaw misalignment will create a .0007 g error in longitudinal acceleration which is within the ±1 mg accuracy requirement. For higher accuracy data, this misalignment must be computed.

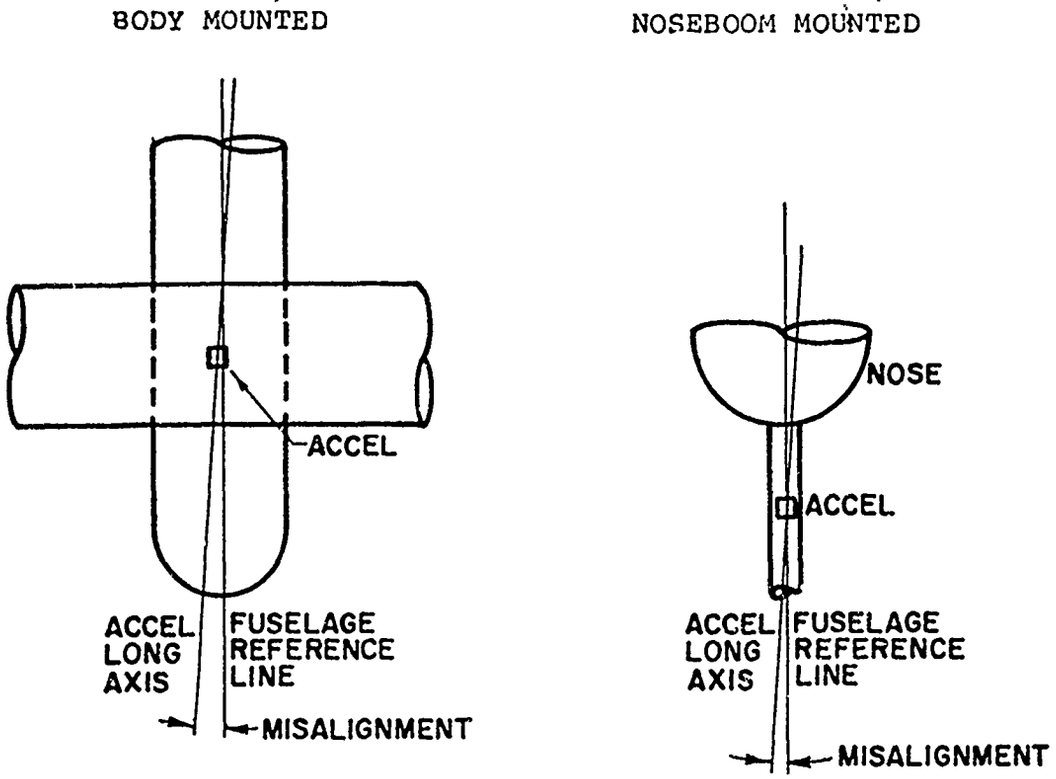

FIG. 6-12: YAW MISALIGNMENTS

ACCELEROMETER TEMPERATURE SENSITIVITY

6.21 Calibrating the accelerometer over a wide temperature range is desirable. For this reason, a temperature probe was mounted on the flight path accelerometer used in the AFFTC program. The probe consisted of a small spool of wire whose resistance was temperature sensitive. The probe used was made of Balco wire - 36 gauge (4.8 ohms/ft @ $0^{\circ}C$), and was wound to 50 ohms (just over 10 feet) for compatibility with output instruments. (Accelerometer models are available with temperature probes installed.) The probe may be calibrated at the same time as the accelerometer. The probe and accelerometer should be calibrated over the useful temperature range of the accelerometer (-40 to $+130^{\circ}F$ for the Systron-Donner Model 4310). The accelerometer is placed on a stand and a pendulum is mounted as shown in figure 6-13. With the vane earth-oriented by the pendulum and the accelerometer vane-oriented, there will be no change in the accelerometer position with the earth's gravitational field due to temperature warpage of the mounting stand or over floor. Standard g is given as the component of the earth's gravitational field. The value of standard g can then be changed by changing the accelerometer orientation with the pendulum as shown in figure 6-14.

6.22 Several results can be obtained. Looking again at the basic mathematical model:

$$g = \left[\frac{V-V_o}{\gamma} + n\right] dg/dstep \quad . \qquad (6\text{-}1)$$

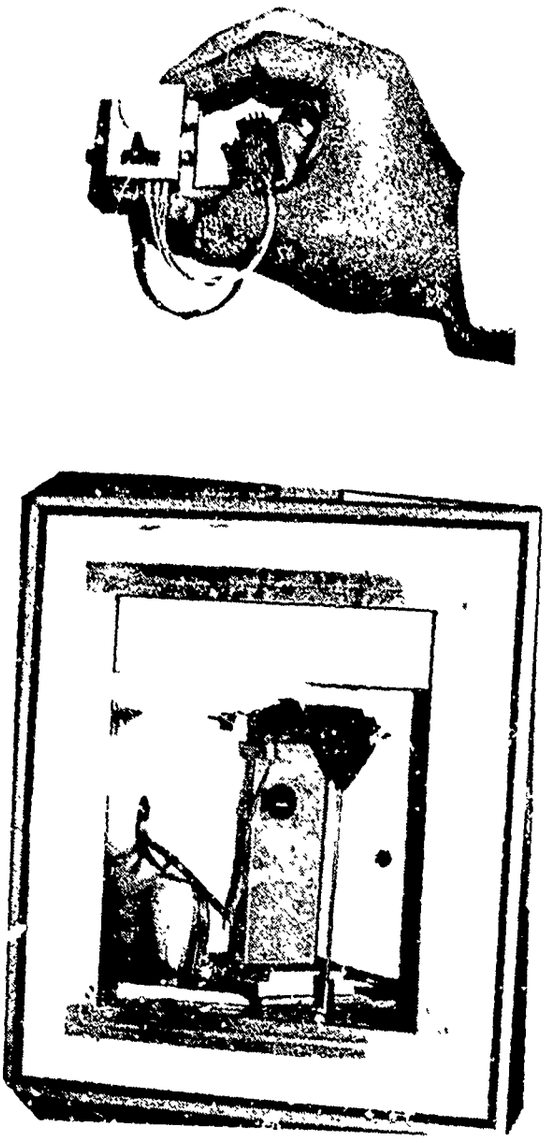

FIG. 6-13: ACCELEROMETER WITH TEMPERATURE PROBE (ABOVE) AND PENDULUM MOUNT IN OVEN (BELOW)

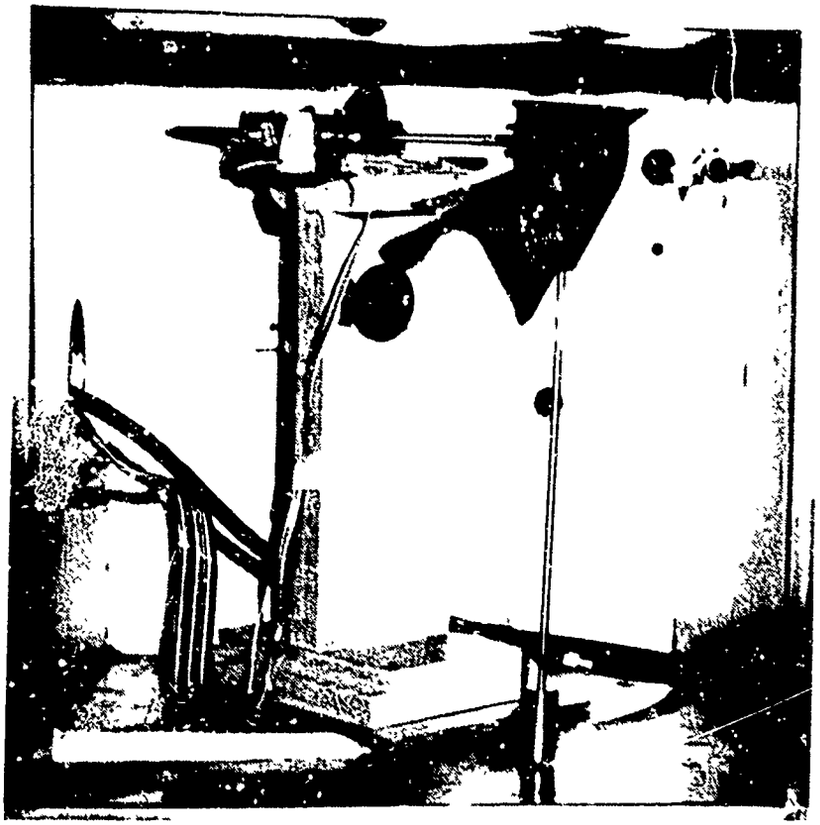

FIG. 6-14: TEMPERATURE CALIBRATION WITH PENDULUM MOUNTED AT ANGLE

The value of the integer step will not change, although the voltage required to give the step may. However, for the systems tested, step levels were 0.2 volts apart and changes with temperature were in the millivolts. Typical results are shown in table 6-1. The main consideration here is to give the computer program an adequate tolerance to determine step number.

6.23 The other voltage terms in the equation can change as follows:

A. Zero voltage (V_o) shift only due to temperature (see figure 6-15).

The adjustment can be made as discussed in paragraph 6.12 and cross-plotted as shown in figure 6-16.

B. Zero voltage (V_o) and sensitivity (γ) change. It was noted in paragraph 6.11 that a sensitivity change rotates the calibration line. Figure 6-17 shows the general case of both zero shift and sensitivity change.

The zero voltage shift can be removed by noting that the sensitivity parameter drops out when $V = V_o$ at zero g s. This deviation can be removed by cross-plotting figure 6-15. The slope of the line can be taken out by calculating a sensitivity (γ) at each temperature as given in paragraph 6.12 and shown in figure 6-18.

C. Non-linear changes. It has been shown that misalignment angle error will cause the calibration curve to become non-linear. Figure 6-19 shows such non-linear changes.

TABLE 6-1

STEP VOLTAGE CHANGE WITH TEMPERATURE

Step Number	Low Temperature Voltage	Room Temperature Voltage	High Temperature Voltage
0	2.431	2.435	2.438
1	2.633	2.636	2.639
2	2.835	2.837	2.840
etc.			

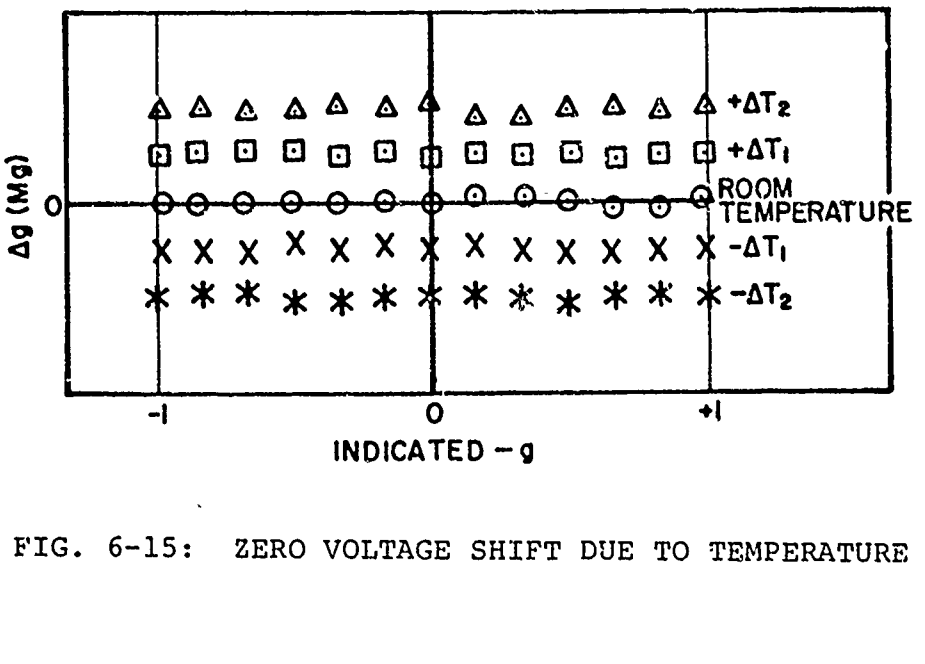

FIG. 6-15: ZERO VOLTAGE SHIFT DUE TO TEMPERATURE

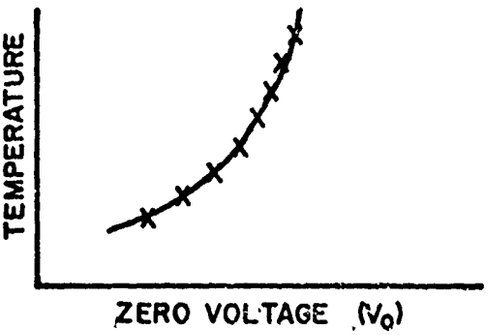

FIG. 6-16: ZERO VOLTAGE CROSSPLOT

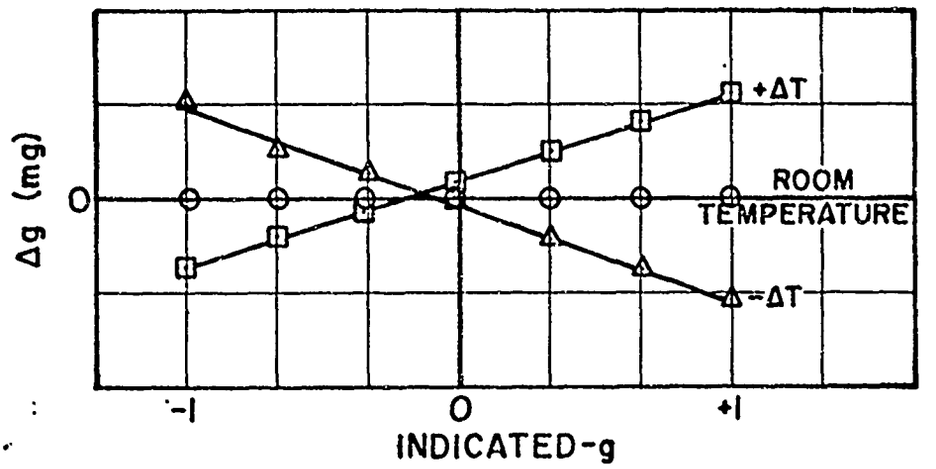

FIG. 6-17: ZERO SHIFT AND SENSITIVITY CHANGE

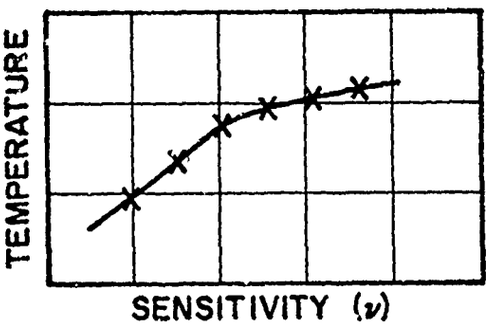

FIG. 6-18: SENSITIVITY/TEMPERATURE CORRECTION

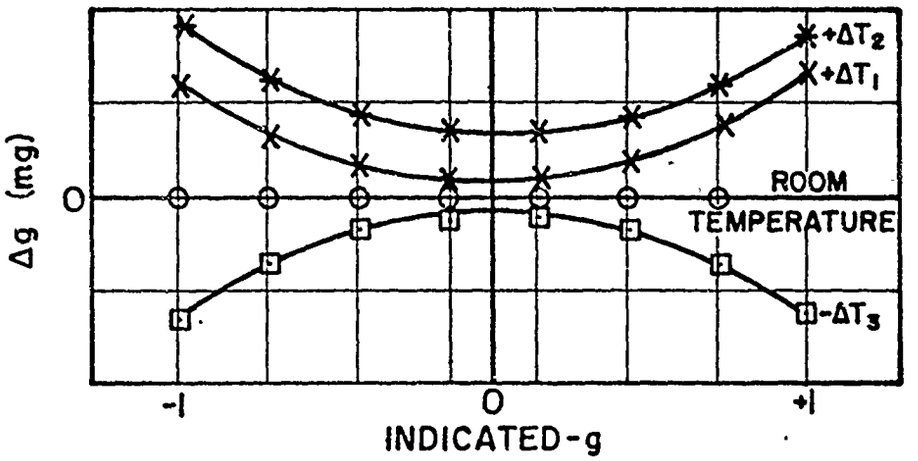

FIG. 6-19: NON-LINEAR TEMPERATURE CHANGES

For this situation, the first step is to make the curve look like a misalignment error as shown in figure 6-6, so that an apparent misalignment angle can be computed. For the normal axis shown here, a zero voltage shift at each temperature would first be generated such that the error in indicated g will be zero at 1 g. (For the flight path axis, the error in indicating g will be zero at zero g.) Once this is done, an apparent misalignment for each temperature can be generated which will linearize the data (to some extent) as explained in paragraph 6.12-D, and as shown in figure 6-20. This misalignment angle may be real or apparent (some vane/accelerometer angular change may occur). It may be multi-valued or monotonic, but it is in reality an adjustment factor which forces the experimental data to match the mathematical model.

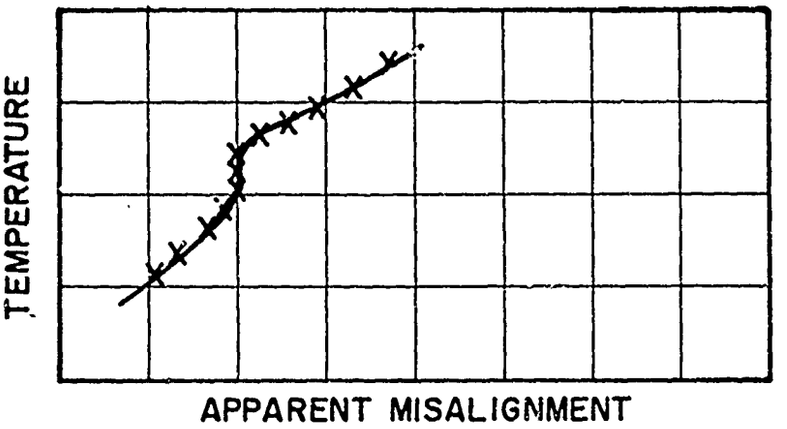

FIG. 6-20: APPARENT MISALIGNMENT CROSSPLOT

POSSIBLE SIMPLIFICATIONS TO THE TEMPERATURE CALIBRATION

HEAT SOAK VERSUS TRANSIENT METHODS

6.24 If the accelerometer and temperature measuring system are well insulated and the accelerometer is small, the heat transfer difference from accelerometer to temperature probe may be small. In this case, the transient method may be used to determine the bulk of the temperature calibration, after a comparison is made between the two for one data set, as shown in figure 6-21.

6.25 The heat soak data points are acquired by allowing the oven temperature to stabilize at each incremental temperature up to the maximum (130°F). The transient points are obtained by turning the oven fan on and opening the oven door. Data are recorded at given time intervals as the oven cools to room temperature. The oven is then taken to minimum temperature (-40°F) and the process repeated. If the data reasonably agrees, as in figure 6-21, the remaining data can be taken by the transient method at a great savings of time. Inflight during accelerations and climbs, the heat transfer rate will generally not be as great as during the transient calibration method for two reasons:

- The temperature differential between the accelerometer and the environment will always be less than the temperature differential taken during the temperature calibration.
- Some shielding of the accelerometer system is afforded by the housing in the boom.

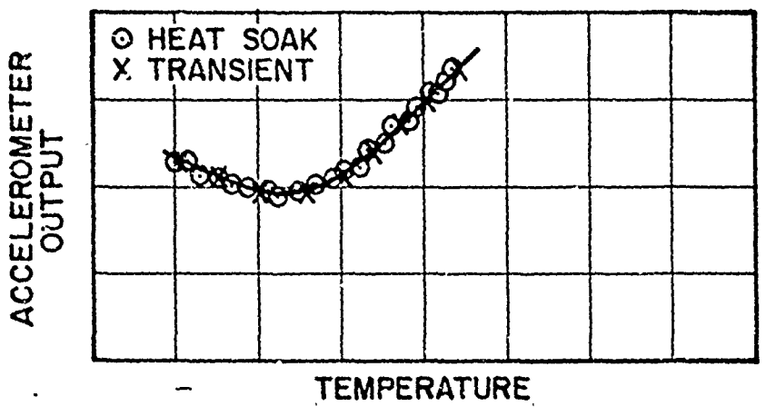

FIG. 6-21: HEAT SOAK VERSUS TRANSIENT METHODS

SIMPLIFIED CASE OF NO ZERO SHIFT

6.26 In this case (as was found for the Systron-Donner Systems tested), the data can be processed more easily and simply. Each data run can be plotted, as shown in figure 6-22.

6.27 The data non-linearity may be due to an internal angular change with temperature creating an apparent misalignment or may be caused by other effects. The data is approximated by two lines, as shown in figure 6-22. Each line has a slope of C± (defined as $(\Delta g/g/^{o}F)$), as calculated above and below the intercept. The values of C± should be fairly constant for the many runs. The mathematical model used is as follows:

$$n_i = \left[\frac{V-V_o}{\gamma} + n\right] dg/dstep \quad , \qquad (6\text{-}1)$$

as obtained from room temperature calibration, and

$$n = n_i\left[\frac{\left[1 - C\pm(T_i - T_o)\right]}{\left[1 - C_{amb}(T_{amb} - T_o)\right]}\right] \quad , \qquad (6\text{-}11)$$

where n = true load factor

n_i = indicated load factor

T_i = indicated temperature

T_{amb} = ambient value where original calibrations were made

T_o = intercept temperature, as shown in figure 6-22

C± = slope on either side of T_o (C+ when $T_i > T_o$; C- when $T_i < T_o$)

C_{amb} = slope through T_{amb} (C+ as shown in figure 6-22).

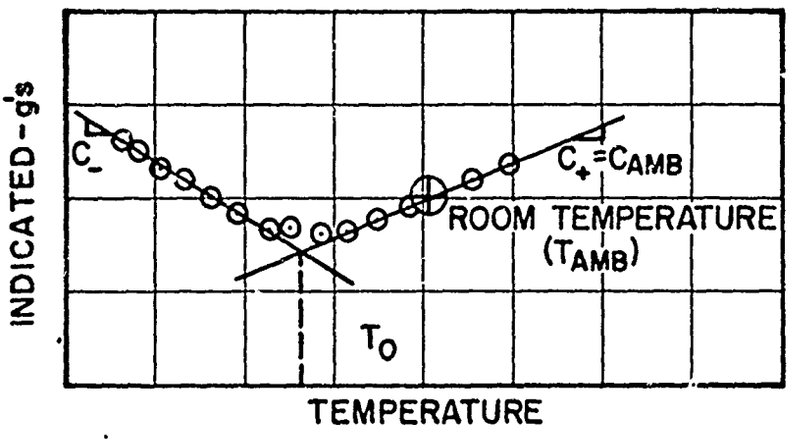

FIG. 6-22: TEMPERATURE CALIBRATION FOR NO ZERO SHIFT

ALTERNATE METHOD OF ANALYSIS

6.28 The data taken during laboratory calibration can be analyzed by regression analysis techniques as presented by reference 6-2. These techniques are especially useful when such parameters as the cross-axis sensitivity are to be included. Such a regression analysis system was used by Gerlach (reference 6-2). The regression model used by Gerlach for a three-axis system is:

$$a_x = C_o + C_1 e_x + C_2 e_x^2 + C_3 e_y + C_4 e_z + C_5 e_x e_y \quad , \qquad (6\text{-}12)$$

where e is the voltage output of the non-range extended accelerometer axes (X, Y, and Z), and C is the coefficient vector determined by the regression analysis. Similar models were used for the a_z and a_y accelerations. The important factor is to be able to correlate voltage with g to within ± 1 mg.

BOOM BENDING

6.29 Loads from aerodynamic forces and inertia cause bending of the boom which results in errors in the measured angle of attack, since the position of the vane is referenced to the axis of the boom. Adjustments for boom bending for loads due to inertia may be made from a calibration of static deflections of the boom when loaded with weights to represent inertial forces experienced inflight, or from mathematical modeling. The best method of determining boom bending is by measuring it inflight with strain gauges on the boom. But, assuming that this instrumentation is not available, a mathematical model of the boom structure must be inferred, as shown in figure 6-23.

6.30 From the simplified model, the following must be inferred:

$w = f(\ell)$; weight/length as function of length

$d = f(\ell)$; boom diameter as function of length

$EI = f(\ell)$; boom strength as function of length.

The static equilibrium for cantilever beams can be used as:

$$\theta_{FPA} = \int_0^x \frac{M}{EI}\, d\ell \ . \qquad (6\text{-}13)$$

Analytic calculations should be made. The boom can then be loaded with point loads and comparisons can be made with the analytic calculations. If suitable agreement is not obtained, the data is used to solve for the mathematical model. The simplified model can be

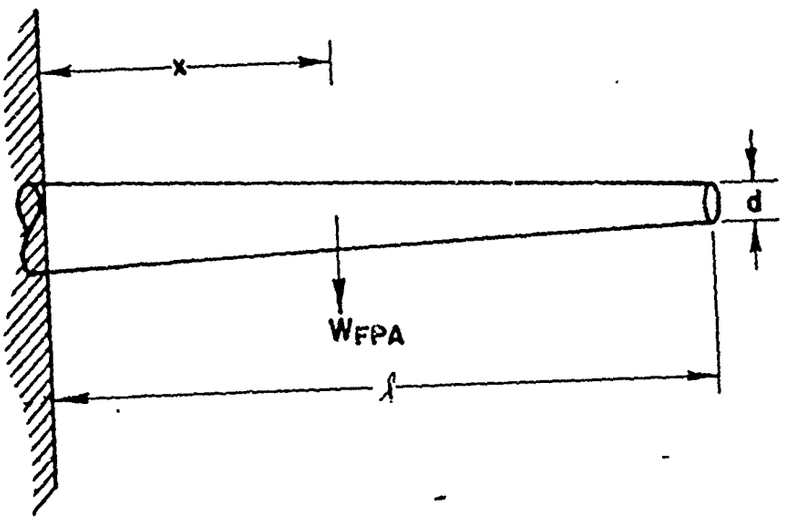

FIG. 6-23: SIMPLIFIED BOOM STRUCTURE MODEL

elevated to any level of complexity for measuring these deflections. With a mathematical model defined, boom bending can be calculated by:

1. Uniform g load

$$w(\ell) = n\, w_o(\ell) \qquad (6\text{-}14)$$

2. Pitch acceleration load

$$w(\ell) = \left(1 + \frac{1\ddot{\theta}}{g}\right) w_o(\ell) \qquad (6\text{-}15)$$

and $$\theta_{FPA} = \int_o^x \frac{M}{EI}\, d\ell \quad , \qquad (6\text{-}13)$$

where $w_o(\ell)$ is the one g weight distribution.

6.31 The measurement of bending under point loads need not be done by complex sight measurements if an FPA system is used. Angular change can be inferred by a change in the FPA reading.

ON BOARD CALIBRATIONS

6.32 In general complete laboratory calibrations are needed only once for each type of accelerometer system. The characteristics of the system being known, some approximations can be made unless extreme accuracy is required. One such example is the rate table calibrations, where high accuracies in the normal axis data are obtained. In general extrapolating from 1 g calibration may introduce additional error, but this error may not be critical (i.e. an error of 24 mg on the normal axis at 6.0 g is 0.4 percent which is usually more than adequate). The flight path axis will, however, require more careful attention since it is the primary instrument for excess thrust. Experience has shown that in general this accelerometer is an excellent experimental tool and is generally more accurate than other on board instrumentation. Generally, greater accuracies can be obtained using this instrument as discussed under angle-of-attack measurement, as compared with normal measurement.

6.33 With the airplane static in the hangar (to avoid wind drafts) and power to the instrumentation equipment, the following additional equipment are required:

a. Voltmeters - one for each output of each axis being calibrated, or one voltmeter than can be switched to read each output.

b. Sensitive inclinometer.

c. Pendulum - The length of the pendulum determines the frequency of the pendulum swing (the longer the pendulum, the lower the frequency). The pendulum should not be so short that its frequency is sufficiently high to introduce electrical lag in the filtering system or so long that it is unwielding. The frequency response will be discussed in a later section.

6.34 The on board calibrations are once again a function of g local, and if comparisons are to be made with laboratory calibrations, then adjustments must be made if g local varies significantly. Assuming one g conditions will be in error by approximately 1 mg for every .03 ft/sec^2 variation in local g.

The first step in the on board calibration is to determine the accelerometer/vane misalignment.

6.35 The vane is taken by hand and very slowly rotated (frequency very low) with the inclinometer in place until the flight path axis changes step near Og right at this break is Og flight path and the inclinometer reading is the flight path angle misalignment. The normal axis can be stepped at 0.667g if enough angular displacement is available. If not, a good first assumption would be to set this equal to flight path axis misalignment and after calibration computations, the error in this assumption can be resolved by knowing the total vector at any point is lg.

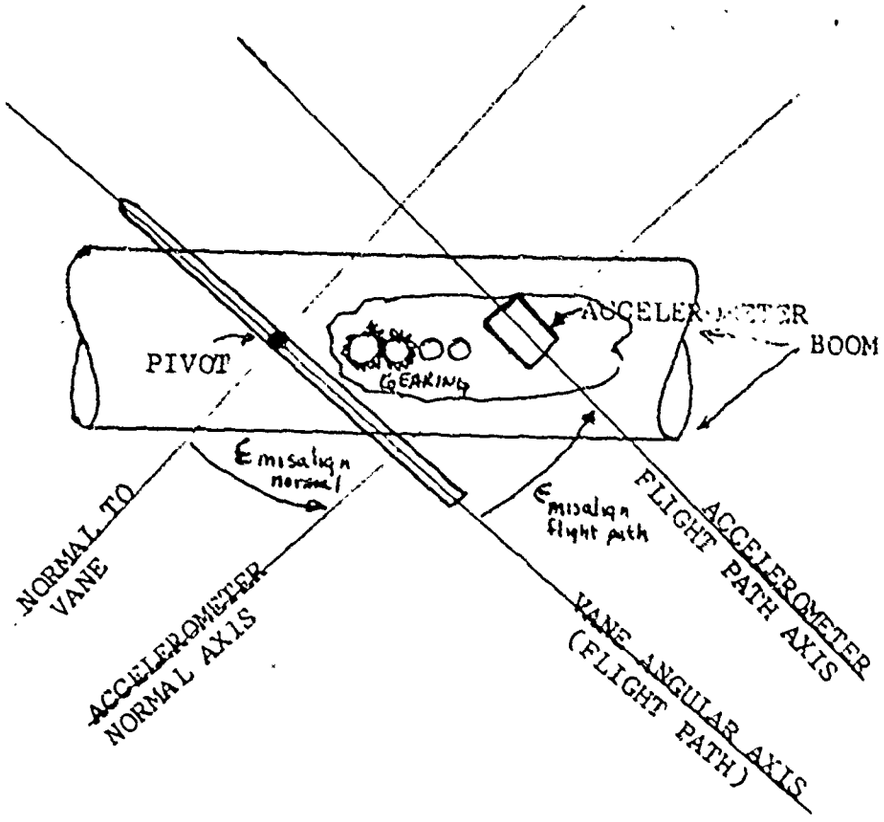

FIG. 6-24: FLIGHT PATH ACCELEROMETER MISALIGNMENTS

6.36 With the accelerometer/vane misalignment known, we can relate vane position to accelerometer reading. Taking points every two degrees up and down from stop to stop, we can get a static calibration over the useful range to be treated the same as a laboratory calibration.

6.37 The angle of attack can be calibrated now by relating it to inclinometer reading. Several pendulum swings averaged give the true zero vane position (should be checked with the inclinometer). If the pendulum is biased (i.e., bent) an error will be introduced so that the pendulum should be reversed and swung on both vanes in both directions. These pendulum swings will be used later to check filter attenuation and phase shift. The last point needed is one with the accelerometer clamped to the boom in the zero degree angle-of-attack (boom relative) position. The inclinometer reading here relates angle-of-attack and inclinometer readings. The inclinometer readings of the calibration can now be used to calibrate the AOA.

6.38 Knowledge of the above relationships relates angle-of-attack to accelerometer readings, and the pendulum swings shown below can be used for attenuation and phase lag checks.

6.39 Since the acceleration is only a function of angle, it should peak and bottom with the AOA. The figure shows some lag due

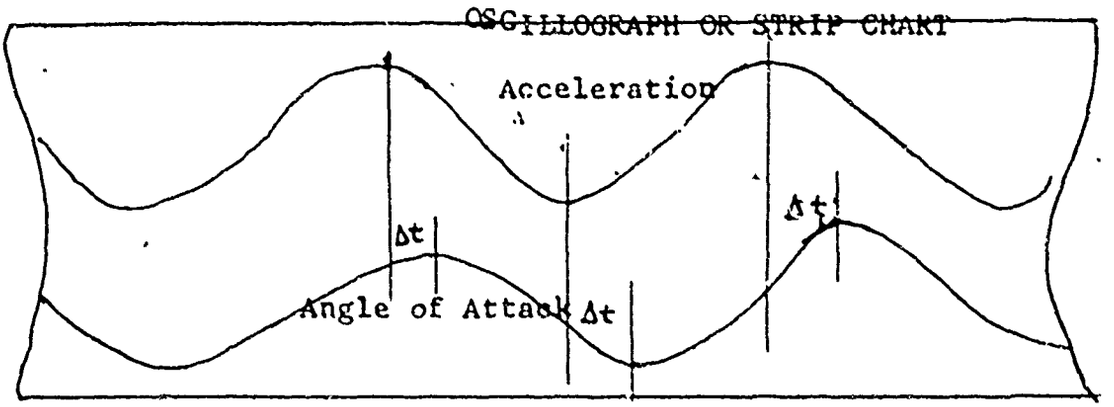

FIG. 6-25: PHASE LAG DETERMINATION

to filtering the number of degrees of phase lag 0 is $\frac{\nabla t}{T} \times 360^0$

where:

∇t = time shift in peaks

T = period of oscillations

6.40 The attenuation characteristics can be found as shown in the next figure.

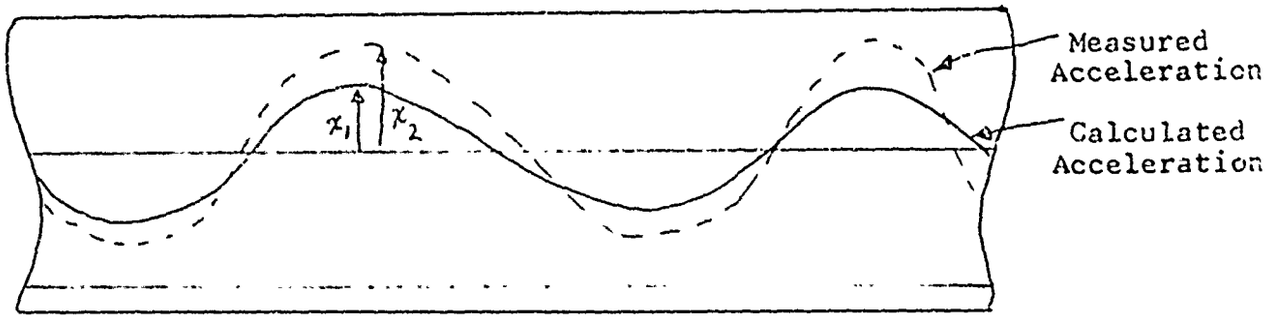

FIG. 6-26: ATTENUATION CHARACTERISTICS

The attenuation here as shown is negative (i.e., gain). The change in value of a number by electronic filtering is usually measured as gain in decibles or

$$G = 20 \log \frac{X_2}{X_1} \text{ db.} \qquad (6.14)$$

It can be seen when the magnitude is attenuated the gain is negative.

6.41 In order to avoid complex frequency response corrections, the filter system should be chosen such that there is zero phase shift, and zero attenuation at the maximum frequency of maneuvers to be considered as shown in the figure.

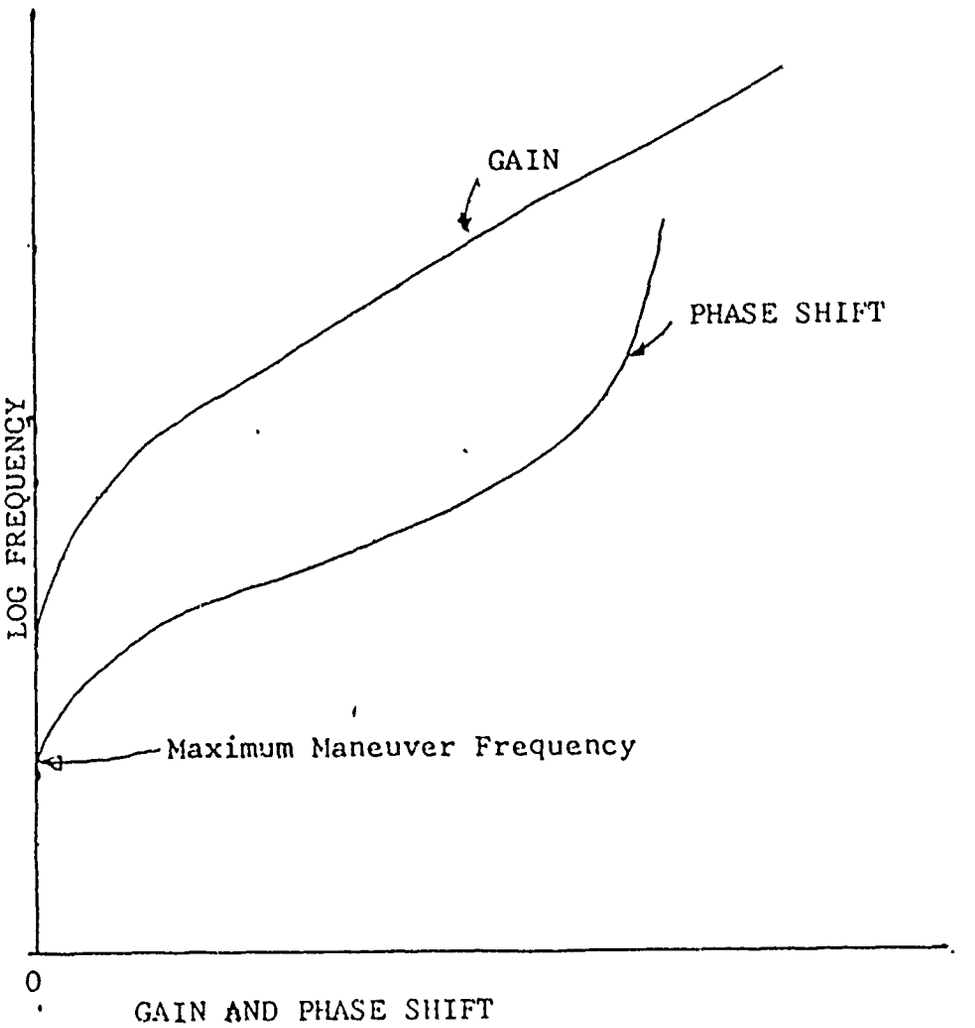

FIG. 6-27: TYPICAL FILTER RESPONSE

CONCLUDING REMARKS TO CHAPTER 6

6.42 It has been demonstrated that 1 mg accuracy in the flight path and normal load factors can be contained in laboratory calibrations. In order to maintain this accuracy in flight, corrections must be made as given in Chapter 2.

6.43 One additional parameter need be discussed because of the increased accuracy requirement when using the accelerometer methods. This parameter is the aircraft angle of attack as discussed in Chapter 7.

REFERENCES FOR CHAPTER 6

6-1. Grumman Aerospace Corporation, Report No. ADR-07-01-70.1, "Development of Dynamic Methods of Performance Flight Testing," by P. Pueschel, Unclassified, Aug 1970

6-2. Gerlach, O.H., "Techniques for Non-Steady Flight Measurements," Flight Test Instrumentation Volume 3, Permagon Press, 1964.

THE ACCELEROMETER METHODS OF DETERMINING AIRCRAFT PERFORMANCE (DYNAMIC PERFORMANCE TESTING)

CHAPTER 7

THE DETERMINATION OF ANGLE OF ATTACK

SUMMARY OF CHAPTER 7

7.1 Recent advances in the state of the art of various categories of flight testing have increased the accuracy requirements for the measurement of aircraft angle of attack. This accuracy requirement may well result in a maximum allowable error of ±0.10 degrees. Angle of attack measurement systems presently available are capable of yielding such an accuracy, but not without correction of the measurements for certain errors. In addition to the classical laboratory instrument calibration, corrections must be made for errors in mechanical positioning, upwash, induced angular flow, vane system lag response, and aeroelastic bending. Several or all of these corrections must be made depending upon the flight test maneuver and basic accuracy sought.

INTRODUCTION TO CHAPTER 7

7.2 Angle of attack is a basic flight parameter in performance, stability and control, weapons delivery , and other types of aircraft flight testing. The degree of accuracy required in the determination of angle of attack varies greatly among the types of tests because of the effect it has in the associated data reduction process. The advent of new methods of determining aircraft performance, aircraft parameter identification concepts, and other test methods have imposed more severe accuracy requirements because of more sophisticated data reduction procedures. In order to realize this high degree of accuracy, methods of ascertaining a standard (an independently derived, true value) angle of attack must be determined, so that corrections can be applied to the measured values. Alternatively, in aircraft maneuvers where standard values cannot be obtained, analytical corrections must be made.

SYMBOLS

7.3 The symbols used in Chapter 7 are defined below.

Symbol	Definition	Common Units	Metric Units
a_x	Longitudinal acceleration	ft/sec^2	(m/sec^2)
b	Span of an aerodynamic surface	ft	(m)
b_α	Random bias	-	-
C_{L_α}	Angle of attack vane lift curve	1/radians	(1/radians)
cg	Aircraft center of gravity	% MAC	(% MAC)
D	Drag	lbs	(N)
E_α	White noise	-	-
F_g	Gross thrust	lbs	(N)
F_r	Ram drag	lbs	(N)
g	Acceleration of gravity	ft/sec^2	(m/sec^2)
h	Altitude	ft	(m)
H_{AGL}	Altitude above ground level	ft	(m)
I	Mass moment of inertia	$lbs\text{-}ft\text{-}sec^2$	$(kg\text{-}m\text{-}sec^2)$
K	Spring constant	lbs/ft	(N/m)
K_α	Random scale factor	-	-
l	Length	ft	(m)
L	Lift	lbs	(N)
m	Mass	slugs	(kg)
M	Mach number	-	-
M	Moment	ft-lbs	(N-m)
n_x	Longitudinal load factor	gs	(gs)
n_z	Normal load factor	gs	(gs)
P_a	Ambient pressure	lbs/ft^2	(N/m^2)

Symbol	Definition	Common Units	Metric Unit
P	Pressure	lbs/ft^2	(N/m^2)
q	Dynamic pressure	lbs/ft^2	(N/m^2)
r	Radius of action	ft	(m)
S_v	Area of angle of attack vane	ft^2	(m^2)
t	Time	sec	(sec)
V_h	Horizontal velocity	ft/sec	(m/sec)
V_t	True velocity (along flight path)	ft/sec	(m/sec)
V_v	Vertical velocity (rate of climb)	ft/sec	(m/sec)
W	Gross weight	lbs	(kg)
Greek Symbols			
α	Angle of attack	deg	(deg)
γ	Flight path angle	deg	(deg)
Δ	Incremental change	-	-
ε	Earth curvature	deg	(deg)
ζ	Damping ratio	-	-
τ	Thrust inclination angle	deg	(deg)
θ	Pitch attitude	deg	(deg)
$\dot{\theta}$	Pitch rate	deg/sec	(deg/sec)
ϕ	Misalignment angle or aircraft bank angle	deg	(deg)
ω_{n_v}	Natural frequency	cycle/sec	(cycle/sec)
Ψ	Yaw angle	deg	(deg)

Subscripts	Definition
$( )_b$	Body-axis accelerometer
$( )_{BB}$	Boom bending
$( )_{FP}$	Flight path
$( )_{FPA}$	Flight path accelerometer
$( )_i$	Indicated
$( )_{1,2,3}$	Condition point
$( )_{LAG}$	Lag
$( )_{PEND}$	Pendulum
$( )_p$	Pitch rate
$( )_t$	True
$( )_u$	Upwash
$( )_v$	Vane
$( )_y$	Rotational axis
$( )_\alpha$	Angle of attack

7.4 The accuracy requirement on angle of attack, for use in aircraft performance flight testing has not, historically, been critical. Examination of the angle of attack parameter during a constant, W/δ point, which is the conventional direct method of determining thrust required and specific range, the following equations result (assumed airspeed and altitude stabilization).

$$L = n_z W - F_g \sin(\alpha + \tau) \tag{7-1}$$

$$D = F_g \cos(\alpha + \tau) - F_r \quad . \tag{7-2}$$

If a nominal set of conditions is assumed:

W	= 50,000 lbs.	α	= 5.0 deg.	F_g	= 16,000 lbs.
n_z	= 1.0	τ	= 0 deg.	F_r	= 4,000 lbs.

An assumed error of 20 percent in angle of attack (1 degree) makes less than 1 percent difference in either lift or drag. Even at high angle of attack values, the effects of inaccurate angle of attack inputs are relatively low.

7.5 With the advent of highly accurate accelerometers, test techniques have changed. Body-axis or flight path accelerometer packages are used to sense vehicle accelerations, from which performance is calculated. Angle of attack is used in the associated coordinate transformations (see Chapter 2), and the required accuracy

is more difficult to obtain. The analysis is a function of the accelerometer package to be used. For body accelerometers:

$$n_z = n_{x_b} \sin\alpha + n_{z_b} \cos\alpha \qquad (7\text{-}3)$$

and

$$n_x = n_{x_b} \cos\alpha - n_{z_b} \sin\alpha \quad . \qquad (7\text{-}4)$$

Assuming the following nominal conditions (where α is the true angle of attack and $\Delta\alpha$ is the total correction to angle of attack):

$n_z = 1.00$

$n_x = 0.30$

$\alpha = 5.0$ degrees

$\Delta\alpha = 0.2$ degrees.

The body accelerometer would yield 0.386 g longitudinal and 0.970 g normal. This assumes misalignment angles and aircraft angular rates are zero.

7.6 The maximum error of present longitudinal accelerometer systems is ±.001 g, including the readout system. To avoid compromising this accuracy, the angle of attack accuracy has to be correspondingly high. Taking the partial derivative of equation 7-4 with respect to α yields:

$$\frac{\partial n_x}{\partial \alpha} = -n_{x_b} \sin\alpha - n_{z_b} \cos\alpha = -n_z = -1.00 \quad . \qquad (7\text{-}5)$$

Thus, to be consistent with the accelerometer accuracy of $\Delta n_x = .001$ g , an angle of attack accuracy of at least $\Delta\alpha = .06$ degrees is required: i.e.,

$$\Delta\alpha = \frac{57.3\ \Delta n_x}{-n_z} = 0.0573 \text{ degrees.} \qquad (7\text{-}6)$$

For practical considerations, the minimum acceptable angle of attack accuracy for performance flight testing using onboard accelerometers is ±0.10 degrees.

7.7 Other areas of flight testing present their own accuracy requirements. For example, in the area of aircraft parameter identification, as cited in reference 7-4, the measurement standard deviation required may be as low as 2 percent with random bias and noise being resolved around a mean of 0 and a standard deviation of 0.05 degrees. The angle of attack measure is then given by:

$$\alpha_i = (1 + K_\alpha)\alpha_V + b_\alpha + E_\alpha \qquad (7\text{-}7)$$

where K_α = random scale factor (7-8)

b_α = random bias (7-9)

E_α = white noise (7-10)

additionally:

$$\alpha_t = \alpha_i + \Delta\alpha \text{ CORRECTIONS.} \qquad (7\text{-}11)$$

These corrective data ($\Delta\alpha$)will be discussed separately. Weapons release, carrier approach, and stall/spin investigations will each

have their own requirements for highly accurate measures of angle of attack. This high degree of accuracy is attainable if consideration is given to the measurement system, dynamics and aerodynamics.

MEASUREMENT OF ANGLE OF ATTACK

7.8 There are basically four generally accepted methods used to measure an aircraft's angle of attack. These methods are:

- Inertial navigation systems
- Differential pressure sensors
- Null seeking differential pressure sensors
- Aerodynamic vanes.

INERTIAL NAVIGATION SYSTEMS

7.9 The use of an inertial navigation system is the most complex method of obtaining angle of attack. Large strides have been made in recent years in the development of inertial navigation systems. The basic function required in the measurement of angle of attack is a gyro stabilized platform with sensitive accelerometers mounted on the platform. The accelerations are continuously integrated to determine rate of climb and horizontal velocity. The flight path angle is then given by:

$$\gamma = \tan^{-1} \frac{V_v}{V_h} \quad . \tag{7-12}$$

The pitch altitude (θ) is given by the angle between the stable platform and the aircraft's reference line, and the angle of attack is given by:

$$\alpha = \theta - \gamma \quad . \tag{7-13}$$

From equations 7-12 and 7-13, the aircraft angle of attack is taken precisely at each point from integrated accelerometer readings. The advantages are an accurate measurement with no flow field errors. Additionally, response lag in this system is negligible. The disadvantages of the inertial navigation system are its inherent complexity, general non-availability on all aircraft, high cost, and the fact that inertial navigation systems have not generally been adapted to flight test work.

DIFFERENTIAL PRESSURE SENSORS

7.10 The second method of obtaining angle of attack is the use of the differential pressure sensor. Figure 7-1 shows the basic system. As shown in the figure, the angle of attack is given as the angle between the probe reference line and the relative wind. This angle is measured, as the probe name implies, by the difference in pressures at points 1 and 2. At a given value of dynamic pressure (q), the $\Delta P(P_1-P_2)$ is linear with angle of attack (α). The calibration of the probe is given by a plot of $\Delta P/q$ versus α. Due to the dependence of q on Mach number, this plot contains a family of straight lines of constant Mach numbers. For increased accuracy levels, wind tunnel calibrations are necessary. The advantages of this system are its structural integrity and negligible response lag. The disadvantages of this system are the limited data due to a small range of angle of attack, the expensive readout system

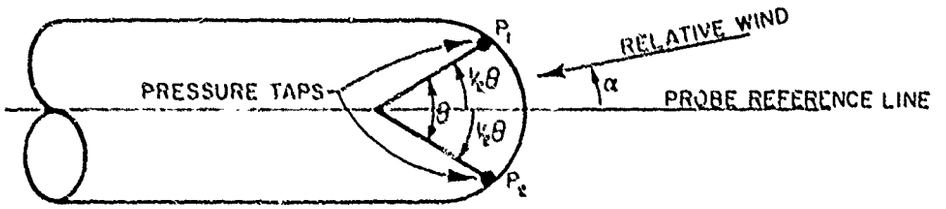

FIG. 7-1: DIFFERENTIAL PRESSURE SENSOR

required, the Mach number relationship in the calibration curves, and the error created by misalignment of the flow at the probe when compared to freestream direction (upwash). This, and all angle of attack systems, are subject to large errors in transonic flow.

NULL-SEEKING DIFFERENTIAL PRESSURE SENSOR

7.11 The third method of obtaining angle of attack is the null-seeking differential pressure sensor. This system is very similar to the differential pressure sensor described in paragraph 7.10, with the following exceptions:

- The nose of the probe is rotatable;
- A servo motor drives the probe to the zero ΔP position; and
- Angle of attack is measured as the angle that the nose makes with the probe reference line.

The advantages of this type of sensor are that the measurements are independent of Mach number and dynamic pressure, and the pressure transducer may be as sensitive as desired since the measured ΔP is always near zero. Additionally, response lag with an adequate servo system is negligible. The disadvantages of the null-seeking sensor are its complexity, cost, and weight. The null-seeking sensor is also subject to flow angularity errors (upwash).

AERODYNAMIC VANE SYSTEMS

7.12 The final system for measuring angle of attack and the most commonly used is the aerodynamic vane system. The system consists of a shaft mounted on a pivot which extends into the airstream. Some type of airfoil is mounted on the shaft to keep it aligned with the relative wind. The angle of the shaft with respect to its mounting is taken as the angle of attack (see figure 7-2). The advantages of this system are its low cost, simplicity, and the fact that its inflight calibration remains essentially constant with Mach number. The disadvantages are structural problems at high q, amplitude, and phase response errors (vane system lag), and local flow angularity (upwash).

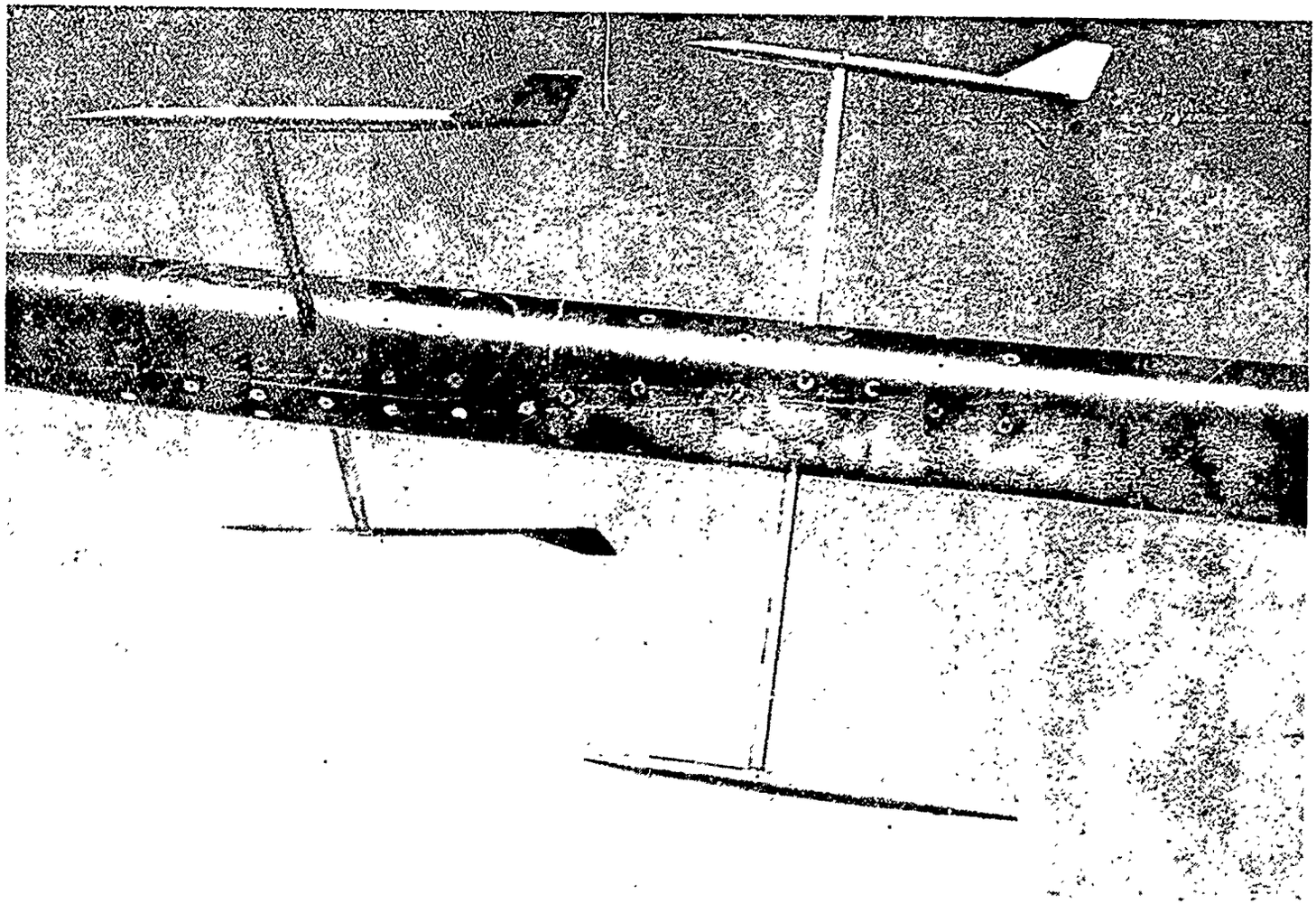

FIG. 7-2: VANE SYSTEM FOR ANGLE OF ATTACK MEASUREMENT

CORRECTION TO MEASURED ANGLE OF ATTACK

7.13 The purpose of the angle of attack system is to measure the true angle between some aircraft reference line and the upstream true flow direction. With the exception of the inertial navigation system, the angle of attack measuring system is usually mounted on a boom extending forward of the aircraft. There are usually several sources of error in the measured angle of attack. Such errors are:

- Errors in mechanical positioning (misalignment);
- Errors due to flow angularity (upwash and induced angular flow);
- Probe response errors (vane system lag); and
- Aeroelastic bending.

Since increased accuracy is required from the angle of attack measuring system, each source of error will be analyzed and an attempt to eliminate these errors will be made.

ERRORS IN MECHANICAL POSITIONING

7.14 Errors in mechanical positioning may be present in the vane system, differential pressure system, or the null-seeking differential pressure system. Precise alignment of the inertial navigation system is a requirement, so that alignment errors are considered eliminated. These errors are created by a misalignment between the measurement system reference line and the aircraft reference line, and are primarily due to installation. Figure 7-3 shows such a mechanical positioning error for the vane system. The mechanical positioning errors are usually very small and are exaggerated in

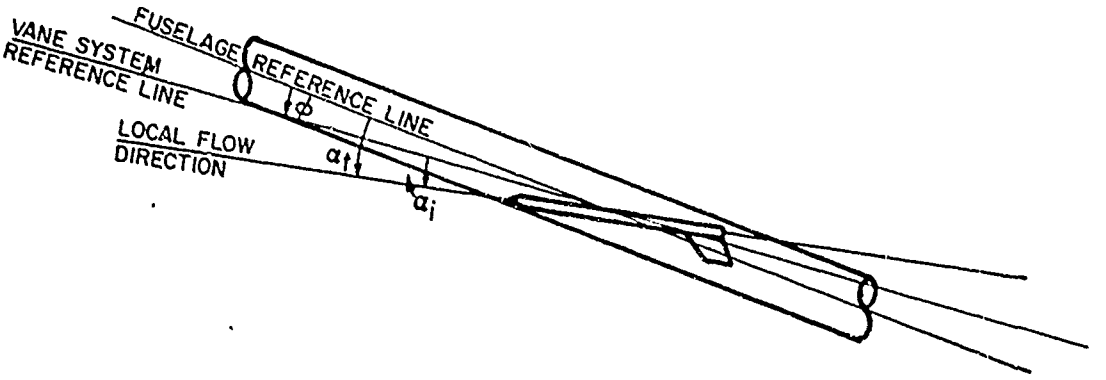

FIG. 7-3: VANE SYSTEM MECHANICAL MISALIGNMENT

figure 7-3, and all subsequent figures for purposes of clarity. The error in alignment (ϕ) is caused by the non-coincidence of the fuselage of aircraft reference line with the vane system reference line, such that

$$\alpha_t = \alpha_i + \phi \quad . \tag{7-14}$$

Figure 7-4 shows the mechanical misalignment of either the differential pressure probe or the null-seeking differential pressure probe. The probes themselves may be misaligned, or not aligned with the reference axis sought to that, in general, there may be more than one misalignment in each system. The misalignment angles can be determined by a variety of means ranging from inclinometer to complex sight measurements. The determination of these misalignment angles is not, however, critical from a standpoint of determining the aircraft true angle of attack, since any error in misalignment not accounted for will show up as a bias in the upwash curve.

ERRORS DUE TO FLOW ANGULARITY

7.15 Errors due to flow angularity are induced by the fact that the flow at the measuring device (local flow) is not aligned with the freestream flow. There are two main contributors to the flow angularity. These contributors are aerodynamic upwash from the boom, fuselage, and wing, and the induced angular flow effects due to angular rates.

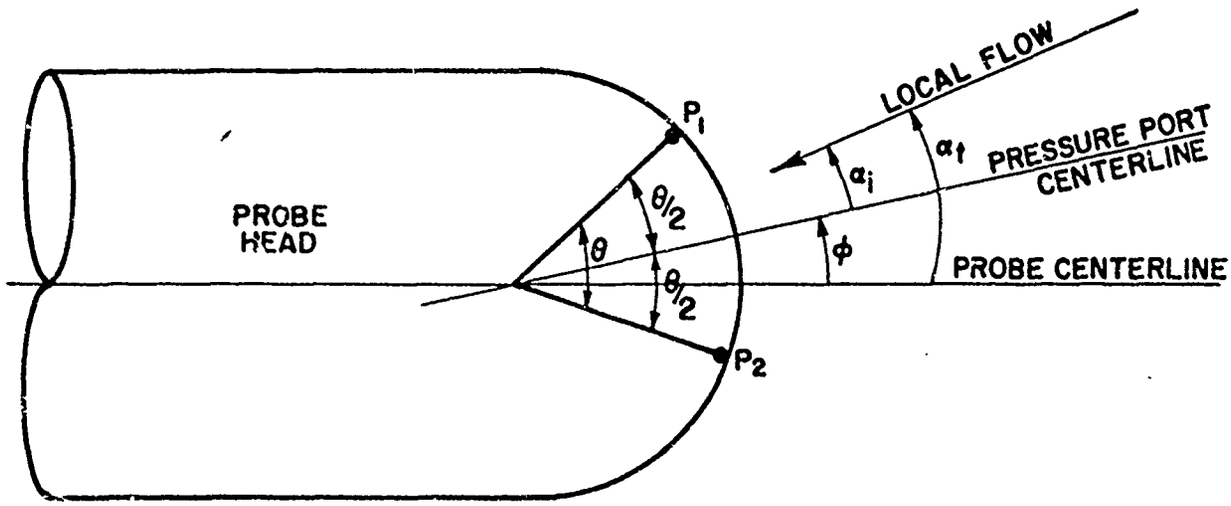

FIG. 7-4: DIFFERENTIAL PRESSURE PROBE MECHANICAL MISALIGNMENT

Upwash

7.16 Errors in measured angle of attack due to aerodynamic upwash are created by disturbances to the flow field which, in turn, are created by the presence of solid bodies moving in the flow field. Figure 7-5 shows the typical flow distribution about an airfoil at a given angle of attack.

7.17 It can be seen from figure 7-5 that the flow angularity at point P differs from the freestream flow angularity. This change in the direction of flow travels upstream due to the pressure distribution of the airfoil. Similar flow perturbations are created by the presence of the aircraft fuselage, noseboom, etc. Complex theoretical methods of determining the upwash at a given point by potential flow theory are given in both references 7-1 and 7-2, but do not yield acceptable accuracy when compared to test results. Flight test determination of aircraft upwash must be used for increased accuracy. The determination can be done by several methods: the attitude gyro method; the horizon reference method; the photographic method; and the energy method. Each of the first three methods calculate upwash by determining the true angle of attack. The energy method by-passes the calculation of true angle of attack by forcing two available flight test methods to agreement. Each of the methods sighted will be reviewed.

Attitude Gyro Method

7.18 The attitude gyro method is based on the defined relation:

$$\theta = \gamma + \alpha \quad . \tag{7-15}$$

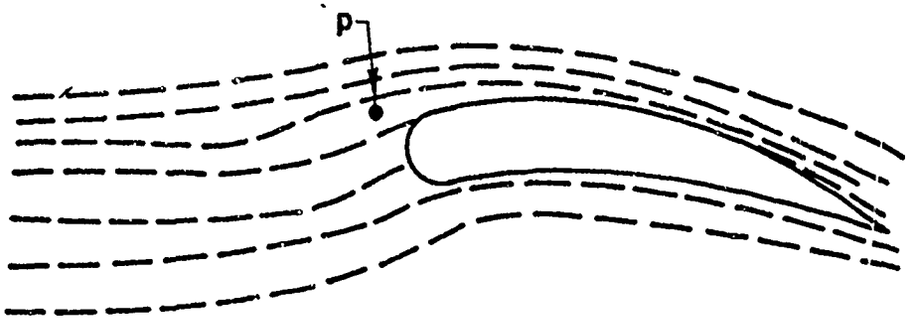

FIG. 7-5: AIRFOIL FLOW PATTERN

The flight path angle, γ , may be determined from the relation defined below:

$$\sin\gamma = \frac{dh}{dt}\frac{1}{V_t} \quad . \tag{7-16}$$

If the aircraft is stabilized with respect to altitude, (dh/dt=0), the flight path angle (γ) equals zero. Under these conditions, the true angle of attack is equal to the pitch attitude, and upwash is given by the difference between pitch attitude and indicated angle of attack:

$$\Delta\alpha_u = \theta - \alpha_i \quad . \tag{7-17}$$

Variations in aircraft angle of attack are obtained by stabilizing at different airspeed/altitude combinations.

7.19 The major advantage of the method is its simplicity. The major disadvantage of the method is the inaccuracy inherent in all presently available vertical gyros and their tendency to drift. In order to maintain the accuracy requirements, the pitch attitude must be as accurate as angle of attack.

Horizon Depression Method

7.20 The principle of the horizon reference method is the same as that of the attitude gyro method, with the exception of the determination of pitch attitude. In the attitude gyro method, the vertical gyro was used to determine pitch attitude. In the horizon reference method, the pilot's gunsight is used. First, on the

ground, the gunsight is bore-sighted to the zero sight line, or to a line parallel to the aircraft fuselage reference line. Inflight then, under stabilized conditions, the zero sight line will yield a line parallel to the aircraft's fuselage.

7.21 As shown in figure 7-6, depression of the gunsight pipper to the horizon will yield pitch attitude information. For a flat earth, the difference between the gunsight setting for zero sight and the gunsight setting for horizon depression will be pitch attitude. For a curved earth over water, the earth's curvature must be subtracted out as given by reference 7-1:

$$\varepsilon = \sqrt{.00319\ H_{AGL}} \quad . \tag{7-18}$$

A more detailed analysis of this procedure, together with an adaptation to over land, is given in reference 7-1. Again, the upwash is given as the difference between pitch attitude and indicated angle of attack. The major advantage of this method is the increased accuracy available when using the gunsight to determine pitch attitude. The major disadvantages are the requirement of a special flight test technique and the requirement to boresight the gunsight. Additionally, all aircraft are not equipped with precision gunsights.

Photographic Method

7.22 The same relationships are again used in the photographic method to obtain aircraft upwash. Here, the aircraft is flown over a test course where it can be photographed by Askania cameras.

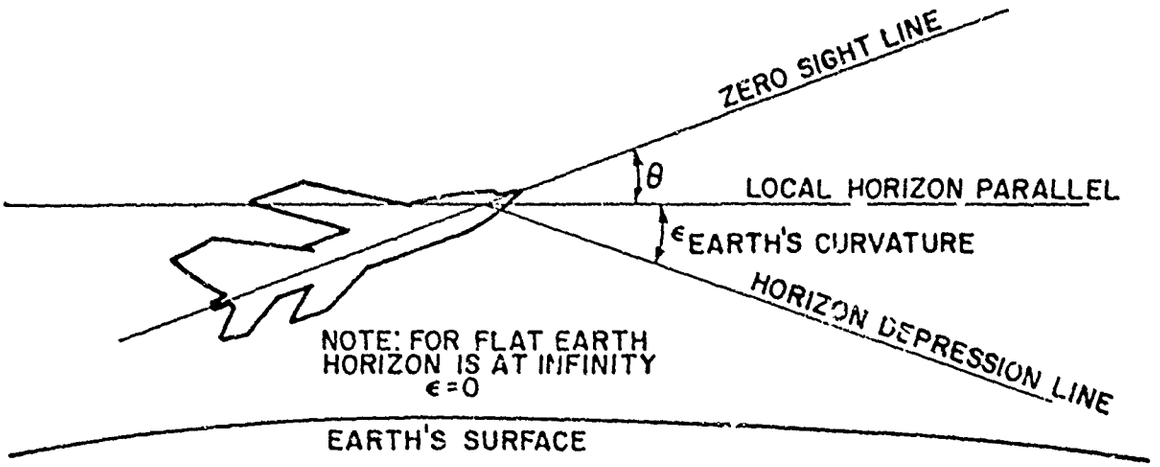

FIG. 7-6: HORIZON REFERENCE METHOD

(three are desired; two are adequate), and the aircraft position is calculated from geometric properties and camera elevation angles. From the space positioning, dh/dt and V_t can be computed and:

$$\sin\gamma = \frac{dh}{dt}\ \frac{1}{V_t} \quad , \tag{7-16}$$

where V_t is along the flight path. For Askania data, the horizontal velocity, V_h, is more easily obtained, so that:

$$\tan\gamma = \frac{dh}{dt}\ \frac{1}{V_h} \quad . \tag{7-19}$$

If appropriate references are available on the aircraft, the pitch attitude (θ) can be measured from the film, so that:

$$\alpha_t = \theta - \gamma \ ,$$

and

$$\Delta\alpha_u = \alpha_t - \alpha_i \ .$$

The advantage of this method is that only angle of attack need be measured onboard the aircraft. The major disadvantages are the degraded accuracy available, the requirement of specialized flight tests, and the time required to manually read the film.

Acceleration Energy Method

7.23 The energy method combines the simplicity of the attitude gyro method with the accuracy of the horizon reference method. Basically, the determination of pitch attitude is bypassed and the

upwash is determined from the accelerometer. Under true stabilized conditions, the resolved flight path acceleration is zero. As shown in figure 7-7, the resolved flight path acceleration (through the coordinate transformation of equations 7-3 and 7-4), using the indicated angle of attack and under stabilized conditions will yield the sine of the upwash angle.

7.24 In reality, true stabilization cannot be accomplished so that the flight path acceleration must be computed as:

$$\frac{a_{x_{FP}}}{g} = \frac{dh}{dt}\frac{1}{V_t} + \frac{dV_t}{dt}\frac{1}{g} \quad . \tag{7-20}$$

The $a_{x_{FP}}$ is then calculated from pitot-static instrumentation, and the smaller this quantity is, the greater the stabilization and consequently, the greater the accuracy. The upwash can then be computed by:

$$\Delta\alpha_U = \sin^{-1}\left(n_{x_{RESOLVED}} - \frac{a_{x_{FP}}}{g}\ \text{COMPUTED}\right) \quad . \tag{7-21}$$

The advantages of the energy method are its accuracy, the fact that a stabilized point technique may be used and the independence of the method from pitch attitude. The disadvantages of the method are the increased analysis time over that of the attitude gyro method.

Upwash Flight Test Determination Summary

7.25 All of the methods outlined can be used to obtain the total aerodynamic upwash. Each has its own advantages and disadvantages.

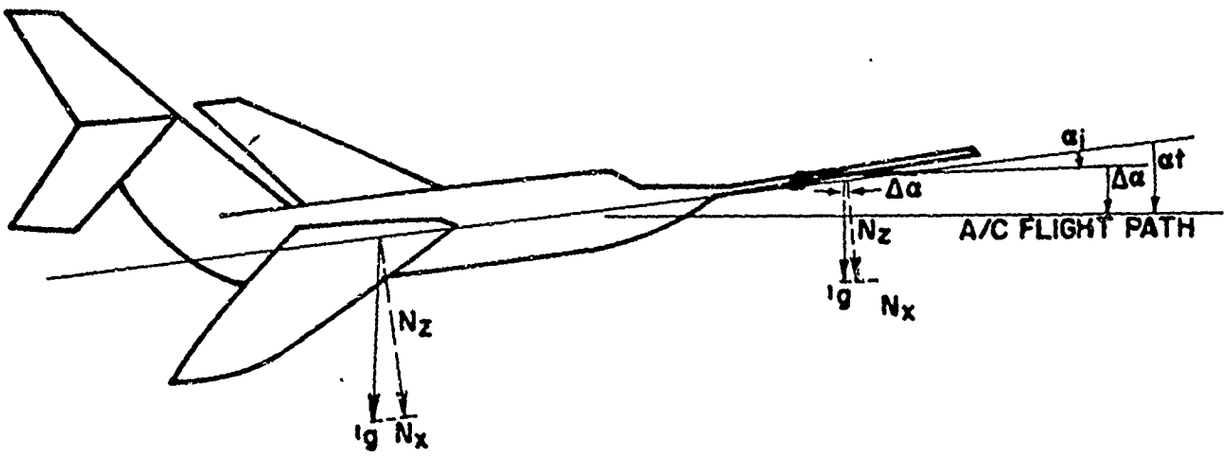

FIG. 7-7: ENERGY METHOD UPWASH DETERMINATION

The energy method is recommended because of its accuracy and the fact that the stabilized point method is used. Any flight testing involving stabilized conditions may be used, so that upwash calibration data need not consume additional flight time.

7.26 Reference 7-1 indicates that in a normal boom-mounted system, the aircraft induced flow field has become negligibly small at approximately 1.5 maximum fuselage diameters ahead of the nose of the aircraft. Under these conditions, a wind tunnel calibrated boom can be used and flight test data from any of the aforementioned methods can be used to ascertain its validity.

Induced Angular Flow

7.27 Induced angular flow corrections can be deduced with the aid of figure 7-8. From the figure, a velocity component equal to $(r\dot{\theta})$ is generated perpendicular to the radius of rotation.

7.28 Detail A of figure 7-8 gives the corresponding component breakdown along and perpendicular to the flight path, and detail B gives the resulting velocity triangle. From detail B , the vane senses two velocity components and is in error in that it tries to follow the resultant velocity vector, such that:

$$\tan\Delta\alpha_p = \frac{r\dot{\theta}(\cos\alpha_t)}{V_t - r\dot{\theta}\sin\alpha_\tau} \qquad (7\text{-}22)$$

or

$$\Delta\alpha_p = \tan^{-1}\frac{r\dot{\theta}\cos\alpha_t}{V_t - r\dot{\theta}\sin\alpha_t} \qquad (7\text{-}23)$$

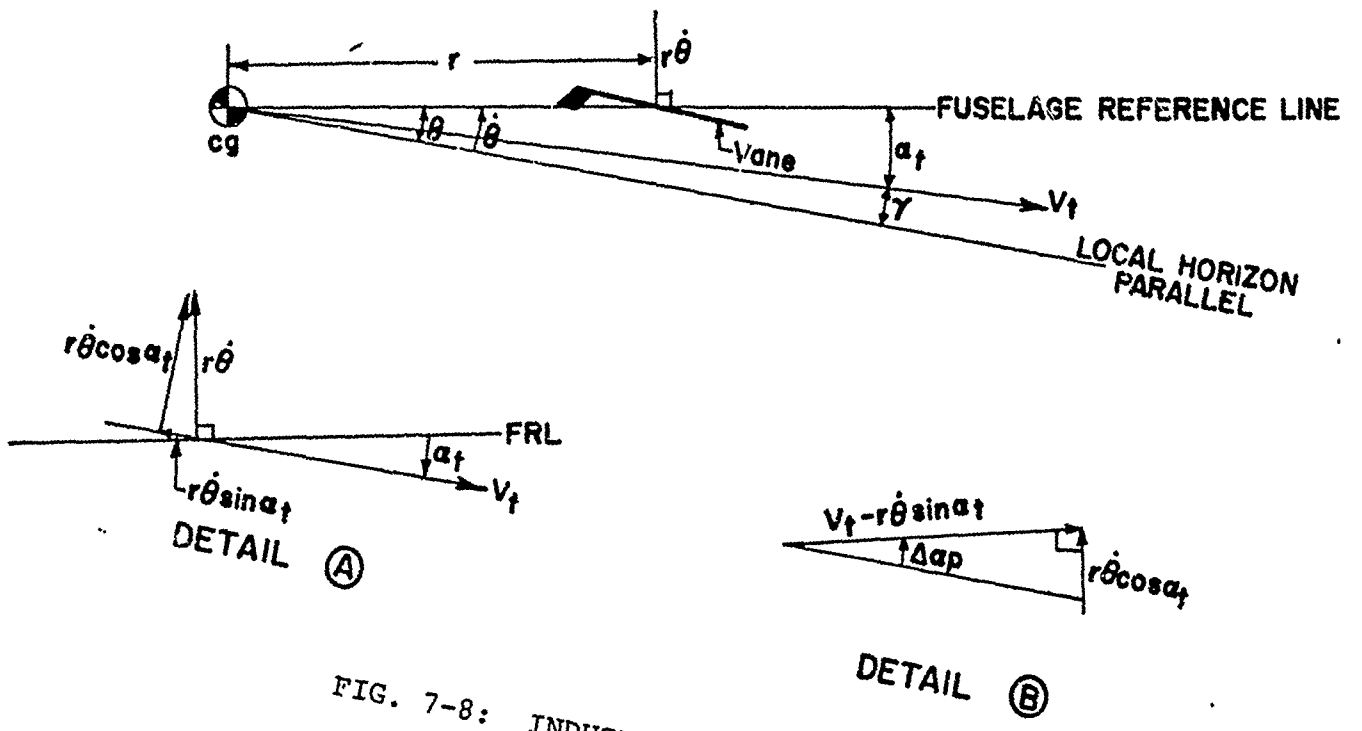

FIG. 7-8: INDUCED ANGULAR FLOW

The equation is unsolvable since:

$$\alpha_t = \alpha_i + \Delta\alpha_u + \Delta\alpha_{BB} + \Delta\alpha_p \quad . \tag{7-24}$$

An exact solution can be obtained by iteration with $\Delta\alpha_p = 0$ as the starting point and repetition of α_t to within a given accuracy as a termination point but in practice the first iteration with $\alpha_t = \alpha_i + \Delta\alpha_u + \Delta\alpha_{BB}$ is accurate enough for most applications. A further derivation and additional information is available in reference 7-2.

VANE SYSTEM LAG RESPONSE

7.29 Corrections for vane system lag response are extremely complicated, and should be avoided if possible. If, for instance, the angle of attack system has a low rotational inertia, and intended aircraft maneuvers are of a slow or moderate rate, the angle of attack system will follow changes in angle of attack closely enough to avoid the correction. If, on the other hand, high system inertias prevail and/or high rate maneuvers are contemplated, the corrections must be made to maintain accuracy. As taken from reference 7-2, an angle of attack vane system constitutes a torsional spring-mass-damper mechanical system having an undamped natural frequency (ω_n) and damping ratio (ζ) that describe its dynamic response characteristics. The vane system includes internal mass balancing, transducer elements, accelerometer package, etc., in addition to the aerodynamic lifting

surfaces. The output of such a system will have errors that are due to signal amplitude and phase-lag characteristics which are functions of the frequency relationship of the exciting signal and the natural frequency of the vane system, as well as its damping ratio. The characteristics of such a system can be determined by analysis of figure 7-9.

7.30 Summing rotational moments about the vane pivot, and solving the resulting differential equation yields the following vane system characteristics:

$$\omega_{n_v} = \left[\frac{q\, S_v\, \ell\, C_{L_{\alpha_v}}}{I_{y_v}}\right]^{\frac{1}{2}} = M\left[\frac{\gamma a}{2}\,\frac{P_a\, S_v\, \ell\, C_{L_{\alpha_v}}}{I_{y_v}}\right]^{\frac{1}{2}} \qquad (7\text{-}25)$$

$$\zeta_v = \frac{1}{2V_t}\,\omega_{n_v} \quad . \qquad (7\text{-}26)$$

A complete derivation of the above equations is given in reference 7-2.

7.31 If equations 7-25 and 7-26 are coupled with a random input to the inertia system, the following differential equation results:

$$\alpha_t = \frac{1}{\omega_{n_v}^2}\left[\ddot{\alpha}_i + 2\zeta_v\omega_{n_v}(\dot{\alpha}_i - \dot{\alpha}_t) + \omega_{n_v}^2\,\alpha_i\right] . \qquad (7\text{-}27)$$

It should be noted that ω_n and ζ are functions of flight parameters and must be calculated for each point.

7.32 In equations 7-25, 7-26, and 7-27, there remain several unknowns which must be determined. The area of the vanes (S_v) and the vane pivot length (ℓ) can be computed knowing the vane system

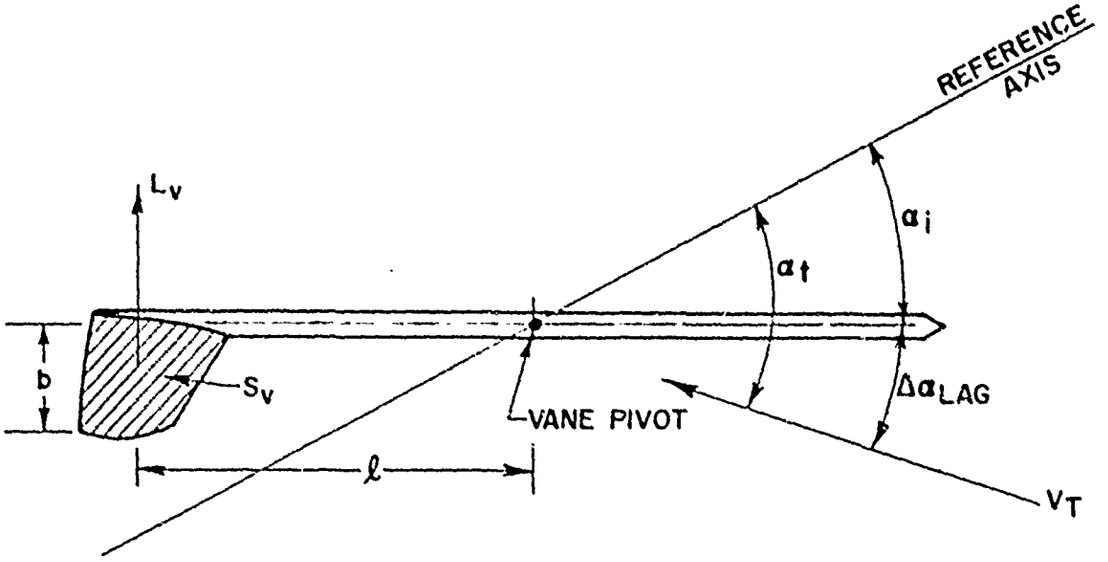

FIG. 7-9: VANE SYSTEM LAG RESPONSE DIAGRAM

geometry, and the flight dynamic pressure (q) can be computed at each flight condition. Using the thin wing approximation for $C_{L_{\alpha_v}}$:

$$C_{L_{\alpha_v}} = \frac{2\pi}{1 + \frac{2S_v}{b^2}} \quad . \tag{7-28}$$

The unknowns in the above equation set have now been reduced to one, the rotational moment of the inertia (I_{y_v}).

Determination of Vane System Inertia

7.33 There are two possible methods of determining the rotational inertia of the vane system; both involve laboratory tests. Figure 7-10 shows the first alternative. A pendulum is mounted on the vane system and given an initial displacement. The frequency and damping of the resulting oscillation are calculated. The natural frequency of such a pendulum with a driving mass m is given by:

$$\omega_1 = \frac{1}{2\pi}\sqrt{\frac{mg\ell}{I_{pend} + I_v}} \quad . \tag{7-29}$$

Next, the pendulum is removed from the vane system, and is allowed to oscillate about its axis. Its natural frequency is given by:

$$\omega_2 = \frac{1}{2\pi}\sqrt{\frac{mg\ell}{I_{pend}}} \quad . \tag{7-30}$$

Solving equations 7-29 and 7-30, the inertia of the vane system is given by:

$$I_v = \frac{mg\ell}{4\pi^2}\left(\frac{1}{\omega_1^2} - \frac{1}{\omega_2^2}\right) . \tag{7-31}$$

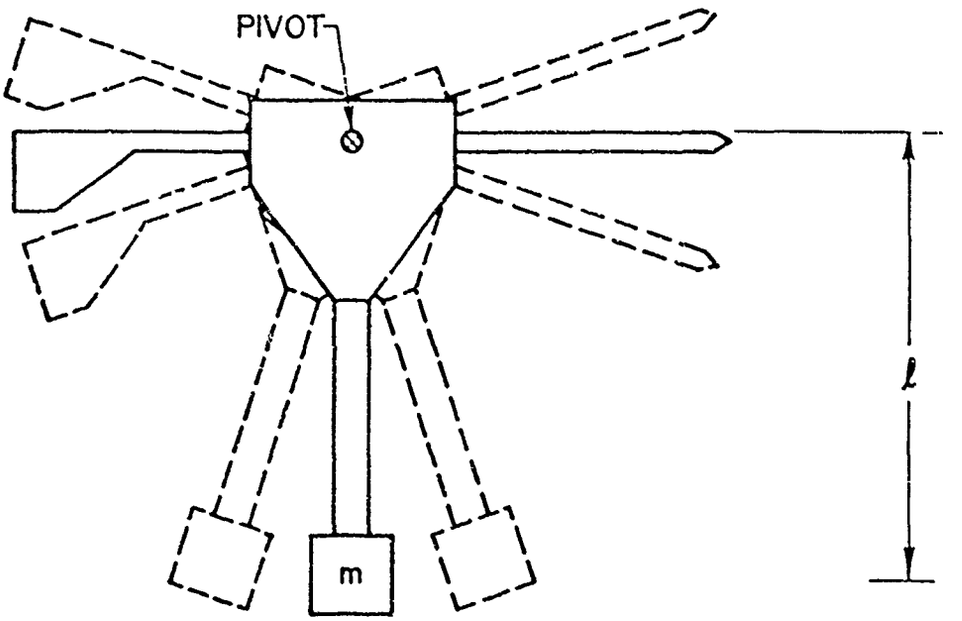

FIG. 7-10: PENDULUM MOUNT FOR INERTIA DETERMINATION

It can be seen that the accuracy of the measurement decreases as $I_{pend} > I_v$, and the calculation can be lost completely if $I_{pend} >> I_v$.

7.34 A more reliable method of obtaining small inertias is by employing an inertia rig, as shown in figure 7-11. The inertia rig consists of a stable platform on which there are points for attachment of springs, as shown in figure 7-12. From figure 7-12, the equation set for the general undamped spring mass system can be derived. Summing moments about the rotational axis: $\Sigma M_y = I\ddot{\theta}$,

$$I_v\ddot{\theta} = -\sum_{i=1}^{n} r_i k_i x_i \quad , \tag{7-32}$$

where x_i is the initial spring deflection. The deflection angle θ can be defined by $\sin\theta = \frac{x_i}{r_i}$, or with the small angle approximation $x_i = r_i\theta$, so that equation 7-32 becomes:

$$I_v\ddot{\theta} = -\sum_{i=1}^{n} r_i^2 k_i \theta \tag{7-33}$$

or

$$I_v = \frac{\theta}{\ddot{\theta}}\left(-\sum_{i=1}^{n} r_i^2 k_i\right) . \tag{7-34}$$

To solve the system, a second order undamped spring mass system is assumed. The characteristics of such a system are such that:

$$\theta = \theta_o \sin \omega_n t \quad . \tag{7-35}$$

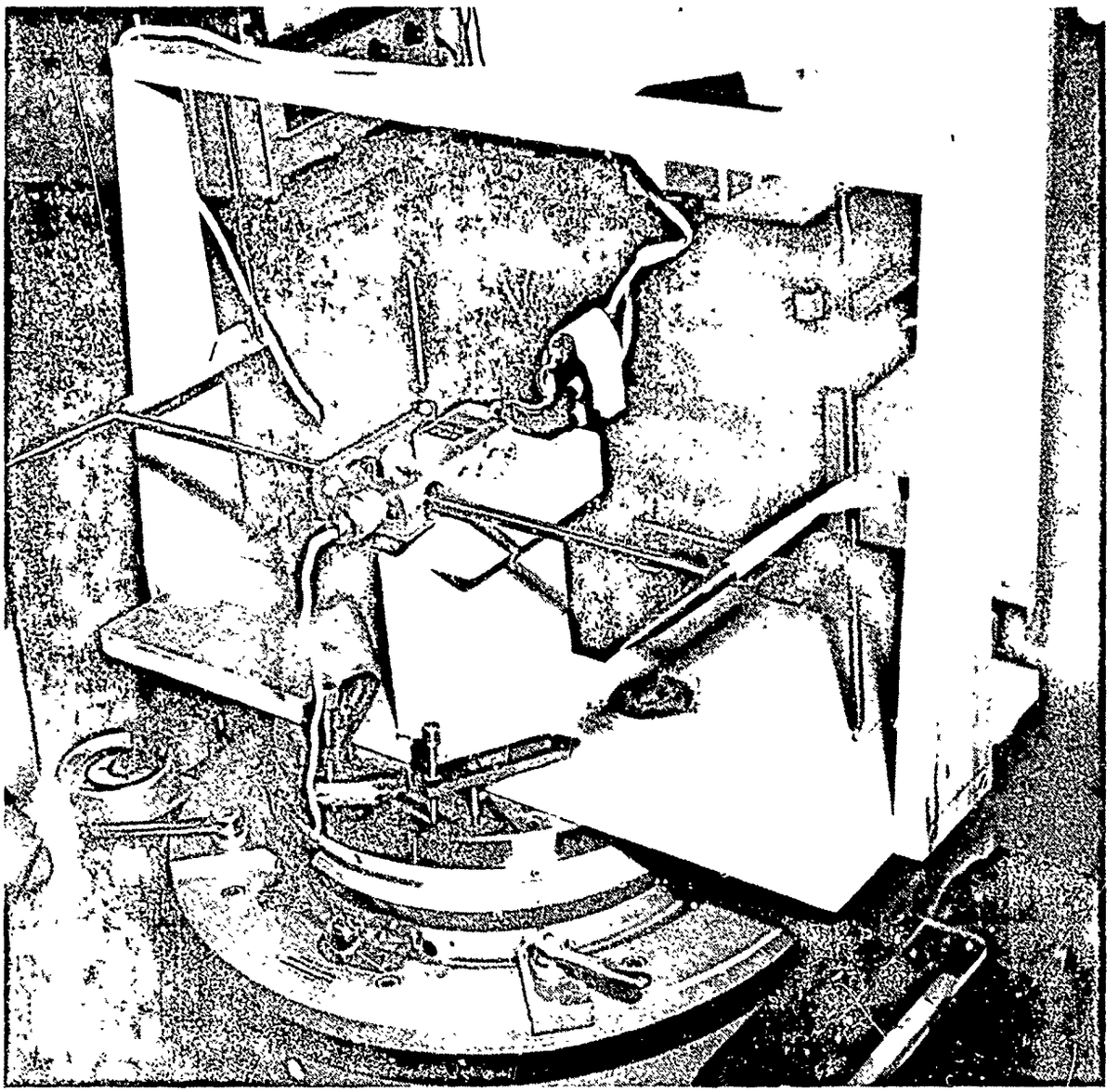

FIG. 7-11: INERTIA RIG WITH VANE SYSTEM MOUNTED

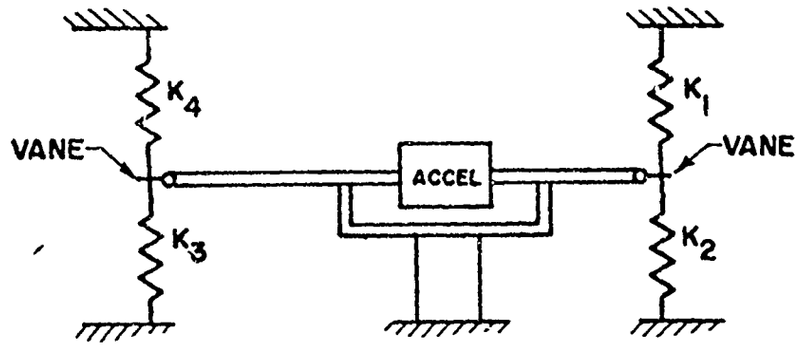

DETAIL Ⓐ FRONT VIEW

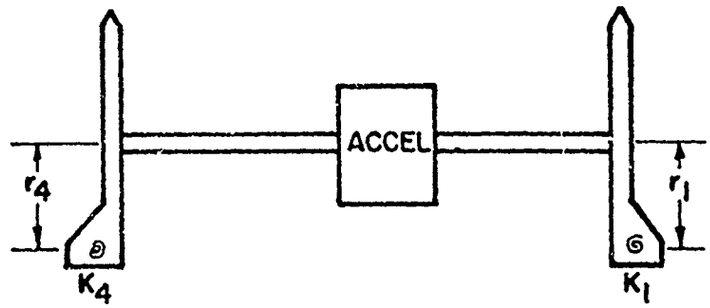

DETAIL Ⓑ TOP VIEW

FIG. 7-12: INERTIA RIG MATHEMATICAL MODEL

This is based on the assumption: $\omega_d \approx \omega_n$ and $\zeta\omega_n \approx 0$. This assumption has proven to be very good for the low inertia system ($\zeta \approx 0.05$). Equation 7-35 is differentiated twice to obtain:

$$\ddot{\theta} = -\theta_o \omega_n^2 \sin \omega_n t \quad , \tag{7-36}$$

so that dividing equation 7-35 by equation 7-36:

$$\frac{\theta}{\ddot{\theta}} = -\frac{1}{\omega_n^2} \quad . \tag{7-37}$$

Equation 7-37 is then combined with equation 7-34 to yield:

$$I_v = \frac{\sum_{i=1}^{n} k_i r_i^2}{\omega_n^2} \quad . \tag{7-38}$$

Vane System Lag Response Summary

7.35 All quantities needed for equation 7-27 are now solved; however, the equation is still unsolvable in that α_t appears on both sides of the equation

$$\alpha_t = \frac{1}{\omega_{n_v}^2}\left[\ddot{\alpha}_i + 2\zeta_v \omega_{n_v}(\dot{\alpha}_i - \dot{\alpha}_t) + \omega^2 n_v \alpha_i\right] \tag{7-27}$$

This equation must be iterated in order to obtain a useful answer. The iteration is taken over the entire time-slice with numerical derivatives taken at each point. Experience has shown that when $\dot{\alpha}_t = \dot{\alpha}_i$ is used as the first iteration guess, a suitable convergence

of α_t is obtained in three iterations. Suitable convergence is taken as magnitude change less than 0.1 degrees at every point.

AEROELASTIC BENDING

7.36 Aeroelastic bending can create errors in angle of attack due to the movement of the angle of attack reference line with respect to the aircraft reference line. There are two primary contributors: boom bending and fuselage bending. The boom bending portion has been obtained in the past by statically loading the boom to predicted flight loads, or by strain gage measurement (reference 7-3 gives additional information on determining boom bending values). Typically, boom bending will be less than 0.1 degree per g , but need be measured for correction where 0.1 degree is the minimum acceptable error.

7.37 Fuselage bending is considerably more complex and generally cannot be calibrated on the ground. One excellent method, as given in reference 7-1, uses two sets of accelerometers mounted in the aircraft. One set is mounted at the vanes and the other set at or near the cg. After correcting the accelerometer readings for dynamic rates, the accelerometers hould read:

$$n_{x_{FPA}} = n_{x_{i_{FPA}}} \cos \Delta\alpha - n_{z_{i_{FPA}}} \sin \Delta\alpha \qquad (7\text{-}39)$$

and

$$n_{x_b} = n_{x_{i_b}} \cos(\alpha_i + \Delta\alpha) - n_{z_{i_b}} \sin(\alpha_i + \Delta\alpha) \quad . \qquad (7\text{-}40)$$

As given in reference 7-1, a rapid solution is obtained by using the first estimate of the Newton-Raphson solution as:

$$\Delta\alpha_{BENDING} = \frac{n_{x_b} - n_{x_{FPA}}}{n_{z_b}} \quad \text{(radians)} \quad , \qquad (7\text{-}41)$$

which is accurate to 0.5 percent at $\Delta\alpha = 5$ with no further calculations. The $\Delta\alpha_{BENDING}$ is then the total bending between the two sets of accelerometers.

CONCLUDING REMARKS TO CHAPTER 7

7.38 It has been shown that when dealing with the accelerometer methods of determining aircraft performance, the minimum acceptable accuracy for angle of attack is ±0.10 degrees. Other flight test data present other accuracy requirements. In order to maintain this accuracy, corrections to the measured angle of attack must be made for errors in mechanical positioning, errors due to flow angularity, probe response errors, and aeroelastic bending. The true angle of attack is then given by:

$$\alpha_t = \alpha_i + \phi + \Delta\alpha_u + \Delta\alpha_{BENDING} + \Delta\alpha_p + \Delta\alpha_{LAG} \quad . \tag{7-42}$$

7.39 Chapter 7 completes the instrumentation requirements for the accelerometer methods. Procedural requirements are given in Chapter 8, and other uses of the accelerometer package are detailed in Chapter 9.

REFERENCES

7-1. Berven, Lester H., "Determination of Aircraft Angle of Attack," Air Force Flight Test Center, Undated, circa 1971

7-2. USAF Edwards AFB, Document No. FTC-TD-71-1, "Theory of the Measurement and Standardization of Inflight Performance of Aircraft," by E.W. Dunlap and M. Porter, Unclassified, Apr 1971

7-3. U.S. Naval Air Test Center, Flight Test Technical Memorandum 5-73, "Developing the Airplane Drag Polar and Lift Slope Curve From Flight Test Data Using Onboard Accelerometers," by W.R. Simpson, Unclassified, 15 May 1973

7-4. Systems Control, Inc., Technical Report No. 1, "Identification of Aircraft Stability Derivatives for the High Angle of Attack Regime," Unclassified, Jun 1973

7-5. U.S. Naval Air Test Center, Flight Test Technical Memorandum 2-75, "The Determination of Aircraft Angle of Attack," by W.R. Simpson, Unclassified, 27 Mar 1975.

THE ACCELEROMETER METHODS OF DETERMINING AIRCRAFT PERFORMANCE (DYNAMIC PERFORMANCE TESTING)

CHAPTER 8
TEST METHODS
(PILOT AND ENGINEERING PROCEDURES)

SUMMARY OF CHAPTER 8

8.1 This chapter presents engineering and pilot procedures for the use of the accelerometer methods of determining aircraft performance. Its primary intent is to bring forth information not discussed elsewhere in the text. Basic aircraft instrumentation considerations (other than accuracy which is dealt with in Chapters 5, 6, and 7), are presented with a detailed procedure given for determining the extent of environmental control required. Pilot maneuver techniques are detailed (the basic maneuvers are discussed as to data content in Chapter 3). Basic data reduction considerations are related (data reduction procedures are given in Chapters 2, 3, and 4). Finally, considerations in the construction of the optimum flight profile are discussed (first introduced in Chapter 3). Each of these topics is considered a detailed expansion of areas previously discussed, and cross-reference is made to the appropriate chapter in each case.

INTRODUCTION TO CHAPTER 8

8.2 To this point, this document has related specific considerations to be made when dealing with the accelerometer methods of obtaining aircraft performance from flight test data. There has been very little in the area of "how-to" do the tests or to make instrumentation or data reduction decisions. This Chapter is intended to fill that need. The details of implementation are omitted since they are given elsewhere in the document, but appropriate cross-reference is made for those seeking more detail. This Chapter is included primarily as a reference for the content of the manual, and partly as a guide to the use of the accelerometer methods.

SYMBOLS

8.3 The following symbols are used in Chapter 8.

Symbol	Definition	Common Units	Metric Units
C_D	Drag coefficient	-	-
C_L	Lift coefficient	-	-
cg	Center of gravity	% MAC	(% MAC)
h	Altitude	ft	(m)
g	Acceleration of gravity	ft/sec^2	(m/sec^2)
F_n	Net thrust	lbs	(N)
M	Mach number	-	-
T_1, T_2, etc	Temperature	deg R	(deg K)
V	Velocity	kts	(km/hr)
V_{MAX}	Maximum airspeed	kts	(km/hr)
W_f	Fuel flow	(lbs/hr)	(kg/sec)
Greek Symbols			
α	Angle of attack	deg	(deg)

AIRCRAFT INSTRUMENTATION CONSIDERATIONS

8.4 The aircraft instrumentation and instrumentation accuracy requirements are reviewed in detail in Chapter 5. The first consideration of any program is the choosing of an accelerometer package. Several items must be ascertained. The most important of these is the extent to which environmental control will be necessary. Figure 8-1 shows the environmental control considerations graphically.

8.5 In the figure, total temperature lines (T_1,T_2,etc.) are plotted on the Mach number altitude plot. Super imposed upon this is the aircraft altitude versus Mach number envelope. Finally, the accelerometer temperature limits are drawn (in cases where the accelerometer has not been chosen, this plot should be made for each type of accelerometer under consideration). The regions of interest are where the aircraft flight envelope intersects the accelerometer temperature limits. This region will determine whether or not environmental control will be required. As shown in the figure, the range of no accelerometer data (electronic elements in the non-linear range) intersects the flight envelope and, therefore, may cause the accelerometer to go beyond the linear range if this temperature is sustained long enough to carry the accelerometer temperature to this level.

8.6 Additionally, the temperature at which damage to the accelerometer will occur may intersect the Mach number-altitude

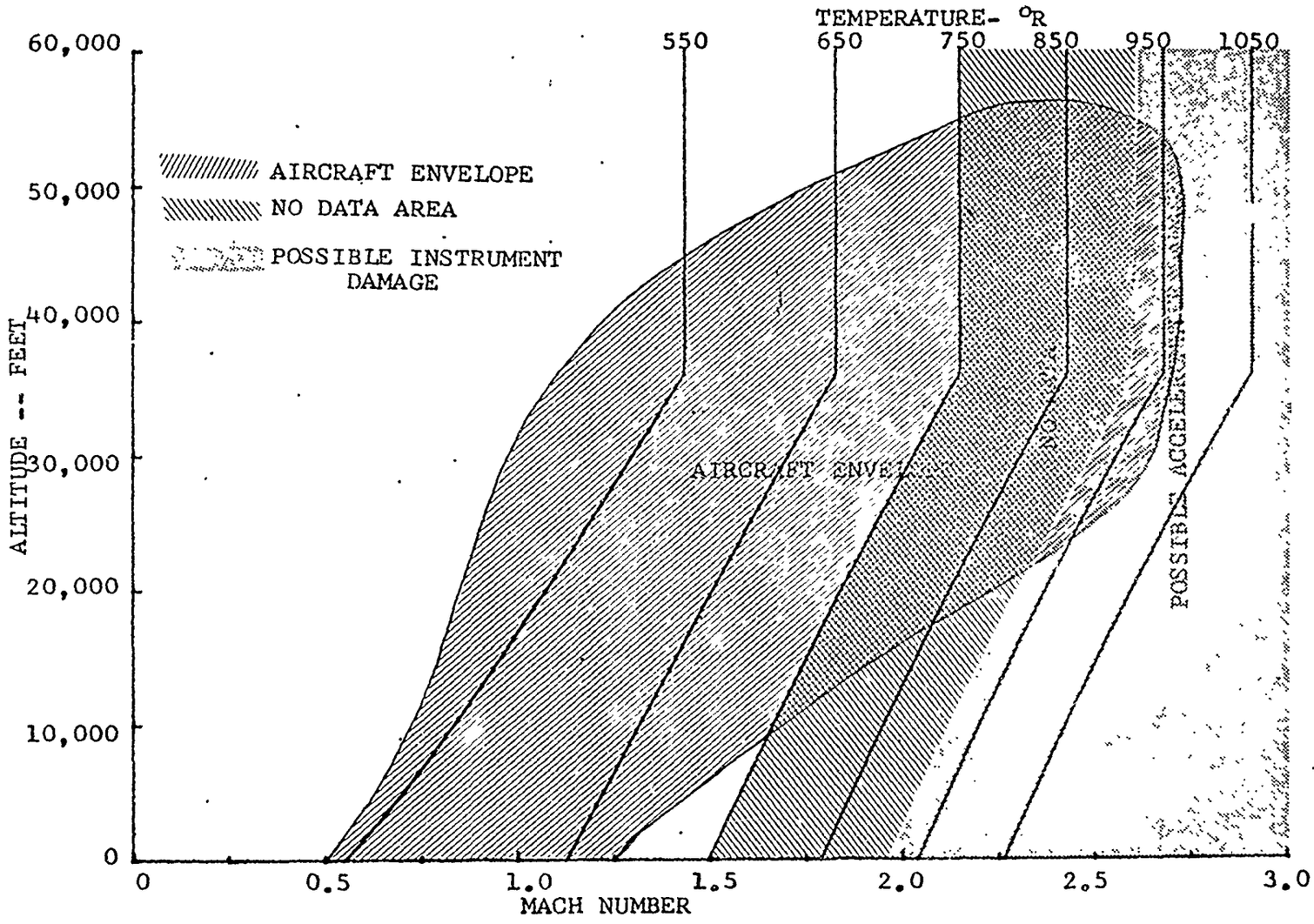

FIG. 8-1: ENVIRONMENTAL CONTROL CONSIDERATIONS

envelope, so that from the plot of figure 8-1, it can be ascertained whether the accelerometer should be environmentally controlled. If environmental control is necessary, then the flight path accelerometer may be necessarily eliminated because of the cost required to cool a boom-mounted accelerometer, and the fact that the additional hardware to cool the accelerometer must be mounted in the boom with the accelerometer.

8.7 Assuming for the moment that the flight path accelerometer has not been eliminated from consideration due to environmental problems, the primary trade-offs to be considered center around the accuracy requirements of angle of attack and angular rates. If high rate maneuvers are not considered, then the flight path accelerometer offers the attractive advantage of being less sensitive to angle of attack measurement errors. If, however, the dynamic maneuvers are needed to obtain flight data within the program constraints, the flight path accelerometer is more sensitive to angular rate corrections because of its increased moment arm to the aircraft cg. These trade-off factors are detailed in Chapters 5 and 7. The body accelerometer can be made almost insensitive to angular rates by placing it at the aircraft cg.

8.8 Additional instrumentation parameters accuracies will then be determined by the accelermoeter package chosen. The cost factor versus accuracy analysis for each instrument can be weighed by the analysis techniques of Chapter 5. For example, an associated

accuracy of ±.2 degrees for angle of attack will be the equivalent of ±0.002 gs in longitudinal acceleration, etc.

PILOT MANEUVER TECHNIQUES

8.9 The pilot maneuver techniques will be the same with both major types of accelerometer packages (flight path and body-mounted). Increased care, however, will be required to keep the maneuver rate and aircraft angular rates low with the flight path system installed. The mathematical model contribution of each of the maneuvers is given in Chapter 3, and this section is intended as a pilot procedure guide.

CLIMBS

8.10 The climb offers the advantage of being capable of execution at a near constant Mach number. It is usually preceded by a low altitude, level acceleration which transitions into the desired climb Mach number. The pull-up is started at some point in advance of the Mach number for the climb, dictated by familiarity with the aircraft and a smooth transition to the climb. The maneuver is done at a constant throttle setting and the primary concern to the pilot is the smooth execution of the maneuver. Small deviations in Mach number or normal load factor are much preferred to jerky or unsmooth aircraft motions. The climb is continued to an altitude selected by the performance engineer and may be segmented. The climb described above is for the production of data for the mathematical model. Additional climbs may be flown on climb schedules or at constant calibrated airspeeds, etc.,

for verification of the mathematical model, and once again, smooth execution is the primary factor.

DESCENTS

8.11 The descent maneuver required for data gathering by accelerometer methods will differ from the conventional test or operational maneuver. It will be flown at constant Mach number, and is usually preceded by a high altitude level acceleration or deceleration. The primary concern is again the smooth transition to the descent schedule. The descent will be done at constant throttle setting and low power setting, but idle has not been found to be a good reference for thrust modeling applications. The low pressure range in the engine and subsequent fluctuations at idle power create problems in calculating thrust by normal parametric methods, and it is recommended that the throttle be placed somewhat above idle. The throttle setting should be such that adequate rates of descent are obtained by the pilot. For example, a Mach .9 descent will require a moderately high power setting to keep the rate of descent from becoming excessive. Or, for a Mach .5 descent, the power must be very low (just above idle) in order to maintain a reasonably high sink rate. Descent rates in the 4,000 fpm - 6,000 fpm are usually desired, although the performance engineer may decide upon higher or lower rates. For Mach numbers less than the lower limit of the pilot's Machmeter, an airspeed versus altitude schedule for the desired constant Mach number must be provided the pilot.

NEAR STABILIZED POINTS

8.12 The stabilized point for accelerometer methods is the same stabilized point done by conventional techniques with the exception that with the accelerometer methods, the requirement for complete stabilization is relaxed. The "near stabilized" point is usually entered from a slow deceleration since this has been found to yield the quickest stabilization time. When the pilot "feels" he has stabilized, he should hold the aircraft at this point for 30 to 45 seconds, and even if there is a small change in airspeed or altitude, the accelerometer method data reduction will compensate. With the accelerometer methods, a one minute stabilization or near stabilization is adequate as opposed to a 2 to 3 minute stabilization by conventional techniques. Stabilization times are further discussed in Chapter 9.

ACCELERATIONS

8.13 The acceleration is performed around a baseline altitude. The pilot will slow the aircraft down to as slow an airspeed as is reasonably possible or to an airspeed selected by the performance engineer. These are not necessarily the same as will be seen in the section on optimum flight profiles. The power is selected as either MIL or MAX and the acceleration is performed as smoothly as possible (jerky or unsmooth aircraft motions avoided). If small deviations in load factor or altitude occur, pilot corrections are to be made slowly and smoothly. If problems exist with pilot-static

instruments in the transonic range (Mach .9 to 1.2), the pilot should select a visual reference (such as nose on the horizon) and hold it. The acceleration is taken to the maximum airspeed or Mach number allowable either by flight operating limits or thrust limited considerations. If the maximum airspeed is thrust limited, "cooking" at V_{MAX} is not desired as this consumes additional flight time. When the acceleration rate becomes sufficiently small (two or three knots per minute), the pilot can initiate a small push-over to several knots beyond the predicted V_{MAX} for extrapolation of the drag polar. The push-over should be a very low smooth g excursion (.80 to 1.0 gs), to prevent sizeable altitude loss. This particular requirement becomes safety of flight at low altitudes.

DECELERATIONS

8.14 The deceleration is usually preceded by an acceleration. Since the end of the acceleration included a small push-over, the pilot should pull smoothly to the near trimmed condition (around V_{MAX} at baseline altitude). This should consume very little flight time if the accelration is done properly. The throttle is reduced smoothly to the desired power setting which, in general, may be anything from MIL to IDLE and depends upon the end point of the deceleration. The deceleration may be segmented for use with the optimum flight profile. Again, thrust should be maintained somewhat above idle for thrust modeling applications. The low speed end of

the deceleration does not usually present problems, but if the deceleration rate is excessively low (less than 2 knots per minute), the pilot can pull-up smoothly into a climb attitude to increase deceleration rate. The g excursion should again be low(1.0 to 1.2 gs) and as in all accelerometer method flight techniques, unsmooth or jerky motion should be avoided.

WIND-UP TURNS

8.15 The wind-up turns are done at constant Mach number and usually preceded by a stabilized point. The stabilized point is necessary for two reasons. It allows the engine to stabilize and gives a reference point from which to start the maneuver and the data reduction. The pilot applies roll control and pulls smoothly to the desired q level losing altitude to hold Mach number and keeping the throttle position constant to avoid transient thrust calculations. The g excursion in the wind-up turn is generally dictated by the acceptable altitude loss (±1,000 feet usually the manuever starts at +1,000 feet above trim altitude and terminates at -1,000 feet below trim altitude). The maximum pull rate is dictated by pitch rate consideration (±10 deg/sec nominal limit on pitch rate, pitch acceleration should be held as small as possible).

WIND-DOWN TURNS

8.16 The wind-down turns are done at constant altitude and usually preceded by a stabilized point. The maneuver is primarily

done for turning performance as discussed in Chapter 9. The pilot applies roll control and smoothly applies g at constant throttle holding altitude with rudder and ailerons. The airspeed will be allowed to decrease to a pre-determined point, where the pilot will release g and roll-out reducing throttle as appropriate. The maximum g applied will be dictated by the maximum deceleration rate desired and the maximum pitch rate allowed as discussed in paragraph 8.15.

ROLLERCOASTER OR PUSH-PULL MANEUVER

8.17 The roller coaster is done at near constant Mach number and is preceded by a stabilized point. The maneuver rate is very important here. If the maneuver is done too quickly, high pitch rates and high pitch accelerations cannot be avoided. If the maneuver rate is too low, sizable excursions in Mach number and altitude cannot be avoided. It is imperative that adequate pilot training be performed in this area to increase the number of useful maneuvers. The maneuver should start from the stabilized point by pulling the aircraft gently to a nose-high altitude causing a small bleed-off in Mach number. The push-over should be smoothly started from this point, and as the nose comes through the trim position, Mach number increases. As the Mach number goes through trim, the pull-up is started and so the maneuver continues for several cycles. The Mach number excursion can be held to a minimum by this method. Large g excursions should be avoided in this maneuver and

0 to 3 gs is adequate under most conditions. A larger C_L variation can be had at higher altitude where the C_L at trim is higher. A 7 g rollercoaster may produce pitch rates in excess of 20 deg/sec while, in most cases, pitch rates less than 10 deg/sec are acceptable.

OTHER MANEUVERS

8.18 Other maneuvers may be requested by the performance engineer for either obtaining data which is not readily available from the above listed maneuvers, or for verification of the mathematical model as discussed in Chapter 3. The primary concern in these maneuvers will be the smooth execution or avoidance of jerky aircraft motions. Individual requirements of maneuvers not listed should be provided by the performance engineer.

BASIC DATA REDUCTION

8.19 The basic philosophy of data reduction as applied to the accelerometer methods of determining an aircraft's performance is the mathematical modeling concept as given in Chapter 3. Each flight data point will be reduced to values of drag (C_D), lift (C_L), thrust (F_n), fuel flow (W_f), and angle of attack (α) . The basic data yield of each maneuver is given in Chapter 3, and can be summarized in table 8-1.

8.20 Additionally, corrective procedures as detailed in Chapter 4 for the lift and drag and Chapter 7 for the angle of attack, must be applied to each of the test maneuvers flown. The basic corrective procedures to be applied are given in table 8-2.

TABLE 8-1

BASIC MANEUVER DATA CONTRIBUTION
TO THE MATHEMATICAL MODEL

(X=Data Available Y=Primary Data Yield)

Maneuver	Drag Polar	Lift Curve	Thrust Available	Thrust Fuel Flow	Thrust RPM
Climb	Y	X	X[a]	Y	Y
Descent	Y	X		Y	Y
Near Stabilized Point	Y	Y		Y	Y
Acceleration	Y	X	Y[a]	X	X
Deceleration	Y	X		X	X
Wind-Down Turn	X	X		X	X
Wind-Up Turn	Y	Y		X	X
Rollercoaster	Y	Y		X	X

[a]Thrust available data is taken in any maneuver at MIL, MAX, or other power settings considered desirable. Climbs and accelerations are usually flown at these power settings but not necessarily so.

TABLE 8-2

CORRECTIVE AND STANDARDIZATION PROCEDURES REQUIRED BY MANEUVERS

(Y=Required X=Not Required M=May Be Required)

Maneuver	L/D[a] Load Factor	L/D Power	L/D Wing Sweep	L/D Pitch Rate	AOA[b] Load Factor	L/D Roll Rate	AOA Upwash	L/D cg	AOA Lag	L/D Mach #	AOA Pitch Rate	Tail Trim
Climb	M	Y	M	M	M	X	Y	Y	X	Y	M	Y
Descent	Y	Y	M	X	X	X	Y	Y	X	Y	X	Y
Stabilized point	Y	Y	M	X	M	X	Y	Y	X	Y	X	Y
Acceleration	Y	Y	M	M	M	X	Y	Y	X	X	M	Y
Deceleration	Y	Y	M	X	M	X	Y	Y	X	X	M	Y
Wind-up Turn	X	Y	M	Y	X	Y	Y	Y	Y	Y	Y	Y
Wind-Down Turn	X	Y	M	Y	X	Y	Y	Y	Y	X	Y	Y
Rollercoaster	X	Y	M	Y	X	X	Y	Y	Y	Y	Y	Y

[a]Lift and drag

[b]Angle of attack

OPTIMUM FLIGHT PROFILE CONSTRUCTION

8 21 The optimum flight profile is used to give the maximum usable flight data in the minimum time and is discussed in detail in Chapter 3. This section then, will deal with the rational in constructing such a profile. The profile should reasonably define each of the five components that make up the mathematical model. These five components are:

- Drag polar
- rust available
- Thrust/fuel flow
- Thrust/rpm
- Lift curve.

8.22 As seen from table 8-1, all of the maneuvers can be used to generate the aircraft drag polar. The thrust available, on the other hand, is generated mainly from the acceleration and data is available on climbs so that the profile should include enough acceleration data to generate the thrust available data. The stabilized point is used as the anchor point for curve fairing, so that it is imperative that an adequate number of stabilized points are incorporated in the profile. As discussed in the section on pilot techniques, the stabilized point is best entered from a deceleration. Additionally, if decelerations are done over the same range of accelerations, the adequacy and magnitude of power corrections can be assessed. The decelerations can then be broken

into parts to allow for the stabilized points at increments. So, for the data thus far discussed, the optimum flight profile consists of accelerations and "decelerations by parts" with stabilized points during the deceleration. Of the data taken so far, no data has been taken during a constant Mach number maneuver, which would essentially define the drag polar curve shape if the maneuver is done over a large C_L range. Such maneuvers would be climbs and descents, so that the optimum profile should include these. Again, if a climb and descent are done at the same Mach number power, effects can be analyzed.

8.23 At this point, then, the optimum flight profile is formulated and it remains only to place the maneuvers in the order of flight sequence. Several additional considerations remain. If there are any peculiarities of the aircraft that are apparent, these should be investigated. In the example of Chapter 3 (figure 3-22), a zoom climb or pull-up to high altitude was initiated to give high altitude fuel flow data. The maneuver also gives high C_L drag and angle of attack data. Predicted performance data should be used to determine the time and fuel used for each maneuver. If additional instrumentation time and onboard fuel permits, additional accelerations or climbs may be performed. Or, if desirable, dynamic maneuvers may be employed after the stabilized points.

8.24 The optimum flight profile can be tailored to fit the individual requirements of the aircraft. For example, if it is

known that power effects are small, or that they create no problems because adequate corrective procedures are available, the acceleration/deceleration pair can be broken, and the climb/descent pair can be done at different Mach numbers. The optimum flight profile should then be tailored to the individual time, fuel, and peculiarities of the aircraft being tested.

8.25 Figure 8-2 shows an optimum flight profile developed for the subsonic determination of the FB-111A at various wing sweep conditions. Extensive use of the vertical was made in order to give constant Mach number maneuvers. Wind-up turns were used to generate lift/drag data under accelerated conditions for comparison with 1 g data. The primary purpose of the profile of figure 8-2 was for the determination of incremental drag of store loading under various flight/wing sweep conditions.

8.26 Figure 8-3 shows an optimum flight profile developed to define the clean drag polar in subsonic and supersonic conditions at fixed wing sweep conditions. Extensive use of the horizontal was made because of excessive fuel consumption in climbs. Note the use of aerial refueling to extend the flight time to that time available in the instrumentation.

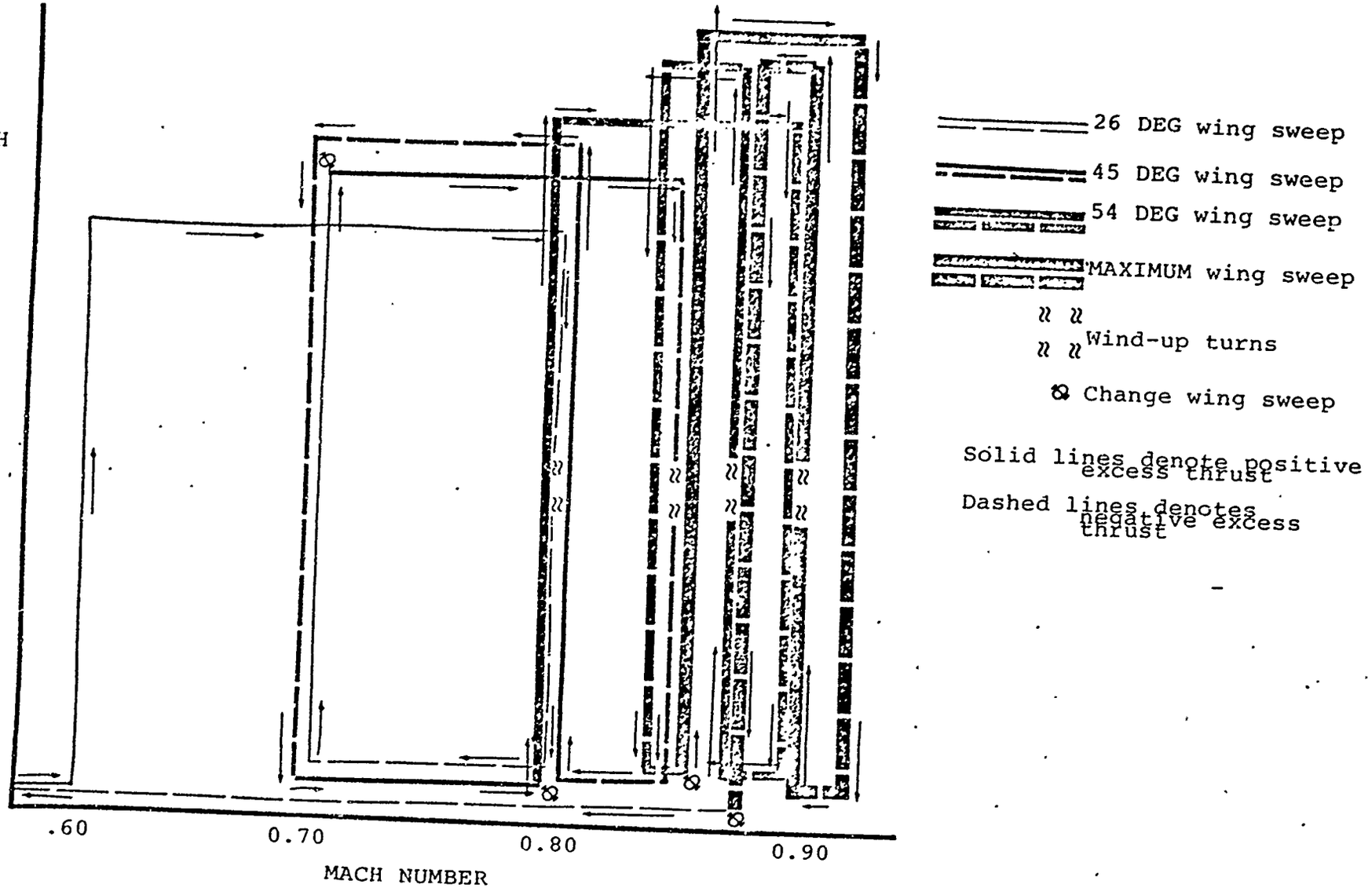

FIG. 8-2: SUBSONIC OPTIMUM FLIGHT PROFILE FOR VARIABLE WING SWEEP AIRCRAFT

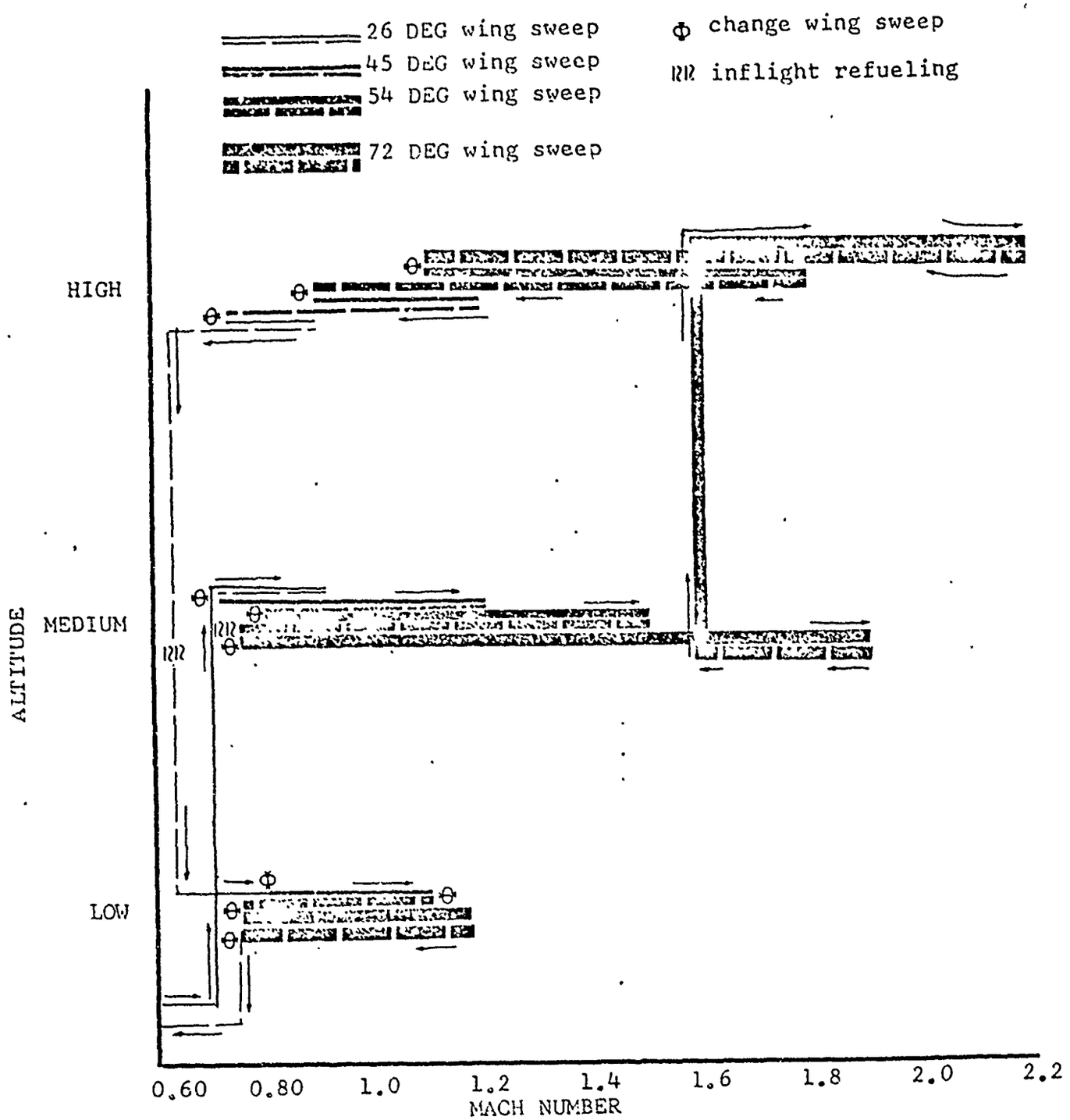

FIG. 8-3: SUBSONIC/SUPERSONIC OPTIMUM FLIGHT PROFILE FOR VARIABLE WING SWEEP AIRCRAFT

CONCLUDING REMARKS TO CHAPTER 8

8.27 Chapter 8 concludes the accelerometer methods as applied to the mathematical modeling concept. One further use will be discussed. This is in the use of onboard accelerometers for securing data in conventional aircraft performance flight tests and is detailed in Chapter 9.

THE ACCELEROMETER METHODS OF DETERMINING AIRCRAFT PERFORMANCE (DYNAMIC PERFORMANCE TESTING)

CHAPTER 9
CONVENTIONAL AIRCRAFT PERFORMANCE FLIGHT TEST USING ONBOARD ACCELEROMETER DATA

SUMMARY OF CHAPTER 9

9.1 Conventional aircraft performance flight tests are reviewed for data obtained when using onboard accelerometer data. Techniques such as the stabilized point, climbs, accelerations, and level flight turning performance are reviewed. Additionally, procedures are given for the integration of accelerometer data during take-offs for the application of self-contained take-off and landing data.

INTRODUCTION TO CHAPTER 9

9.2 To this point, the accelerometer methods of obtaining aircraft performance have been treated as significantly different from conventional methods. This is inherently true because of the radically different approach pursued (the indirect or math modeling approach as detailed in the preface). This radically different approach to flight test is only possible because of the "instantaneous" measure of excess thrust available with accelerometer measurements of an appropriate accuracy level.

9.3 The direct methods, however, offer the attractive advantage of self-verification. That is, the data should be a direct reflection of the test (such as specific range or endurance - as opposed to drag polar). In many instances, the direct method may be used even when instrumentation for the indirect method is available. Such cases may typically be in areas of limited interest or for direct verification of performance characteristics in a specific flight regime.

9.4 Onboard accelerometers may be used in these instances to more accurately reflect the test data and to verify the proper functioning of other instrumentation. In the case of transonics or take-off data, they may allow direct methods not available with conventional instrumentation. These cases are the subject of this chapter.

SYMBOLS

9.5 The following symbols are used in Chapter 9.

Symbol	Definition	Common Units	Metric Units
A_f	Acceleration factor $1+\frac{V}{g}\frac{dV}{dh}$	-	(-)
a_z	Acceleration flight path normal	ft/sec^2	(m/sec^2)
C_D	Drag coefficient	-	(-)
C_L	Lift coefficient	-	(-)
F_{ex}	Excess thrust	lbs	(N)
F_g	Gross thrust	lbs	(N)
F_n	Net thrust	lbs	(N)
g	Acceleration of gravity	ft/sec^2	(m/sec^2)
h	Height	ft	(m)
h'	Height derivative	ft/sec	(m/sec)
H_p	Pressure altitude	ft	(m)
M	Mach number	-	(-)
n_x	Longitudinal load factor	-	(-)
n_z	Normal load factor	-	(-)
P_s	Specific excess power	ft/sec	(m/sec)
RPM	Engine speed or wheel speed	RPM	(RPM)
S	Distance	ft	(m)
$\dot{S}$	Distance derivative	ft/sec	(m/sec)
S.R.	Specific range	air n.mi./lbs	(air km/kg)
t	Time	sec	(sec)

Symbol	Definition	Common Units	Metric Units
V	Velocity	ft/sec	(m/sec)
$\dot{V}$	Velocity derivative	ft/sec^2	(m/sec^2)
W	Weight	lbs	(kg)
W_f	Fuel flow	lbs/hr	(kg/sec)
Greek Symbols			
α	Angle of attack	deg	(deg)
Δ	Increment	-	(-)
δ	Pressure ratio	-	(-)
ϕ	Runway slope	deg	(deg)
θ	Temperature ratio	-	(-)
θ	Pitch attitude	deg	(deg)
$\dot{\theta}$	Pitch rate	deg/sec	(deg/sec)
γ	Flight path angle	deg	(deg)

Subscripts

$( )_{POFF}$	Power off
$( )_{1,2,3,4,etc.}$	Condition state
$( )_{AVAIL}$	Available
$( )_{T,t}$	True
$( )_i$	Indicated
$( )_u$	Upwash
$( )_{FP}$	Flight path

Others

$\equiv$	Equal by definition

CONVENTIONAL TECHNIQUES

9.6 Conventional flight test techniques to determine aircraft performance are reviewed extensively in references 9-1 through 9-7 and will not be dealt with in this paper except by reference. A general knowledge of these techniques is assumed. For detailed derivations of equations and methods, the reader is referred to the references. An attempt will be made to further refine the data obtained by these techniques by using the accelerometer as the primary determinant of aircraft excess thrust. In addition, presupposing an accurate value of excess thrust taken "instantaneously" will lead to more sophisticated analysis methods as in the case of level flight turning performance. Each technique will be discussed separately.

STABILIZED POINT DATA

9.7 In conventional flight testing, the stabilized point is taken to avoid several corrections to the data. These corrections include power and excess thrust. The stabilized point is done at power for level flight at zero excess thrust, and is usually flown along a constant W/δ line . Dimensional analysis yields the functionality of specific range as Mach and W/δ . In addition, the specific range at a given point on a standard day is given by V_t/W_f . Complete stabilization is seldom obtained, and the average velocity and fuel flow are corrected by the average excess thrust obtained by airspeed altitude energy method over the two or three minute interval. The length of stabilization is dictated by the sensitivity of airspeed altitude energy method to differentiation. If the energy equation is examined:

$$\frac{F_{ex}}{W} = \frac{\dot{h}}{V} + \frac{\dot{V}}{g} = n_{x_{Fp}} \quad . \tag{9-1}$$

(A complete derivation of this equation is given in Chapter 2.) It can be seen that onboard accelerometers can yield excess thrust point by point and there is no need for mathematical differentiation. Further, the length of the stabilized point can be reduced to a shorter period of time since neither differentiation nor complete stabilization are required.

9.8 Each point then can be corrected by normal means (i.e., assuming $F_{ex}=\Delta F_n$ and obtaining a ΔW_f at each point for specific range determination. A one-minute stabilized point will yield several data points on the specific range curve as shown in figure 9-1. There will be a total of six points if the stabilized run was reduced very 10 seconds, as opposed to one point by conventional methods. Since the data points are very close to one another, they can be averaged to give one point on the curve, or we can take a point during the run at true zero excess thrust as measured by the accelerometer so that the corrections are truly zero. Utilizing this method can be a real advantage on the back side of the power curve, at low Mach numbers or any place where true stabilization is difficult, because true stabilization is not required.

9.9 We can additionally take the matrix of points generated by the W/δ flights and mathematically model the data as discussed in Chapter 3. Here each data point can be used to generate drag polar data and thrust fuel flow relations as shown in figure 9-2. The stabilized data reduced by dynamic methods are shown as clusters of points. The faired curve can then be used to generate figure 9-1. With sparse data, the figures of the mathematical model may be easier to fair, especially if we have the availability of previous flight test data to show curve shapes and families. As in conventional techniques, one method should be played against the other to yield the most accurate fairing of the range data.

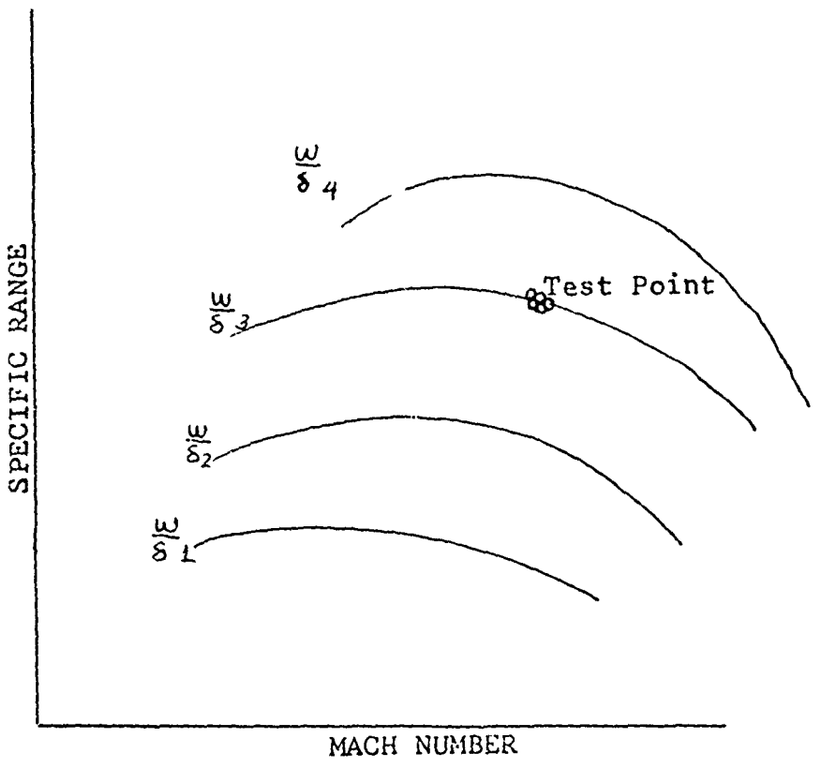

FIG. 9-1: SPECIFIC RANGE DATA

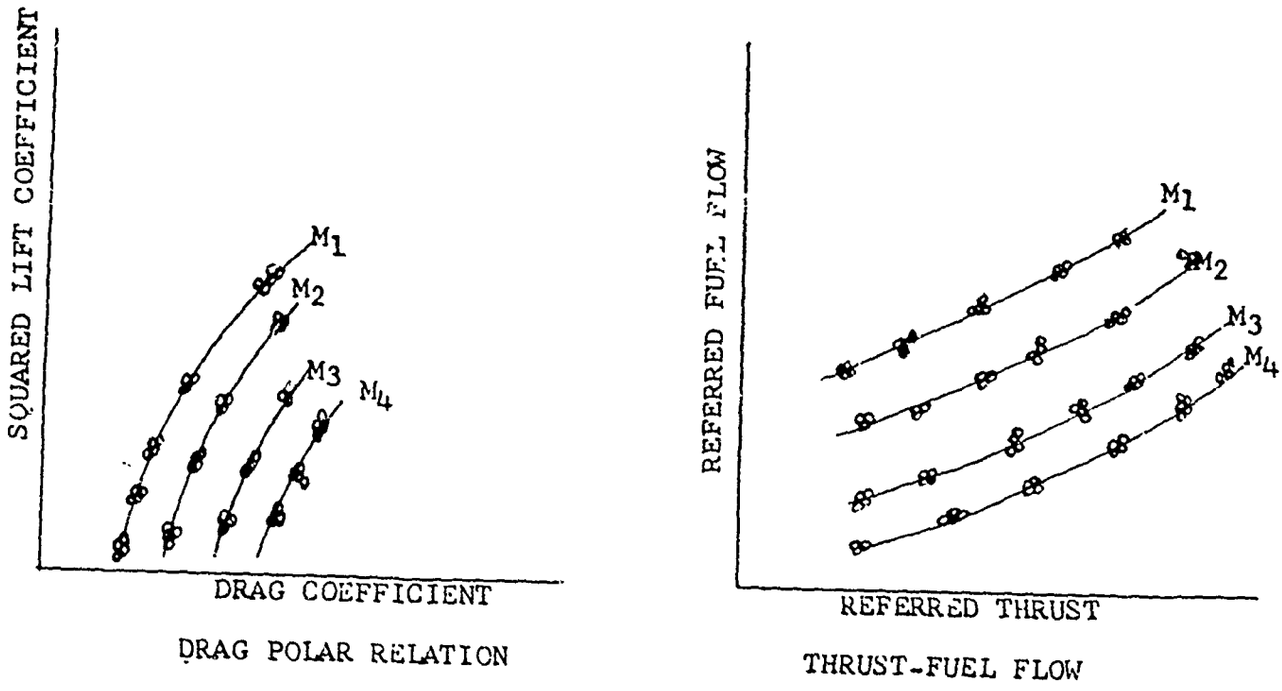

FIG. 9-2: MATH MODELING APPROACH

ACCELERATION DATA

9.10 Acceleration data taken by dynamic techniques is the same as that taken by conventional techniques with the exception that the accelerometer is used to determine excess thrust. At first, the accelerometer method appeared more scattered than the airspeed time method as shown in figure 1-3 of Chapter 1. The apparent scatter is due to the g sensitivity of the dynamic methods as opposed to the airspeed/time method which affords a time averaging and tends to follow more closely the average g over the time interval considered. This may be an advantage in slow smooth accelerations where the pilot is near 1g conditions. But for high excess thrust conditions, it becomes hard to hold 1g and the conventional airspeed/time method may be in error. The Accelerometer data may be corrected for the g effect point by point (see Chapter 4 for complete discussion) by adding or subtracting drag from the drag polar or points may be taken at 1g as shown in figure 1-3. The data can then be cross-plotted as thrust available and thrust required as shown in figure 9-3. The thrust required data will be a primary funciton of load factor as can be seen on the drag polar for a comparable change in C_L. The thrust available is obtained through the normal parametric measurement of thrust or inferred by fuel flow and the assumed thrust fuel flow relation (see Chapters 1 and 3). The thrust required at a given g level is simply the thrust available less the measured excess thrust for the given Mach number and g combination.

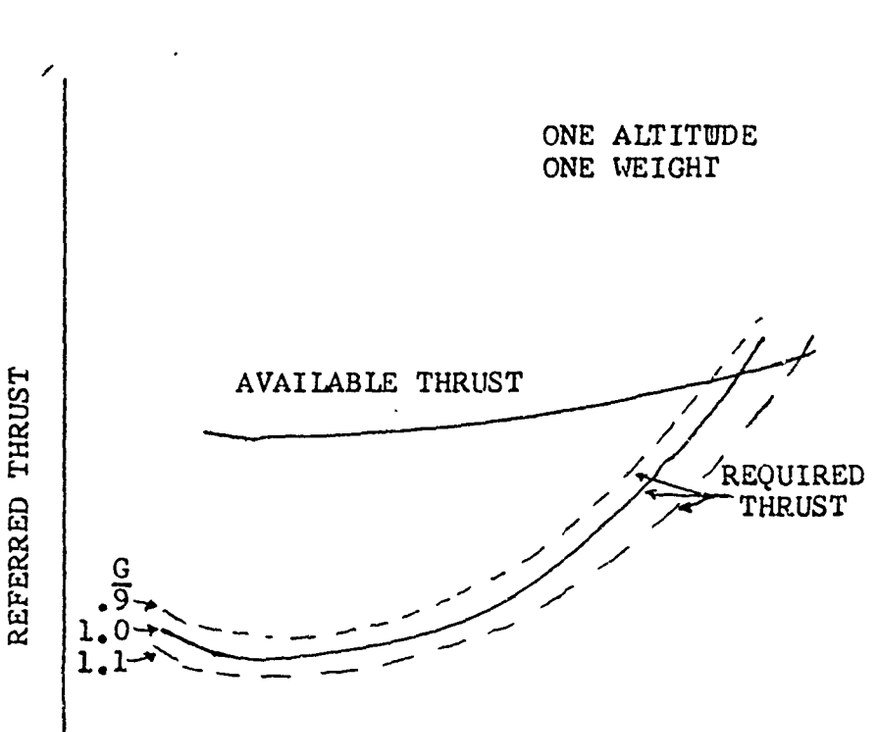

FIG. 9-3: ACCELERATION DATA

9.11 From the cross-plot of figure 9-3, the climb potential can be standardized at a given altitude by noting the given relationship for excess thrust in the unaccelerated case:

$$\frac{F_{ex}}{W} = \frac{\dot{h}}{V} = \sin \gamma \qquad \text{assuming } \frac{\dot{V}}{g} = 0 \tag{9-2}$$

and noting that:

$$n_z = \cos \gamma \text{ for the climb condition.} \tag{9-3}$$

Where excess thrust is a function of g , there is a small iteration required to get the parameters straight. The rate of climb under various acceleration factors as given by:

$$A_f = 1 + \frac{V}{g}\frac{dV}{dh} \quad , \tag{9-4}$$

can also be computed by the equations:

$$\frac{F_{ex}}{W} = \frac{\dot{h}}{V} + \frac{\dot{V}}{g} \tag{9-1}$$

and

$$\sin \gamma = \frac{\dot{h}}{V} \tag{9-5}$$

with

$$\cos \gamma = n_z \tag{9-3}$$

Again, an iteration is required, and the data should be cross-plotted as shown in figure 9-4. At the same time, the flight path angle calculated should be plotted as shown in figure 9-5. With this information for several altitudes, climb performance can be predicted or corrected to various climb schedules.

9.12 There is probably no need to calculate climb parameters at Mach numbers below the minimum thrust required since there is a speed stability problem here and there will not be a climb schedule which places the pilot on the back side of the power curve. Varying the weight in an accel has the same effect as varying N_Z as shown on the drag polar in figure 9-6. So that the data of figure 9-4 can be shown for lines of weight at 1g as well as lines of N_Z at one weight. A small correction does appear in the C_L for weight variation or N_Z variation as given by:

$$C_{L_{POFF}} = \frac{N_Z \cdot W - F_g \sin(\alpha+\tau)}{qs} \qquad (2\text{-}66)$$

and it can be seen that a 10 percent change in weight is equivalent to a 10 percent change in N_Z.

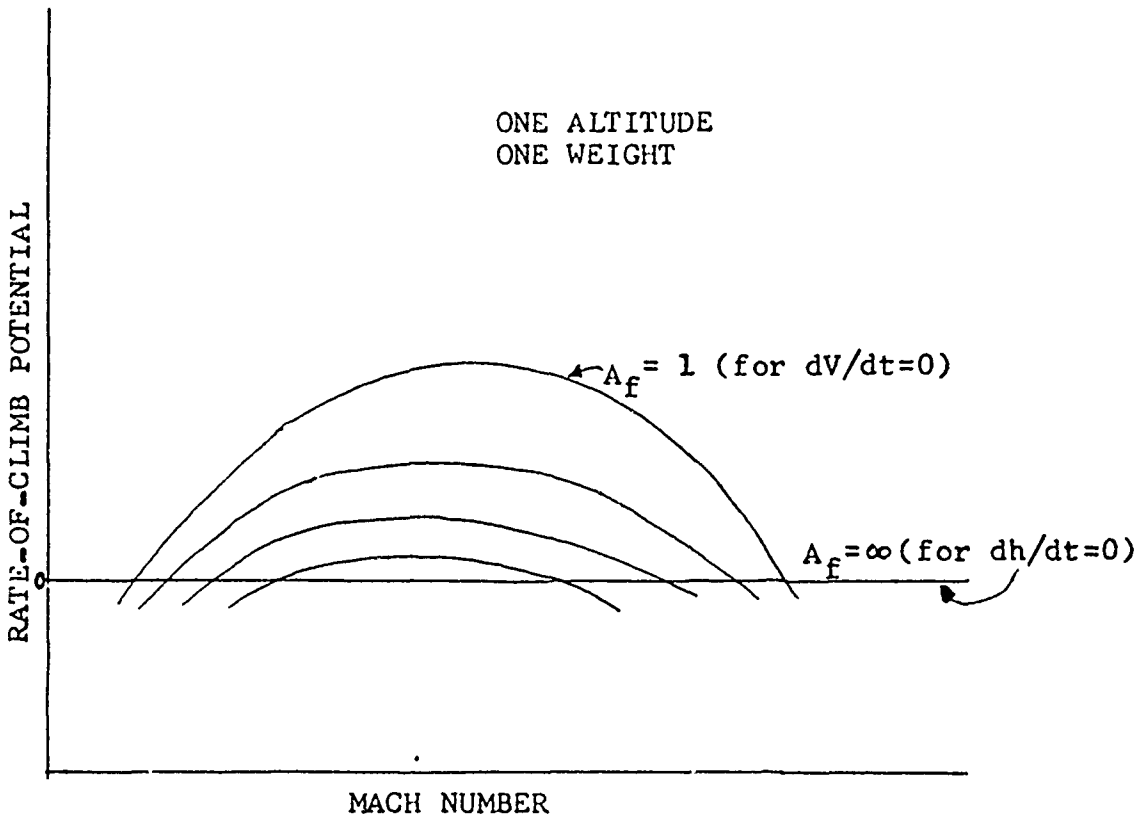

FIG. 9-4: RATE-OF-CLIMB POTENTIAL CROSS-PLOT

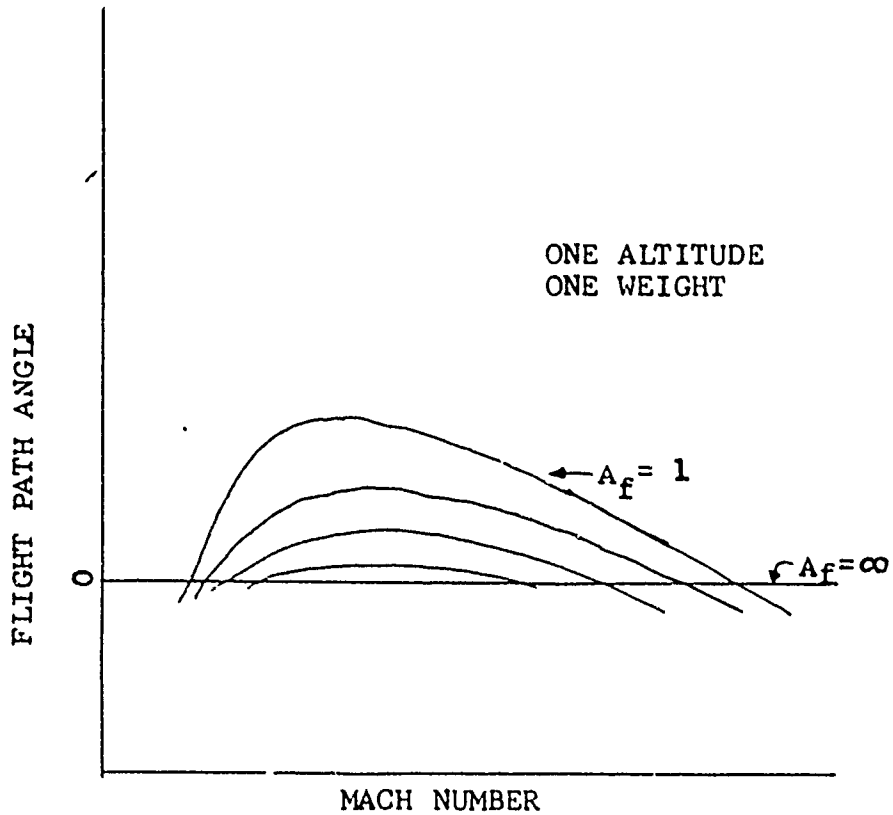

FIG. 9-5: ACCELERATION FACTOR/FLIGHT PATH ANGLE DATA

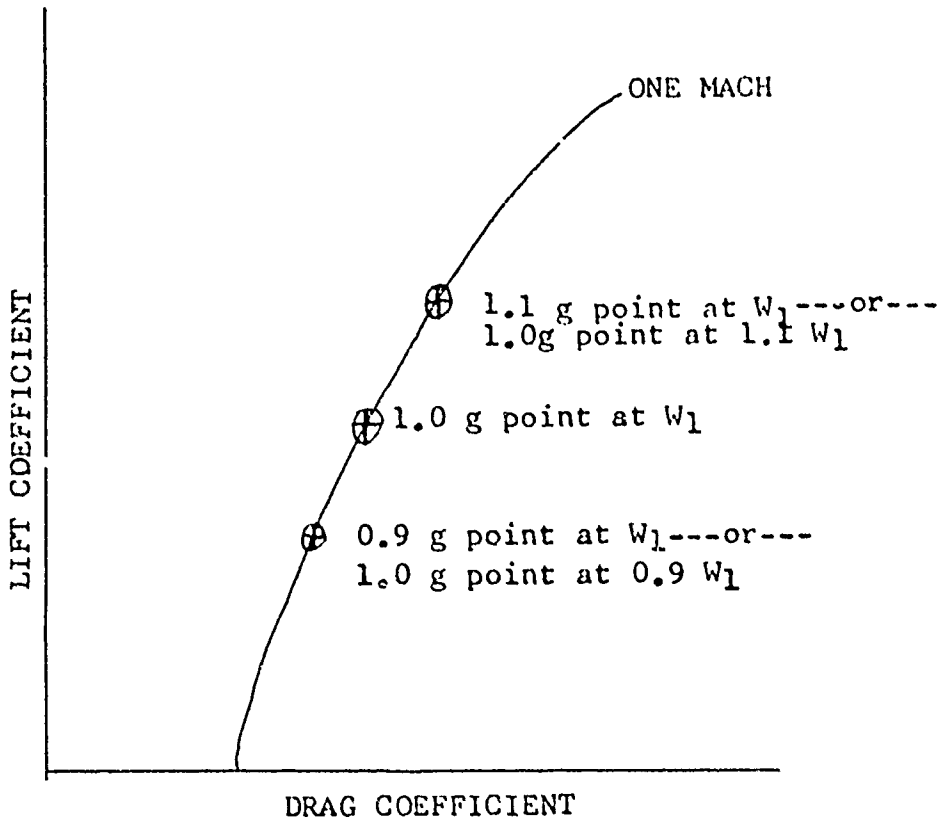

FIG. 9-6: CLIMB POTENTIAL WEIGHT/
NORMAL LOAD FACTOR RELATION

9.13 To correct the climb or standardize it, a flight path angle versus altitude relation must first be calculated. This can be taken from the acceleration data for the criteria dictated by the climb. For example, if minimum time to climb is desired, it can be computed by taking maximum rate of climb at each altitude for the Mach number and acceleration factor. For climb schedules, there is a Mach number and acceleration factor at each altitude defined. The data should be plotted as shown in figure 9-7.

9.14 Figure 9-7 also shows the normal load factor versus aititude as given by:

$$n_z = \cos \gamma \qquad (9\text{-}3)$$

Each point in the climb then can be corrected to $n_z=\cos\gamma$ from the climb scheduled flight path angle as well as to the acceleration factor dictated by the climb schedule. The difference between this and the so called "lg" climb may be small in low performance aircraft or in supersonic aircraft at mil power, but can become significant at high F_{ex}/W values. The data can once again be calculated from the mathematical model and compared to the corrected climb to test the predictive qualities of the model.

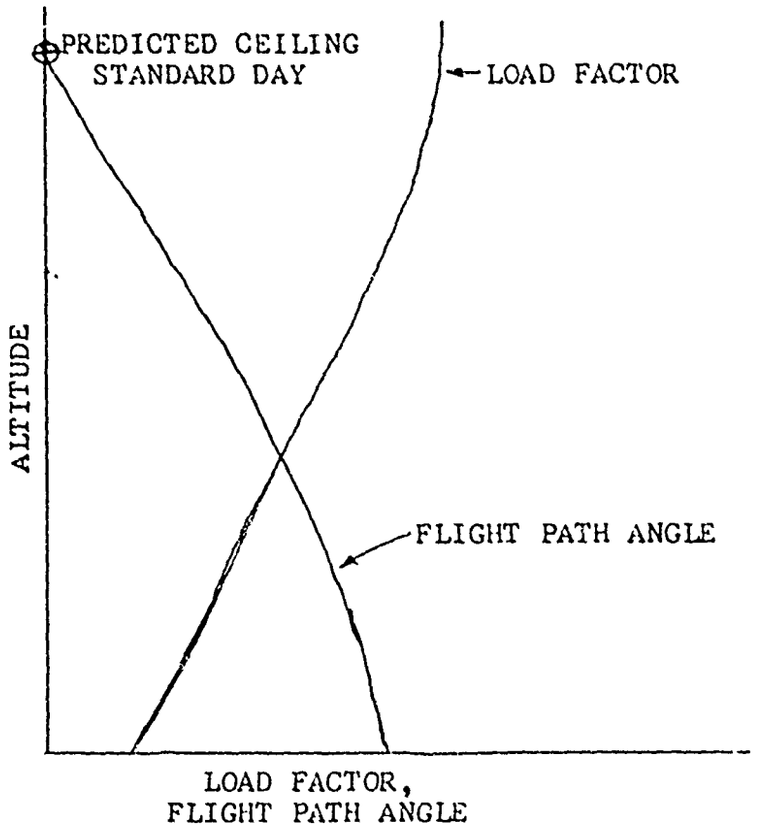

FIG. 9-7: CLIMB SCHEDULED FLIGHT PATH ANGLE

TURNING PERFORMANCE (LEVEL FLIGHT)

9.15 The conventional approach to level flight turning performance as given by reference 9-4 can be further refined as follows. Over a given data point of turning performance, small bobbles in g will occur. No change in flight techniques are required as these excursions in g are an outgrowth of the pilot seeking the stabilized load factor for steady state turning. This small bobbling in g creates a change in C_L which can be plotted as shown in figure 9-8. The F_{ex} is simply (n_x)(weight). Since at a given $C_{L_{POFF}}$ we do not vary the drag, the $C_{L_{POFF}}$ available becomes g available for a given weight so that generalized turning performance for a given altitude can be cross-plotted as shown in figure 9-9.

9.16 A C_L limit placed on this plot allows a precise definition of low speed turning performance. The C_L limited turning performand is shown in figure 9-10. This data can then be cross-plotted to load factor for a given weight, and a structural limit can be applied as shown in figure 9-11.

9.17 The turning performance can then be generalized for altitudes and plotted as shown in figure 9-12. For a given weight/altitude combination, we can generate n_z versus Mach as shown in figure 9-11 Radius of turn, and turn rate are generated by n_z versus Mach, such that all turning performance data can be obtained from figure 9-12.

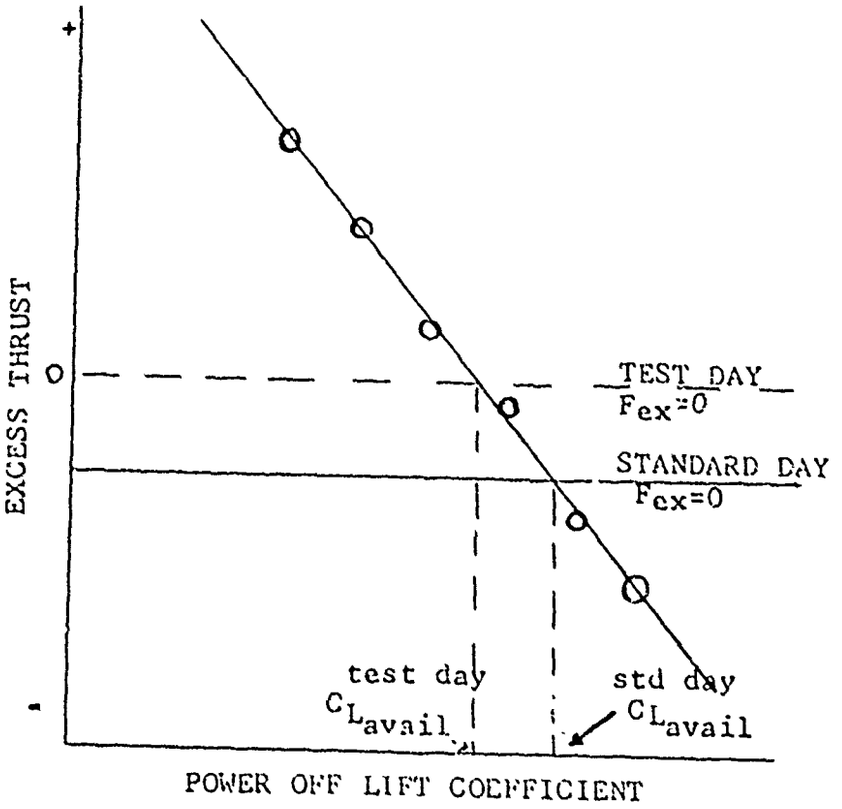

FIG. 9-8: TURNING PERFORMANCE C_L AVAILABLE PLOT

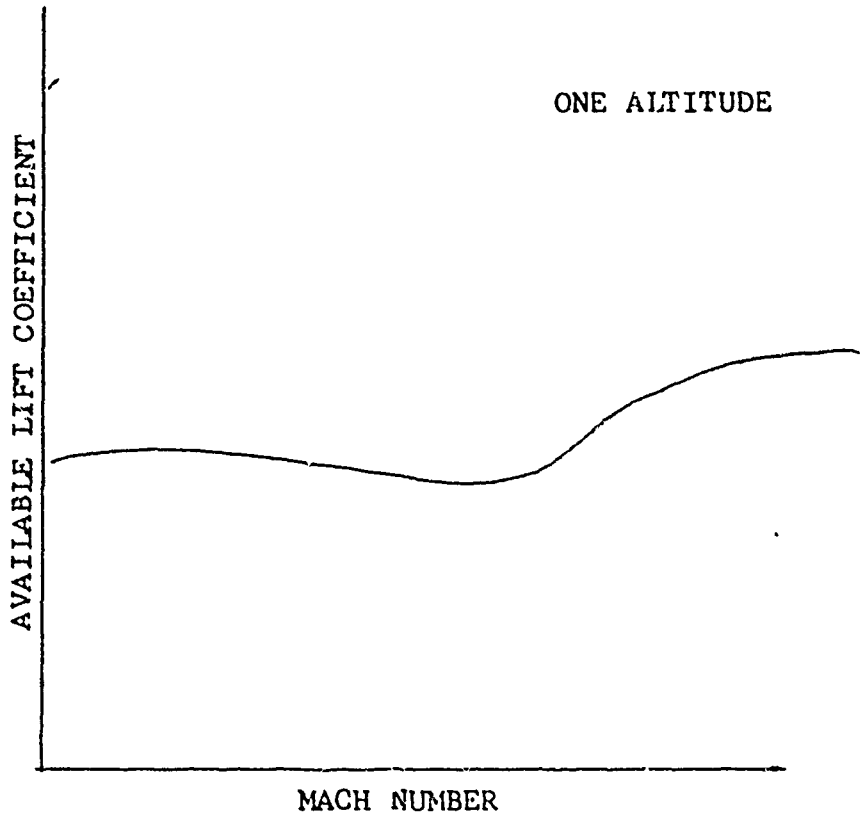

FIG. 9-9: GENERALIZED THRUST LIMITED TURNING PERFORMANCE

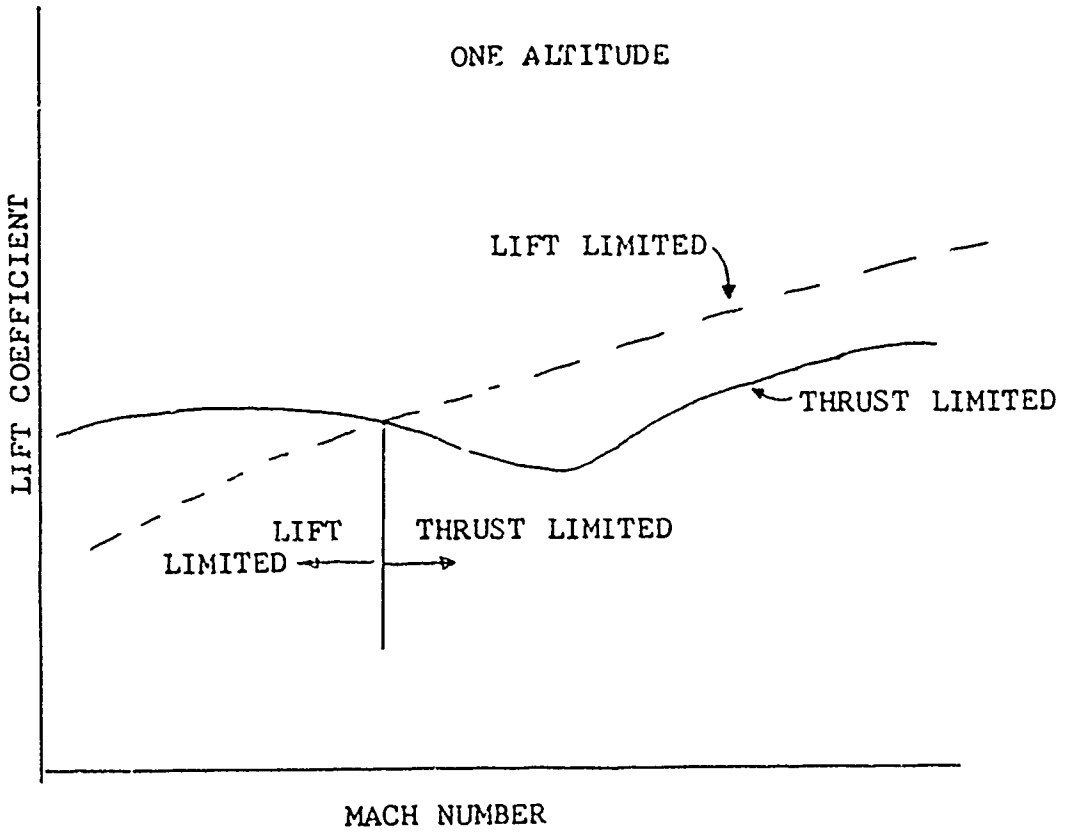

FIG. 9-10: GENERALIZED TURNING PERFORMANCE AT CONSTANT ALTITUDE

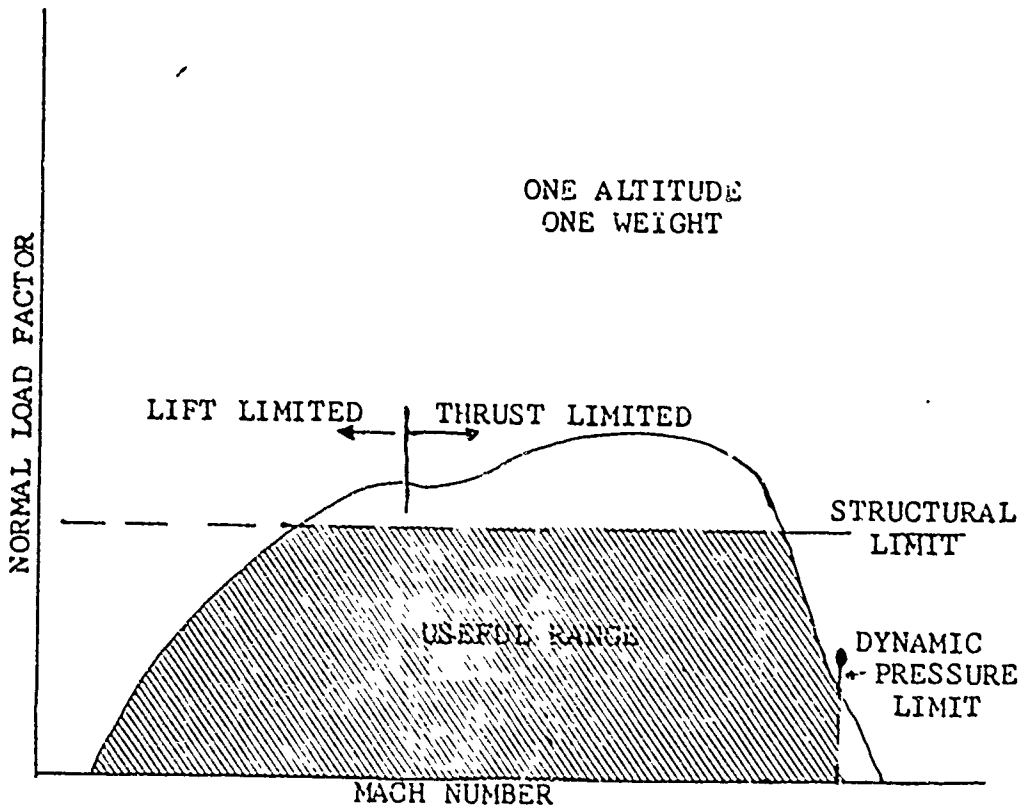

FIG. 9-11: GENERALIZED TURNING PERFORMANCE CROSS-PLOT AT CONSTANT ALTITUDE

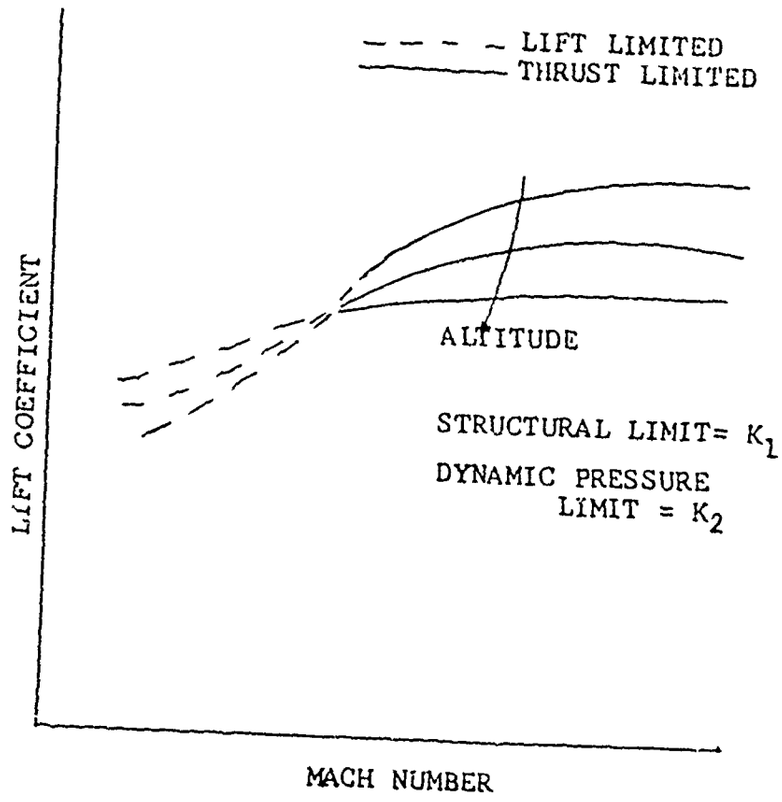

FIG. 9-12: GENERALIZED TURNING PERFORMANCE MAP

9.18 Self-contained take-off and landing data can be obtained by integrating accelerometer data. Preliminary investigations have indicated that suitable data can be obtained. Figure 1-9 of Chapter 1 shows the results of one such analysis. The data was generated as outlined in the following steps:

GROUND PHASE

a. Ground roll true angle of attack is taken to be pitch attitude. (This is reasonable because it forces the flight path to be parallel to the runway.)

b. $\alpha_t = \theta$ so $\alpha_t - \alpha_i = \Delta\alpha$ correction for flight path accelerometers (upwash and misalignment).

c. n_X and n_Z are rotated to the proper axis for integration (runway and runway normal).

d. Compute V_T airspeed by pitot-static using in ground effect position error.

e. While in ground roll phase, compute velocity by integration as follows:

$$n_X = \frac{\dot{V}}{g} + \frac{\dot{h}}{V} \qquad (9\text{-}6) \qquad \text{where } \frac{\dot{h}}{V} = \sin\gamma \qquad (9\text{-}7)$$

for ground roll the flight path angle is equal to the runway slope such that:

$$n_X = \frac{\dot{V}}{g} + \sin\phi \qquad (9\text{-}8)$$

or

$$\dot{V} = g(n_x - \sin\phi) \tag{9-9}$$

which can be numerically integrated.

f. The difference between (d) and (e) gives a time history of wind on the aircraft nose.

g. Runway distance is again obtained by numerically integrating the relation:

$$\dot{S} = V \ . \tag{9-10}$$

AIR PHASE

h. Determine lift-off point by wheel rpm as shown in figure 9-13. At the time the aircraft wheel leaves the runway, there is an abrupt change from acceleration to deceleration of main wheel rpm.

i. After lift-off, the assumption $\Delta\alpha=\Delta\alpha_u$ is valid because we have reached a high enough speed for aerodynamic forces to dominate any inertial forces in the vane system due to slow airspeed.

j. After lift-off, an iteration is required as follows:

$$\frac{a_z}{g} = (n_z - \cos\gamma) \tag{9-11}$$

$$\ddot{h} = a_z\cos\gamma = g(n_z - \cos\gamma)\cos\gamma \tag{9-12}$$

initial guess for γ is $=\frac{\dot{h}}{V}$ from altimeter or $\gamma=0$.

Integrate $\ddot{h}$ to obtain $\dot{h}$.

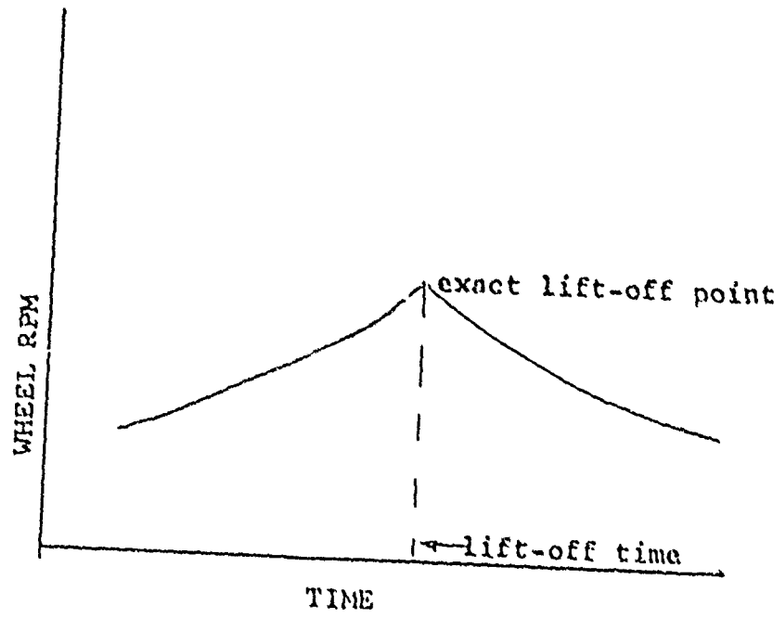

FIG. 9-13: WHEEL RPM TIME HISTORY

Next, integrate $\dot{V}=q(n_x-\frac{\dot{h}}{V})$ using initial guess for $\frac{\dot{h}}{V}$. Now, using the solved h and V the process is started over again until the values of $\dot{h}$ and V repeat within a given tolerance. This yields $\dot{h}$ and V where V is inertially oriented.

k. V_T airspeed can be obtained as $\frac{V}{\cos\gamma}$ (not including wind component).

l. Runway distance is computed as the integral of V.

m. Altitude can be computed as the integral of $\dot{h}$.

Typical results are again shown in figure 1-9 of Chapter 1.

LANDING

n. For landings, the sign of the whole problem changes and the solution is obtained by integrating backwards from full stop.

9.19 If the data of figure 1-9 is reduced with impressed errors in each of the primary parameters, and the Askania data is taken as standard, an appreciation of the sensitivities of the data reduction procedure to small errors can be obtained. Table 9-2 gives the result of such an analysis. For take-off, the listed errors in parameters are equivalent with the exception of lift-off time which showed no correlation, but did show the highest sensitivity. Since the lift-off time is obtained by the abrupt sign change of wheel acceleration, it should be as accurate as time is recorded. For digital systems then, data should be recorded at short time intervals (.1 sec. or less) to assure an accurate lift-off time.

TABLE 9-1

TAKE-OFF DATA REDUCTION SENSITIVITY STUDY

Parameter	Impressed Error	% Error distance @t=10sec	% Error distance @t=20sec	% Error distance @liftoff	% Error distance @t=30sec	% Error altitude @t=30sec
Standard value	-	543 ft	2351 ft	2845 ft	4806 ft	263 ft
N_z NORMAL	+.001	0.2%	0.0%	0.0%	0.1%	4.6%
N_x LONGITUDINAL	+.001	0.4%	0.1%	0.3%	0.2%	4.5%
θPITCH RATE	+.1	-1.0%	-0.6%	-0.8%	-0.6%	4.5%
θPITCH ALTITUDE	+.1	-0.5%	-1.4%	-0.4%	-0.6%	4.5%
αANGLE OF ATTACK	+.1	+0.5%	1.4%	0.4%	0.6%	4.5%
$V_{PITOT\ STATIC}$	+1.0	0.0%	0.0%	0.1%	0.1%	4.5%
$t_{liftoff}$	-1.0	0.0%	0.0%	0.0%	0.0%	-13.0%
$t_{liftoff}$	-4.0	0.0%	0.0%	-8.9%	0.8%	16.5%

CONCLUDING REMARKS TO CHAPTER 9

9.20 It has been shown that, in general, conventional aircraft performance flight test can yield more information in the case of accelerations and climbs when using onboard accelerometers. Stabilized points can be done more quickly with accelerometers onboard. Additionally, turning performance data can be analyzed with more sophisticated analysis techniques. Finally, onboard accelerometers can give a self-contained take-off and landing data capability.

REFERENCES TO CHAPTER 9

9-1. USAF, Edwards AFB, Technical Report #6273, "Flight Test Engineering Handbook," R.M. Herrington, et al, Unclassified, Jan 1966.

9-2. Wright Patterson AFB, Foreign Technology Division Report HT-23-95-69, " Flight Testing of Aircraft," (Letnyye Ispytaniya Samoletov), Translation from Russian, Unclassified, Sep 1969.

9-3. U.S. Naval Test Pilot School, Patuxent River, Maryland, "Performance Testing Manual," M.W. Townsend, Unclassified, Aup 1966.

9-4. USNTPS-FTM-#104, Patuxent River, Maryland, "Fixed Wing Performance Theory and Flight Test Techniques," S.M.Small and J.W. Prueher, Unclassified, Jul 1972.

9-5. Air Force Flight Test Center, Technology Document #71-1, "Theory of the Measurement and Standardization of Inflight Performance of Aircraft," E.W. Dunlop and M.B. Porter, Unclassified, Apr 1971.

9-6. Boeing Corporation, Document #D6-1420, "Jet Transport Performance Methods," Unclassified, May 1969.

9-7. USAF Aerospace Research Pilots' School, FTC-TIA-70-1001, "Performance," Unclassified, 1970.